

AWARD NUMBER: W81XWH-15-1-0372

TITLE: Discovery of Novel N-Nicotinamide Methyltransferase Inhibitors to Combat Obesity-Linked Osteoarthritis and Metabolic Disease Among Veterans and Beneficiaries

PRINCIPAL INVESTIGATOR: Watowich, Stanley J.

CONTRACTING ORGANIZATION: University of Texas Medical Branch at Galveston
Galveston, TX 77555

REPORT DATE: June 2018

TYPE OF REPORT: Final

PREPARED FOR: U.S. Army Medical Research and Materiel Command
Fort Detrick, Maryland 21702-5012

DISTRIBUTION STATEMENT: Approved for Public Release;
Distribution Unlimited

The views, opinions and/or findings contained in this report are those of the author(s) and should not be construed as an official Department of the Army position, policy or decision unless so designated by other documentation.

REPORT DOCUMENTATION PAGE

Form Approved
OMB No. 0704-0188

Public reporting burden for this collection of information is estimated to average 1 hour per response, including the time for reviewing instructions, searching existing data sources, gathering and maintaining the data needed, and completing and reviewing this collection of information. Send comments regarding this burden estimate or any other aspect of this collection of information, including suggestions for reducing this burden to Department of Defense, Washington Headquarters Services, Directorate for Information Operations and Reports (0704-0188), 1215 Jefferson Davis Highway, Suite 1204, Arlington, VA 22202-4302. Respondents should be aware that notwithstanding any other provision of law, no person shall be subject to any penalty for failing to comply with a collection of information if it does not display a currently valid OMB control number. **PLEASE DO NOT RETURN YOUR FORM TO THE ABOVE ADDRESS.**

1. REPORT DATE June 2018		2. REPORT TYPE Final		3. DATES COVERED 30 Sep 2015 – 29 Mar 2018	
4. TITLE AND SUBTITLE Discovery of Novel N-Nicotinamide Methyltransferase Inhibitors to Combat Obesity-Linked Osteoarthritis and Metabolic Disease Among Veterans and Beneficiaries				5a. CONTRACT NUMBER	
				5b. GRANT NUMBER W81XWH-15-1-0372	
				5c. PROGRAM ELEMENT NUMBER	
6. AUTHOR(S) Stanley J. Watowich E-Mail: watowich@xray.utmb.edu				5d. PROJECT NUMBER	
				5e. TASK NUMBER	
				5f. WORK UNIT NUMBER	
7. PERFORMING ORGANIZATION NAME(S) AND ADDRESS(ES) AND ADDRESS(ES) University of Texas Medical Branch 301 University Blvd Galveston, TX 77555-5302				8. PERFORMING ORGANIZATION REPORT NUMBER	
9. SPONSORING / MONITORING AGENCY NAME(S) AND ADDRESS(ES) U.S. Army Medical Research and Materiel Command Fort Detrick, Maryland 21702-5012				10. SPONSOR/MONITOR'S ACRONYM(S)	
				11. SPONSOR/MONITOR'S REPORT NUMBER(S)	
12. DISTRIBUTION / AVAILABILITY STATEMENT Approved for Public Release; Distribution Unlimited					
13. SUPPLEMENTARY NOTES					
14. ABSTRACT Nicotinamide N-methyltransferase (NNMT) has been implicated in osteoarthritis, metabolic disorders, cardiovascular disease, cancer, kidney disease, and Parkinson's disease that impact the military, their dependents, and the general population. This project is developing drug candidates that specifically target NNMT and produce targeted reductions in white adipose tissue, leading to significant weight loss and improvements in obesity-linked comorbidities. Towards this end, we developed the first assay to directly monitor NNMT product formation and activity in real-time, resulting in the enhanced capacity to collect accurate NNMT kinetic data. Detailed kinetic data analysis has resulted in the detailed molecular characterization of NNMT reaction mechanism, and, importantly, discovery of novel drug-like nanomolar NNMT inhibitors. These drug candidates showed attractive cellular permeability flux when tested in membrane transport assays. Synthesis scale-up of the most promising drug candidates has been achieved. Proof-of-concept evaluation in mouse models of diet-induced obesity has been completed and shows promising activity.					
15. SUBJECT TERMS metabolic disease; obesity; osteoarthritis; drug candidates					
16. SECURITY CLASSIFICATION OF:			17. LIMITATION OF ABSTRACT	18. NUMBER OF PAGES	19a. NAME OF RESPONSIBLE PERSON
a. REPORT	b. ABSTRACT	c. THIS PAGE			USAMRMC
Unclassified	Unclassified	Unclassified	Unclassified	98	19b. TELEPHONE NUMBER (include area code)

Table of Contents

	<u>Page</u>
1. Introduction.....	4
2. Keywords.....	5
3. Accomplishments.....	6
4. Impact.....	14
5. Changes/Problems.....	15
6. Products.....	16
7. Participants & Other Collaborating Organizations.....	18
8. Special Reporting Requirements.....	20
9. Appendices.....	21

1. Introduction

Our project aligned with FY14 PRMRP Topic Areas metabolic disease (including obesity, obesity-associated metabolic disease, and type 2 diabetes) and osteoarthritis. Das et al. reported that over one-third of US veterans and their post-adolescent dependents were clinically obese, making obesity and obesity-linked comorbidities one of the top health issues faced by the DoD healthcare system. Treating obesity-linked chronic diseases currently accounts for ~10% of veteran's healthcare expenditures. Unfortunately, the vast majority of efforts to reduce obesity through diet, exercise, and/or appetite suppression have not had long-term success, and bariatric surgery carries many risks including death. In this project, we proposed a radical rethinking of this problem to move away from failed efforts to reduce calorie input relative to calorie expenditure in the hope that body fat (white adipose tissue) and excess body mass will decrease. Instead, we developed and tested novel small molecule drugs that were predicted to directly increase white adipose tissue energy expenditures, thus reducing body fat and total body mass. To achieve this anti-obesity drug breakthrough, our project exploited recent observations that down-regulation of the enzyme nicotinamide N-methyltransferase (NNMT) could shrink white adipose tissue and produce significant weight loss in animal models, without the necessity of reducing calorie intake. To validate the in vitro activity of novel NNMT inhibitors, we developed the first assay capable of directly monitoring NNMT product formation and activity in real-time, resulting in the enhanced capacity to collect accurate NNMT kinetic data. Using this assay, and accessory tests, we validated a series of novel drug-like nanomolar NNMT inhibitors. Importantly, these drug candidates showed attractive cellular permeability flux when tested in membrane transport assays and in cells. Synthesis scale-up of the most promising drug candidates was achieved. Proof-of-concept evaluations of individual drug candidates in mouse models of diet-induced obesity were completed and showed that our NNMT inhibitors could safely produce significant weight-loss in obese animals without changes in food intake. Work is continuing, beyond the scope of this award, to determine the impact of NNMT inhibitors on obesity-linked Type 2 diabetes.

2. Keywords

metabolic disease

obesity and obesity-linked comorbidities

osteoarthritis

drug candidates

3. Accomplishments

Major goals of the project

Task 1: *In vitro* testing of *in silico* hits

1.1. Complete project hiring

Research scientists hired February 1, 2016 and February 15, 2016. Research technician hired August 8, 2016.

1.2. Order 70 small molecules for testing

Small molecules with good Vina “docking” (or virtual screening) scores were ordered for testing. To date, ~40-50 commercially available compounds have been testing in NNMT inhibition assays (see Figure 1). Based on initial results, novel analogs of a promising scaffold hit were evaluated using virtual screening protocols, and ~20-30 best scoring compounds synthesized and tested in NNMT inhibition assays. Drug-like nanomolar small molecule inhibitors of NNMT have been validated (see Table 1-5; published and reproduced in Appendix 2). Tested compounds have been analyzed and 2-dimensional and 3-dimensional structure-activity relationships have been established.

□

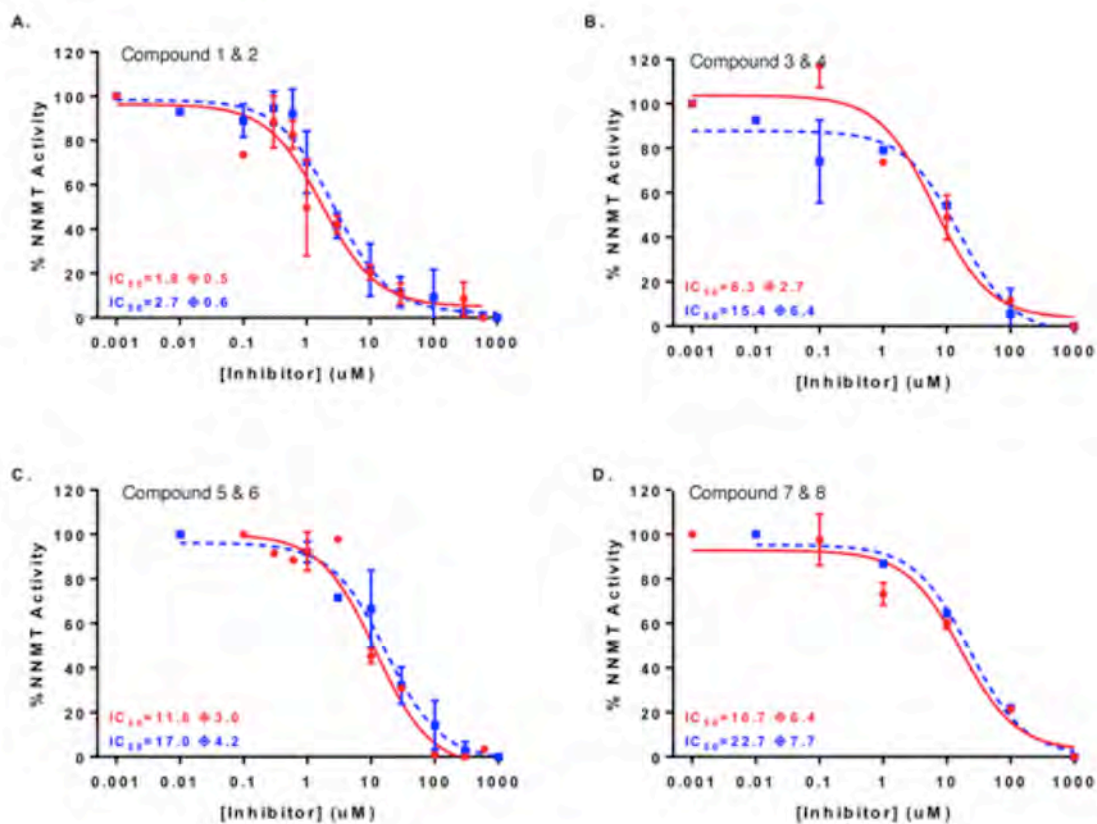
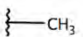
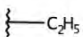
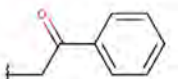
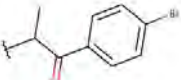
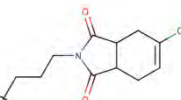
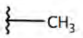
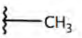
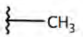
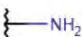
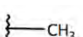
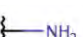

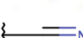

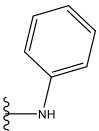
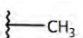
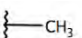
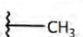





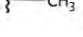

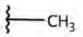
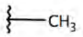










Figure 1. IC₅₀ curves for the representative potent small molecule NNMT inhibitors within four different core scaffolds (A-D).

Table 1. NNMT inhibitory activity of scaffold A compounds with single positional substitutions

Compound Name	R1	R2	R3	R4	R5	R6	R7	R8	IC ₅₀ ± S.E. (uM)
1a		H	H	H	H	H	H	H	12.1 ± 3.1
1b		H	H	H	H	H	H	H	27.5 ± 4.4
1c	Methoxy-ethyl	H	H	H	H	H	H	H	165.1 ± 298
1d		H	H	H	H	H	H	H	>1000
1e		H	H	H	H	H	H	H	>1000
1f		H	H	H	H	H	H	H	>1000
1g			H	H	H	H	H	H	16.5 15.3 *
1h			H	H	H	H	H	H	6.3 ± 1.1
1i		H		H	H	H	H	H	2.6 ± 0.6
1j		H		H	H	H	H	H	23.8 ± 5.6
1k		H		H	H	H	H	H	>1000
1l		H	H		H	H	H	H	7.5 ± 2.2
1m		H	H		H	H	H	H	11.3 ± 11.7(R)
1n		H	H	H		H	H	H	0.9 ± 0.3
1o		H	H	H	H		H	H	5.7 ± 1.8
1p		H	H	H	H		H	H	13.1 ± 5.1
1q		H	H	H	H		H	H	52.4 ± 31
1r		H	H	H	H		H	H	468 ± 309?
1s		H	H	H	H	H		H	2.0 ± 0.5
1t		H	H	H	H	H		H	709 +/- 179 680?
1u		H	H	H	H	H	H		1.8 ± 0.5

1v		H	H	H	H	H	H		48.7 ± 19.3
-----------	--	---	---	---	---	---	---	--	-------------

Table 2. NNMT inhibitory activity of scaffold A compounds with dual positional substitutions

Compound Name	R1	R2	R3	R4	R5	R6	R7	R8	IC ₅₀ ± S.E. (uM)
2a		H		H	H	H	H	H	>1000
2b		H	H		H	H	H	H	9.8 ± 5.2
2c		H	H		H	H	H	H	33.5 ± 9.9
2d		H	H	H	H		H	H	>1000
2e		H	H	H	H		H	H	>1000
2f		H	H	H	H		H	H	>1000
2g		H	H	H	H		H	H	NI
2h		H	H	H	H	H	H		3.1 ± 1.4
2i		H	H	H	H	H	H		40.6 ± 13

Table 3. NNMT inhibitory activity of scaffold A compounds with multi-positional substitutions

Compound Name	R1	R2	R3	R4	R5	R6	R7	R8	IC ₅₀ ± S.E. (uM)
3a		H		H	H		H	H	1.1
3b		H	H		H		H	H	3.6 ± 1.5
3c			H	H	H		H	H	>1000
3d		H	H		H		H	H	>1000
3e		H	H		H	H	H		>1000??
3f			H		H		H		>1000

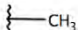
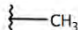
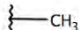
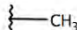
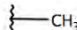
3g			H		H	H			>1000
-----------	---	---	---	---	---	---	---	---	-------

Table 4. NNMT inhibitory activity of compounds containing scaffold B

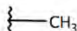
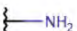
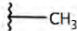
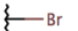
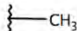
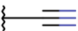
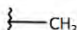
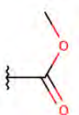
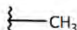
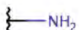
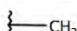

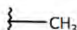

Compound Name	R1	R2	R3	R4	R5	R6	R7	R8	IC ₅₀ ± S.E. (uM)
4b	H			H	H	H	H	H	6.3 ± 2.7
4c	H		H		H	H	H	H	29.4 ± 6.4
4d	H		H		H	H	H	H	201.5 ± 204
4e	H		H		H	H	H	H	NI??
4f	H		H	H	H		H	H	29.9 ± 9.1
4g	H		H	H	H		H	H	>1000??
4h	H		H	H	H	H		H	>1000??

Table 5. NNMT inhibitory activity of compounds containing scaffold C

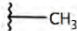
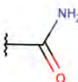
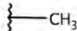
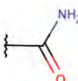
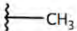
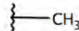
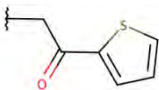
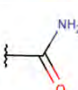
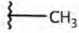
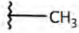
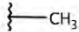
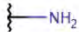
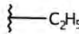
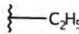
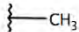
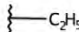
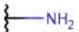
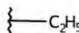
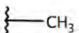
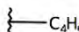
Compound Name	R1	R3	R4	R6	IC ₅₀ ± S.E. (uM)
5a			H	H	16.7 ± 3.8
5b					11.8 ± 3.0
5c			H	H	>1000

Table 6. NNMT inhibitory activity of compounds containing scaffold D.

Core/ Compound Name	R1	R3	R6	R7	X	IC ₅₀ ± S.E. (μ M)
6a			H	H	N	16.7 ± 6.4
6b			H	H	N	82.4 ± 17.4
6c			H	H	N	22.7 ± 7.7
6d				H	N	>1000
6e		-		H	S	>1000
6f		-	H	H	S	>1000

1.3. Complete turbidity measurements in physiological buffer to determine solubility limits Completed for each tested molecule.

1.4. Complete methyltransferase kinetic assay on initial set of soluble compounds
As noted under item 1.2, NNMT inhibition assays have been completed for 60+ compounds. Drug-like nanomolar small molecule inhibitors of NNMT have been validated. Tested compounds have been analyzed and 2-dimensional and 3-dimensional structure-activity relationships have been established. This process is continuing as we utilize existing data and improved predictive algorithms to design more effective small molecule inhibitors.

Milestone: Identify small molecule(s) NNMT inhibitor for subsequent cell culture study.

Achieved - small molecules for use as potential NNMT inhibitors in cell culture studies were proposed in November 2015. Following additional testing and validation, additional small molecule NNMT inhibitors were proposed in May, 2016 for testing in cell culture The list of validated small molecule NNMT inhibitors appropriate for efficacy testing in adipocyte cell culture system is undergoing continual refinement as new compounds are tested.

1.5. Complete cell culture studies of 10 top-ranked compounds

Approximately 4 compounds have been tested to determine their effect on oxygen consumption in adipocyte cell culture. These studies used the Oxygraph system to measure oxygen flux, and collected data have suggested the tested compounds produce a phenotypic effect. We have recently developed a LC/MS assay to directly measure NNMT activity in cultured adipocytes; once fully characterized, this assay will be used to characterize the mechanistic activity of NNMT inhibitors in cell culture.

1.6. Complete metabolic stability of 5 top-ranked compounds

Initial compounds were tested for metabolic stability using human and mouse microsomes. Studies were performed by Cypotex (Watertown, MA), a valued Contract Research Organization, and completed December 3, 2015. We are currently refining our list of the most promising small molecule NNMT inhibitors for use in additional metabolic stability studies.

Task 2: *In vivo* testing of *in silico* hits

2.1. Local IRB/IACUC approval

IACUC protocol approval for treatment studies in diet-induced obesity (DIO) mouse models was obtained May 15, 2016. IACUC approval is required for each additional unique small molecule used to treat DIO mice.

Milestone: ACURO approval

Achieved – ACURO approval received on October 9, 2015.

2.2. Complete PK study of 4 top-ranked compounds

Pharmacokinetic (PK) studies of small molecule compounds completed on December 3, 2015 and August 8, 2016 using the Cyprotex (Watertown, MA), a valued Contract Research Organization. PK studies were performed in triplicate using mice, with compounds administered by subcutaneous injection. Plasma samples were collected at 7 time points over a 24 hr period. Test compounds were quantified by LC/MS and the time-dependent data used to calculate PK parameters (e.g., half-life, C_{max}).

2.3. Complete NOAEL study of top-ranked compounds

Preliminary NOAEL studies completed for lead NNMT inhibitor 5-amino-1-methylquinoline.

Milestone: Identify small molecule(s) NNMT inhibitor for *in vivo* obesity-reversal study.

Achieved – a novel small molecule validated NNMT inhibitor (~1 μ M IC_{50}) was selected for proof-of-concept *in vivo* efficacy studies in DIO mice. Studies commenced January 2017, following a 1-month acclimation period for the subject animals. Test compound has been synthesized in amounts > 1 g for use in these studies.

2.4. Complete diet-induced obesity-reversal study of top-ranked cmpds

Completed. Approximately 20 DIO mice were ordered and used in weight loss study. Study results published and attached as Appendix 3.

Milestone achieved: Completed preliminary proof-of-concept study to validate NNMT inhibitor as an anti-obesity lead.

Task 3: Synthesis of novel transition-state (ts) analogs

3.1. Develop a multi-step synthesis of the novel transition-state inhibitor, which will be synthesized via a 9-step process based on some prior literature precedent.

A synthesis route has been designed, and we are currently troubleshooting the initial steps of this challenging reaction path.

3.2. Design and synthesis of 6 unique analogs of **SW-ts-0001**

Delayed; resources have been focused on advancing the more promising anti-obesity small molecule inhibitors described in Tasks 1-2.

3.3. Design and synthesis of additional 6 unique analogs of **SW-ts-0001**

Delayed; resources have been focused on advancing the more promising anti-obesity small molecule inhibitors described in Tasks 1-2.

Milestone: Complete *de novo* synthesis of **SW-ts-0001** and ts analogs.
~25% completed.

Task 4: *In vitro* testing of novel transition-state (ts) analogs

4.1 Turbidity measurements of ts analogs in physiological buffer

Delayed; resources have been focused on advancing the more promising anti-obesity small molecule inhibitors described in Tasks 1-2.

4.2. Complete methyltransferase kinetic assays of ts analogs

Delayed; resources have been focused on advancing the more promising anti-obesity small molecule inhibitors described in Tasks 1-2.

4.3. Complete cell culture studies of ts analogs

Delayed; resources have been focused on advancing the more promising anti-obesity small molecule inhibitors described in Tasks 1-2.

Milestone: Identify ts analog NNMT inhibitor for *in vivo* obesity-reversal study.
~20% completed.

Task 5: *In vivo* testing of novel transition state analogs

5.1. Complete PK study of 2 top-ranked ts analogs

Delayed; resources were refocused to advance the more promising anti-obesity small molecule inhibitors described in Tasks 1-2.

5.2. Complete NOAEL study of 2 top-ranked ts analogs

Delayed; resources were refocused to advance the more promising anti-obesity small molecule inhibitors described in Tasks 1-2.

5.3. Complete diet-induced obesity-reversal study of top-ranked ts analog

Delayed; resources were refocused to advance the more promising anti-obesity small molecule inhibitors described in Tasks 1-2.

Milestone: Complete proof-of-concept study to validate ts analog NNMT inhibitor as an anti-obesity lead.

Delayed; resources were refocused to advance the more promising anti-obesity small molecule inhibitors described in Tasks 1-2.

What was accomplished under these goals?

We discovered and developed novel first-in-class small molecule therapeutics that target a new mechanism-of-action to combat obesity and obesity-linked type 2 diabetes (T2D). During this project award period, we completed lead optimization and preliminary safety studies to successfully translate our academic benchtop discoveries into promising and game-changing drug candidates for obesity and T2D. Our compelling drug candidates promise to greatly

improve the health and well-being of a vast majority of US Veterans, military service members, and beneficiaries (as well as the general US population) impacted by obesity and chronic T2D.

What opportunities for training and professional development has the project provided?

Nothing to Report.

How were the results disseminated to communities of interest?

Three high-profile manuscripts were published (see Appendix), including significant media reporting of the results obtained for our anti-obesity drug leads.

What do you plan to do during the next reporting period to accomplish the goals?

Nothing to Report.

4. Impact

What was the impact on the development of the principal discipline(s) of the project?

With pivotal support from a FY14 Discovery Award, we discovered and developed novel first-in-class small molecule therapeutics that target a new mechanism-of-action to combat obesity and obesity-linked type 2 diabetes (T2D). During this project award period, we completed lead optimization and preliminary safety studies to successfully translate our academic benchtop discoveries into promising and game-changing drug candidates for obesity and T2D. Our compelling drug candidates promise to greatly improve the health and well-being of a vast majority of US Veterans, military service members, and beneficiaries (as well as the general US population) impacted by obesity and chronic T2D.

All major milestones proposed in our high-risk, high-reward FY14 DA project were successfully completed. These milestones provided a solid foundation for our ongoing T2D drug development program, centered on potent and selective candidate inhibitors of nicotinamide N-methyltransferase (NNMT) as a novel strategic target to combat obesity and T2D. Several challenges (e.g., cell permeability) were encountered during the discovery and identification of our lead series analogues, which were overcome by rigorous structure-based computational and medicinal chemistry efforts. This strikingly resulted in detailed structure activity relationships for our 1st-generation selective and potent small molecule inhibitors of NNMT (see Appendix 2). Potent “hits” within the lead series were rapidly validated for mechanism-of-action in optimized biochemical (see Appendix 1) and cellular assays, with a lead inhibitor successfully demonstrating potent efficacy in a translationally-relevant diet-induced obese (DIO) mouse model (see Appendix 3).

What was the impact on other disciplines?

The above promising outcomes in diet-induced obese mouse models suggest our drug leads will have significant impact at improving comorbidities associated with chronic obesity, most importantly Type 2 diabetes and non-alcoholic steatohepatitis (NASH).

What was the impact on technology transfer?

The important and successful outcomes from our FY14 Discovery Award project resulted in 3 publications in high-impact internationally-recognized journals, as well as international patent protection under Patent Cooperation Treaty (PCT) covering “composition of matter” and “use” with no freedom to operate barriers.

What was the impact on society beyond science and technology?

The above promising outcomes have successfully positioned our drug leads to advance to preclinical development and IND-enabling studies needed to secure US FDA approval for first-in-human clinical trials as new mechanism-of-action treatments to reduce obesity and reverse Type 2 diabetes.

5. Changes/Problems

Changes in approach and reasons for change

Resources were refocused to advance the more promising anti-obesity small molecule inhibitors described in Tasks 1-2.

Actual or anticipated problems or delays and actions or plans to resolve them

Our research team increasingly focused its limited resources on efforts to rapidly capitalize on the discoveries that were rapidly made in Aim 1; this refocusing of effort was made in consultation with Project Officials. As such, work on synthesizing and testing transition-state analogs as NNMT inhibitors (Aim 2) was deemed low-priority.

Changes that had a significant impact on expenditures

Nothing to Report.

Significant changes in use or care of human subjects, vertebrate animals, biohazards, and/or select agents

Nothing to Report.

Significant changes in use or care of human subjects

Not applicable.

Significant changes in use or care of vertebrate animals

Nothing to Report.

Significant changes in use of biohazards and/or select agents

Not applicable.

6. Products

Publications, conference papers, and presentations

Published manuscripts:

Neelakantan H, Vance V, Wang HY, McHardy SF, Watowich SJ. Non-coupled fluorescent assay for direct real-time monitoring of nicotinamide N-methyltransferase activity. *Biochem.* 56, 824, 2017.

Neelakantan H, Wang HY, Vance V, Hommel JD, McHardy SF, Watowich SJ. Structure–activity relationship for small molecule inhibitors of nicotinamide N-methyltransferase. *J. Med. Chem.* 60, 5015, 2017.

Neelakantan H, Vance V, Wetzel M, Wang HY, McHardy SF, Finnerty C, Hommel JD, Watowich SJ. Selective and membrane permeable small molecule inhibitor of nicotinamide N-methyltransferase reverses diet-induced obesity in mice. *Biochemical Pharmacology* 147, 141, 2018.

Journal publications

Neelakantan H, Vance V, Wang HY, McHardy SF, Watowich SJ. Non-coupled fluorescent assay for direct real-time monitoring of nicotinamide N-methyltransferase activity. *Biochem.* 56, 824, 2017.

Neelakantan H, Wang HY, Vance V, Hommel JD, McHardy SF, Watowich SJ. Structure–activity relationship for small molecule inhibitors of nicotinamide N-methyltransferase. *J. Med. Chem.* 60, 5015, 2017.

Neelakantan H, Vance V, Wetzel M, Wang HY, McHardy SF, Finnerty C, Hommel JD, Watowich SJ. Selective and membrane permeable small molecule inhibitor of nicotinamide N-methyltransferase reverses diet-induced obesity in mice. *Biochemical Pharmacology* 147, 141, 2018.

Books or other non-periodical, one-time publications

Nothing to Report.

Other publications, conference papers, and presentations

Nothing to Report.

Website(s) or other Internet site(s)

Nothing to Report.

Technologies or techniques

We have developed the first assay to utilize fluorescence spectroscopy to directly monitor NNMT product formation and activity in real-time. This assay provides accurate kinetic data that can be used to understand the molecular mechanistic details of the NNMT reaction. Our novel assay offers a robust detection technology for use in SAM substrate competition assays for the discovery and development of inhibitors of the large class of medically relevant SAM-dependent methyltransferases. As such, this research is of interest to pharmaceutical and academic researchers involved in drug discovery and enzyme structure-function studies. Additionally, we identified small molecule NNMT inhibitors that promote weight loss in diet-induced obese animals without concomitant changes in food intake. As such, this research is of interest to

pharmaceutical companies developing therapeutics to treat obesity and obesity-related comorbidities.

Inventions, patent applications, and/or licenses

An international patent protection was filed under Patent Cooperation Treaty (PCT) covering “composition of matter” and “use” with no freedom to operate barriers. This patent describes novel small molecule chemical entities that are to be used to inhibit the enzymatic activity of human nicotinamide N-methyltransferase (NNMT; CAS registry # 9029-74-7; EC 2.1.1.1). NNMT has been implicated in a number of diseases, including osteoarthritis, metabolic disorders (including, but not limited to, abnormal BMI, obesity, type 2 diabetes), cardiovascular disease, cancer (including, but not limited to, colorectal, breast, kidney, digestive tract, prostate, esophageal, pancreatic, endometrial, thyroid, gallbladder), metastatic progression, Parkinson's disease, kidney disease, and other neurovascular-related (e.g., migraine) and neurological dysfunctions (e.g., epilepsy). The described small molecule chemical entities could be used to treat and/or prevent some or all NNMT-associated diseases and/or their progression. These entities would be administered to people who are at risk for developing or are afflicted with NNMT-associated diseases.

Other Products

Nothing to Report.

7. Participants & Other Collaborating Organizations

What individuals have worked on the project?

Name:	Stanley Watowich
Project Role:	PI
Researcher Identifier (e.g. ORCID ID):	ORCID ID: 0000-0002-1660-1818
Nearest person month worked:	3
Contribution to Project:	Project coordination and director; data analysis; computational SAR; assay design and development; inhibitor design
Funding Support:	DoD and UTMB
Name:	Stanton McHardy
Project Role:	PI of subcontract to University of Texas San Antonio
Researcher Identifier (e.g. ORCID ID):	
Nearest person month worked:	1
Contribution to Project:	Supervises all aspects of chemical synthesis related to this project
Funding Support:	UTSA
Name:	Harshini Neelakantan
Project Role:	Research scientist
Researcher Identifier (e.g. ORCID ID):	
Nearest person month worked:	12
Contribution to Project:	Designs, develops, optimizes, and performs biochemical and cell-based assays, and animal studies
Funding Support:	
Name:	Hua-Yu Wang
Project Role:	Research scientist
Researcher Identifier (e.g. ORCID ID):	
Nearest person month worked:	3
Contribution to Project:	Performs chemical synthesis of novel inhibitors; quality control and validation of commercial reagents
Funding Support:	UTSA
Name:	Virginia Vance

Project Role:	Research technician
Researcher Identifier (e.g. ORCID ID):	
Nearest person month worked:	12
Contribution to Project:	Optimizes and performs biochemical and cell-based assays
Funding Support:	

Has there been a change in the active other support of the PD/PI(s) or senior/key personnel since the last reporting period?

Nothing to Report.

What other organizations were involved as partners?

Nothing to Report.

8. Special Reporting Requirements

9. Appendices

Published manuscripts attached.

Appendix 1: Neelakantan H, Vance V, Wang HY, McHardy SF, Watowich SJ. Non-coupled fluorescent assay for direct real-time monitoring of nicotinamide N-methyltransferase activity. *Biochem.* 56, 824, 2017.

Appendix 2: Neelakantan H, Wang HY, Vance V, Hommel JD, McHardy SF, Watowich SJ. Structure–activity relationship for small molecule inhibitors of nicotinamide N-methyltransferase. *J. Med. Chem.* 60, 5015, 2017.

Appendix 3: Neelakantan H, Vance V, Wetzel M, Wang HY, McHardy SF, Finnerty C, Hommel JD, Watowich SJ. Selective and membrane permeable small molecule inhibitor of nicotinamide N-methyltransferase reverses diet-induced obesity in mice. *Biochemical Pharmacology* 147, 141, 2018.

Appendix 1: Neelakantan H, Vance V, Wang HY, McHardy SF, Watowich SJ. Non-coupled fluorescent assay for direct real-time monitoring of nicotinamide N-methyltransferase activity. *Biochem.* 56, 824, 2017.

series of enzyme-coupled SAH detection colorimetric assays are used to probe the activity of many disease-linked MTs where the catalytic product readouts are single-point, indirect, slow with multiple steps, labor intensive, insensitive, and/or incorporate radioactive materials.^{28–37} These assays can be challenging and expensive to adapt for high-throughput screening of large chemical libraries to identify MT inhibitors.³³

To date, there appears to be only one assay (for catechol *O*-methyltransferase) described to directly detect methyltransferase product fluorescence,^{38,39} and no current detection method provides direct, continuous, real-time, and sensitive monitoring of NNMT product formation. Herein, we describe a sensitive noncoupled fluorescence-based assay that monitors NNMT kinetic activity. Importantly, our fluorescent assay provides direct, continuous, and quantitative readout of the NNMT reaction, thus allowing detailed characterization of the NNMT reaction, inhibition constants, and the inhibitor's mechanism of action. To the best of our knowledge, this is the first assay that allows direct real-time spectroscopic monitoring of NNMT product formation. This assay relies upon the NNMT selective substrate quinoline¹² that is methylated by SAM to form the product 1-methylquinolinium (1-MQ) with characteristic fluorescent properties. Direct real-time fluorescent readout of 1-MQ was used to define the NNMT reaction kinetic parameters (e.g., $K_{d,SAM}$, $K_{d,substrate}$, and k_{cat}) and mechanism (e.g., product inhibition, sequential bimolecular binding, or random-order substrate binding) in contrast to most MT activity assays noted earlier for which complete kinetic characterization has been rather challenging.³⁰

EXPERIMENTAL PROCEDURES

Chemicals and Reagents. Chemicals for the enzyme activity assays, including the cosubstrates quinoline and SAM, the NNMT inhibitors 1-MNA and SAH, and 1-MQ for calibration curves, were obtained from established commercial vendors. SAM, SAH, quinoline, and 1-MQ were obtained from Sigma-Aldrich (St. Louis, MO), and 1-MNA chloride was obtained from the Cayman Chemical Co. (Ann Arbor, MI). All compounds were reconstituted in doubly distilled water at the required concentrations. The identities of quinoline, 1-MQ, and 1-MNA were validated in house using nuclear magnetic resonance and mass spectroscopy, and purities of the compounds were confirmed to be >95% (conducted in the Center for Innovative Drug Discoveries at the University of Texas at San Antonio).

Expression and Purification of Recombinant Human NNMT. A codon-optimized plasmid [isopropyl β -D-1-thiogalactopyranoside (IPTG)-inducible plasmid pJ401] corresponding to His-tagged human NNMT⁴⁰ was produced by DNA 2.0 (Menlo Park, CA). The recombinant human NNMT protein was expressed and purified to homogeneity by using protocols adapted and modified from ref 40. Briefly, the expression vector was used to transform chemically competent *Escherichia coli* BL21 (DE3) cells. The BL21 transformants were plated on an LB agar plate with kanamycin (KAN) (30 μ g/mL) and incubated overnight at 37 °C, which was used to inoculate 1 L of medium along with magnesium and calcium chloride (0.5 mM each) for protein overexpression. The culture was placed in a shaker at 37 °C until the OD₆₀₀ reached 0.7–0.8 (~2–3 h) before induction with 0.5 mM IPTG and incubated for an additional 3 h. Cells were harvested by centrifugation at 10 °C and 4000 rpm for 20 min and removal of the supernatant. For purification, harvested cells were first resuspended in chilled

lysis buffer [20 mM Tris (pH 7.9), 0.5 M NaCl, 5 mM imidazole, 10% glycerol, 1 mM DTT (dithiothreitol), and 1 mM PMSF (phenylmethanesulfonyl fluoride)], and the lysis mixture was sonicated on ice. Cell lysates were centrifuged at 4 °C and 15000 rpm for 30 min. The soluble fraction was loaded onto a nickel affinity column formed from nickel sepharose beads (GE Biosciences) pre-equilibrated with lysis buffer. The column was washed with lysis buffer (5 mM imidazole in lysis buffer) and increasing concentrations of NaCl (from 0.5 to 1 M) followed by increasing concentrations of imidazole (from 5 to 20 mM, in lysis buffer) to remove contaminating proteins. Bound human NNMT was eluted from the column with lysis buffer and 150 mM imidazole, 200 mM salt, and 5% glycerol in 1 mL aliquots. Collected fractions were run on sodium dodecyl sulfate–polyacrylamide gel electrophoresis (SDS–PAGE) and Coomassie stained to verify purity and dialyzed into storage buffer [25 mM Tris (pH 8.6), 20% glycerol, 100 mM NaCl, and 1 mM DTT]. The pooled protein dialysate concentration was determined by UV spectroscopy, and the pooled protein dialysate was portioned into 100 μ L aliquots (final stock concentration of 25 μ M), flash-frozen in liquid nitrogen, and stored at –80 °C for future use. Approximately 5 mg of purified NNMT was generated per liter of bacterial culture, and the identity of the protein was confirmed by separation via SDS–PAGE followed by Western blotting using an anti-NNMT primary antibody (ab119758, Abcam; 1:2000 dilution).

Steady-State Kinetic Assays for NNMT Activity.

Reactions were performed at room temperature (25 °C) in buffer consisting of 5 mM Tris (pH 8.6) and 1 mM DTT. Immediately prior to the initiation of each set of reactions, freshly thawed NNMT was added to reaction buffers at a final concentration of 100 nM. Initial velocities were measured for independent reactions using varying quinoline concentrations (25, 100, 200, 400, 600, and 800 μ M) at different fixed concentrations of SAM (4, 8, 12, 20, 80, and 120 μ M). Separate reactions were performed in individual wells of a 96-well plate, and all reactions were initiated by addition of SAM substrate. Because global fits of enzyme kinetic data can be sensitive to small differences in reaction concentrations, master stocks were used to minimize the number of titration steps required to prepare each individual reaction, thereby reducing potential differences in initial reaction concentrations due to pipetting errors. Following addition of NNMT and substrates, reaction progress was immediately monitored using a Micromax 96-well plate reader integrated into a double-monochromator Fluorolog-3 spectrofluorometer (Horiba Jobin Yvon, Edison, NJ), and reaction data were collected approximately every minute for 10 min. The production of 1-MQ reaction product in each well was monitored by recording fluorescence emission intensities at 405 nm [excitation wavelength (λ_{ex}) of 330 nm] with detector excitation and emission slit widths positioned at 4 nm. To compensate for potential fluctuations in instrument sensitivity between different experiments and across days, calibration curve data ([1-MQ] vs fluorescence intensity) were collected in parallel for each experiment and used to construct progress curves specific to each experiment.

NNMT Inhibition Assays. NNMT reactions were performed at room temperature in 96-well plates as described above, using reaction buffer containing 5 mM Tris (pH 8.6), 1 mM DTT, and 10 μ M SAM. Immediately prior to the initiation of the reactions, 100 nM freshly thawed NNMT was added and the reactions were initiated by adding 100 μ M quinoline substrate. Substrate concentrations were chosen such that they

were substantially below the saturating concentrations that produced the maximal initial reaction velocity yet were high enough to permit the noninhibited (control) reaction to produce 1-MQ significantly above background detection limits during the first 5 min of the reaction. Well-studied MT/NNMT inhibitors SAM⁴¹ and 1-MNA⁸ were added as inhibitors to each reaction mixture at half-log dilutions to generate concentration–response data that uniformly spanned a logarithmic scale. Fluorescence intensities were recorded, and data from the first 3 min (linear range of progress curves) of all reactions were used to calculate initial velocities at each inhibitor concentration.

Data Analysis. Fluorescence data obtained were transferred to GraphPad Prism (version 7.0b; GraphPad Software, La Jolla, CA), which was used to perform linear regression analysis of replicate data to generate calibration curves and initial velocity measurements for all reactions. Initial velocities were measured for the linear portion of each reaction progress curve (initial 3–5 min) and under conditions where the total amount of product formed was less than <10% of the limiting substrate. The calculated steady-state initial velocity measurements and associated error estimates were used in Prism to generate individual Michaelis–Menten curves and kinetic parameters (i.e., $K_{m,substrate}$ and V_{max}) for reaction data sets where one substrate concentration was fixed and the second substrate was varied as described above. The analysis of competing reaction models was performed using the DynaFit software package (BioKin, Watertown, MA). Each reaction model was automatically converted to a series of coupled ordinary differential equations (ODEs) under the assumption of rapid equilibrium, and nonlinear regression methods were used to calculate ODE parameters (corresponding to steady-state kinetic variables) that produced the best global fit of all kinetic data. Goodness-of-fit R^2 statistics provided a measure of the curve fit quality, and the computed Akaike Information Criterion was used as the statistical measure to discriminate between competing models of the NNMT reaction mechanism.

Progress curve data (1-MQ fluorescence intensity vs time) for replicate dose–response experiments (fixed substrate and enzyme concentrations, half-log dilutions of inhibitor concentration) for each inhibitor were transferred to Prism and analyzed using the least-squares linear regression that was used to convert replicate kinetic data from the first 3 min of the reaction to initial velocity measurements. Initial velocities were then normalized (0–100%), and a single-parameter (Hill slope of -1) dose–response model [$\text{normalized velocity} = 100/(1 + [\text{inhibitor}]/IC_{50})$] was fit to the data using least-squares nonlinear regression to calculate IC_{50} values and associated error estimates and to generate dose–response curves.

RESULTS AND DISCUSSION

Protein Activity. Approximately 5 mg of purified NNMT was generated per liter of bacterial culture. The activity of newly purified protein was confirmed using well-established and endogenous cosubstrates, nicotinamide (NA; final concentration of 100 μM) and *S*-adenosylmethione (SAM; final concentration of 10 μM), and monitoring 1-methylnicotinamide (1-MNA) and *S*-adenosylhomocysteine (SAH) product formation in an HPLC-based absorbance assay as described previously.⁴⁰ Aliquots of NNMT stored at -80°C for at least 6 months did not show an appreciable change in enzymatic activity relative to that of freshly purified protein (data not shown).

Fluorescent Assay Development. NNMT was observed to methylate several substrates analogous to pyridines, including quinoline, similar to earlier reports.^{9,27} 1-MQ was strongly fluorescent with an emission maximum of 405 nm. The fluorescence excitation spectra ($\lambda_{em} = 405$ nm) of quinoline (Q) and 1-MQ were appreciably different; 1-MQ showed a large excitation peak between 280 and 350 nm, whereas quinoline showed little appreciable excitation at wavelengths longer than 320 nm (Figure 1). The differential

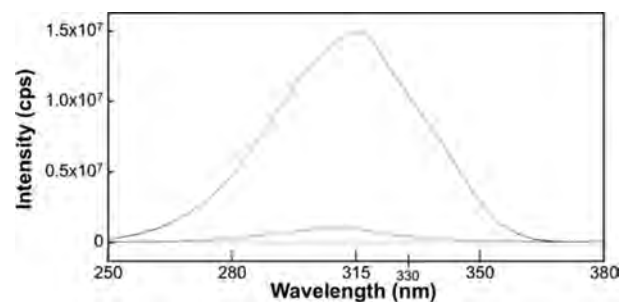


Figure 1. Comparative fluorescence excitation spectra for 10 μM solutions of 1-methylquinolinium (1-MQ, top curve) and quinoline (Q, bottom curve). Fluorescence emission intensities (counts per seconds) were recorded at a λ_{em} of 405 nm.

excitation profile between 1-MQ and quinoline in reaction buffer (Table 1) suggested that a spectrofluoroscopic approach

Table 1. Relative Fluorescence of 1-Methylquinolinium (1-MQ) and Quinoline (Q)^a

λ_{ex} (nm)	λ_{em} (nm)	Fl_{1-MQ}/Fl_Q
310	405	15
320	405	20
330	405	25
340	405	25

^aFluorescence intensity measurements were performed in 96-well plates using 10 μM solutions of compound and a buffer of 5 mM Tris (pH 8.6) and 1 mM DTT. The excitation and emission wavelengths at which a maximal difference in signal was observed (i.e., $\lambda_{ex} = 330$ nm; $\lambda_{em} = 405$ nm) in the instrument configuration were chosen for the fluorescence assay.

might be used to directly observe NNMT reaction progress. The fluorescence intensity for 1-MQ at 405 nm was significantly greater than that of either quinoline in reaction buffer or reaction buffer alone, indicating fluorescence detection of the 1-MQ reaction product could be used to directly monitor NNMT activity. Importantly, in 96-well plates, the fluorescence signal ($\lambda_{ex} = 330$ nm; $\lambda_{em} = 405$ nm) of 1-MQ in NNMT reaction buffer was linearly correlated ($R^2 = 1$) with 1-MQ concentration over several orders of magnitude with a detection limit of 100 nM in 5 mM Tris (pH 8.6) reaction buffer (Figure 2A). The fluorescent signal was invariant with quinoline concentration (Figure 2B); the fluorescent signals from quinoline in reaction buffer and reaction buffer alone were similar (data not shown). Figure 2A (inset) highlights the linear correlation between the fluorescence signal and 1-MQ concentration over the concentration range most relevant to the measurement of initial product formation velocities for NNMT reactions. The 1-MQ detection limit could be lowered to ~ 40 nM when the reaction buffer contained 1 mM Tris (data not shown). Moreover, the slope of the 1-MQ calibration

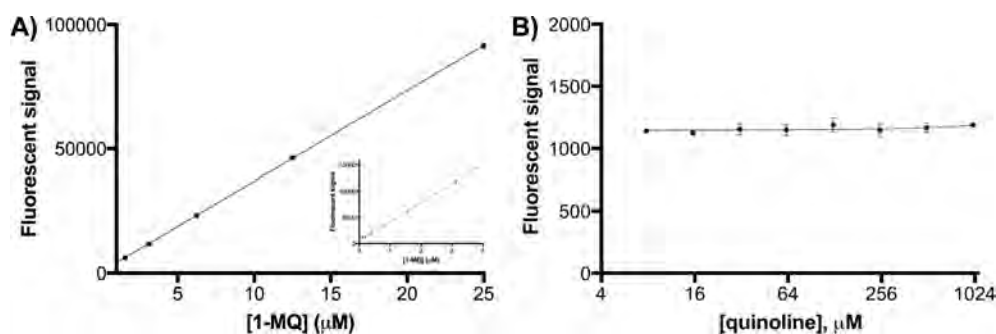


Figure 2. Fluorescent signals for 1-MQ and quinoline ($\lambda_{\text{ex}} = 330 \text{ nm}$; $\lambda_{\text{em}} = 405 \text{ nm}$). (A) Representative calibration curve showing the linear response ($R^2 = 1$) between 1-MQ concentrations and the fluorescent signal. The inset shows data points for the lower 1-MQ concentrations. The slope and y -intercept values (\pm the standard error) of the linear regression curve were 3642 ± 4.9 and 576 ± 46.7 , respectively. (B) Representative curve showing the fluorescent signal over the range of quinoline concentrations typically used in NNMT assays. The slope of the linear regression curve was not significantly different from zero. The buffer included 5 mM Tris (pH 8.6) and 1 mM DTT. Data points and errors bars (which in all cases are similar in size to the data point symbol) represent averages and standard deviations from nine replicate experiments. Figures and linear regression generated with GraphPad Prism.

curve was essentially unchanged when 800 μM quinoline and/or 120 μM SAM was included in the reaction buffer (data not shown), suggesting that the substrates in a reaction mixture do not interfere with the signal generated from the NNMT reaction.

The molecular mechanism and the values of the kinetic parameters associated with the NNMT reaction can be determined from accurate initial rate enzyme kinetics measured at varied SAM and quinoline substrate concentrations, with the assumption that the reaction achieves a rapid substrate binding equilibrium. Progress curves of 1-MQ product formation as a function of time could be reproducibly measured from NNMT reactions performed in 96-well plates. As expected for enzyme kinetic studies, the collected progress curves were hyperbolic, with an initial rapid linear reaction rate ($[1\text{-MQ}] \text{ s}^{-1}$) followed by progressively slower reaction rates until the 1-MQ concentration plateaued. The enzyme concentration in the NNMT reaction was adjusted to allow multiple fluorescent measurements to be simultaneously recorded from several dozen reaction wells during the initial linear velocity phase of the reaction. Using a NNMT concentration of 100 nM for the kinetic reactions, the velocities of product formation were highly linear during the first 3–5 min of the reaction for all tested SAM substrate concentrations (Figure 3). Moreover, most reactions converted <1% of the limiting substrate to product during the initial linear velocity phase, and even reactions using the lowest tested initial SAM concentrations converted <8% of the starting substrate to product during the initial linear velocity phase. Linear regression analysis of the time-dependent kinetic data was used to calculate initial reaction velocities for SAM substrate concentrations ranging from 4 to 120 μM and quinoline substrate concentrations ranging from 25 to 800 μM ; goodness-of-fit R^2 values for the linear regression analysis ranged from 0.93 for the lowest tested substrate concentrations (4 μM SAM and 25 μM quinoline) to >0.99 for the majority of tested substrate concentrations. Over the tested concentration ranges, initial velocity measurements had error estimates of $\sim 10^{-5} \mu\text{M s}^{-1}$. The relative error in the initial velocity measurements ranged from 0.3 to 19%, with lower relative errors associated with the higher initial velocities that occurred at high substrate concentrations. The average and median relative errors observed with several dozen velocity measurements were 4.8 and 4.0%, respectively. Taken together, this noncoupled fluorescent assay provides a direct, continuous,

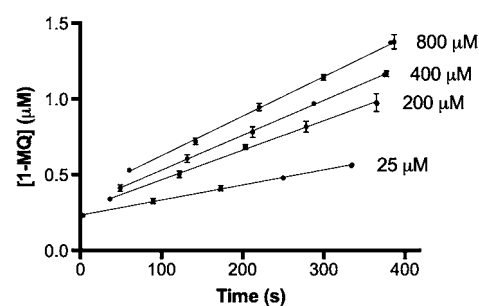


Figure 3. Real-time progress curves for representative NNMT reactions showing linear response data used to calculate initial reaction velocities (v_0). Fluorescence intensities ($\lambda_{\text{ex}} = 330 \text{ nm}$; $\lambda_{\text{em}} = 405 \text{ nm}$) from 1-MQ product generation were continuously recorded and converted to molar concentrations using simultaneously measured calibration curve data. For these representative reactions, assay conditions included 5 mM Tris (pH 8.6), 1 mM DTT, 80 μM SAM, and 100 nM NNMT, with quinoline concentrations ranging from 25 to 800 μM . Error bars represent standard deviations from three experiments. Linear regression analysis for the representative curves had a goodness-of-fit R^2 of >0.9988.

sensitive, and quantitative readout of the NNMT reaction allowing kinetic characterization of the NNMT reaction mechanism (discussed in the section below). Progress curves for 1-MQ product formation are rapidly obtained (<10 min) at ambient temperature, allowing for immediate generation of IC_{50} curves for NNMT inhibitors (see the section below) and the determination of inhibitor kinetic parameters and the mechanism of action. These features make our assay a valuable alternative to the previously published NNMT-coupled chemical assay that, although sensitive, required long chemical reaction times and extreme reaction conditions, making it unsuitable for real-time detection and HTS.²⁵

NNMT Kinetic Assay and Reaction Mechanism. Initial velocities were measured for reaction conditions with a fixed NNMT concentration and a comprehensive matrix of substrate concentrations (SAM concentrations of 4, 8, 12, 20, 80, and 120 μM ; quinoline concentrations of 25, 100, 200, 400, 600, and 800 μM). Initial velocity data sets consisting of a single SAM concentration and a range of quinoline concentrations were plotted in conventional Michaelis–Menten format (initial velocity of 1-MQ product formation vs $[Q]$), and independent two-parameter steady-state Michaelis–Menten curves [$v_0 =$

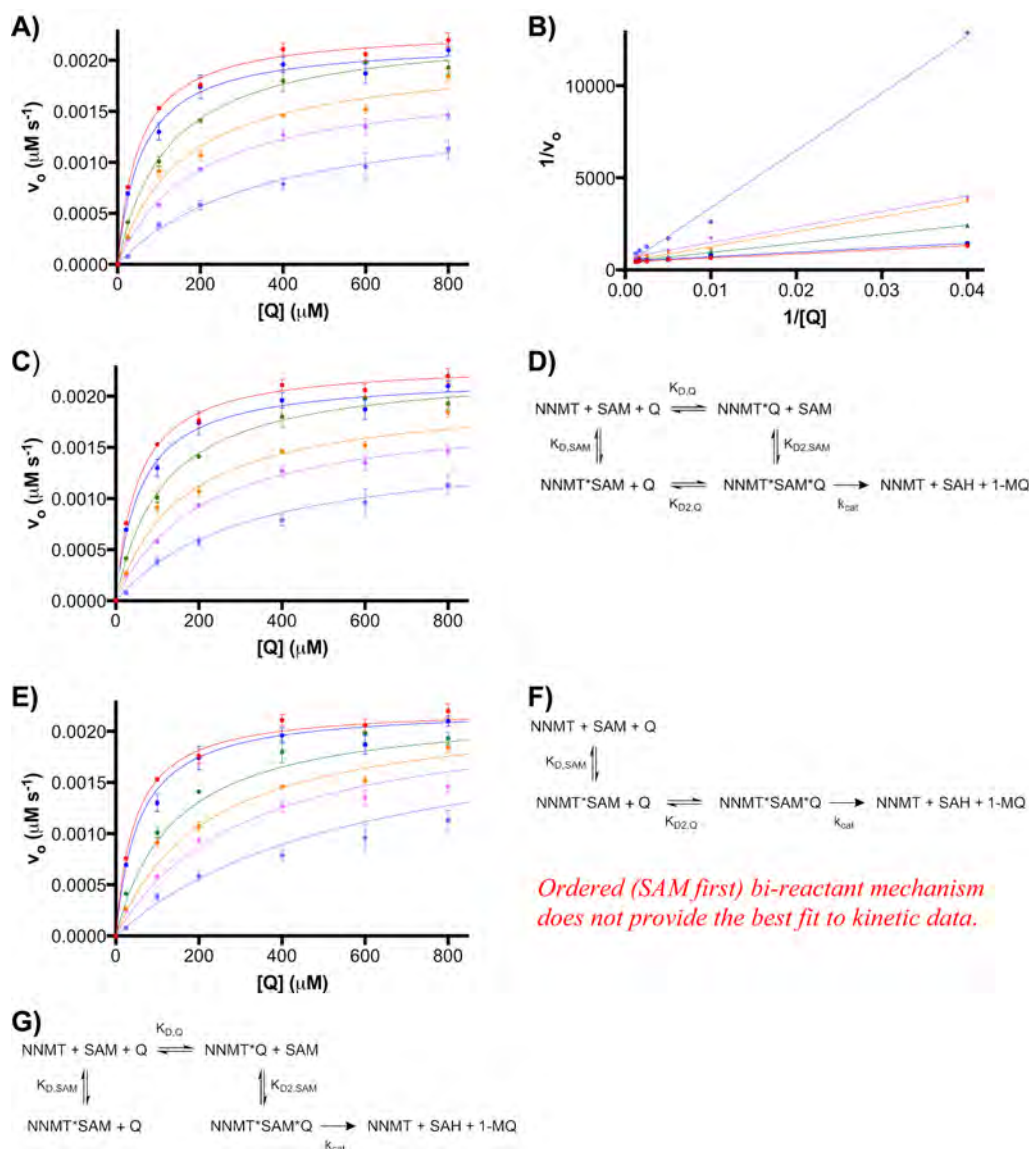


Figure 4. Michaelis–Menten plots for NNMT kinetic data. Data sets represent initial velocities (average value; $n = 3$) measured over a range of quinoline concentrations and at fixed SAM concentrations. (A) Data sets for reactions performed at several SAM concentrations were independently fit to single-substrate Michaelis–Menten curves [$v_o = v_{\text{max,app}}[Q]/(K_{\text{m,app}} + [Q])$]. Goodness-of-fit R^2 values were 0.996, 0.991, 0.997, 0.983, 0.997, and 0.994 for curves corresponding to 120, 80, 20, 12, 8, and 4 μM SAM, respectively. (B) Double-reciprocal plot for kinetic reactions performed over a range of quinoline concentrations, where each line corresponds to a fixed SAM reaction concentration. Linear regression R^2 values were >0.99 for all fitted lines. (C) Global fit (nonlinear regression analysis sum of squares = 1.3×10^{-7}) of all kinetic data measurements using a random bi-reactant reaction mechanism. (D) Schematic of the random bi-reactant reaction mechanism that produces the global curve fits shown in panel C. (E) Optimal global fit (nonlinear regression analysis sum of squares = 3.2×10^{-7}) of all kinetic data using an ordered (SAM first) bi-reactant reaction mechanism. (F) Schematic of the ordered (SAM first) bi-reactant reaction mechanism that produces the global curve fits shown in panel E. (G) Schematic of a random bi-reactant reaction mechanism with a kinetically blocked binding step that would similarly produce the global curve fits shown in panel C. Curves in panels A–C and E correspond to reactions with 120 μM (red curve), 80 μM (blue curve), 20 μM (green curve), 12 μM (orange curve), 8 μM (magenta curve), and 4 μM SAM (cyan curve). Error bars represent standard deviations ($n = 3$). Chemical reaction schematics prepared with ChemDraw (version 13.0).

$v_{\text{max,app}}[Q]/(K_{\text{m,app}} + [Q])$ were fit to each data set with a goodness-of-fit R^2 of >0.98 (Figure 4A). Similarly, the collected data could be transposed, and individual steady-state Michaelis–Menten curves could be accurately fit to data sets consisting of a fixed quinoline concentration and a range of SAM concentrations. All curves asymptotically approached a maximal initial velocity at high substrate concentration, with no apparent substrate inhibition⁴² observed over the tested reaction conditions. The lack of observed substrate inhibition is in contrast to results reported using HPLC and mass

spectrometry to separate and characterize the NNMT reaction products.²⁷

Historically, steady-state kinetic studies of two substrate (or bi-reactant) enzymes have been analyzed using reciprocal plots (e.g., Lineweaver–Burk⁴³) that linearized the Michaelis–Menten equation (see ref 44 and references therein). This approach was popularized by Cleland^{45,46} as providing a graphical diagnostic to discriminate between conventional “ping-pong” and “sequential” reaction mechanisms that could be reduced to a closed-form analytical solution. Following this

Table 2. Kinetic Parameters Derived for Competing NNMT Reaction Mechanisms

mechanism	AIC ^a	$K_{d,SAM}$ (μM) ^b	$K_{d,Q}$ (μM) ^b	$K_{d2,SAM}$ (μM) ^b	$K_{d2,Q}$ (μM) ^b	k_{cat} (s^{-1}) ^b
random bireactant	0.997	45.1 ± 8.8	842.0 ± 233.7	2.1 ± 0.4	39.2 ± 5.4	0.024 ± 0.0005
random bireactant (fixed [NNMT])	0.003	39.9 ± 9.3	848.9 ± 299.0	2.0 ± 0.5	41.5 ± 6.7	0.023 ± 0.0005
random bireactant with a constant $K_{d,substrate}$	0.0	5.7 ± 0.6	92.2 ± 11.0	5.7 ± 0.6	92.2 ± 11.0	0.026 ± 0.001
ordered (SAM first) bireactant	0.0	82.9 ± 18.8	–	–	27.3 ± 5.8	0.022 ± 0.0005
ordered (Q first) bireactant	0.0			no convergence		

^aAkaike Information Criterion. ^bReaction parameters \pm the standard error estimates were calculated within the Dynafit program using nonlinear regression to provide the best fit to the experimental data.

historical convention, initial velocity data sets consisting of a single SAM concentration and a range of quinoline concentrations were converted to double-reciprocal plots (Figure 4B), where each data set fit to a linear equation with high accuracy (linear regression $R^2 > 0.99$). The lines corresponding to constant SAM concentrations in the double-reciprocal plot intersect at a single point, indicating a bireactant (also termed sequential) reaction mechanism in which NNMT forms a ternary complex with SAM and quinoline substrates, followed by the methyl transfer reaction that forms a transient complex of NNMT and the SAH and 1-MQ products. Because the constant SAM data sets did not form a series of parallel lines in the double-reciprocal plot, it is unlikely that NNMT operates via a “ping-pong” reaction mechanism.

The use of reciprocal plots to analyze bireactant kinetic data has largely been superseded by more accurate and robust nonlinear regression methods that calculate kinetic parameters by fitting ordinary differential equations corresponding to potential reaction mechanisms to all available initial velocity data.^{47–49} Moreover, modern global fitting methods can provide a rigorous statistical basis for discriminating between alternative reaction mechanisms (e.g., random bireactant and ordered bireactant).^{50,51} A number of NNMT bireactant molecular models were constructed and simultaneously fit to all kinetic data using nonlinear regression analysis with a rapid equilibrium approximation (Table 2). Akaike model discrimination, performed within the Dynafit suite, consistently selected a random bireactant reaction model with nonequivalent binding constants (Figure 4C,D) as the model that provided the best fit of the initial velocity data. In this comparative analysis, competing models (listed in Table 2) that did not provide good global fits of the initial velocity data included ordered bireactant models (also termed ordered sequential models) in which either SAM (Figure 4E,F) or quinoline was required to first bind NNMT and random bireactant models with constant substrate binding constants (e.g., $K_{d,Q} = K_{d2,Q}$ and $K_{d,SAM} = K_{d2,SAM}$).

It is interesting to note that the nonoptimal model termed “random bi-reactant with constant $K_{d,substrate}$ ” produced binding constants [$K_{d,Q} = K_{d2,Q} = 92.2 \mu\text{M}$, and $K_{d,SAM} = K_{d2,SAM} = 5.7 \mu\text{M}$ (Table 2)] that were largely equivalent to the K_m parameters ($K_{m,NA} = 105 \mu\text{M}$, and $K_{m,SAM} = 5 \mu\text{M}$) determined in earlier enzyme kinetic studies⁴⁰ with an equivalent NNMT construct (triple-mutant hNNMT) and NA and SAM substrates. Furthermore, the binding constants generated by the nonoptimal model were different from K_m parameters ($K_{m,Q} = 609 \mu\text{M}$, and $K_{m,SAM} = 8.5 \mu\text{M}$) determined in a recent enzyme kinetic study²⁷ with a human wild-type NNMT construct. However, the rigorous kinetic analysis performed in our current study suggested that the “random bireactant with constant $K_{d,substrate}$ ” model did not provide the best global fit of

our extensive set of initial velocity data, and thus, its associated kinetic parameters likely do not accurately reflect details of the NNMT molecular mechanism. Instead, the NNMT mechanism was best described as a random bireactant reaction model with nonequivalent binding constants (Table 2 and Figure 4C,D). This model, which is likely generally applicable for all NNMT xenobiotic reactants, implies that SAM or quinoline can initially bind to the NNMT apoenzyme, although the quinoline binding constant is ~ 20 -fold higher than the SAM binding constant. Both SAM and quinoline have an ~ 20 -fold improved binding affinity for the binary complex compared to their binding affinities for the apoenzyme, suggesting that either (1) the binding of the first substrate perturbs the adjacent second substrate binding site to make it more favorable for coreactant binding or (2) the first bound substrate provides favorable intermolecular interactions of 7.4 kJ mol^{-1} ($1.77 \text{ kcal mol}^{-1}$) that stabilize the binding of the second substrate.

The kinetic parameters for the random bireactant reaction model with nonequivalent binding constants (reaction scheme in Figure 4D) could be refined to produce a slightly improved fit to the kinetic data by accounting for potential differences in NNMT concentrations in the different reaction data sets that might arise from small titration errors. Treating the NNMT concentration as a potentially adjustable parameter between independent reactions did not change the reaction model that was selected as producing the best fit of the kinetic data; however, adjusting by $\sim 5\%$ the enzyme concentration associated with two SAM data sets (80 and $20 \mu\text{M}$ SAM) produced optimal global curve fits of the kinetic data as judged by Akaike weights and sum-of-squares statistics (Table 2 and Figure 4C). The accuracy of the optimal global curve fits was essentially identical to that of the curve fits generated when Michaelis–Menten equations were independently fit to each separate data set (compare panels A and C of Figure 4); however, the global fits required fewer parameters and resulted in single values for all kinetic parameters. Moreover, the kinetic parameters calculated for these optimal global curve fits and the global fits calculated when the NNMT concentration was not treated as an adjustable parameter (compare “random bireactant” and “random bireactant fixed [NNMT]” models in Table 2) were within the calculated error of each other.

Upon evaluation of enzyme catalytic mechanisms, it is important to remember that a detailed analysis of kinetic data can identify models that are consistent with, or at odds with, experimental data. Such analysis can eliminate a proposed reaction model from consideration as being responsible for an enzyme’s mechanism of action, but as noted in studies dating back to that of Lineweaver and Burk,⁴³ this analysis cannot prove that a particular model correctly describes the enzyme’s reaction mechanism. The random bireactant reaction model with nonequivalent binding constants is most consistent with all currently available initial velocity data, although this model

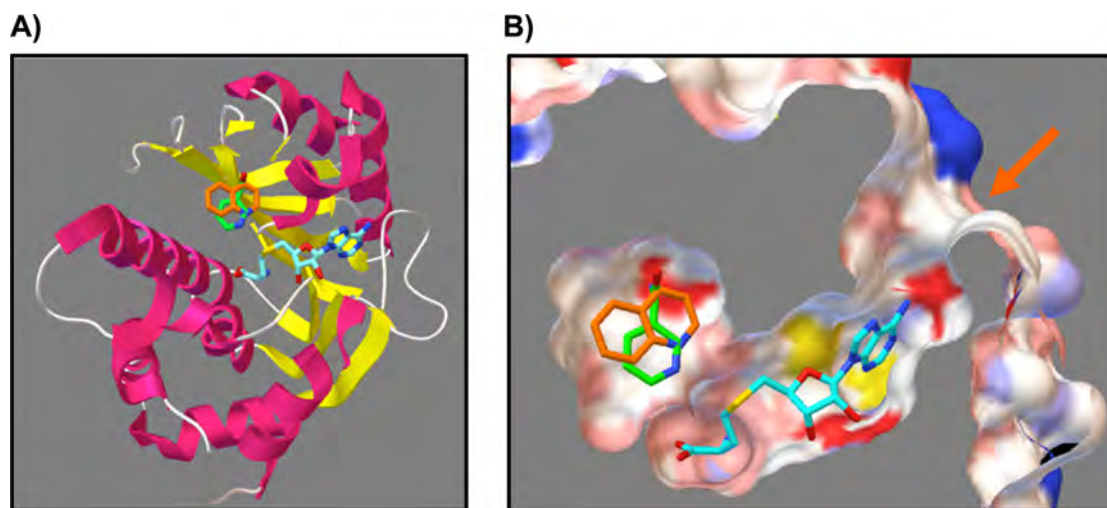


Figure 5. Model structure of the quinoline substrate bound to the NNMT nicotinamide (NA) substrate binding site. (A) Ribbon representation of NNMT with NA (green molecule) and SAH (teal molecule) as bound in the X-ray cocrystal structure (PDB entry 3ROD⁴⁰). The bound conformation of quinoline (orange molecule) is predicted to overlap with the NA substrate, with the methyl-accepting nitrogen atoms positioned in essentially equivalent positions. (B) Surface representation for NNMT highlighting the deep internal cavity that encloses the NA, quinoline, and SAM binding sites. The arrow indicates where the internal cavity opens to the bulk solvent surrounding NNMT. Figures produced with AutoDock Tools.⁵³

may require modification as additional experimental data are collected. For example, the random bireactant reaction model assumes NNMT, substrate–NNMT binary species, and the ternary complex satisfy a closed thermodynamic cycle with equilibrium binding constants linked as $K_{d,Q}K_{d2,SAM} = K_{d,SAM}K_{d2,Q}$ (reaction scheme in Figure 4D). However, nonlinear regression analysis of initial velocity kinetic data with a steady-state approximation cannot discriminate between models in which a slow rate constant for the binding step essentially prevents the formation of one of the steady-state species. For example, a random bireactant reaction model that proposes binding of quinoline to the NNMT·SAM binary complex is a kinetically disallowed event (reaction scheme in Figure 4G) that would fit the initial velocity data in the exact same manner as the random bireactant reaction model shown in Figure 4D. This is an intriguing model, because molecular docking studies predict that quinoline (and all NNMT xenobiotic substrates) would bind NNMT in an orientation similar to that of nicotinamide (Figure 5A), with the N1 atom of the methyl accepting the substrate directed toward the reactive methyl moiety of SAM. In this orientation, quinoline is positioned at the terminus of a narrow closed tunnel that holds both SAM and the xenobiotic substrate (Figure 5B). Binding of SAM to the NNMT apoenzyme could effectively occlude this tunnel and conceivably prevent (or dramatically slow) quinoline from reaching its binding site. Subsequent studies will further refine the molecular binding events and rate constants associated with the NNMT reaction mechanism.

Inhibition Studies. The described real-time direct NNMT fluorescent assay can be utilized for robust high-throughput screening to identify small molecule inhibitors of NNMT and any SAM-dependent methyltransferase. In addition, this assay can facilitate detailed characterization of NNMT inhibitors, either through rigorous kinetic inhibition studies to determine an inhibitor's mechanism of action and binding affinity (K_i) or via IC_{50} studies to rapidly establish a compound's relative inhibitory potential. These applications will be expanded upon in future studies. However, as a proof of concept, we completed

IC_{50} studies to determine if NNMT reaction products could function as inhibitors (Figure 6). These studies serve as a

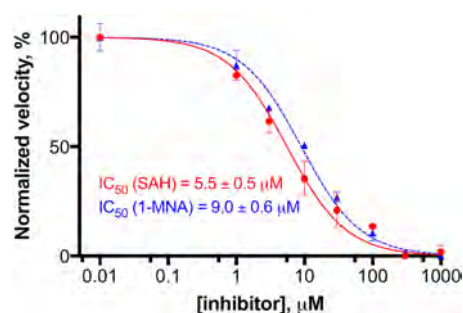


Figure 6. Normalized response curves (Hill slope of -1) for NNMT inhibitors (SAH, solid red curve; 1-MNA, dashed blue curve). Data points represent the average and standard deviation of normalized initial reaction velocities measured from replicate ($n = 3$) experiments. For both compounds, the goodness-of-fit R^2 between the fitted curves and data was 0.98.

foundation for developing small molecule NNMT inhibitors and for investigating product inhibition as a component of the NNMT reaction mechanism. Both SAH and 1-MNA (the presumed major physiological NNMT reaction product) strongly inhibited NNMT, with IC_{50} values of 5.5 ± 0.5 and $9.0 \pm 0.6 \mu\text{M}$, respectively, calculated from dose–response curves. The IC_{50} (SAH) value determined in this assay was comparable to the low micromolar value recently reported by van Harren,²⁷ although an IC_{50} value of 1-MNA was not reported. Importantly, in our fluorescent assay, the data of measured NNMT initial velocity versus inhibitor concentration could be accurately fit ($R^2 = 0.98$) by a standard dose–response inhibition curve (Hill slope of -1) that displayed well-defined plateaus at both high and low inhibitor concentrations. These fits generated highly reproducible IC_{50} measurements with errors of $<10\%$. The low micromolar inhibitory activity determined for SAH and 1-MNA suggests that physiological

concentrations of NNMT reaction products may modulate *in vivo* NNMT activity.

CONCLUSION

We describe a rapid, direct, ultrasensitive, convenient, cost-effective, noncoupled, and real-time analytical assay for monitoring NNMT activity based on the fluorescence properties of a NNMT reaction product. This assay can generate accurate steady-state and pre-steady-state kinetic data that help delineate the detailed reaction mechanism and kinetic parameters associated with NNMT-mediated catalysis. As demonstrated in our current studies, NNMT appears to operate through a random bireactant reaction mechanism, where each substrate can independently bind the apoenzyme. Significantly, the kinetic data allow detailed analysis that further showed both substrates bound their complementary binary complexes with an affinity ~20-fold stronger compared to their binding to the apoenzyme. Future broad-ranging kinetic studies with this assay will greatly facilitate our mechanistic understanding of NNMT and related methyltransferases. Importantly, this assay can be directly used for the discovery, development, and characterization of NNMT inhibitors with the potential to fully understand the mechanism of action and inhibition constants via detailed kinetic inhibition studies. In addition, this NNMT fluorescent assay could be adapted to anchor a SAM substrate competition assay⁵² to permit the identification of inhibitors of other SAM-dependent methyltransferases. Given the expanding role of NNMT and other methyltransferases as molecular targets for the development of therapeutics to combat numerous diseases, our robust 96-well plate format fluorescence-based assay will likely be of great utility for academic and pharmaceutical researchers and can be further miniaturized for efficient and effective high-throughput screening. However, intrinsic assay limitations in the detection of inhibitors with overlapping excitation wavelengths as 1-MQ and the parallel use of orthogonal assays to minimize detection of false positives will need to be carefully considered.

AUTHOR INFORMATION

Corresponding Author

*E-mail: watowich@xray.utmb.edu. Phone: (409) 747-4749.

ORCID

Stanley J. Watowich: 0000-0002-1660-1818

Funding

This work was supported by Department of Defense Peer Reviewed Medical Research Program Grant PR141776 (S.J.W.) and a University of Texas Medical Branch Technology Commercialization Award (S.J.W.).

Notes

The authors declare no competing financial interest.

ACKNOWLEDGMENTS

We thank Drs. J. Lee and C. Finnerty for helpful discussions and Dr. P. Kuzmic for developing the Dynafit program and making it freely available for use.

ABBREVIATIONS

DTT, dithiothreitol; HPLC, high-performance liquid chromatography; KAN, kanamycin; IPTG, isopropyl β -D-1-thiogalactopyranoside; 1-MNA, 1-methylnicotinamide; MTs, methyltransferases; 1-MQ, 1-methylquinolinium; NA, nicotinamide; NAD⁺, nicotinamide adenine dinucleotide; NNMT, nicotina-

mid N-methyltransferase; PMSF, phenylmethanesulfonyl fluoride; Q, quinoline; SAH, S-S'-adenosylhomocysteine; SAM, S-S'-adenosyl-L-methionine.

REFERENCES

- (1) Syed, S. K., Kim, S., and Paik, W. K. (1993) Comparative studies on S-adenosyl-L-methionine binding sites of protein N-methyltransferases, using 8-azido-S-adenosyl-L-methionine as photoaffinity probe. *J. Protein Chem.* 12, 603–612.
- (2) Martin, J. L., and McMillan, F. M. (2002) SAM (dependent) I AM: the S-adenosylmethionine-dependent methyltransferase fold. *Curr. Opin. Struct. Biol.* 12, 783–793.
- (3) Zhang, X., and Cheng, X. (2006) Structure of protein arginine methyltransferases. *Enzymes* 24, 105–121.
- (4) Copeland, R. A., Solomon, M. E., and Richon, V. M. (2009) Protein methyltransferases as a target class for drug discovery. *Nat. Rev. Drug Discovery* 8, 724–732.
- (5) Schapira, M., and Ferreira de Freitas, R. (2014) Structural biology and chemistry of protein arginine methyltransferases. *MedChemComm* 5, 1779–1788.
- (6) Kaniskan, H. U., Konze, K. D., and Jin, J. (2015) Selective inhibitors of protein methyltransferases. *J. Med. Chem.* 58, 1596–1629.
- (7) Hu, H., Qian, K., Ho, M. C., and Zheng, Y. G. (2016) Small Molecule Inhibitors of Protein Arginine Methyltransferases. *Expert Opin. Invest. Drugs* 25, 335–358.
- (8) Aksoy, S., Szumlanski, C. L., and Weinshilboum, R. M. (1994) Human liver nicotinamide N-methyltransferase. cDNA cloning, expression, and biochemical characterization. *J. Biol. Chem.* 269, 14835–14840.
- (9) Alston, T. A., and Abeles, R. H. (1988) Substrate specificity of nicotinamide methyltransferase isolated from porcine liver. *Arch. Biochem. Biophys.* 260, 601–608.
- (10) Kraus, D., Yang, Q., Kong, D., Banks, A. S., Zhang, L., Rodgers, J. T., Pirinen, E., Pulinilkunnil, T. C., Gong, F., Wang, Y. C., Cen, Y., Sauve, A. A., Asara, J. M., Peroni, O. D., Monia, B. P., Bhanot, S., Alhonen, L., Puigserver, P., and Kahn, B. B. (2014) Nicotinamide N-methyltransferase knockdown protects against diet-induced obesity. *Nature* 508, 258–262.
- (11) Cantoni, G. L. (1951) Methylation of nicotinamide with soluble enzyme system from rat liver. *J. Biol. Chem.* 189, 203–216.
- (12) Rini, J., Szumlanski, C., Guercioli, R., and Weinshilboum, R. M. (1990) Human liver nicotinamide N-methyltransferase: ion-pairing radiochemical assay, biochemical properties and individual variation. *Clin. Chim. Acta* 186, 359–374.
- (13) Yan, L., Otterness, D. M., Craddock, T. L., and Weinshilboum, R. M. (1997) Mouse liver nicotinamide N-methyltransferase: cDNA cloning, expression, and nucleotide sequence polymorphisms. *Biochem. Pharmacol.* 54, 1139–1149.
- (14) Riederer, M., Erwa, W., Zimmermann, R., Frank, S., and Zechner, R. (2009) Adipose tissue as a source of nicotinamide N-methyltransferase and homocysteine. *Atherosclerosis* 204, 412–417.
- (15) Giuliante, R., Sartini, D., Bacchetti, T., Rocchetti, R., Kloting, I., Polidori, C., Ferretti, G., and Emanuelli, M. (2015) Potential involvement of nicotinamide N-methyltransferase in the pathogenesis of metabolic syndrome. *Metab. Syndr. Relat. Disord.* 13, 165–170.
- (16) Kannt, A., Pfenninger, A., Teichert, L., Tonjes, A., Dietrich, A., Schon, M. R., Kloting, N., and Bluher, M. (2015) Association of nicotinamide-N-methyltransferase mRNA expression in human adipose tissue and the plasma concentration of its product, 1-methylnicotinamide, with insulin resistance. *Diabetologia* 58, 799–808.
- (17) Parsons, R. B., Smith, M. L., Williams, A. C., Waring, R. H., and Ramsden, D. B. (2002) Expression of nicotinamide N-methyltransferase (E.C. 2.1.1.1) in the Parkinsonian brain. *J. Neuropathol. Exp. Neurol.* 61, 111–124.
- (18) Roessler, M., Rollinger, W., Palme, S., Hagmann, M. L., Berndt, P., Engel, A. M., Schneidinger, B., Pfeffer, M., Andres, H., Karl, J., Bodenmuller, H., Ruschoff, J., Henkel, T., Rohr, G., Rossol, S., Rosch, W., Langen, H., Zolg, W., and Tacke, M. (2005) Identification of

- nicotinamide N-methyltransferase as a novel serum tumor marker for colorectal cancer. *Clin. Cancer Res.* 11, 6550–6557.
- (19) Salek, R. M., Maguire, M. L., Bentley, E., Rubtsov, D. V., Hough, T., Cheeseman, M., Nunez, D., Sweatman, B. C., Haselden, J. N., Cox, R. D., Connor, S. C., and Griffin, J. L. (2007) A metabolomic comparison of urinary changes in type 2 diabetes in mouse, rat, and human. *Physiol. Genomics* 29, 99–108.
- (20) Sartini, D., Muzzonigro, G., Milanese, G., Pierella, F., Rossi, V., and Emanuelli, M. (2006) Identification of nicotinamide N-methyltransferase as a novel tumor marker for renal clear cell carcinoma. *J. Urol.* 176, 2248–2254.
- (21) Sartini, D., Santarelli, A., Rossi, V., Goteri, G., Rubini, C., Ciavarella, D., Lo Muzio, L., and Emanuelli, M. (2007) Nicotinamide N-methyltransferase upregulation inversely correlates with lymph node metastasis in oral squamous cell carcinoma. *Mol. Med.* 13, 415–421.
- (22) Tomida, M., Mikami, I., Takeuchi, S., Nishimura, H., and Akiyama, H. (2009) Serum levels of nicotinamide N-methyltransferase in patients with lung cancer. *J. Cancer Res. Clin. Oncol.* 135, 1223–1229.
- (23) Williams, A. C., and Ramsden, D. B. (2005) Autotoxicity, methylation and a road to the prevention of Parkinson's disease. *J. Clin. Neurosci.* 12, 6–11.
- (24) Xu, J., Moatamed, F., Caldwell, J. S., Walker, J. R., Kraiem, Z., Taki, K., Brent, G. A., and Hershman, J. M. (2003) Enhanced expression of nicotinamide N-methyltransferase in human papillary thyroid carcinoma cells. *J. Clin. Endocrinol. Metab.* 88, 4990–4996.
- (25) Sano, A., Endo, N., and Takitani, S. (1992) Fluorometric assay of rat tissue N-methyltransferases with nicotinamide and four isomeric methylnicotinamides. *Chem. Pharm. Bull.* 40, 153–156.
- (26) Patel, M., Vasaya, M. M., Asker, D., and Parsons, R. B. (2013) HPLC-UV method for measuring nicotinamide N-methyltransferase activity in biological samples: evidence for substrate inhibition kinetics. *J. Chromatogr. B: Anal. Technol. Biomed. Life Sci.* 921–922, 87–95.
- (27) van Haren, M. J., Sastre Torano, J., Sartini, D., Emanuelli, M., Parsons, R. B., and Martin, N. I. (2016) A Rapid and Efficient Assay for the Characterization of Substrates and Inhibitors of Nicotinamide N-Methyltransferase. *Biochemistry* 55, 5307–5315.
- (28) Barrow, E. W., Clinkenbeard, P. A., Duncan-Decocq, R. A., Perteet, R. F., Hill, K. D., Bourne, P. C., Valderas, M. W., Bourne, C. R., Clarkson, N. L., Clinkenbeard, K. D., and Barrow, W. W. (2012) High-throughput screening of a diversity collection using biodefense category A and B priority pathogens. *J. Biomol. Screening* 17, 946–956.
- (29) Drake, K. M., Watson, V. G., Kisielewski, A., Glynn, R., and Napper, A. D. (2014) A sensitive luminescent assay for the histone methyltransferase NSD1 and other SAM-dependent enzymes. *Assay Drug Dev. Technol.* 12, 258–271.
- (30) Duchin, S., Vershinin, Z., Levy, D., and Aharoni, A. (2015) A continuous kinetic assay for protein and DNA methyltransferase enzymatic activities. *Epigenet. Chromatin* 8, 56.
- (31) Jurkowska, R. Z., Ceccaldi, A., Zhang, Y., Arimondo, P. B., and Jeltsch, A. (2011) DNA methyltransferase assays. *Methods Mol. Biol.* 791, 157–177.
- (32) Kumar, S., King, L. E., Clark, T. H., and Gorovits, B. (2015) Antibody-drug conjugates nonclinical support: from early to late nonclinical bioanalysis using ligand-binding assays. *Bioanalysis* 7, 1605–1617.
- (33) Luo, M. (2012) Current chemical biology approaches to interrogate protein methyltransferases. *ACS Chem. Biol.* 7, 443–463.
- (34) Rye, P. T., Frick, L. E., Ozbal, C. C., and Lamarr, W. A. (2011) Advances in label-free screening approaches for studying histone acetyltransferases. *J. Biomol. Screening* 16, 1186–1195.
- (35) Su, Y., Hickey, S. F., Keyser, S. G., and Hammond, M. C. (2016) In Vitro and In Vivo Enzyme Activity Screening via RNA-Based Fluorescent Biosensors for S-Adenosyl-l-homocysteine (SAH). *J. Am. Chem. Soc.* 138, 7040–7047.
- (36) Wood, R. J., McKelvie, J. C., Maynard-Smith, M. D., and Roach, P. L. (2010) A real-time assay for CpG-specific cytosine-C5 methyltransferase activity. *Nucleic Acids Res.* 38, e107.
- (37) Wu, Q., Gee, C. L., Lin, F., Tyndall, J. D., Martin, J. L., Grunewald, G. L., and McLeish, M. J. (2005) Structural, mutagenic, and kinetic analysis of the binding of substrates and inhibitors of human phenylethanolamine N-methyltransferase. *J. Med. Chem.* 48, 7243–7252.
- (38) Barrow, J. C. (2012) Inhibitors of Catechol-O-Methyltransferase. *CNS Neurol. Disord.: Drug Targets* 11, 324–332.
- (39) Kimos, M., Burton, M., Urbain, D., Caudron, D., Martini, M., Famelart, M., Gillard, M., Barrow, J., and Wood, M. (2016) Development of an HTRF Assay for the Detection and Characterization of Inhibitors of Catechol-O-Methyltransferase. *J. Biomol. Screening* 21, 490–495.
- (40) Peng, Y., Sartini, D., Pozzi, V., Wilk, D., Emanuelli, M., and Yee, V. C. (2011) Structural basis of substrate recognition in human nicotinamide N-methyltransferase. *Biochemistry* 50, 7800–7808.
- (41) Borchardt, R. T., Huber, J. A., and Wu, Y. S. (1974) Potential inhibitor of S-adenosylmethionine-dependent methyltransferases. 2. Modification of the base portion of S-adenosylhomocysteine. *J. Med. Chem.* 17, 868–873.
- (42) Tomlinson, S. M., and Watowich, S. J. (2008) Substrate inhibition kinetic model for West Nile virus NS2B-NS3 protease. *Biochemistry* 47, 11763–11770.
- (43) Lineweaver, H., and Burk, D. (1934) The Determination of Enzyme Dissociation Constants. *J. Am. Chem. Soc.* 56, 658–666.
- (44) Segel, I. H. (1975) *Enzyme kinetics: behavior and analysis of rapid equilibrium and steady state enzyme systems*, Wiley, New York.
- (45) Cook, P. F., and Cleland, W. W. (2007) *Enzyme kinetics and mechanism*, Garland Science, London.
- (46) Morrison, J. F., and Cleland, W. W. (1980) A kinetic method for determining dissociation constants for metal complexes of adenosine 5'-triphosphate and adenosine 5'-diphosphate. *Biochemistry* 19, 3127–3131.
- (47) Kuzmic, P. (1996) Program DYNAFIT for the analysis of enzyme kinetic data: application to HIV proteinase. *Anal. Biochem.* 237, 260–273.
- (48) Kuzmic, P. (2006) A generalized numerical approach to rapid-equilibrium enzyme kinetics: application to 17beta-HSD. *Mol. Cell. Endocrinol.* 248, 172–181.
- (49) Kuzmic, P. (2009) DynaFit—a software package for enzymology. *Methods Enzymol.* 467, 247–280.
- (50) Collom, S. L., Laddusaw, R. M., Burch, A. M., Kuzmic, P., Perry, M. D., Jr., and Miller, G. P. (2008) CYP2E1 substrate inhibition. Mechanistic interpretation through an effector site for monocyclic compounds. *J. Biol. Chem.* 283, 3487–3496.
- (51) Kuzmic, P., Cregar, L., Millis, S. Z., and Goldman, M. (2006) Mixed-type noncompetitive inhibition of anthrax lethal factor protease by aminoglycosides. *FEBS J.* 273, 3054–3062.
- (52) Vainshtein, I., Silveria, S., Kaul, P., Rouhani, R., Eglén, R. M., and Wang, J. (2002) A high-throughput, nonisotopic, competitive binding assay for kinases using nonselective inhibitor probes (ED-NSIP). *J. Biomol. Screening* 7, 507–514.
- (53) Sanner, M. F. (1999) Python: a programming language for software integration and development. *J. Mol. Graphics Modell.* 17, 57–61.

Appendix 2: Neelakantan H, Wang HY, Vance V, Hommel JD, McHardy SF, Watowich SJ. Structure–activity relationship for small molecule inhibitors of nicotinamide N-methyltransferase. *J. Med. Chem.* 60, 5015, 2017.

Structure–Activity Relationship for Small Molecule Inhibitors of Nicotinamide *N*-Methyltransferase

Harshini Neelakantan,[†] Hua-Yu Wang,[‡] Virginia Vance,[†] Jonathan D. Hommel,[§] Stanton F. McHardy,[‡] and Stanley J. Watowich^{*,†,§}

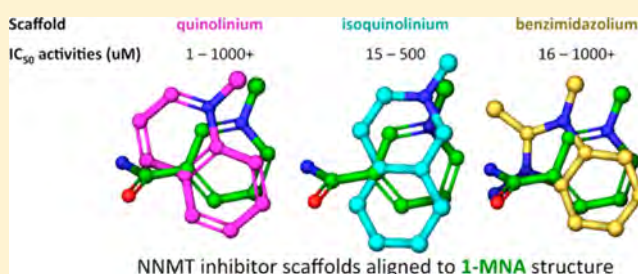
[†]Department of Biochemistry and Molecular Biology, University of Texas Medical Branch, Galveston, Texas 77550 United States

[‡]Department of Chemistry and Center for Innovative Drug Discovery, University of Texas at San Antonio, San Antonio, Texas 78249 United States

[§]Department of Pharmacology and Toxicology, University of Texas Medical Branch, Galveston, Texas 77550 United States

S Supporting Information

ABSTRACT: Nicotinamide *N*-methyltransferase (NNMT) is a fundamental cytosolic biotransforming enzyme that catalyzes the *N*-methylation of endogenous and exogenous xenobiotics. We have identified small molecule inhibitors of NNMT with >1000-fold range of activity and developed comprehensive structure–activity relationships (SARs) for NNMT inhibitors. Screening of *N*-methylated quinolinium, isoquinolinium, pyridinium, and benzimidazolium/benzothiazolium analogues resulted in the identification of quinoliniums as a promising scaffold with very low micromolar ($IC_{50} \sim 1 \mu M$) NNMT inhibition. Computer-based docking of inhibitors to the NNMT substrate (nicotinamide)-binding site produced a robust correlation between ligand–enzyme interaction docking scores and experimentally calculated IC_{50} values. Predicted binding orientation of the quinolinium analogues revealed selective binding to the NNMT substrate-binding site residues and essential chemical features driving protein–ligand intermolecular interactions and NNMT inhibition. The development of this new series of small molecule NNMT inhibitors direct the future design of lead drug-like inhibitors to treat several metabolic and chronic disease conditions characterized by abnormal NNMT activity.



■ INTRODUCTION

Nicotinamide *N*-methyltransferase (NNMT) is a cytosolic enzyme that catalyzes the transfer of methyl group from the cofactor *S*-(*S*'-adenosyl)-*L*-methionine (SAM) to substrates such as nicotinamide (NCA), pyridine, and related analogues (e.g., quinoline, isoquinoline, 1,2,3,4-tetrahydroisoquinoline¹), directly regulating the detoxification of endogenous and exogenous drugs/xenobiotics by the formation of methylated metabolic products (1-methyl nicotinamide [1-MNA], methylated pyridiniums, and methylated related analogues).² Given its primary metabolizing function, NNMT is predominantly expressed in the liver,^{3–5} but significant levels of the enzyme are also present in other tissues, including the adipose tissue, kidney, brain, lung, heart, and muscle.^{2,6} Enhanced expression and enzymatic activity of NNMT has been linked to a number of chronic disease conditions, making it a significant and relevant target for drug development. For example, several studies have demonstrated a causal relationship between increased NNMT expression and enhanced cell proliferation/progression in a variety of cancer cell lines with potential implications for NNMT as a biomarker for cancer prognosis and a target for anticancer therapeutic development.^{7–11} NNMT expression has also been reported to be upregulated in patients with Parkinson's disease, which is suggested to be

linked to the production of neurotoxins such as *N*-methylpyridinium ions that underlie neurodegeneration.^{12,13} Furthermore, studies in both animals^{14,15} and humans^{14,16,17} have shown that NNMT expression and activity was increased in obesity and related chronic metabolic conditions (e.g., type-2 diabetes). Knockdown of NNMT expression using an antisense oligonucleotide was reported to suppress body weight gain, reduce fat mass, and increase energy expenditure in mice fed a high fat diet.¹⁵ While the underlying molecular mechanisms that link decreased NNMT activity to increased adipocyte metabolism are not well understood, NNMT may modulate intracellular metabolite turnover in the methionine–homocysteine cycle and/or the nicotinamide adenine dinucleotide (NAD⁺) synthesis pathway critical for cellular energy expenditure.¹⁵ Therefore, targeted small molecule inhibitors of the NNMT could be significantly beneficial as molecular probes for mechanistic investigations and for the development of therapeutics to treat metabolic and chronic diseases that are characterized by abnormal NNMT activity.

SAM-dependent methyltransferases represent a major class of biotransforming enzymes that catalyze the methylation of

Received: March 15, 2017

Published: May 26, 2017

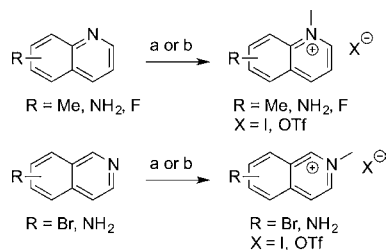
various substrates, including proteins, nucleic acids, and endogenous small molecules (e.g., intracellular metabolites) using the cofactor SAM as a universal methyl donor.^{18–20} Many inhibitors of SAM-dependent methyltransferases (e.g., the broad-spectrum methyltransferase inhibitor sinefungin, histone methyltransferase inhibitor EPZ-5676) mimic the chemical structure of SAM and interact with the SAM-binding site,^{21,22} thereby lacking selectivity for specific methyltransferase enzymes.²³ However, the recent determination of the structure of NNMT bound to the NCA substrate and SAH product²⁴ provide information that can be used to design selective and specific small molecule NNMT inhibitors.

On the basis of consistent observations of 1-MNA, the primary endogenous *N*-methylated product of NNMT, as an NNMT inhibitor in biochemical and pharmacological studies *in vitro* and *in vivo*,^{2,15} in the present study we explored the NNMT inhibitory activity of *N*-methylated heterocyclic small molecules containing several different aromatic scaffolds including quinoline, isoquinoline, pyridine, benzimidazole, and benzothiazole.^{1,25} Preliminary sets of *N*-methylated analogues for each of the chemical scaffolds were purchased from commercial suppliers and screened for NNMT inhibitory activity using purified recombinant protein. We expanded several promising chemical series to develop predictive structure–activity relationships (SARs) with emphasis on substitution effect on aryl ring and the N1 atom for each chemical series. Further, computer-based docking of inhibitors to the NNMT NCA substrate-binding site yielded a correlation between inhibitor–enzyme interaction docking scores and experimentally determined IC₅₀ values that served as a guiding tool to identify NNMT residues responsible for protein–ligand interactions and further generate binding hypotheses to design novel inhibitors with improved binding. The SAR described herein demonstrates significant promise for future exploration of the chemical space surrounding the template moieties to develop potent, selective, and drug-like NNMT inhibitors.

RESULTS AND DISCUSSION

Chemistry. The general approach to prepare the N1-methylated quinolinium and N2-methylated isoquinolinium salts was carried out as shown in Scheme 1. Commercially

Scheme 1. General Method for Synthesis of *N*-Methylated Quinolinium and Isoquinolinium Analogues^a



^aReagents and conditions: (a) MeI, IPA, 90 °C, 12 h; (b) MeOTf, toluene, 100 °C, 12 h.

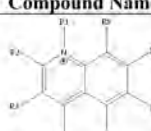
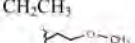



available and/or synthesized quinoline and isoquinoline with various substitution patterns were treated with iodomethane (MeI) in 2-propanol (IPA) or methyl trifluoromethanesulfonate (MeOTf) in toluene to give the corresponding analogues in good yields. Full details on the synthesis of the substituted

amino-quinoline and per-methylated quinoline intermediates/precursors are described in the Supporting Information.

Biological Evaluation of 1-Methylquinolinium (1-MQ) Analogues. To test the hypothesis that *N*-methylated quinolinium containing compounds function as NNMT inhibitors, we began by probing the NNMT inhibitory activity of 1-MQ (**1a**), which exhibited an IC₅₀ value of 12 μM (Table 1). On the basis of the activity exhibited by **1a**, we explored SAR for NNMT inhibition on the 1-MQ scaffold by testing 48 additional analogues (obtained either from commercial suppliers or synthesized in-house) using a modified HPLC-based biochemical assay.^{25,26} In the first series of compounds, we explored the inhibitory activities of monosubstituted 1-MQ with various polar/apolar substituents and different N1-substituted quinolinium analogues (**1b–z**; Table 1). Generally, small substituents such as methyl or amine groups were well tolerated in different substitution patterns on the 1-MQ ring with NNMT inhibitory activity in the low micromolar range (Table 1). Among all the monomethylated quinolinium analogues tested with various substitution patterns at C2–C8-positions of 1-MQ (**1b**, **1e**, **1i**, **1l**, **1n**, **1r**, and **1t**; Table 1), a methyl substituent at the C8-position (**1t**) gave the most significant improvement in inhibition (6.7-fold lower IC₅₀ value, IC₅₀ = 1.8 μM) as compared to the parent compound 1-MQ (**1a**). While a methyl substituent at the C3-position also exhibited low micromolar NNMT inhibition (**1e**, IC₅₀ = 4.1 μM; Table 1), an amino substitution at the same position further improved the IC₅₀ value to 2.9 μM (**1d**), suggesting relatively favorable interactions between the NNMT residues and the C3-amino substitution. To further explore the favorable nature of polar groups at the C3-position, we tested analogues **1f–h**; analogue **1f** with a C3-methylamino substitution and analogue **1g** with a cyano substituent at the C3-position had ~3-fold and ~8-fold higher IC₅₀ values, respectively, relative to compound **1d**. Importantly, analogue **1h** with a bulky phenyl ring at the C3-position had significantly reduced inhibitory activity (IC₅₀ > 1 mM). Taken together, the data suggests that potentially favorable interactions can be imparted by small polar group substituents such as an amine, while unfavorable steric interactions occur when large chemical groups occupy the C3-position of the 1-MQ scaffold.

To further explore 1-MQ scaffold positions that could form favorable hydrogen-bonding interactions with NNMT binding site residues to improve inhibitory activity, a systematic SAR was conducted among different amino-quinolinium derivatives (**1c**, **1d**, **1j**, **1k**, **1o**, **1q**; Table 1). Many of the 1-MQ analogues with amino pharmacophores (e.g., **1c**, **1k**, **1q**) demonstrated excellent inhibitory activities that were comparable to **1d** (IC₅₀ = 2.9 μM); the exceptions were analogues **1j** (C4-amino substituent) and **1o** (C6-amino substituent) that exhibited ~4-fold and ~10-fold reduction in activity (IC₅₀ = 11 μM and 34 μM), respectively, compared to **1d**. An amino substitution at the C5-position (**1k**) produced potent NNMT inhibition (IC₅₀ = 1.2 μM) with 10- and 2.4-fold lower IC₅₀ values compared to **1a** and **1d**, respectively (Figure 1; Table 1). This suggests that the polar amine group at the C5-position favors strong intermolecular interactions with the backbone serine residues in the NNMT substrate-binding site (refer to Molecular Docking discussion below). In contrast to amino substitutions, 1-MQ analogues with other polar substitutions such as hydroxyl (**1s** and **1u**) and methoxy (**1p**) showed significantly weaker NNMT inhibition activities compared to the parent compound **1a**. For example, a hydroxyl group substituent at the C7-

Table 1. NNMT Inhibitory Activity of 1-Methylquinolinium Scaffold Compounds with Single Positional Substitutions

Core/ Compound Name	R1	R2	R3	R4	R5	R6	R7	R8	NNMT Inhibition IC ₅₀ (μM) ^a
									
Quinoline									
1a (1-MQ)	CH ₃	H	H	H	H	H	H	H	12.1 ± 3.1
1b	CH ₃	CH ₃	H	H	H	H	H	H	21.03 ± 2.1 ^b
1c	CH ₃	NH ₂	H	H	H	H	H	H	6.3 ± 1.1 ^b
1d	CH ₃	H	NH ₂	H	H	H	H	H	2.9 ± 0.7 ^b
1e	CH ₃	H	CH ₃	H	H	H	H	H	6.9 ± 3.01 ^b
1f	CH ₃	H	NHCH ₃	H	H	H	H	H	9.9 ± 3.4 ^b
1g	CH ₃	H	CN	H	H	H	H	H	23.8 ± 5.6
1h	CH ₃	H	NHPh	H	H	H	H	H	>1000 ^b
1i	CH ₃	H	H	CH ₃	H	H	H	H	7.5 ± 2.2
1j	CH ₃	H	H	NH ₂	H	H	H	H	11.4 ± 2.1 ^b
1k	CH ₃	H	H	H	NH ₂	H	H	H	1.2 ± 0.1 ^b
1l	CH ₃	H	H	H	CH ₃	H	H	H	4.6 ± 1.8 ^b
1m	CH ₃	H	H	H	H	F	H	H	5.7 ± 1.8 ^b
1n	CH ₃	H	H	H	H	CH ₃	H	H	13.1 ± 5.1
1o	CH ₃	H	H	H	H	NH ₂	H	H	34.4 ± 9.6 ^b
1p	CH ₃	H	H	H	H	OCH ₃	H	H	119.9 ± 50.1
1q	CH ₃	H	H	H	H	H	NH ₂	H	2.6 ± 0.5 ^b
1r	CH ₃	H	H	H	H	H	CH ₃	H	12.01 ± 4.5 ^b
1s	CH ₃	H	H	H	H	H	OH	H	709.2 ± 178.9
1t	CH ₃	H	H	H	H	H	H	CH ₃	1.8 ± 0.5
1u	CH ₃	H	H	H	H	H	H	OH	95.2 ± 21.02
1v	CH ₂ CH ₃	H	H	H	H	H	H	H	27.1 ± 5.4
1w		H	H	H	H	H	H	H	>1000
1x		H	H	H	H	H	H	H	>1000
1y		H	H	H	H	H	H	H	>1000
1z		H	H	H	H	H	H	H	>1000

^aIC₅₀ values are represented at mean ± SD of duplicate or more measurements. ^bCompounds synthesized in-house.

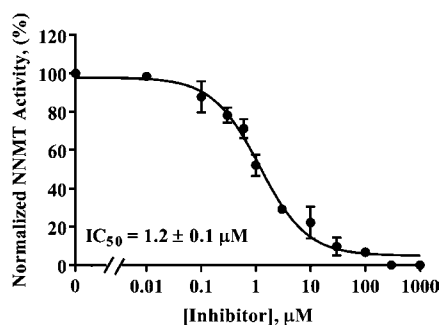









Figure 1. Normalized response curve for NNMT inhibitor **1k** (5-amino-1-methylquinolinium analogue). Data points represent average and standard deviation of normalized NNMT activity. Data points were normalized to no inhibitor condition (0 μM) within each experiment ($n = 5$). The goodness-of-fit R^2 between the fitted curves and data was 0.97.

position demonstrated ~50% inhibition of NNMT at nearly a millimolar concentration (**1s**, IC₅₀ = 709 μM), whereas the comparable amino-substituted analogue (**1q**) was a potent NNMT inhibitor (IC₅₀ = 2.6 μM). While this observation remains intriguing, it can be speculated based on our molecular docking analyses using predicted binding orientations of the analogues **1s** and **1q** that the N atom of the C7-amino forms a

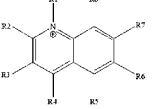
stronger hydrogen bond to the carbonyl oxygen side chain of Ser213 residue of NNMT, relative to the more repulsive hydrogen bond interaction between donor hydrogen atom of C7-hydroxyl and the Ser213 residue. Additionally, under the aqueous buffer reaction condition (pH 8.6) used in the current study, it is likely that the C7-hydroxy quinolinium analogue undergoes tautomerization into its dominant form (i.e., C7-oxo-dihydroquinolinium analogue), losing the charge on the N1 atom and significantly diminishing the overall binding within the NNMT substrate-binding site. Similarly, replacement of the methyl group (**1t**) by a polar hydroxyl substituent at the C8-position exhibited >50-fold lower IC₅₀ (**1u**, IC₅₀ = 95.2 μM) that may also be due to preferred ionization of the polar hydroxyl group in aqueous buffer, resulting in potential disruption of the tight binding within the apolar pocket of the NNMT binding site (refer to [Molecular Docking](#) discussion below). Lastly, we examined the relationship between quinolinium analogues containing N1 substitutions with varied steric and electronic properties (**1v–z**; [Table 1](#)) and NNMT inhibition. The results revealed that the activity of N1-substituted quinoliniums was inversely correlated with the size of the substituent. For example, N1-ethyl quinolinium analogue **1v** was an ~2-fold weaker inhibitor compared to 1-MQ (**1a**) and analogues with bulky substituents (**1w–z**) showed very poor inhibition (IC₅₀ > 1000 μM). These data

Table 2. NNMT Inhibitory Activity of 1-Methylquinolinium Scaffold Compounds with Dual Positional Substitutions^c

Core/ Compound Name	R1	R2	R3	R4	R5	R6	R7	R8	NNMT Inhibition IC ₅₀ (μM) ^d
									
Quinoline									
2a	CH ₂ CH ₃	H	H	CH ₃	H	H	H	H	8.7 ± 2.6
2b	CH ₂ CH ₃	H	H	H	H	H	H	CH ₃	3.1 ± 1.4
2c		H	H	CH ₃	H	H	H	H	33.5 ± 9.9
2d		H	H	H	H	H	H	OH	40.6 ± 13.01
2e		H	Br	H	H	H	H	H	>1000
2f	CH ₂ CH ₂ CH ₃	H	H	H	H	CH ₃	H	H	>1000
2g		H	H	H	H	Cl	H	H	>1000
2h		H	H	H	H	OH	H	H	>1000
2i		H	H	H	H	CH ₃	H	H	NI
2j	CH ₃	H	NH ₂	H	H	F	H	H	1.2 ± 0.2 ^b
2k	CH ₃	H	H	H	CF ₃	H	H	CH ₃	87.01 ± 26.1 ^b
2l	CH ₃	H	H	Cl	H	H	H	CF ₃	>1000 ^b
2m	CH ₃	NH ₂	NH ₂	H	H	H	H	H	2.8 ± 0.5 ^b
2n	CH ₃	CH ₃	H	H	H	H	H	CH ₃	15.9 ± 7.9 ^b
2o	CH ₃	CH ₃	H	H	H	CH ₃	H	H	>1000 ^b

^aIC₅₀ values are represented at mean ± SD of duplicate or more measurements. ^bCompounds synthesized in-house. ^cNI: No inhibition and area product peak was higher compared to control reaction.

Table 3. NNMT Inhibitory Activity of 1-Methylquinolinium Scaffold Compounds with Multipositional Substitutions

Core/ Compound Name	R1	R2	R3	R4	R5	R6	R7	R8	NNMT Inhibition IC ₅₀ (μM) ^d
									
Quinoline									
3a	CH ₂ CH ₃	H	H	CH ₃	H	F	H	H	3.6 ± 1.5
3b	CH ₂ CH ₃	H	H	CH ₃	H	CF ₃	H	H	>1000
3c	CH ₃	CH ₃	H	CH ₃	H	H	H	CH ₃	115.4 ± 41.01 ^b
3d	CH ₃	CH ₃	H	CH ₃	CH ₃	H	H	CH ₃	>1000 ^b
3e	CH ₃	CH ₃	H	CH ₃	H	CH ₃	H	CH ₃	>1000 ^b
3f	CH ₃	CH ₃	H	CH ₃	H	H	CH ₃	CH ₃	>1000 ^b
3g	CH ₃	CH ₃	H	CH ₃	F	H	H	CH ₃	94.6 ± 76.3 ^b
3h	CH ₃	CH ₃	H	CH ₃	H	H	F	CH ₃	109.2 ± 58.5 ^b

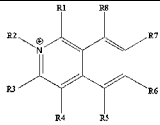
^aIC₅₀ values are represented at mean ± SD of duplicate or more measurements. ^bCompounds synthesized in-house.

suggest that small moieties such as methyl or ethyl groups directly adjacent to the N1 position may be crucial for maintaining potent NNMT inhibitory activity of the quinolinium scaffold.

To further develop an SAR model for the quinolinium scaffold, we next explored the activities of analogues with dual (2a–o; Table 2) and multipositional substitutions (3a–h; Table 3). Consistent with our previously observed inverse relationship between NNMT inhibition and N1 substituent size, N1-ethyl quinolinium analogues with C4- and C8-methyl substituents (2a,b; Table 2) showed lower activities compared to N1-methyl quinolinium congeners (1i and 1t; Table 1). Substituting a hydroxyethyl (2c) for an ethyl group (2a) at the

N1 position further reduced the activity by ~3.5-fold, reinforcing the observation that a smaller alkyl group (e.g., methyl) at the N1 position is valuable for maintaining good inhibitory potency. The relationship between NNMT inhibition and likely steric effects from N1 substitutions was further exemplified by analogues 2e–i, which displayed IC₅₀ values that either exceeded 1000 μM or showed no inhibition of NNMT, regardless of the pharmacophore (i.e., methyl, chloro, and hydroxyl groups) placed at the C6-position. Single-point SAR studies indicated that a C8-hydroxyl containing analogue (1u; Table 1) decreased the IC₅₀ value by ~50-fold relative to a more favorable methyl substituent (1t), while two-point SAR studies incorporating a hydroxyl group at the C8-position and a

Table 4. NNMT Inhibitory Activity of Compounds Containing 2-Methyl Isoquinolinium Scaffold

Core/ Compound Name	R1	R2	R3	R4	R5	R6	R7	R8	NNMT Inhibition IC ₅₀ (μM) ^a
 Isoquinoline									
4a	H	CH ₃	H	H	H	H	H	H	14.9 ± 6.1
4b	H	CH ₃	NH ₂	H	H	H	H	H	6.3 ± 2.7 ^b
4c	H	CH ₃	H	Br	H	H	H	H	30.3 ± 7.02 ^b
4d	H	CH ₃	H	H	H	NH ₂	H	H	29.9 ± 9.1 ^b
4e	H	CH ₃	H	H	H	Br	H	H	505.7 ± 199.1 ^b
4f	H	CH ₃	H	H	H	H	NH ₂	H	39.4 ± 18.02 ^b

^aIC₅₀ values are represented at mean ± SD of duplicate or more measurements. ^bCompounds synthesized in-house.

relatively bulky C2-oxopropyl at the N1 position (**2d**) did not additively impair activity; instead, the IC₅₀ value for **2d** was ~2-fold lower relative to **1u**. This may imply that substitutions at C8-position combined with branched groups at the N1 position might alter the binding mode of the analogue and disrupt the steric-dependent inhibition pattern observed with bulky groups at the quinolinium N1 position.

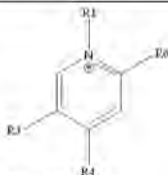
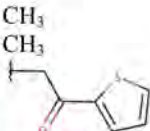
Interestingly, when a fluorine was added to the C6-position of the C3-amino-analogue (**1d**), we observed supra-additive effects on NNMT inhibition; the C3-amino C6-fluoro-1-MQ analogue (**2j**) had an IC₅₀ of 1.2 μM, which was ~2.5-fold more potent than the nonfluorinated derivative **1d** (IC₅₀ = 2.9 μM) and ~5-fold more potent than the C6-fluoro-1-MQ analogue (**1m**; IC₅₀ = 5.7 μM), highlighting the significance of both C3-amino and C6-fluoro substituents in improving activity. The improvement observed in NNMT inhibitory activity with the introduction of a fluorine substituent is consistent with the general observation that electron-withdrawing halogen groups such as fluorine may engage in multipolar interactions (e.g., orthogonal-type dipolar interaction with carbonyl groups in the binding pocket of a target protein), causing improvements in compound binding and affinity.^{27,28} Analogues with CF₃ substitutions have also been observed to form strong multipolar intermolecular interactions and improve binding affinities relative to the corresponding methyl derivatives.²⁹ CF₃ substituents were tested using several 1-MQ analogues; CF₃ substituent (**2k**; Table 2) placed at C5-position within the 1-MQ scaffold impaired activity relative to an analogue lacking this substituent (**1t**) and a CF₃ substituent at the C8-position (**2l**; Table 2) in addition to an impairing chloro substituent at the C4-position significantly deteriorated the activity of the compound. Further, we tested for other potentially synergistic effects by screening dual-substituent 1-MQ analogues containing numerous small apolar and amino pharmacophores. We found that the C2,3-diamino-1-MQ analogue **2m** showed inhibitory activity (IC₅₀ = 2.8 μM; Table 2) that was similar to the C3-amino 1-MQ analogue **1d** (IC₅₀ = 2.9 μM; Table 1) without additive improvements, reinforcing the observation that an amino-substituent at the C3-position is an important feature among 1-MQ analogues to maintain potent inhibitory activity. Similarly, other dimethyl substitutions in analogues (**2n–o**; Table 2) did not cause synergistic improvements in compound activity compared to the corresponding mono-methyl substitutions (**1b**, **1n**, **1t**; Table 1) but instead rendered the dimethyl quinolinium compounds as poor inhibitors of NNMT (5–50-fold higher IC₅₀ values, **2n–o**; Table 2).

In our studies of the activity of multipositionally substituted N1-quinoliniums, a C6-fluorinated analogue **3a** (IC₅₀ = 3.6 μM; Table 3) showed a ~2.5-fold increase in NNMT inhibitory activity compared to the nonfluorinated derivative **2a** (IC₅₀ = 8.7 μM; Table 2), consistent with earlier observations that C6-fluoro substitution positively impacts quinolinium inhibitory activity. Substitution of the C6-fluoro of analogue **3a** to a C6-trifluoromethyl group (**3b**) resulted in a significant loss of compound inhibitory activity (IC₅₀ > 1000 μM), comparable to the drastic reductions in NNMT inhibition observed when CF₃ substituents were incorporated into the quinolinium scaffold (analogues **2k–l**; Table 2).

General synthetic approaches were applied to improve the lipophilicity and drug-like properties (e.g., permeability) of this class of quinolinium-based NNMT inhibitors, in which the lipophilicity was evaluated in silico by measuring the calculated logarithmic form of the partition coefficient using ChemAxon software.³⁰ To this end, we tested several per-methylated quinolinium analogues with methyl substituents at multiple ring positions (C2–C8). Similar to the results obtained with dimethyl-substituted analogues, the addition of multiple methyl substituents largely decreased the ability of the analogues to inhibit NNMT (**3c–f**; Table 3). A C2,C4,C8-trimethyl-analogue **3c** showed ~5–64-fold lower inhibitory activity (IC₅₀ = 115.4 μM) as compared to monomethylated analogues such as **1b** (IC₅₀ = 21 μM), **1h** (IC₅₀ = 7.5 μM), and **1q** (IC₅₀ = 1.8 μM). Graphical analysis of molecular docking simulations suggested that multimethylated 1-MQ analogues make intermolecular apolar contacts with several hydrophobic residues within the NNMT binding site that are likely detrimental to the overall binding energetics between the ligand and enzyme; this conclusion was supported by poor docking scores generated by Vina ligand docking program. Furthermore, unlike the activity improvements observed for 1-MQ analogues with C6-fluoro group substitutions (see compounds **1k**, **2j**, **3a**), the addition of a fluoro group to the C5 or C7 positions of a per-methylated quinolinium scaffold (**3c**) did not improve analogue inhibitory potency (**3g**, IC₅₀ = 94.6 μM; **3h**, IC₅₀ = 109.2 μM; Table 3), suggesting that the C6-position may be highly “fluorophilic” to promote dipole-type interactions within the NNMT substrate-binding site. However, additional analogues with positional fluoro substitutions within the 1-MQ scaffold need to be tested to confirm this hypothesis.

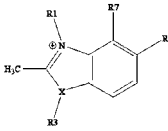
Biological Evaluation of N2-Methyl Isoquinolinium Analogues. Previous studies have shown that the isoquinoline

Table 5. NNMT Inhibitory Activity of Compounds Containing Pyridinium Scaffold

Core/ Compound Name	R1	R3	R4	R6	NNMT Inhibition IC ₅₀ (μM) ^a
 Pyridine					
5a		CONH ₂	H	H	9.0 ± 0.6 ^b
5b	CH ₃	CONH ₂	CH ₃	CH ₃	11.8 ± 3.04
5c		CONH ₂	H	H	>1000

^aIC₅₀ values are represented at mean ± SD of duplicate or more measurements. ^b1-MNA (5a) is a reaction product of NNMT; IC₅₀ curve for 5a was determined using a fluorescence assay that utilizes quinoline as an NNMT substrate and monitors formation of 1-MQ.

Table 6. NNMT Inhibitory Activity of Compounds Containing Benzimidazolium/Benzothiazolium Scaffold

Core/ Compound Name	R1	R3	R6	R7	X	NNMT Inhibition IC ₅₀ (μM) ^a
 Benzimidazol/ Benzothiazole						
6a	CH ₃	CH ₃	H	H	N	16.7 ± 6.4
6b	CH ₃	NH ₂	H	H	N	82.4 ± 17.4
6c	CH ₂ CH ₃	CH ₂ CH ₃	H	H	N	22.8 ± 7.8
6d	CH ₃	CH ₂ CH ₃	NH ₂	H	N	>1000
6e	CH ₂ CH ₃	-	CH ₃	H	S	>1000
6f	CH ₂ CH ₂ CH ₂ CH ₃	-	H	H	S	>1000

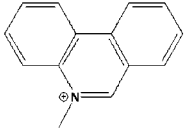
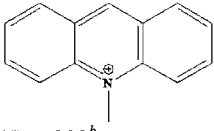
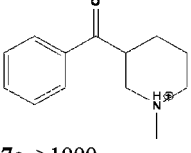
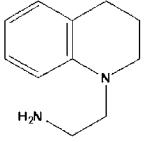
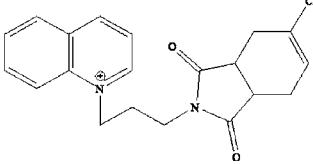
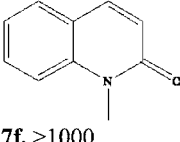
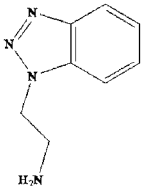
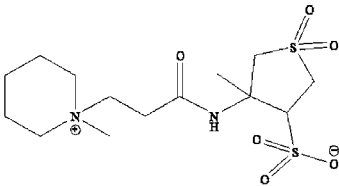
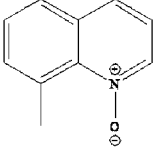
^aIC₅₀ values are represented at mean ± SD of duplicate or more measurements.

scaffold is amendable to the development of drug-like small molecule inhibitors.^{31,32} Because isoquinoline is also an NNMT substrate,^{1,25} we examined the NNMT inhibitory activities of a series of analogues designed around the *N*2-methyl isoquinolinium chemotype (Table 4). NNMT methylates isoquinoline to produce the reaction product *N*2-methyl isoquinolinium (4a),^{1,25} which inhibits NNMT with an IC₅₀ of 14.9 μM similar to that of 1-MQ (1a; IC₅₀ = 12.1 μM). Guided in part by the SAR established for the 1-MQ scaffold (Tables 1–3) and molecular docking calculations, we explored the activities of a small series of monosubstituted isoquinoline analogues (4b–f; Table 4). As summarized in Table 4, a C3-amino substituent (4b) improved compound activity ~2.4-fold (IC₅₀ = 6.3 μM) compared to the parent *N*2-methyl isoquinolinium (4a); the relative improvement in activity that resulted from adding a C3-amino group to the isoquinoline parent was smaller compared to the activity increase observed when the substitutional congener was added to the 1-MQ scaffold (1d, IC₅₀ = 2.9 μM). Instead, 4b had activity similar to analogue 1c (IC₅₀ = 6.3 μM); both analogues have an amino group adjacent to the *N*-methyl moiety, which could potentially shift the binding orientations of these analogues and disrupt some of the hydrophobic interactions within the NNMT substrate-binding site (a detailed discussion is presented in the Molecular Docking section below). Incorporation of a bromo group at the C4-

position (4c) or an amino group at the C6-position (4d) reduced the potency of these analogues by ~2-fold relative to the parent analogue (4a) while adding a bromo group at the C6-position (4e) significantly decreased analogue activity (IC₅₀ = 505.7 μM). In contrast to the 1-MQ chemotype (1a) where a C7-amino (1n) improved analogue potency by 5-fold, a comparable amino substitution pattern on the *N*2-methyl isoquinolinium scaffold decreased analogue potency by ~3-fold (4f; IC₅₀ = 39.4 μM). These observations are consistent with calculated changes to the binding orientations and intermolecular interactions between NNMT and N1-MQ and *N*2-methyl isoquinolinium analogues, respectively (refer to Molecular Docking discussion below).

Inhibitory Activities of 1-Methylpyridinium Analogues. 1-Methylnicotinamide (1-MNA; 5a) is the endogenous product of the NNMT catalyzed reaction and an established NNMT inhibitor.^{2,15} Using a recently developed sensitive fluorescence-based assay,³³ we determined the IC₅₀ of 1-MNA to be 9.0 μM (Table 5), which is comparable to the IC₅₀ value determined for 1-MQ (1a). On the basis of this result, 1-MNA analogues with dimethyl groups at C4- and C6-positions (5b) and a sterically demanding C2-acyl-thiofuranyl group at the N1 position (5c) were tested. Compound 5b exhibited slightly decreased potency (IC₅₀ = 11.8 μM) relative to 5a (Table 5) and was similar to that of 1-MQ (1a). Again,

Table 7. Related Structural Analogues with Poor NNMT Inhibitory Activity

Structure	Compound name, IC ₅₀ (μM) ^a	Structure	Compound name, IC ₅₀ (μM) ^a	Structure	Compound name, IC ₅₀ (μM) ^a
	7a, 161.4 ± 272.9		7b, >300 ^b		7c, >1000
	7d, >1000		7e, >1000		7f, >1000
	7g, >1000		7h, >1000		7i, >1000

^aIC₅₀ values are represented at mean ± SD of duplicate or more measurements. ^bCompound precipitated in solution at concentration >300 μM. Exact IC₅₀ could not be determined.

consistent with the general observations that sterically hindered substituents at the N1 position significantly reduce the activity of analogues within the NNMT substrate-binding site, analogue 7c was observed to have very poor activity (IC₅₀ > 1000 μM).

Inhibitory Activities of Benzimidazolium/Benzothiazolium and Other Structural Analogues. Lastly, other structurally related chemotypes, i.e., compounds containing benzimidazolium and benzothiazolium scaffolds (6a–f; Table 6) and other heteroaryl templates (7a–i; Table 7) were tested for NNMT inhibition. Compound 6a, with apolar methyl group substituents at both the N1 and N3 positions of the benzimidazole scaffold exhibited an IC₅₀ value of 16.7 μM, which was ~2-fold lower relative to 1-MNA (5a), 1-MQ (1a), and N2-methyl isoquinolinium analogue (4a). Consistent with results observed for additive groups to the 1-MQ scaffold, an ethyl substitution at the N1 position (6b) was well tolerated and generated comparable activity (IC₅₀ = 22.8 μM) to the parent structure 6a. This is supported, in part, by overlapping intermolecular interactions that are predicted to occur between ligands containing distinct core scaffolds (1-MQ, N2-methyl isoquinolinium, pyridinium, and benzimidazolium/benzothiazolium) and NNMT substrate-binding site residues; however, molecular docking studies also revealed dissimilar interactions for the ligands with the different scaffolds within the NNMT substrate-binding site (refer to Molecular Docking discussion below). For example, the C3-amino benzimidazolium analogue 6c demonstrated a ~5-fold higher IC₅₀ value (IC₅₀ = 82.4 μM) relative to the parent structure 6a; this was in contrast to the 1-MQ and N2-methyl isoquinolinium scaffolds where an amino group at the C3-position improved ligand activity (1d and 4b). Other analogues composed of the benzimidazolium (6d) and benzothiazolium scaffolds (6e) were very poor inhibitors of NNMT (IC₅₀ > 1000 μM). As summarized in Table 7, only analogues (7a,b) containing phenanthridinium and acridinium

structures showed even modest ability to inhibit NNMT (IC₅₀ values, 100–300 μM); all other tested chemotypes (7c–i) showed very poor NNMT inhibition (IC₅₀ > 1000 μM). Importantly, analogues containing tetrahydroquinoline/quinolone scaffolds (e.g., 7d, 7f) that were uncharged exhibited very poor NNMT inhibition, suggesting that a positive charge at the N1 position may be a necessary chemical feature for small molecule inhibitors of NNMT.

Structure-Based Docking between NNMT and Small Molecule Inhibitors. The Vina computer docking program was able to reproduce the NCA molecular orientation observed in the X-ray structure of the NNMT–NCA–SAH ternary complex²⁴ with an all atom root-mean-square deviation of 0.74 Å, suggesting that these calculations would be suitable to investigate likely orientations and intermolecular interactions of small molecule inhibitors bound to NNMT. Binding orientations and docking scores between NNMT and each of the ~44 combined quinolinium, isoquinolinium, pyridinium, and benzimidazolium analogues containing N-methyl substituents, respectively, were calculated. As shown in Figure 2 for the combined set of analogues, a positive linear correlation ($r = 0.63$, $R^2 = 0.4$, $P[\text{two-tailed}] = 0.0003$) was observed between Vina docking score and log(IC₅₀) values. In these calculations, low (i.e., more negative) docking scores suggest more favorable binding conformations and intermolecular interactions between the ligand and macromolecular target. Consistent with this observation, analogues that were potent NNMT inhibitors (e.g., compounds 1k, 1t; IC₅₀ = 1.2–1.8 μM) had the lowest calculated Vina docking scores (scores between –8.3 and –8.1). Conversely, many analogues (e.g., per-methylated compounds 3e,f) that were either poor NNMT inhibitors (IC₅₀ > 1000 μM) or failed to inhibit NNMT had higher calculated Vina docking scores (scores between –6.0 and –5.0) or did not bind in the nicotinamide binding pocket. Taken

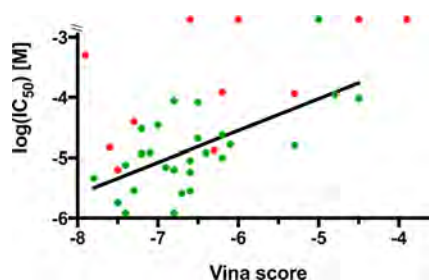


Figure 2. Correlation between the Vina docking scores and experimentally measured IC_{50} values for all analogues with methyl substitution at the N-position in each of the core scaffolds (41 compounds). Data points colored red correspond to analogues that docked outside the NNMT substrate-binding site. Pearson's correlation analysis performed on analogues that docked in the substrate-binding site (represented by green markers) indicated a positive linear correlation between calculated docking scores and $\log(IC_{50})$ ($r = 0.63$, $R^2 = 0.4$, $P[\text{two-tailed}] = 0.0003$).

together, Vina docking scores and inhibitor potencies were modestly correlative for many analogues containing the N1-methyl quinolinium scaffold (Figure 2), suggesting that docking calculations could serve as a predictive tool to guide the identification and design of small molecule NNMT inhibitors similar to other reported systems.³⁴ However, there were

exceptional N1-methylquinolinium ligands and analogues containing other chemical scaffolds (e.g., N2-methyl isoquinolinium, benzimidazolium) that were inconsistent, likely, in part, due to inherent limitations of the Vina computational program and/or inherent analogue properties. The Vina program makes assumptions on the protonation states/partial charge distribution in molecules not accounting for solvent, dipole, entropic, and tautomerization effects.³⁵ As a result, disparity between calculated docking scores and experimentally generated IC_{50} values were observed for some of the tested analogues. For example, analogues with relatively good docking scores (e.g., analogues **1s**, **2l**; docking scores between -7 and -8) exhibited poor IC_{50} values ($>500 \mu\text{M}$) and improvements imparted by C6-fluoro substitutions in the IC_{50} values compared to the nonfluorinated derivatives, presumably via enhanced dipolar interactions, were not truly reflected in the docking scores generated by the Vina calculations [e.g., analogues **1a** ($IC_{50} = 12.1 \mu\text{M}$) and **1m** ($IC_{50} = 5.7 \mu\text{M}$) had similar Vina docking scores ~ -7.7].

Vina docking calculations can predict likely orientations and conformations of small molecules bound to a target protein. 1-methylquinolinium (**1a**) was used to establish a prototypical structure for 1-MQ analogues bound to the NNMT substrate-binding pocket (Figure 3). The predicted binding orientation of 1-MQ (and related analogues) was similar to the bound

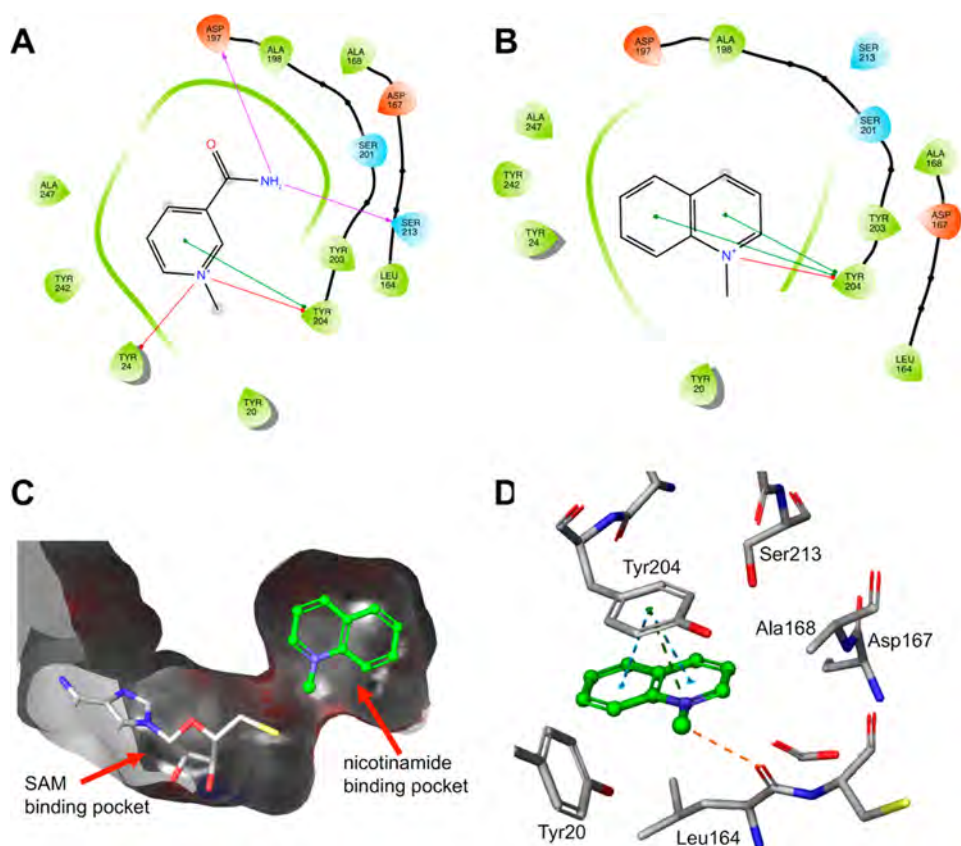


Figure 3. Bound orientation and intermolecular interactions between representative inhibitors and NNMT as calculated by the Vina molecular docking program. (A) 2-D schematic of the intermolecular interactions between NNMT and bound 1-methylnicotinamide (**1a**). (B) 2-D schematic of the intermolecular interactions between NNMT and bound 1-methylquinolinium (**1a**). (C) 3-D representation of the orientation of 1-methylquinolinium (**1a**) in the NNMT substrate-binding site and positioned relative to the SAM binding pocket. (D) 3-D representation of the intermolecular interactions between NNMT and bound 1-methylquinolinium (**1a**). Potential cation- π interactions are depicted by red arrows, π - π interactions are shown by green arrows, and hydrogen bonds are shown by purple arrows. Figures were produced with Maestro 11 (Schrodinger LLC, New York, NY).³⁷

structures of the endogenous substrate NCA and docked 1-MNA, with the N1 atoms of these ligands superimposable and with similar intermolecular interactions to residues within the NNMT substrate-binding pocket (Figure 3A,B). Moreover, the inhibitors were positioned in the nicotinamide binding pocket such that their N1-methyl groups were directed toward the adjacent SAM binding pocket (Figure 3C). 1-MQ and related analogues are predicted to form strong π - π , cation- π , and hydrophobic interactions with residues Tyr204 and Leu164 that define the apolar pocket surrounding the quinolinium N1-containing ring (Figure 3B,D), similar to the manner in which these aromatic residues interact with the pyridine ring of NCA in the NNMT substrate-binding site.²⁴ In addition, NNMT residues Ala198, Tyr242, and Tyr 24 were also indicated to contact via hydrophobic interactions with the quinolinium ring of 1-MQ (Figure 3B,D), two of which (Ala198 and Tyr242) have also been indicated to contact with the pyridinium ring of the substrate NCA and 1-MNA (Figure 3A). Further, the NCA amide group has been reported to form hydrogen bonds with the hydroxyl groups of Ser201/Ser213 residues and the Asp197 carboxylate.^{24,24} The predicted binding orientation of quinolinium analogue **1k**, however, suggests that the C5-amino group forms hydrogen bonds with Ser201 and hydrophobic interactions with Ser213 and Tyr20 (figure not shown). These distinct predicted interactions between analogue **1k** and NNMT compared to NCA suggest more favorable intermolecular bonding interactions with residues within the NNMT substrate-binding pocket, which is supported by a lower Vina docking score (Vina score = -8.1) for **1k** relative to 1-MNA (Vina score = -6.8) and the potent inhibitory activity exhibited by this analogue ($IC_{50} = 1.2 \mu M$).

The predicted conformations, binding orientations, and intermolecular interactions with NNMT residues for the most potent analogues with the pyridinium scaffold (1,2,4-trimethyl-5-carboxamidepyridinium, **5b**), benzimidazolium scaffold (1,2,3-trimethyl-1*H*-3,1-benzimidazol-3-ium, **6a**), and *N*2-methyl isoquinolinium scaffold (3-amine-2-methylisoquinolinim, **4b**) were examined and are summarized below. Inhibitors with different chemotypes were predicted to bind NNMT via hydrophobic interactions with the same aromatic residues (Leu164 and Tyr204) in the apolar substrate-binding pocket and make additional contacts with apolar atoms of Tyr24, Tyr242, and Ala198 around the respective scaffold ring structures relative to the prototype analogue **1k**. Analogues **5b** and **6a** with the pyridinium and benzimidazolium scaffolds, respectively, either formed only hydrogen bonds or hydrophobic contacts with Ser201/213 residues and made additional hydrophobic contacts with NNMT residues (e.g., **5b**, Asp167, Ala247; **6a**, Ala168, Asp167, Asp197) compared to **1k**, which potentially rendered these inhibitors less potent (at least ~10-fold lower potency relative to **1k**). Lastly, the predicted orientation of isoquinolinium analogues (e.g., **4b**) was shifted within the NNMT substrate-binding pocket relative to the quinolinium analogues. Specifically, the carbon atoms around the *N*2-methyl isoquinolinium rings were predicted to form distinct hydrophobic interactions with NNMT residues Tyr203 and Ala247 and more importantly form hydrogen bond and hydrophobic interactions with the phenol hydroxyl group and ring carbon atoms in the backbone of Tyr20 residue, respectively. Given that Tyr20 is critical for the functional activity of NNMT²⁴ and the alignment of both methyl donor and acceptor molecules (SAM and NCA) in the binding

pocket,²⁴ interactions with this residue might be relevant in guiding the inhibitor activity.

Summary of SAR for 1-MQ Analogues. The most potent NNMT inhibitor analogues identified in the current study (e.g., **1k**, **2j**; $IC_{50} \sim 1.2 \mu M$) contained the quinolinium scaffold. These compounds were predicted to bind the NNMT substrate-binding pocket analogous to NCA and exhibited favorable intermolecular interactions with NNMT residues. A predictive SAR developed for this series of analogues highlights a few important chemical features required for potent NNMT inhibition as summarized in Figure 4: (i) apolar methyl

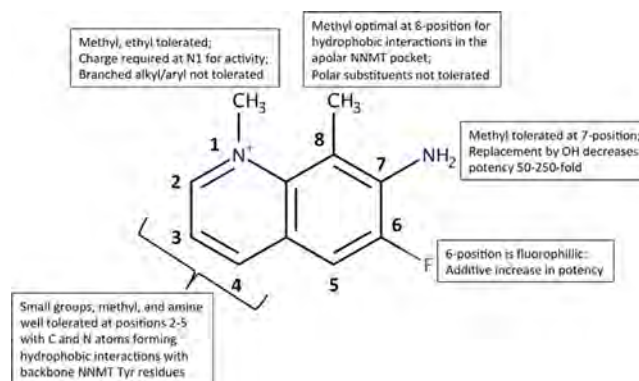


Figure 4. SAR summary for analogues containing the quinolinium scaffold (information abstracted from Tables 1–3).

substitutions at N1 and C8 positions promote strong hydrophobic interactions with aromatic NNMT residues (Leu164, Tyr204), and the positive charge on the N1 atom is required to retain potent inhibitory activity; (ii) methyl or amino substituents at C2–C5-, and C7-positions provide favorable C and N atoms that can contact with Tyr (Tyr20, Tyr24, Tyr242) and Ser (Ser201 and Ser213) residues via multiple hydrophobic and/or hydrogen bond interactions; and (iii) an electron-withdrawing fluoro substitution at the C6-position engages in multipolar interactions and significantly enhances analogue potency.

CONCLUSIONS

Exploration of an initial series of commercially available and synthesized *N*-methylated analogues of different chemotypes, including quinolinium, isoquinolinium, pyrididum, and benzimidazolium/benzothiazolium, resulted in the rapid development of structure–activity relationships (SARs) for NNMT inhibitors demonstrating >1000-fold range of activity. Computer-based docking of inhibitors to the NNMT NCA substrate-binding site produced a robust correlation between ligand–enzyme interaction docking scores and experimentally established IC_{50} values. Computational calculations and predicted binding orientation of inhibitors enabled identification of NNMT residues responsible for protein–ligand intermolecular interactions. The quinolinium analogue series that demonstrated significant NNMT inhibition were further expanded by synthesis, guided in part by calculations to identify analogues with improved docking scores and binding. Potent quinolinium analogues identified in the current study exhibited very low micromolar potency ($IC_{50} \sim 1 \mu M$) that fully correlated with very low ligand–enzyme docking scores. The SAR described herein demonstrates quinolinium as a promising scaffold to selectively bind to the NNMT substrate-binding site

with a confirmation analogous to the endogenous NNMT substrate NCA and highlights some of the key structural features of quinolinium analogues for NNMT inhibition. These SAR results motivate future exploration of the chemical space surrounding the template moieties to develop potent, selective, and drug-like NNMT inhibitors. Ongoing research will investigate selectivity, confirm inhibitor activities using orthogonal assays, and develop potent NNMT inhibitors with improved “drug-like” physicochemical properties. Future studies will elucidate inhibitor mechanism-of-action and the structures of the NNMT–SAM–inhibitor ternary complexes, which will validate the molecular predictions derived from the current findings.

EXPERIMENTAL SECTION

Chemistry. Analogues and Chemicals. PubChem and Zinc similarity search programs were employed to identify commercially available analogues containing quinolinium, isoquinolinium, pyridinium, benzimidazolium, and benzothiazolium core structures and the analogues were purchased from established commercial suppliers, including Sigma-Aldrich (St. Louis, MO), Chembridge Corporation (San Diego, CA), ChemDiv (San Diego, CA), Specs (Hopkinton, RI), Cayman (Ann Arbor, MI), and Pfaltz & Bauer (Waterbury, CT). The identity of all the tested compounds was confirmed by ^1H NMR and HPLC-MS, and the purity was ensured to be $\geq 95\%$ (see Supporting Information for representative examples of HPLC analyses for compound purity). SAM was obtained from Sigma-Aldrich and nicotinamide from Fluka Analytical (Kwazulu Natal, South Africa; distributed by Sigma-Aldrich in the USA). 1-MNA chloride and S-5'-adenosylhomocysteine (SAH) were obtained from Cayman Chemical Company (Ann Arbor, MI). All compounds were made in double-distilled water.

General Procedures. Unless otherwise indicated, all reactions were conducted in standard commercially available glassware using standard synthetic chemistry methods and setup. All air- and moisture-sensitive reactions were performed under nitrogen atmosphere with dried solvents and glassware under anhydrous conditions. Starting materials and reagents were commercial compounds of the highest purity available and were used without purification. Solvents used for reactions were indicated as of commercial dry or extra-dry or analytical grade. Analytical thin layer chromatography was performed on aluminum plates coated with Merck Kieselgel 60F254 and visualized by UV irradiation (254 nm) or by staining with a solution of potassium permanganate. Flash column chromatography was performed on Biotage Isolera One 2.2 using commercial columns that were prepacked with Merck Kieselgel 60 (230–400 mesh) silica gel. Final compounds for biological testing are all $\geq 95\%$ purity as determined by HPLC-MS and ^1H NMR.

NMR. ^1H NMR experiments were recorded on Agilent DD2 400 MHz spectrometers at ambient temperature. Samples were dissolved and prepared in deuterated solvents (CDCl_3 , CD_3OD , and $\text{DMSO}-d_6$) with residual solvents being used as the internal standard in all cases. All deuterated solvent peaks were corrected to the standard chemical shifts (CDCl_3 , $d_{\text{H}} = 7.26$ ppm; CD_3OD , $d_{\text{H}} = 3.31$ ppm; $\text{DMSO}-d_6$, $d_{\text{H}} = 2.50$ ppm). Spectra were all manually integrated after automatic baseline correction. Chemical shifts (δ) are given in parts per million (ppm), and coupling constants (J) are given in Hertz (Hz). The proton spectra are reported as follows: d (multiplicity, coupling constant J , number of protons). The following abbreviations were used to explain the multiplicities: app = apparent, b = broad, d = doublet, dd = doublet of doublets, ddd = doublet of doublet of doublets, dddd = doublet of doublet of doublet of doublets, m = multiplet, s = singlet, t = triplet.

HPLC-MS. All samples were analyzed on Agilent 1290 series HPLC system comprised of binary pumps, degasser, UV detector, and autosampler coupled to an Agilent 6150 mass spectrometer. Purity was determined via UV detection with a bandwidth of 170 nm in the range from 230 to 400 nm. The general LC parameters were as follows:

Column, Zorbax Eclipse Plus C18, size 2.1 mm \times 50 mm; solvent A, 0.10% formic acid in water; solvent B, 0.00% formic acid in acetonitrile; flow rate, -0.7 mL/min; gradient, 5% B to 95% B in 5 min and hold at 95% B for 2 min; UV detector, channel 1 = 254 nm, channel 2 = 254 nm. Mass detector Agilent Jet Stream–Electron Ionization (AJS-ES).

General Procedure A: Quinolinyl or Isoquinolinyl Ring N-Alkylation Using MeI. A mixture of appropriate quinoline or isoquinoline derivative (1 equiv) and MeI (1.5 equiv unless otherwise indicated) in IPA (0.5M) was heated at 90 $^\circ\text{C}$ for 12 h. The reaction was cooled to ambient temperature, and the resulting precipitate was isolated by vacuum filtration, washed with a mixture of IPA/ Et_2O (v:v/1:1), and dried in vacuo.

General Procedure B: Quinolinyl or Isoquinolinyl Ring N-Alkylation Using MeOTf. A mixture of appropriate quinoline or isoquinoline derivative (1 equiv) and MeOTf (3 equiv unless otherwise indicated) in toluene (0.2M) was heated at 100 $^\circ\text{C}$ for 12 h. The reaction was cooled to ambient temperature and Et_2O added to induce precipitation. The resulting precipitate was isolated by vacuum filtration, washed with Et_2O , and dried in vacuo.

1,2-Dimethylquinolin-1-ium Trifluoromethanesulfonate (1b). According to general procedure B, the title compound was obtained as pale-orange powder (89% yield). ^1H NMR (400 MHz, $\text{DMSO}-d_6$) δ 9.08 (d, $J = 8.4$ Hz, 1H), 8.58 (d, $J = 9.2$ Hz, 1H), 8.39 (d, $J = 8.0$ Hz, 1H), 8.22 (dd, $J = 8.4, 7.6$ Hz, 1H), 8.10 (d, $J = 8.8$ Hz, 1H), 7.99 (dd, $J = 8.4, 7.6$ Hz, 1H), 4.44 (s, 3H), 3.07 (s, 3H). HPLC-MS (AJS-ES): R_t 1.13 min, m/z 158.2 [$\text{M}-\text{OSO}_2\text{CF}_3$].

2-Amino-1-methylquinolin-1-ium iodide (1c). According to general procedure A, the title compound was obtained as gray powder (26% yield). ^1H NMR (400 MHz, $\text{DMSO}-d_6$) δ 9.45 (br, 1H), 8.87 (br, 1H), 8.34 (d, $J = 9.2$ Hz, 1H), 8.01 (d, $J = 8.8$ Hz, 1H), 7.98 (d, $J = 8.8$ Hz, 1H), 7.87 (dd, $J = 8.4, 7.6$ Hz, 1H), 7.57 (dd, $J = 7.6, 7.6$ Hz, 1H), 7.17 (d, $J = 9.2$ Hz, 1H), 3.87 (s, 3H). HPLC-MS (AJS-ES): R_t 1.31 min, m/z 159.1 [$\text{M}-\text{I}$].

3-Amino-1-methylquinolin-1-ium iodide (1d). According to general procedure A, the title compound was obtained as orange powder (33% yield). ^1H NMR (400 MHz, $\text{DMSO}-d_6$) δ 8.81 (s, 1H), 8.21 (d, $J = 8.8$ Hz, 1H), 8.07 (d, $J = 7.2$ Hz, 1H), 7.98 (s, 1H), 7.78 (m, 2H), 6.56 (br, 2H), 4.51 (s, 3H). HPLC-MS (AJS-ES): R_t 1.08 min, m/z 159.1 [$\text{M}-\text{I}$].

1,3-Dimethylquinolin-1-ium trifluoromethanesulfonate (1e). According to general procedure A, the title compound was obtained as white powder (93% yield). ^1H NMR (400 MHz, $\text{DMSO}-d_6$) δ 9.47 (s, 1H), 9.08 (s, 1H), 8.46 (d, $J = 9.2$ Hz, 1H), 8.35 (d, $J = 9.2$ Hz, 1H), 8.21 (ddd, $J = 7.6, 6.8, 1.6$ Hz, 1H), 8.02 (ddd, $J = 7.6, 7.6, 0.8$ Hz, 1H), 4.60 (s, 3H), 2.64 (s, 3H). HPLC-MS (AJS-ES): R_t 0.39 min, m/z 158.1 [$\text{M}-\text{OSO}_2\text{CF}_3$].

1-Methyl-3-(methylamino)quinolin-1-ium iodide (1f). According to general procedure A, the title compound was obtained as orange powder (72% yield). ^1H NMR (400 MHz, $\text{DMSO}-d_6$) δ 8.90 (d, $J = 2.4$ Hz, 1H), 8.22 (dd, $J = 4.8, 4.4$ Hz, 1H), 8.10 (dd, $J = 4.8, 4.4$ Hz, 1H), 7.97 (d, $J = 1.6$ Hz, 1H), 7.78 (dd, $J = 4.8, 4.4$ Hz, 1H), 7.13 (br, 1H), 4.54 (s, 3H), 2.90 (s, 3H). HPLC-MS (AJS-ES): R_t 0.78 min, m/z 173.1 [$\text{M}-\text{I}$].

1-Methyl-3-(phenylamino)quinolin-1-ium iodide (1h). According to general procedure A, the title compound was obtained as orange–yellow powder (59% yield). ^1H NMR (400 MHz, $\text{DMSO}-d_6$) δ 9.33 (s, 1H), 9.17 (d, $J = 2.4$ Hz, 1H), 8.57 (d, $J = 2.0$ Hz, 1H), 8.31 (d, $J = 8.8$ Hz, 1H), 8.23 (d, $J = 8.0$ Hz, 1H), 7.93 (dd, $J = 8.0, 7.6$ Hz, 1H), 7.85 (dd, $J = 8.0, 6.8$ Hz, 1H), 7.44 (d, $J = 8.0$ Hz, 1H), 7.41 (d, $J = 7.6$ Hz, 1H), 7.34 (s, 1H), 7.32 (s, 1H), 7.11 (dd, $J = 8.0, 7.2$ Hz, 1H), 4.59 (s, 3H). HPLC-MS (AJS-ES): R_t 1.48 min, m/z 235.2 [$\text{M}-\text{I}$].

4-Amino-1-methylquinolin-1-ium iodide (1j). According to general procedure A, the title compound was obtained as gray powder (78% yield). ^1H NMR (400 MHz, $\text{DMSO}-d_6$) δ 8.97 (s, 2H), 8.51 (d, $J = 7.6$ Hz, 1H), 8.48 (d, $J = 8.4$ Hz, 1H), 8.06 (d, $J = 3.6$ Hz, 2H), 7.77 (m, 1H), 6.78 (d, $J = 7.2$ Hz, 1H), 4.11 (s, 3H). HPLC-MS (AJS-ES): R_t 0.69 min, m/z 159.1 [$\text{M}-\text{I}$].

5-Amino-1-methylquinolin-1-ium iodide (1k). According to general procedure A, the title compound was obtained using

stoichiometric amount of MeI (1 equiv) to isolate the product as red powder (62% yield). $^1\text{H NMR}$ (400 MHz, $\text{DMSO-}d_6$) δ 9.32 (d, $J = 8.4$ Hz, 1H), 9.28 (d, $J = 5.6$ Hz, 1H), 7.89 (dd, $J = 8.4, 8.0$ Hz, 1H), 7.85 (d, $J = 5.6$ Hz, 1H), 7.35 (d, $J = 8.8$ Hz, 1H), 7.11 (br, 2H), 7.02 (d, $J = 8.0$ Hz, 1H), 4.42 (s, 3H). HPLC-MS (AJS-ES): R_t 0.39 min, m/z 159.1 [M-I].

1,5-Dimethylquinolin-1-ium trifluoromethanesulfonate (1l). According to general procedure B, the title compound was obtained as white powder (99% yield). $^1\text{H NMR}$ (400 MHz, $\text{DMSO-}d_6$) δ 9.48 (d, $J = 5.6$ Hz, 1H), 9.35 (d, $J = 8.8$ Hz, 1H), 8.35 (d, $J = 8.8$ Hz, 1H), 8.17 (dd, $J = 8.4, 1.6$ Hz, 1H), 8.16 (d, $J = 8.8$ Hz, 1H), 7.90 (d, $J = 7.2$ Hz, 1H), 4.63 (s, 3H), 2.86 (s, 3H). HPLC-MS (AJS-ES): R_t 0.41 min, m/z 158.1 [M-OSO₂CF₃].

6-Fluoro-1-methylquinolin-1-ium iodide (1m). According to general procedure A, the title compound was obtained as yellow powder (75% yield). $^1\text{H NMR}$ (400 MHz, $\text{DMSO-}d_6$) δ 9.52 (s, 1H), 9.23 (d, $J = 8.8$ Hz, 1H), 8.64 (dd, $J = 9.6, 4.4$ Hz, 1H), 8.37 (dd, $J = 8.8, 2.8$ Hz, 1H), 8.26 (dddd, $J = 9.2, 9.2, 2.8, 2.0$ Hz, 1H), 8.21 (dd, $J = 8.4, 5.6$ Hz, 1H), 4.66 (s, 3H). HPLC-MS (AJS-ES): R_t 0.37 min, m/z 162.1 [M-I].

6-Amino-1-methylquinolin-1-ium iodide (1o). According to general procedure A, the title compound was obtained as orange-brown powder (58% yield). $^1\text{H NMR}$ (400 MHz, $\text{DMSO-}d_6$) δ 8.94 (s, 1H), 8.77 (d, $J = 9.2$ Hz, 1H), 8.18 (d, $J = 9.2$ Hz, 1H), 7.83 (m, 1H), 7.58 (d, $J = 9.2$ Hz, 1H), 7.11 (s, 1H), 6.46 (br, 2H), 4.48 (s, 3H). HPLC-MS (AJS-ES): R_t 0.74 min, m/z 159.1 [M-I].

7-Amino-1-methylquinolin-1-ium iodide (1q). According to general procedure A, the title compound was obtained using stoichiometric amount of MeI (1 equiv) to isolate the product as orange-brown powder (56% yield). $^1\text{H NMR}$ (400 MHz, $\text{DMSO-}d_6$) δ 8.92 (d, $J = 5.6$ Hz, 1H), 8.71 (d, $J = 8.0$ Hz, 1H), 8.02 (d, $J = 9.2$ Hz, 1H), 7.46 (dd, $J = 7.6, 6.4$ Hz, 1H), 7.38 (br, 2H), 7.29 (dd, $J = 9.2, 1.6$ Hz, 1H), 6.93 (d, $J = 1.2$ Hz, 1H), 4.23 (s, 3H). HPLC-MS (AJS-ES): R_t 0.52 min, m/z 159.1 [M-I].

1,7-Dimethylquinolin-1-ium Trifluoromethanesulfonate (1r). According to general procedure B, the title compound was obtained as white powder (87% yield). $^1\text{H NMR}$ (400 MHz, $\text{DMSO-}d_6$) δ 9.41 (d, $J = 6.0$ Hz, 1H), 9.20 (d, $J = 8.4$ Hz, 1H), 8.36 (d, $J = 8.4$ Hz, 1H), 8.34 (s, 1H), 8.08 (dd, $J = 8.4, 6.0$ Hz, 1H), 7.91 (d, $J = 8.4$ Hz, 1H), 4.59 (s, 3H), 2.72 (s, 3H). HPLC-MS (AJS-ES): R_t 0.41 min, m/z 158.1 [M-OSO₂CF₃].

3-Amino-6-fluoro-1-methylquinolin-1-ium iodide (2j). According to general procedure A, the title compound was obtained as yellow powder (58% yield). $^1\text{H NMR}$ (400 MHz, $\text{DMSO-}d_6$) δ 8.84 (d, $J = 2.0$ Hz, 1H), 8.35 (dd, $J = 9.6, 4.4$ Hz, 1H), 7.99 (dd, $J = 9.2, 2.8$ Hz, 1H), 7.94 (d, $J = 2.0$ Hz, 1H), 7.76 (ddd, $J = 8.8, 8.8, 3.2$ Hz, 1H), 6.78 (br, 2H), 4.56 (s, 3H). HPLC-MS (AJS-ES): R_t 0.22 min, m/z 177.1 [M-I].

1,8-Dimethyl-5-(trifluoromethyl)quinolin-1-ium Trifluoromethanesulfonate (2k). According to general procedure B, the title compound was obtained using excess amount of MeOTf (5 equiv) to isolate the product as pale-gray powder (69% yield). $^1\text{H NMR}$ (400 MHz, $\text{DMSO-}d_6$) δ 9.56 (d, $J = 6.0$ Hz, 1H), 9.24 (d, $J = 8.8$ Hz, 1H), 8.38 (d, $J = 7.6$ Hz, 1H), 8.29 (dd, $J = 8.8, 5.6$ Hz, 1H), 8.21 (d, $J = 7.6$ Hz, 1H), 4.89 (s, 3H), 3.15 (s, 3H). HPLC-MS (AJS-ES): R_t 0.92 min, m/z 226.1 [M-OSO₂CF₃].

4-Chloro-1-methyl-8-(trifluoromethyl)quinolin-1-ium Trifluoromethanesulfonate (2l). According to general procedure B, the title compound was obtained using excess amount of MeOTf (5 equiv) to isolate the product as pale gray powder (88% yield). $^1\text{H NMR}$ (400 MHz, $\text{DMSO-}d_6$) δ 8.56 (m, 1H), 8.33–8.10 (m, 2H), 7.59 (m, 1H), 6.47 (m, 1H), 3.93 (m, 3H). HPLC-MS (AJS-ES): R_t 3.01 min, m/z 246.1 [M-OSO₂CF₃].

2,3-Diamino-1-methylquinolin-1-ium iodide (2m). According to general procedure A, the title compound was obtained as tan powder (30% yield). $^1\text{H NMR}$ (400 MHz, $\text{DMSO-}d_6$) δ 8.76 (br, 2H), 7.89 (d, $J = 8.4$ Hz, 1H), 7.72 (d, $J = 8.0$ Hz, 1H), 7.54 (dd, $J = 8.0, 7.2$ Hz, 1H), 7.43 (dd, $J = 7.6, 7.6$ Hz, 1H), 7.35 (br, 1H), 5.94 (br, 2H), 3.95 (s, 3H). HPLC-MS (AJS-ES): R_t 1.41 min, m/z 174.1 [M-I].

1,2,8-Trimethylquinolin-1-ium Trifluoromethanesulfonate (2n).

According to general procedure B, the title compound was obtained as pale-tan powder (84% yield). $^1\text{H NMR}$ (400 MHz, $\text{DMSO-}d_6$) δ 9.01 (d, $J = 8.4$ Hz, 1H), 8.18 (d, $J = 8.0$ Hz, 1H), 8.04 (d, $J = 8.4$ Hz, 1H), 8.02 (d, $J = 8.4$ Hz, 1H), 7.83 (dd, $J = 7.6, 7.6$ Hz, 1H), 4.45 (s, 3H), 3.03 (s, 3H), 2.97 (s, 3H). HPLC-MS (AJS-ES): R_t 0.31 min, m/z 172.1 [M-OSO₂CF₃].

1,2,6-Trimethylquinolin-1-ium iodide (2o). According to general procedure A, the title compound was obtained as yellow-orange powder (36% yield). $^1\text{H NMR}$ (400 MHz, $\text{DMSO-}d_6$) δ 8.98 (d, $J = 8.4$ Hz, 1H), 8.49 (d, $J = 9.2$ Hz, 1H), 8.16 (s, 1H), 8.08 (m, 1H), 8.06 (m, 1H), 4.42 (s, 3H), 3.05 (d, $J = 4.0$ Hz, 3H), 2.60 (s, 3H). HPLC-MS (AJS-ES): R_t 1.00 min, m/z 172.1 [M-I].

1,2,4,8-Tetramethylquinolin-1-ium Trifluoromethanesulfonate (3c). According to general procedure B, the title compound was obtained as white powder (94% yield). $^1\text{H NMR}$ (400 MHz, $\text{DMSO-}d_6$) δ 8.25 (d, $J = 8.4$ Hz, 1H), 8.00 (d, $J = 6.8$ Hz, 1H), 7.96 (s, 1H), 7.84 (dd, $J = 8.0, 7.6$ Hz, 1H), 4.36 (s, 3H), 2.96 (s, 3H), 2.93 (s, 3H), 2.88 (s, 3H). HPLC-MS (AJS-ES): R_t 0.85 min, m/z 186.2 [M-OSO₂CF₃].

1,2,4,5,8-Pentamethylquinolin-1-ium Trifluoromethanesulfonate (3d). According to general procedure B, the title compound was obtained as tan powder (93% yield). $^1\text{H NMR}$ (400 MHz, $\text{DMSO-}d_6$) δ 7.83 (s, 1H), 7.80 (d, $J = 7.6$ Hz, 1H), 7.61 (d, $J = 8.0$ Hz, 1H), 4.24 (s, 3H), 3.04 (s, 3H), 2.91 (s, 6H), 2.78 (s, 3H). HPLC-MS (AJS-ES): R_t 1.01 min, m/z 200.2 [M-OSO₂CF₃].

1,2,4,6,8-Pentamethylquinolin-1-ium Trifluoromethanesulfonate (3e). According to general procedure B, the title compound was obtained as white powder (70% yield). $^1\text{H NMR}$ (400 MHz, $\text{DMSO-}d_6$) δ 8.03 (s, 1H), 7.91 (s, 1H), 7.85 (s, 1H), 4.35 (s, 3H), 2.93 (s, 3H), 2.90 (s, 3H), 2.85 (s, 3H), 2.55 (s, 3H). HPLC-MS (AJS-ES): R_t 1.11 min, m/z 200.2 [M-OSO₂CF₃].

1,2,4,7,8-Pentamethylquinolin-1-ium Trifluoromethanesulfonate (3f). According to general procedure B, the title compound was obtained as white powder (87% yield). $^1\text{H NMR}$ (400 MHz, $\text{DMSO-}d_6$) δ 8.13 (d, $J = 8.4$ Hz, 1H), 7.87 (s, 1H), 7.79 (d, $J = 8.4$ Hz, 1H), 4.28 (s, 3H), 2.94 (s, 3H), 2.86 (s, 3H), 2.67 (s, 3H), 2.57 (s, 3H). HPLC-MS (AJS-ES): R_t 1.04 min, m/z 200.2 [M-OSO₂CF₃].

5-Fluoro-1,2,4,8-tetramethylquinolin-1-ium Trifluoromethanesulfonate (3g). According to general procedure B, the title compound was obtained as tan powder (89% yield). $^1\text{H NMR}$ (400 MHz, $\text{DMSO-}d_6$) δ 7.99 (dd, $J = 7.6, 6.8$ Hz, 1H), 7.95 (s, 1H), 7.70 (dd, $J = 11.2, 8.8$ Hz, 1H), 4.32 (s, 3H), 2.95 (s, 6H), 2.86 (s, 3H). HPLC-MS (AJS-ES): R_t 0.87 min, m/z 204.2 [M-OSO₂CF₃].

7-Fluoro-1,2,4,8-tetramethylquinolin-1-ium Trifluoromethanesulfonate (3h). According to general procedure B, the title compound was obtained as white powder (78% yield). $^1\text{H NMR}$ (400 MHz, $\text{DMSO-}d_6$) δ 8.37 (dd, $J = 9.6, 6.8$ Hz, 1H), 7.95 (s, 1H), 7.89 (dd, $J = 9.2, 9.2$ Hz, 1H), 4.35 (s, 3H), 2.96 (s, 3H), 2.89 (s, 3H), 2.74 (s, 3H). HPLC-MS (AJS-ES): R_t 0.86 min, m/z 204.2 [M-OSO₂CF₃].

3-Amino-2-methylisoquinolin-1-ium iodide (4b). According to general procedure A, the title compound was obtained as tan-orange powder (40% yield). $^1\text{H NMR}$ (400 MHz, $\text{DMSO-}d_6$) δ 9.36 (s, 1H), 7.93 (d, $J = 8.4$ Hz, 1H), 7.81 (d, $J = 8.8$ Hz, 1H), 7.75 (dd, $J = 6.4, 0.8$ Hz, 1H), 7.71 (br, 2H), 7.41 (ddd, $J = 7.6, 7.6, 0.8$ Hz, 1H), 7.34 (s, 1H), 4.03 (s, 3H). HPLC-MS (AJS-ES): R_t 1.25 min, m/z 159.1 [M-I].

4-Bromo-2-methylisoquinolin-2-ium iodide (4c). According to general procedure A, the title compound was obtained using excess MeI (5 equiv) to isolate the product as tan-yellow powder (99% yield). $^1\text{H NMR}$ (400 MHz, $\text{DMSO-}d_6$) δ 10.09 (m, 1H), 9.24 (s, 1H), 8.56 (d, $J = 8.0$ Hz, 1H), 8.43–8.33 (m, 2H), 8.17 (dd, $J = 8.0, 8.0$ Hz, 1H), 4.45 (d, $J = 4.0$ Hz, 3H). HPLC-MS (AJS-ES): R_t 0.63 min, m/z 222.0, 224.0 [M-I].

6-Amino-2-methylisoquinolin-2-ium iodide (4d). According to general procedure A, the title compound was obtained as tan powder (68% yield). $^1\text{H NMR}$ (400 MHz, $\text{DMSO-}d_6$) δ 9.21 (s, 1H), 8.14 (dd, $J = 6.8, 1.2$ Hz, 1H), 8.00 (d, $J = 8.8$ Hz, 1H), 7.81 (d, $J = 6.8$ Hz, 1H), 7.35 (br, 2H), 7.27 (dd, $J = 8.8, 2.0$ Hz, 1H), 6.89 (d, $J = 1.6$ Hz, 1H), 4.16 (s, 3H). HPLC-MS (AJS-ES): R_t 0.78 min, m/z 159.1 [M-I].

6-Bromo-2-methylisoquinolin-2-ium Iodide (4e). According to general procedure A, the title compound was obtained using excess MeI (5 equiv) to isolate the product as brown–gray powder (99% yield). ¹H NMR (400 MHz, DMSO-*d*₆) δ 10.04 (s, 1H), 8.74 (d, *J* = 6.4 Hz, 1H), 8.69 (s, 1H), 8.49 (d, *J* = 6.4 Hz, 1H), 8.41 (d, *J* = 8.8 Hz, 1H), 8.21 (m, 1H), 4.45 (s, 3H). HPLC-MS (AJS-ES): *R*_f 1.25 min, *m/z* 222.0, 224.0 [M-1].

7-Amino-2-methylisoquinolin-2-ium Iodide (4f). According to general procedure A, the title compound was obtained as orange–yellow powder (53% yield). ¹H NMR (400 MHz, DMSO-*d*₆) δ 9.48 (s, 1H), 8.23 (d, *J* = 6.8 Hz, 1H), 8.20 (d, *J* = 6.8 Hz, 1H), 7.99 (d, *J* = 8.8 Hz, 1H), 7.55 (dd, *J* = 8.8, 2.4 Hz, 1H), 7.13 (d, *J* = 2.0 Hz, 1H), 6.52 (br, 2H), 4.34 (s, 3H). HPLC-MS (AJS-ES): *R*_f 0.78 min, *m/z* 159.1 [M-1].

Biology. Expression and Purification of Recombinant hNNMT. Because previous studies had demonstrated that a triple mutant human NNMT (tm-hNNMT; containing three site-directed mutations at surface exposed residues well removed from the catalytic sites) and wild-type NNMT had similar activities and kinetic parameters,²⁴ the tm-hNNMT enzyme was utilized in these current studies to facilitate planned crystallographic analysis of inhibitor:NNMT complexes and to enable direct comparison to previous kinetic studies. The tm-hNNMT sequence was cloned into an isopropyl-β-D-1-thiogalactopyranoside (IPTG)-inducible plasmid pJ401 expression vector was purchased from DNA 2.0 (Menlo Park, CA). tm-hNNMT was expressed in competent *Escherichia coli* BL21/DE3 cells and purified using a nickel-based ion affinity chromatography procedure as described in detail previously.³³

NNMT Activity Assay: HPLC Instrumentation and Chromatographic Conditions. An HPLC-UV method for the detection of NNMT catalyzed product 1-MNA was developed by modifying a previously reported protocol.²⁶ A Shimadzu 10AVP HPLC System (Shimadzu, Kyoto, Japan) with manual sample injector was used to run the HPLC-UV method with mobile phase comprising of 10 mM 1-heptanesulfonate, 20 mM potassium phosphate monobasic [pH 3.1], 4% methanol, and 3% acetonitrile. Chromatographic separation was achieved on a Platinum EPS C18 100 Å 3 μm (length, 53 mm; internal diameter, 7 mm; maximum pressure, 5000 PSIG) analytical column (Alltech Associates, Inc., Deerfield, IL) at ambient temperature with a flow rate of the mobile phase maintained at 1 mL/min. Sample injection volume was 100 μL with a run time of 20 min per sample.

1-MNA Calibration Curve and NNMT Activity Assay. To establish a linear curve for the detection of 1-MNA peak, 10–0.3125 μM/100 μL half-fold serially diluted samples of 1-MNA were prepared in reaction buffer containing 1 mM Tris [pH 8.6], 1 mM DTT, 10% TCA, 4% methanol, and water. Similarly, samples of substrate NCA (100 μM), methyl donor SAM (5 μM), and SAH (5 μM) were run individually in reaction buffer (1 mM Tris [pH 8.6], 1 mM DTT, 10% TCA, 4% methanol, and water) to identify elution times and define substrate, cofactor, and product peaks. 1-MNA, NCA, SAM, and SAH peaks were detected using a wavelength of 265 nm. To determine NNMT activity, 5 μL of 10 mM NCA (in water) and 2.5 μL of 1 mM SAM (in water) were added/500 μL of reaction buffer. The reaction was initiated by adding 4 μL of 25 μM stock purified NNMT protein (final concentration of NNMT in the reaction was 200 nM) and incubated on a heat block at 37 °C for 6 min, following which the reaction was terminated by the addition of a mixture of 10% TCA and 4% methanol, vortexing for 5 s, and centrifuging at 14000g for 2 min to precipitate the protein. Peak area and peak height for 1-MNA were determined by running 100 μL of the supernatant using the chromatographic conditions described above. Reactions were run in the absence of NNMT as control samples in each experiment.

NNMT IC₅₀ Curves for Inhibitors. NNMT reaction products were analyzed by HPLC as described above and used to construct inhibition curves for 1-MQ, 1-MQ analogues, 2-methylisoquinolinium, 2-methylisoquinolinium analogues, and analogues containing pyridinium, benzimidazolium, and benzothiazolium cores. Compounds were initially tested for NNMT inhibition activity at 100 μM or 1 mM concentration (compounds with no activity at 100 μM were tested at 1 mM concentration). Compounds with >50% inhibitory activity at 1

mM were advanced to comprehensive concentration–response analysis (concentration range of 10 nM–1 mM/100 μL reaction). Otherwise, IC₅₀ values are reported as either >1000 μM or no observable inhibition (NI). Data were normalized and reported as % NNMT activity against concentrations tested (μM). IC₅₀ values were determined by three parameter nonlinear regression [inhibitor conc vs normalized % NNMT activity] fitted by least-squares method (Graphpad Prism 7.0, GraphPad Software Inc., La Jolla, CA). For compounds with IC₅₀ values lower than 20 μM and/or *R*² values for the curve fit <0.8, data sets were run in duplicates or triplicates and averaged for analyses.

Molecular Docking. Quinolinium, isoquinolinium, pyridinium, benzimidazolium, and benzothiazolium analogues were docked to substrate-binding site of NNMT [PDB 3ROD, monomer chain A]²⁴ using the AutoDock Vina program.³⁵ AutoDockTools (ADT) was used to add polar hydrogen atoms to the NNMT structure and parametrize the resultant structure using Autodock4 default atom types. Three-dimensional conformations for each small molecule structure was produced in MarvinSketch, converted to Mol2 format, and parametrized with ADT to establish rotatable bonds and atom types. The Vina program was used to calculate the lowest scoring pose/conformation for each analogue bound to NNMT, using a search box (24 × 24 × 24) centered within the nicotinamide binding pocket (search space centered at -29, -20, 4 Å) and an “exhaustiveness” parameter of 20. During docking calculations, the protein structure was fixed as determined from the crystal structure while docked ligands had conformational flexibility around identified rotatable bonds. Analogue conformations with the lowest (i.e., most negative) Vina docking scores corresponded to the bound inhibitor conformation with most favorable interactions within the substrate-binding site of the NNMT protein. A linear analysis using Pearson’s correlation was performed between calculated Vina docking scores and the logarithm of experimentally determined IC₅₀ [log(IC₅₀)] for the respective compounds (Graphpad Prism 7.0, GraphPad Software Inc., La Jolla, CA).

The predicted orientations and conformations generated from the Vina docking for analogues with the lowest IC₅₀ values within each scaffold series were analyzed using the AutoDock Tools (ADT) molecular graphics program. The structure of ligands docked to NNMT (PDB 3ROD) were also used in LigPlot+³⁶ and Maestro 11 (Schrodinger LLC, New York, NY)³⁷ to analyze hydrogen bonding patterns and intermolecular interactions within 4 Å distance between residues in the NNMT substrate-binding pocket and the inhibitor analogues. The NCA substrate site in NNMT/inhibitor contact diagrams was used to describe and develop the initial SAR parameters for this system.

■ ASSOCIATED CONTENT

Supporting Information

The Supporting Information is available free of charge on the ACS Publications website at DOI: 10.1021/acs.jmedchem.7b00389.

Detailed synthesis of reaction intermediates and quinoline/isoquinoline precursors; ¹H NMR spectra of analogues synthesized in house and reaction intermediates; table of analogues purchased from commercial vendors; table of IC₅₀ and Vina scores for *N*-methyl analogues (PDF)

Molecular formula strings (CSV)

■ AUTHOR INFORMATION

Corresponding Author

*Phone: (409) 747-4749. Fax: (409) 747-4745. Email: watowich@xray.utmb.edu.

ORCID

Stanley J. Watowich: 0000-0002-1660-1818

Author Contributions

All authors contributed in a significant way to the manuscript. H.N. conducted experiments, data analysis, and interpretation, prepared the manuscript, and participated in the conceptualization of the project and design of analogues. H.L.W. participated in the design of analogues, synthesized all analogues reported in the manuscript, and wrote/edited the manuscript. V.V. conducted biochemical assays and performed IC₅₀ calculations. J.D.H., S.F.M., and S.J.W. conceptualized the project, designed analogues, analyzed and interpreted data, and edited the manuscript. All authors have read and approved the final manuscript.

Notes

The authors declare no competing financial interest.

ACKNOWLEDGMENTS

We thank Drs. C. Finnerty and C. Porter for helpful discussions. This work was supported by Department of Defense Peer Reviewed Medical Research Program grant PR141776 (S.J.W.) and a University of Texas Medical Branch Technology Commercialization Award (S.J.W.).

ABBREVIATIONS USED

NNMT, nicotinamide-*N*-methyltransferase; SAR, structure–activity relationship; SAM, *S*-(*S*'-adenosyl)-*L*-methionine; NCA, nicotinamide; 1-MNA, 1-methylnicotinamide; SAH, *S*-*S*'-adenosylhomocysteine; 1-MQ, 1-methylquinolinium; hNNMT, human nicotinamide-*N*-methyltransferase; hPNMT, human phenylethanolamine-*N*-methyltransferase; IPTG, isopropyl- β -D-1-thiogalactopyranoside; IPA, 2-propanol; MeOTf, methyl trifluoromethanesulfonate; MeI, iodomethane

REFERENCES

- (1) Alston, T. A.; Abeles, R. H. Substrate specificity of nicotinamide methyltransferase isolated from porcine liver. *Arch. Biochem. Biophys.* **1988**, *260* (2), 601–608.
- (2) Aksoy, S.; Szumlanski, C. L.; Weinshilboum, R. M. Human liver nicotinamide *N*-methyltransferase. cDNA cloning, expression, and biochemical characterization. *J. Biol. Chem.* **1994**, *269* (20), 14835–14840.
- (3) Cantoni, G. L. Methylation of nicotinamide with soluble enzyme system from rat liver. *J. Biol. Chem.* **1951**, *189* (1), 203–216.
- (4) Rini, J.; Szumlanski, C.; Guercioli, R.; Weinshilboum, R. M. Human liver nicotinamide *N*-methyltransferase: ion-pairing radiochemical assay, biochemical properties and individual variation. *Clin. Chim. Acta* **1990**, *186* (3), 359–374.
- (5) Yan, L.; Otterness, D. M.; Craddock, T. L.; Weinshilboum, R. M. Mouse liver nicotinamide *N*-methyltransferase: cDNA cloning, expression, and nucleotide sequence polymorphisms. *Biochem. Pharmacol.* **1997**, *54* (10), 1139–1149.
- (6) Riederer, M.; Erwa, W.; Zimmermann, R.; Frank, S.; Zechner, R. Adipose tissue as a source of nicotinamide *N*-methyltransferase and homocysteine. *Atherosclerosis* **2009**, *204* (2), 412–417.
- (7) Xu, J.; Moatamed, F.; Caldwell, J. S.; Walker, J. R.; Kraiem, Z.; Taki, K.; Brent, G. A.; Hershman, J. M. Enhanced expression of nicotinamide *N*-methyltransferase in human papillary thyroid carcinoma cells. *J. Clin. Endocrinol. Metab.* **2003**, *88* (10), 4990–4996.
- (8) Roessler, M.; Rollinger, W.; Palme, S.; Hagmann, M. L.; Berndt, P.; Engel, A. M.; Schneider, B.; Pfeffer, M.; Andres, H.; Karl, J.; Bodenmuller, H.; Ruschoff, J.; Henkel, T.; Rohr, G.; Rossol, S.; Rosch, W.; Langen, H.; Zolg, W.; Tacke, M. Identification of nicotinamide *N*-methyltransferase as a novel serum tumor marker for colorectal cancer. *Clin. Cancer Res.* **2005**, *11* (18), 6550–6557.
- (9) Sartini, D.; Muzzonigro, G.; Milanese, G.; Pierella, F.; Rossi, V.; Emanuelli, M. Identification of nicotinamide *N*-methyltransferase as a

novel tumor marker for renal clear cell carcinoma. *J. Urol.* **2006**, *176* (5), 2248–2254.

- (10) Sartini, D.; Santarelli, A.; Rossi, V.; Goteri, G.; Rubini, C.; Ciavarella, D.; Lo Muzio, L.; Emanuelli, M. Nicotinamide *N*-methyltransferase upregulation inversely correlates with lymph node metastasis in oral squamous cell carcinoma. *Mol. Med.* **2007**, *13* (7–8), 415–421.

- (11) Tomida, M.; Mikami, I.; Takeuchi, S.; Nishimura, H.; Akiyama, H. Serum levels of nicotinamide *N*-methyltransferase in patients with lung cancer. *J. Cancer Res. Clin. Oncol.* **2009**, *135* (9), 1223–1229.

- (12) Parsons, R. B.; Smith, M. L.; Williams, A. C.; Waring, R. H.; Ramsden, D. B. Expression of nicotinamide *N*-methyltransferase (E.C. 2.1.1.1) in the Parkinsonian brain. *J. Neuropathol. Exp. Neurol.* **2002**, *61* (2), 111–124.

- (13) Williams, A. C.; Ramsden, D. B. Autotoxicity, methylation and a road to the prevention of Parkinson's disease. *J. Clin. Neurosci.* **2005**, *12* (1), 6–11.

- (14) Salek, R. M.; Maguire, M. L.; Bentley, E.; Rubtsov, D. V.; Hough, T.; Cheeseman, M.; Nunez, D.; Sweatman, B. C.; Haselden, J. N.; Cox, R. D.; Connor, S. C.; Griffin, J. L. A metabolomic comparison of urinary changes in type 2 diabetes in mouse, rat, and human. *Physiol. Genomics* **2007**, *29* (2), 99–108.

- (15) Kraus, D.; Yang, Q.; Kong, D.; Banks, A. S.; Zhang, L.; Rodgers, J. T.; Pirinen, E.; Pulinilkunnil, T. C.; Gong, F.; Wang, Y. C.; Cen, Y.; Sauve, A. A.; Asara, J. M.; Peroni, O. D.; Monia, B. P.; Bhanot, S.; Alhonen, L.; Puigserver, P.; Kahn, B. B. Nicotinamide *N*-methyltransferase knockdown protects against diet-induced obesity. *Nature* **2014**, *508* (7495), 258–262.

- (16) Kannt, A.; Pfenninger, A.; Teichert, L.; Tonjes, A.; Dietrich, A.; Schon, M. R.; Kloting, N.; Bluher, M. Association of nicotinamide-*N*-methyltransferase mRNA expression in human adipose tissue and the plasma concentration of its product, 1-methylnicotinamide, with insulin resistance. *Diabetologia* **2015**, *58* (4), 799–808.

- (17) Liu, M.; Li, L.; Chu, J.; Zhu, B.; Zhang, Q.; Yin, X.; Jiang, W.; Dai, G.; Ju, W.; Wang, Z.; Yang, Q.; Fang, Z. Serum *N*(1)-methylnicotinamide is associated with obesity and diabetes in Chinese. *J. Clin. Endocrinol. Metab.* **2015**, *100* (8), 3112–3117.

- (18) Martin, J. L.; McMillan, F. M. SAM (dependent) I AM: the *S*-adenosylmethionine-dependent methyltransferase fold. *Curr. Opin. Struct. Biol.* **2002**, *12* (6), 783–793.

- (19) Syed, S. K.; Kim, S.; Paik, W. K. Comparative studies on *S*-adenosyl-*L*-methionine binding sites of protein *N*-methyltransferases, using 8-azido-*S*-adenosyl-*L*-methionine as photoaffinity probe. *J. Protein Chem.* **1993**, *12* (5), 603–612.

- (20) Copeland, R. A.; Solomon, M. E.; Richon, V. M. Protein methyltransferases as a target class for drug discovery. *Nat. Rev. Drug Discovery* **2009**, *8* (9), 724–732.

- (21) Borchardt, R. T.; Eiden, L. E.; Wu, B.; Rutledge, C. O. Sinefungin, a potent inhibitor of *S*-adenosylmethionine: protein *O*-methyltransferase. *Biochem. Biophys. Res. Commun.* **1979**, *89* (3), 919–924.

- (22) Daigle, S. R.; Olhava, E. J.; Therkelsen, C. A.; Basavapathruni, A.; Jin, L.; Boriack-Sjodin, P. A.; Allain, C. J.; Klaus, C. R.; Raimondi, A.; Scott, M. P.; Waters, N. J.; Chesworth, R.; Moyer, M. P.; Copeland, R. A.; Richon, V. M.; Pollock, R. M. Potent inhibition of DOT1L as treatment of MLL-fusion leukemia. *Blood* **2013**, *122* (6), 1017–1025.

- (23) Cai, X. C.; Kapilashrami, K.; Luo, M. Synthesis and assays of inhibitors of methyltransferases. *Methods Enzymol.* **2016**, *574*, 245–308.

- (24) Peng, Y.; Sartini, D.; Pozzi, V.; Wilk, D.; Emanuelli, M.; Yee, V. C. Structural basis of substrate recognition in human nicotinamide *N*-methyltransferase. *Biochemistry* **2011**, *50* (36), 7800–7808.

- (25) van Haren, M. J.; Sastre Torano, J.; Sartini, D.; Emanuelli, M.; Parsons, R. B.; Martin, N. I. A rapid and efficient assay for the characterization of substrates and inhibitors of nicotinamide *N*-methyltransferase. *Biochemistry* **2016**, *55* (37), 5307–5315.

- (26) Patel, M.; Vasaya, M. M.; Asker, D.; Parsons, R. B. HPLC-UV method for measuring nicotinamide *N*-methyltransferase activity in

biological samples: evidence for substrate inhibition kinetics. *J. Chromatogr. B: Anal. Technol. Biomed. Life Sci.* **2013**, *921–922*, 87–95.

(27) Bissantz, C.; Kuhn, B.; Stahl, M. A medicinal chemist's guide to molecular interactions. *J. Med. Chem.* **2010**, *53* (14), 5061–5084.

(28) Muller, K.; Faeh, C.; Diederich, F. Fluorine in pharmaceuticals: looking beyond intuition. *Science* **2007**, *317* (5846), 1881–1886.

(29) Cowan-Jacob, S. W.; Fendrich, G.; Floersheimer, A.; Furet, P.; Liebetanz, J.; Rummel, G.; Rheinberger, P.; Centeleghe, M.; Fabbro, D.; Manley, P. W. Structural biology contributions to the discovery of drugs to treat chronic myelogenous leukaemia. *Acta Crystallogr., Sect. D: Biol. Crystallogr.* **2007**, *63* (1), 80–93.

(30) Hann, M. M.; Keseru, G. M. Finding the sweet spot: the role of nature and nurture in medicinal chemistry. *Nat. Rev. Drug Discovery* **2012**, *11* (5), 355–365.

(31) Yang, W.; Li, L.; Wang, Y.; Wu, X.; Li, T.; Yang, N.; Su, M.; Sheng, L.; Zheng, M.; Zang, Y.; Li, J.; Liu, H. Design, synthesis and biological evaluation of isoquinoline-based derivatives as novel histone deacetylase inhibitors. *Bioorg. Med. Chem.* **2015**, *23* (17), 5881–5890.

(32) Nishikawa-Shimono, R.; Sekiguchi, Y.; Koami, T.; Kawamura, M.; Wakasugi, D.; Watanabe, K.; Wakahara, S.; Kimura, K.; Yamanobe, S.; Takayama, T. Isoquinoline derivatives as potent CRTH2 antagonists: design, synthesis and SAR. *Bioorg. Med. Chem.* **2013**, *21* (24), 7674–7685.

(33) Neelakantan, H.; Vance, V.; Wang, H. L.; McHardy, S. F.; Watowich, S. J. Noncoupled fluorescent assay for direct real-time monitoring of nicotinamide N-methyltransferase activity. *Biochemistry* **2017**, *56* (6), 824–832.

(34) Viswanathan, U.; Tomlinson, S. M.; Fonner, J. M.; Mock, S. A.; Watowich, S. J. Identification of a novel inhibitor of dengue virus protease through use of a virtual screening drug discovery Web portal. *J. Chem. Inf. Model.* **2014**, *54* (10), 2816–2825.

(35) Trott, O.; Olson, A. J. AutoDock Vina: improving the speed and accuracy of docking with a new scoring function, efficient optimization, and multithreading. *J. Comput. Chem.* **2010**, *31* (2), 455–461.

(36) Wallace, A. C.; Laskowski, R. A.; Thornton, J. M. LIGPLOT: a program to generate schematic diagrams of protein-ligand interactions. *Protein Eng., Des. Sel.* **1995**, *8* (2), 127–134.

(37) *Schrödinger Release 2017-1: Maestro*; Schrödinger, LLC: New York, 2017.

Supporting Information

Structure Activity Relationship for Small Molecule Inhibitors of Nicotinamide N-Methyltransferase

Harshini Neelakantan,¹ Hua-Yu Leo Wang,² Virginia Vance,¹ Jonathan D. Homme,¹ Stanton F. McHardy,² Stanley J. Watowich^{1}*

¹Department of Biochemistry and Molecular Biology, University of Texas Medical Branch, Galveston, Texas 77550 USA

²Department of Chemistry and Center for Innovative Drug Discovery, The University of Texas at San Antonio, San Antonio, Texas 78249 USA

³Department of Pharmacology and Toxicology, University of Texas Medical Branch, Galveston, Texas 77550 USA

Corresponding Author

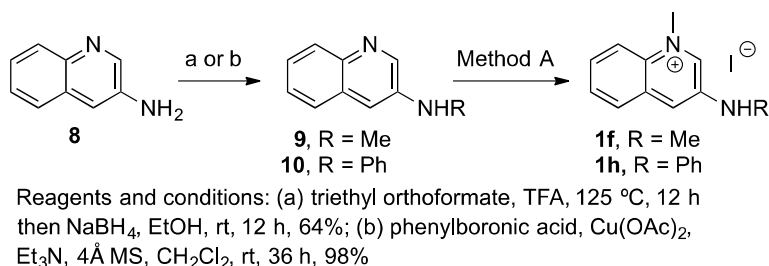
*Phone: (409) 747-4749. Email: watowich@xray.utmb.edu.

Table of Contents

Section 1.	Experimental procedures	S4
Section 2.	¹ H NMR spectra of analogs synthesized in house	
	¹ H NMR of 1b	S13
	¹ H NMR of 1c	S13
	¹ H NMR of 1d	S14
	¹ H NMR of 1e	S14
	¹ H NMR of 1f	S15
	¹ H NMR of 1h	S15
	¹ H NMR of 1j	S16
	¹ H NMR of 1k	S16
	¹ H NMR of 1l	S17
	¹ H NMR of 1m	S17
	¹ H NMR of 1o	S18
	¹ H NMR of 1q	S18
	¹ H NMR of 1r	S19
	¹ H NMR of 2j	S19
	¹ H NMR of 2k	S20
	¹ H NMR of 2l	S20
	¹ H NMR of 2m	S21
	¹ H NMR of 2n	S21
	¹ H NMR of 2o	S22
	¹ H NMR of 3c	S22
	¹ H NMR of 3d	S23
	¹ H NMR of 3e	S23
	¹ H NMR of 3f	S24
	¹ H NMR of 3g	S24
	¹ H NMR of 3h	S25
	¹ H NMR of 4b	S25

	¹ H NMR of 4c	S26
	¹ H NMR of 4d	S26
	¹ H NMR of 4e	S27
	¹ H NMR of 4f	S27
Section 3.	¹ H NMR spectra of reaction intermediates	
	¹ H NMR of 9	S28
	¹ H NMR of 10	S28
	¹ H NMR of 12	S29
	¹ H NMR of 12	S29
	¹ H NMR of 13	S30
	¹ H NMR of 14	S30
	¹ H NMR of 15	S31
	¹ H NMR of 15a	S31
	¹ H NMR of 16	S32
	¹ H NMR of 19c	S32
	¹ H NMR of 19d	S33
	¹ H NMR of 19e	S33
	¹ H NMR of 19f	S34
	¹ H NMR of 19g	S34
	¹ H NMR of 19h	S35
Section 4.	Representative examples of HPLC/MS purity	S35
Table S1.	Analogs purchased from commercial vendors	S38
Table S2.	Vina docking scores	S39

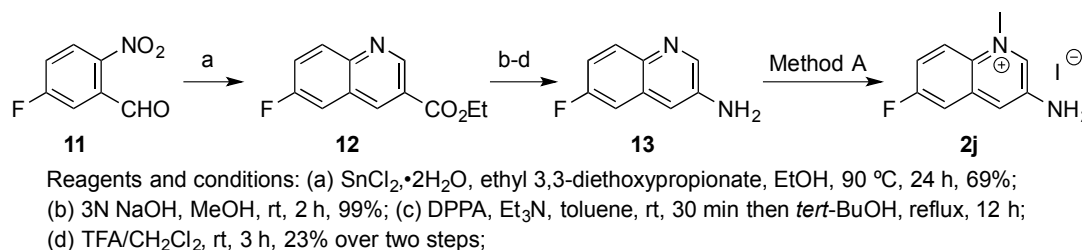
Section 1. Experimental procedures



N-methylquinolin-3-amine (9). To a 250 mL pressure vessel was added 3-amino-quinoline **8** (1 g, 6.94 mmol) and triethyl orthoformate (7.0 mL), followed by addition of TFA (79 mg, 0.69 mmol). The reaction vessel was sealed and heated to 125 °C for 12 h. The reaction mixture was then concentrated under reduced pressure, and the residue was re-dissolved in EtOH (10 mL), followed by addition of NaBH₄ (1.44 g, 38.2 mmol). The mixture was stirred at rt overnight. H₂O (10 mL) was added to the reaction and extracted with CH₂Cl₂ (15 mL x3). The combined CH₂Cl₂ extracts were washed with brine and dried over Na₂SO₄. The crude material was filtered and concentrated under reduced pressure, and purified by Biotage flash chromatography (gradient elution, 0-50% EtOAc in hexanes) to obtain the title compound **9** as orange solid (701 mg, 4.43 mmol, 64% yield). ¹H NMR (400 MHz, DMSO-d₆) δ 8.41 (d, *J* = 2.8 Hz, 1H), 7.74 (d, *J* = 8.0 Hz, 1H), 7.63 (d, *J* = 8.0 Hz, 1H), 7.36 (dd, *J* = 8.0, 6.8 Hz, 1H), 7.28 (dd, *J* = 7.6, 7.6 Hz, 1H), 6.93 (d, *J* = 2.4 Hz, 1H), 6.29 (d, *J* = 4.4 Hz, 1H), 2.75 (d, *J* = 5.2 Hz, 3H); HPLC-MS (AJS-ES): Rt 1.87 min, m/z 159.1 [M+H].

N-phenylquinolin-3-amine (10). To a mixture of 3-amino-quinoline **8** (500 mg, 3.47 mmol) and 4 Å Molecular Sieve in anhydrous CH₂Cl₂ (18 mL) was added phenylboronic acid (1.27 g, 10.4 mmol), TEA (1.05 g, 10.4 mmol) and Cu(OAc)₂ (1.58 g, 8.67 mmol). The resulting mixture was stirred at rt for 36 h. The reaction was quenched with 5% NH₃ (aq) (20 mL) and extracted with

EtOAc (20 mL x3). The combined EtOAc extracts were washed with brine and dried over Na₂SO₄. The crude material was filtered and concentrated under reduced pressure, and purified by Biotage flash chromatography (gradient elution, 0-60% EtOAc in hexanes) to obtain the title compound **10** as yellow solid (755 mg, 3.43 mmol, 98% yield). ¹H NMR (400 MHz, DMSO-d₆) δ 8.71 (d, *J* = 2.8 Hz, 1H), 8.04 (d, *J* = 1.2 Hz, 1H), 7.89 – 7.76 (m, 3H), 7.47 (m, 1H), 7.41 – 7.24 (m, 4H), 6.95 (dd, *J* = 7.2, 7.2 Hz, 1H); HPLC-MS (AJS-ES): Rt 3.12 min, m/z 221.1 [M+H].



Ethyl 6-fluoroquinoline-3-carboxylate (12). The 2,4-unsubstituted quinoline-3-ester was prepared by following the literature procedure.¹ To a 250 mL pressure vessel was added 5-fluoro-2-nitro-benzaldehyde **11** (3 g, 17.7 mmol) and EtOH (88 mL), followed by addition of SnCl₂·2H₂O (16 g, 70.9 mmol) and ethyl 3,3-diethoxypropionate (8.4 g, 44.3 mmol). The reaction vessel was sealed and heated to 90 °C for 24 h. The reaction mixture was concentrated under reduced pressure, and the residue was diluted with EtOAc (50 mL) and washed with saturated NaHCO₃ solution (20 mL). The resulting emulsion was filtered through Celite and washed with EtOAc until complete recovery of the product (monitored by TLC; 20% EtOAc in hexanes). The combined filtrate was washed with brine and dried over Na₂SO₄. The crude material was filtered and concentrated under reduced pressure, and purified by Biotage flash

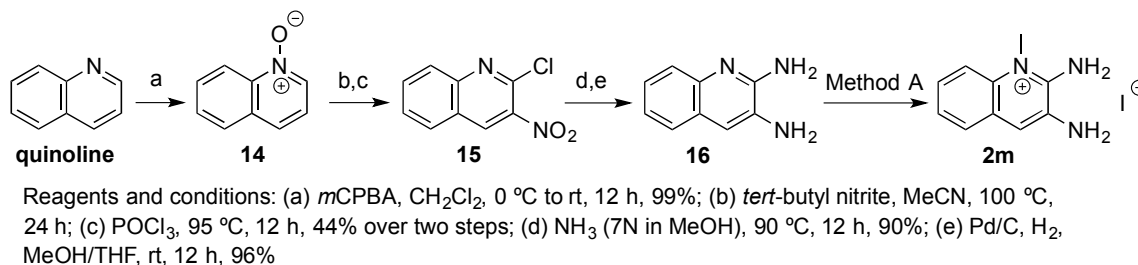
¹ Venkatesan, H.; Hocutt, F. M.; Jones, T. K.; Rabinowitz, M. H. A one-step synthesis of 2,4-unsubstituted quinoline-3-carboxylic acid esters from o-nitrobenzaldehydes. *J. Org. Chem.* **2010**, *75*, 3488-3491.

chromatography (gradient elution, 0-30% EtOAc in hexanes) to obtain the title compound **12** as yellow solid (2.68 g, 12.2 mmol, 69% yield). ¹H NMR was in accordance with the literature data reported by Venkatesan et al. ¹H NMR (400 MHz, CDCl₃) δ 9.41 (d, *J* = 2.0 Hz, 1H), 8.79 (d, *J* = 1.6 Hz, 1H), 8.17 (dd, *J* = 9.2, 5.2 Hz, 1H), 7.60 (ddd, *J* = 7.6, 7.6, 2.8 Hz, 1H), 7.55 (dd, *J* = 8.4, 2.8 Hz, 1H), 4.48 (q, *J* = 6.8 Hz, 2H), 1.46 (t, *J* = 7.2 Hz, 3H).

6-fluoroquinolin-3-amine (13). Ethyl 6-fluoroquinoline-3-carboxylate **12** (2.68 g, 12.2 mmol) was dissolved in methanol (120 mL) and added 3N NaOH (aq) (6.1 mL, 18.3 mmol). The reaction was stirred at rt for 2 h and monitored by LC/MS. Upon reaction completion, 1N HCl (aq) was carefully added to the reaction mixture until pH < 6. The reaction mixture was concentrated under reduced pressure, and the slurry was diluted with H₂O (50 mL). The precipitate was isolated by vacuum filtration and washed repeatedly with H₂O. Any residual amount of H₂O was further removed by azeotropic distillation with toluene and by high-vacuum overnight to obtain the title compound acid **12a** as pale yellow-orange solid (2.33 g, 12.1 mmol, 99% yield). ¹H NMR (400 MHz, DMSO-d₆) δ 9.33 (d, *J* = 1.6 Hz, 1H), 8.86 (s, 1H), 8.11 (dd, *J* = 9.2, 5.2 Hz, 1H), 7.93 (dd, *J* = 9.2, 2.4 Hz, 1H), 7.74 (ddd, *J* = 8.8, 8.8, 2.8 Hz, 1H); HPLC-MS (AJS-ES): Rt 2.04 min, m/z 192.0 [M+H].

To a suspension of 6-fluoroquinoline-3-carboxylic acid **12a** (2.33 g, 12.1 mmol) in anhydrous toluene (120 mL) was added triethylamine (1.89 g, 14.6 mmol), followed by addition of DPPA (4.03 g, 14.6 mmol). The reaction mixture was stirred at rt for 30 min and added *tert*-butanol (3.61 g, 48.8 mmol), and the resulting mixture was heated to reflux for 12 h. Noted that LC/MS showed both NH-Boc intermediate and the title amine product. The mixture was concentrated under reduced pressure and purified by Biotage flash chromatography (gradient elution, 0-50%

EtOAc in hexanes) to obtain the NH-Boc intermediate as white solid (170 mg, 0.65 mmol) and switched the gradient to 0-20% MeOH in CH₂Cl₂ to obtain the title compound **13** as pale orange solid (350 mg, 2.16 mmol, 18% yield). The NH-Boc intermediate (170 mg, 0.65 mmol) was dissolved in CH₂Cl₂ (2.5 mL) and added TFA/CH₂Cl₂ (v:v/1:1, 2.5 mL) and stirred at rt for 3 h. The mixture was concentrated under reduced pressure and neutralized by 3M NH₃/MeOH solutions, and purified by Biotage flash chromatography (gradient elution, 0-5% 3M NH₃/MeOH in CH₂Cl₂) to recover the title compound **13** (98 mg, 0.60 mmol, 93% yield; 23% yield over two steps). ¹H NMR (400 MHz, DMSO-d₆) δ 8.39 (d, *J* = 2.4 Hz, 1H), 7.78 (d, *J* = 9.2, 5.6 Hz, 1H), 7.37 (d, *J* = 10.0, 2.0 Hz, 1H), 7.16 (dddd, *J* = 8.8, 8.8, 2.0, 2.0 Hz, 1H), 7.09 (d, *J* = 2.0 Hz, 1H), 5.82 (br, 2H); HPLC-MS (AJS-ES): Rt 1.79 min, m/z 163.1 [M+H].



Quinoline-1-oxide (14). To a solution of quinoline (5g, 38.7 mmol) in anhydrous CH₂Cl₂ (120 mL) was added *m*CPBA in several portion over 1 h at 0 °C. The reaction mixture was left stirring for 12 h without replenishing the ice-bath. The mixture was washed with 1M NaOH aqueous solution and extracted with IPA/CHCl₃ (v:v 1:4) until complete recovery of the desired product (monitored by TLC; 5% MeOH in CH₂Cl₂). The combined organic layer was washed with brine and dried over Na₂SO₄. The crude material was filtered and concentrated under reduced pressure, and purified by Biotage flash chromatography (gradient elution, 0-8% MeOH in CH₂Cl₂) to obtain the quinoline-1-oxide **14** as pale yellow gel (5.60 g, 38.6 mmol, 99% yield). ¹H NMR

(400 MHz, DMSO- d_6) δ 8.59 (d, J = 6.4 Hz, 1H), 8.53 (d, J = 8.8 Hz, 1H), 8.09 (d, J = 7.6 Hz, 1H), 7.94 (d, J = 8.4 Hz, 1H), 7.82 (dd, J = 8.4, 7.2 Hz, 1H), 7.73 (dd, J = 8.4, 7.2 Hz, 1H), 7.48 (dd, J = 8.0, 6.0 Hz, 1H); HPLC-MS (AJS-ES): Rt 1.47 min, m/z 146.1 [M+H].

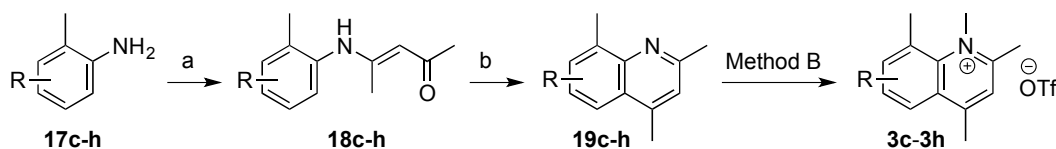
2-Chloro-3-nitroquinoline (15). The intermediate **15** was prepared by following the literature procedure reported by Zhao et al.² Quinoline-1-oxide **14** (4 g, 27.5 mmol) was dissolved in acetonitrile (140 mL) and added *tert*-butyl nitrite (14 g, 135.8 mmol). The resulting mixture was heated at 100 °C for 24 h in a pressure-vessel. Yellow precipitate was formed upon cooling to ambient temperature and triturated with Et₂O (100 mL). The precipitate was collected through filtration and was used directly for the following step without further purification. 3-nitroquinoline 1-oxide (2.2 g, 11.5 mmol) was heated for 12 h in neat POCl₃ (20 mL) in a pressure-sealed vessel. The reaction was cooled to 0 °C and quenched with 10% aqueous ammonia solution until pH > 8. The mixture was extracted with EtOAc (2x 50 mL), and the combined organic layer was washed with brine and dried over Na₂SO₄. The crude material was filtered and concentrated under reduced pressure, and purified by Biotage flash chromatography (gradient elution, 0-20% EtOAc in hexanes) to obtain 2-chloro-3-nitroquinoline **15** as orange-yellow solid (2.4 g, 11.5 mmol, 99% yield). ¹H NMR (400 MHz, CDCl₃) δ 8.74 (s, 1H), 8.13 (d, J = 8.0 Hz, 1H), 7.98 (d, J = 8.4 Hz, 1H), 7.95 (ddd, J = 7.6, 7.6, 1.2 Hz, 1H), 7.74 (ddd, J = 7.4, 7.4, 1.2 Hz, 1H).

Quinoline-2,3-diamine (16). A mixture of 2-chloro-3-nitroquinoline **15** (2.4 g, 11.5 mmol) in NH₃ (40 mL, 7N solution in MeOH) was heated to 100 °C for 24 h in a pressure-sealed vessel.

² Zhao, J. L., P.; Xia, C.; Li, F. Metal-free regioselective C-3 nitration of quinolone N-oxides with *tert*-butyl nitrite. *RSC Advances* **2015**, *5*, 32835-32838.

Orange color precipitate was formed upon cooling to ambient temperature and triturated with Et₂O (100 mL). The precipitate was collected through filtration and was used directly for the following step without further purification. 3-Nitroquinolin-2-amine **15a** (1.96 g, 10.3 mmol, 90%); ¹H NMR (400 MHz, CDCl₃) δ 8.99 (s, 1H), 7.77–7.71 (m, 2H), 7.65 (d, *J* = 8.4 Hz, 1H), 7.34 (dd, *J* = 7.2, 7.2 Hz, 1H), 6.64 (br, 2H).

3-Nitroquinolin-2-amine **15a** (1.26 g, 6.68 mmol) was dissolved in MeOH/THF (v:v, 1:1, 66 mL) and added Pd/C (10% on activated carbon, 710 mg). The reaction mixture was degassed and re-purged with H₂ via a hydrogen-filled balloon, and this process was repeated three times. The mixture was left stirring under hydrogen-filled balloon for 12 h. The mixture was filtered through a celite pad and washed repeatedly with MeOH until complete recovery of the desired product (monitored by TLC; 10% MeOH in CH₂Cl₂). The filtrate was concentrated under reduced pressure to give the title compound **16**, which was used directly for the following step without further purification. Quinolin-2,3-diamine **16** (1.02 g, 6.41 mmol, 96% crude yield); ¹H NMR (400 MHz, CDCl₃) δ 7.65 (d, *J* = 8.0 Hz, 1H), 7.51 (d, *J* = 8.0 Hz, 1H), 7.40 (dd, *J* = 8.0, 7.2 Hz, 1H), 7.24 (d, *J* = 7.2 Hz, 1H), 7.20 (s, 1H), 4.78 (br, 2H), 3.57 (br, 2H); HPLC-MS (AJS-ES): Rt 1.35 min, m/z 160.1 [M+H].



Method C: (a) acetylacetone, 150 °C microwave, 1 h; (b) conc. H₂SO₄, rt, 12 h, 77-92% over two steps

General Procedure C: Combes quinoline synthesis using the literature procedure reported

by Evans et al.³ A mixture of appropriate methylated or fluorinated aniline derivative **17c-h** (1 equiv) and acetylacetone (1.1 equiv) was heated to 150 °C for 1 h in a microwave reactor. The reaction mixture was then partitioned between H₂O (100 mL) and CH₂Cl₂ (100 mL), and the aqueous layer was extracted with CH₂Cl₂ (100 mL x2). The combined CH₂Cl₂ extracts were washed with brine and dried over Na₂SO₄. The crude material was filtered and concentrated under reduced pressure to give the anilide intermediate **18c-h** and was used for the subsequent step without further purification. Anilide intermediate **18c-h** (1 equiv) was dissolved in concentrated sulfuric acid (40 mL or overall concentration at 1M) and stirred at rt for 12 h. The reaction mixture was transferred to a Erlenmeyer flask containing ice-cold water (100 mL) and carefully added NaOH pallet in portions until pH>9. The mixture was extracted with CH₂Cl₂ (100 mL x2). The combined CH₂Cl₂ extracts were washed with brine and dried over Na₂SO₄. The crude material was filtered and concentrated under reduced pressure, and purified by Biotage flash chromatography to obtain the quinoline intermediates **19c-h**.

2,4,8-trimethylquinoline (19c). According to general procedure C, the crude material was purified by Biotage flash chromatography (gradient elution, 0-10% EtOAc in hexanes) to obtain the title compound as pale yellow solid (5.7 g, 33.3 mmol, 88% yield). ¹H NMR (400 MHz, DMSO-d₆) δ 7.85 (d, *J* = 8.4 Hz, 1H), 7.55 (d, *J* = 7.0 Hz, 1H), 7.41 (dd, *J* = 7.6, 7.6 Hz, 1H), 7.25 (s, 1H), 2.69 (s, 3H), 2.61 (s, 6H); HPLC-MS (AJS-ES): Rt 2.75 min, m/z 172.1 [M+H].

2,4,5,8-tetramethylquinoline (19d). According to general procedure C, the crude material was purified by Biotage flash chromatography (gradient elution, 0-15% EtOAc in hexanes) to obtain

³ Evans, P. H., P.; Grigg, R.; Nurnabi, M.; Hinsley, J.; Sridharan, V.; Suganthan, S.; Korn, S.; Collard, S.; Muir, J. E. 8-Methylquinoline palladacycles: stable and efficient catalysts for carbon-carbon bond formation. *Tetrahedron* **2005**, *61*, 9696-9704.

the title compound as orange solid (6.5 g, 35.1 mmol, 92% yield). ¹H NMR (400 MHz, DMSO-d₆) δ 7.37 (d, *J* = 6.8 Hz, 1H), 7.17 (s, 1H), 7.15 (d, *J* = 8.4 Hz, 1H), 2.83 (s, 3H), 2.80 (s, 3H), 2.61 (s, 3H), 2.57 (s, 3H); HPLC-MS (AJS-ES): Rt 2.83 min, m/z 186.1 [M+H].

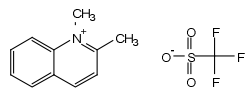
2,4,6,8-tetramethylquinoline (19e). According to general procedure C, the crude material was purified by Biotage flash chromatography (gradient elution, 0-15% EtOAc in hexanes) to obtain the title compound as pale orange solid (3.27 g, 17.6 mmol, 78% yield). ¹H NMR (400 MHz, DMSO-d₆) δ 7.61 (s, 1H), 7.39 (s, 1H), 7.20 (s, 1H), 2.64 (s, 3H), 2.58 (s, 6H), 2.44 (s, 3H); HPLC-MS (AJS-ES): Rt 3.04 min, m/z 186.1 [M+H].

2,4,7,8-tetramethylquinoline (19f). According to general procedure C, the crude material was purified by Biotage flash chromatography (gradient elution, 0-15% EtOAc in hexanes) to obtain the title compound as pale orange solid (845 mg, 4.56 mmol, 93% yield). ¹H NMR (400 MHz, CDCl₃) δ 7.70 (d, *J* = 8.4 Hz, 1H), 7.31 (d, *J* = 8.3 Hz, 1H), 7.05 (s, 1H), 2.78 (s, 3H), 2.70 (s, 3H), 2.62 (s, 3H), 2.50 (s, 3H); HPLC-MS (AJS-ES): Rt 2.54 min, m/z 186.1 [M+H].

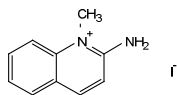
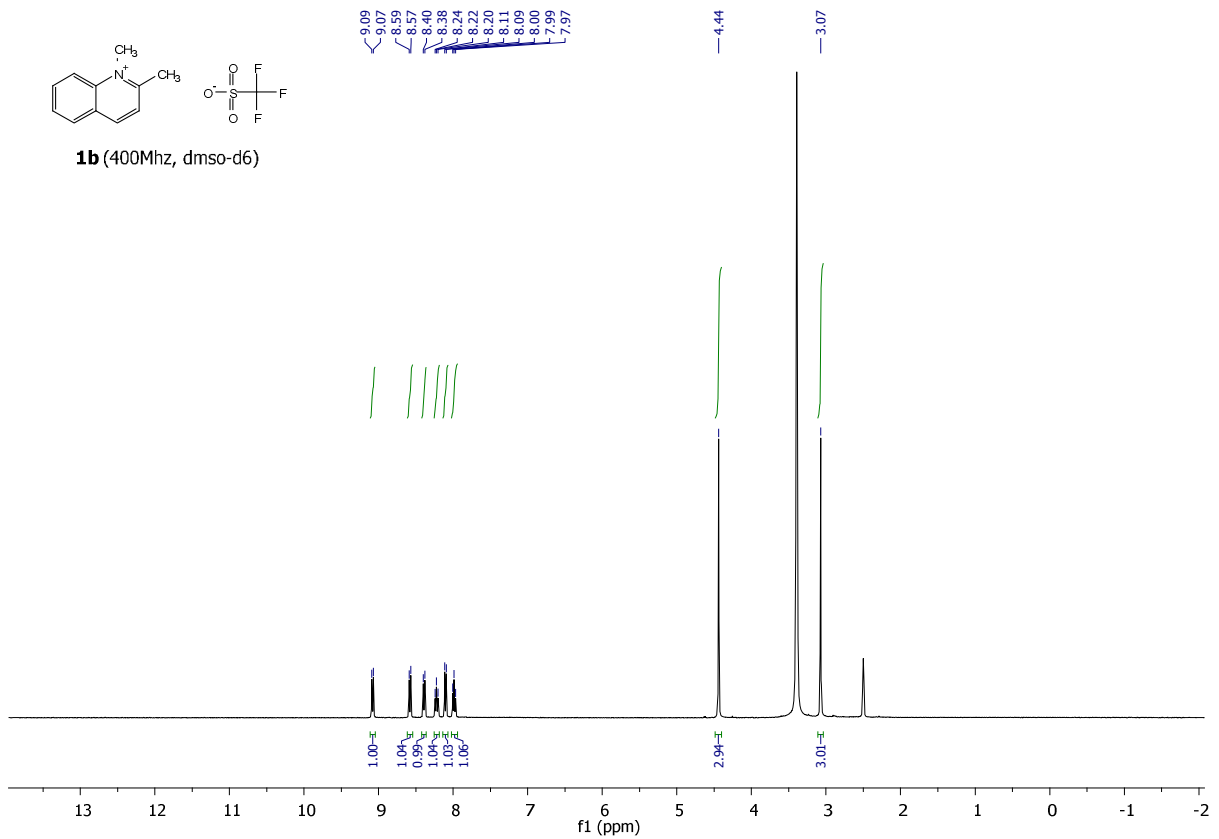
5-fluoro-2,4,8-trimethylquinoline (19g). According to general procedure C, the crude material was purified by Biotage flash chromatography (gradient elution, 0-12% EtOAc in hexanes) to obtain the title compound as yellow solid (4.8 g, 25.4 mmol, 77% yield). ¹H NMR (400 MHz, DMSO-d₆) δ 7.50 (dd, *J* = 6.8, 6.8 Hz, 1H), 7.28 (s, 1H), 7.18 (dd, *J* = 12.4, 7.6 Hz, 1H), 2.73 (d, *J* = 6.8 Hz, 3H), 2.61 (s, 6H); HPLC-MS (AJS-ES): Rt 5.10 min, m/z 190.1 [M+H].

7-fluoro-2,4,8-trimethylquinoline (19h). According to general procedure C, the crude material

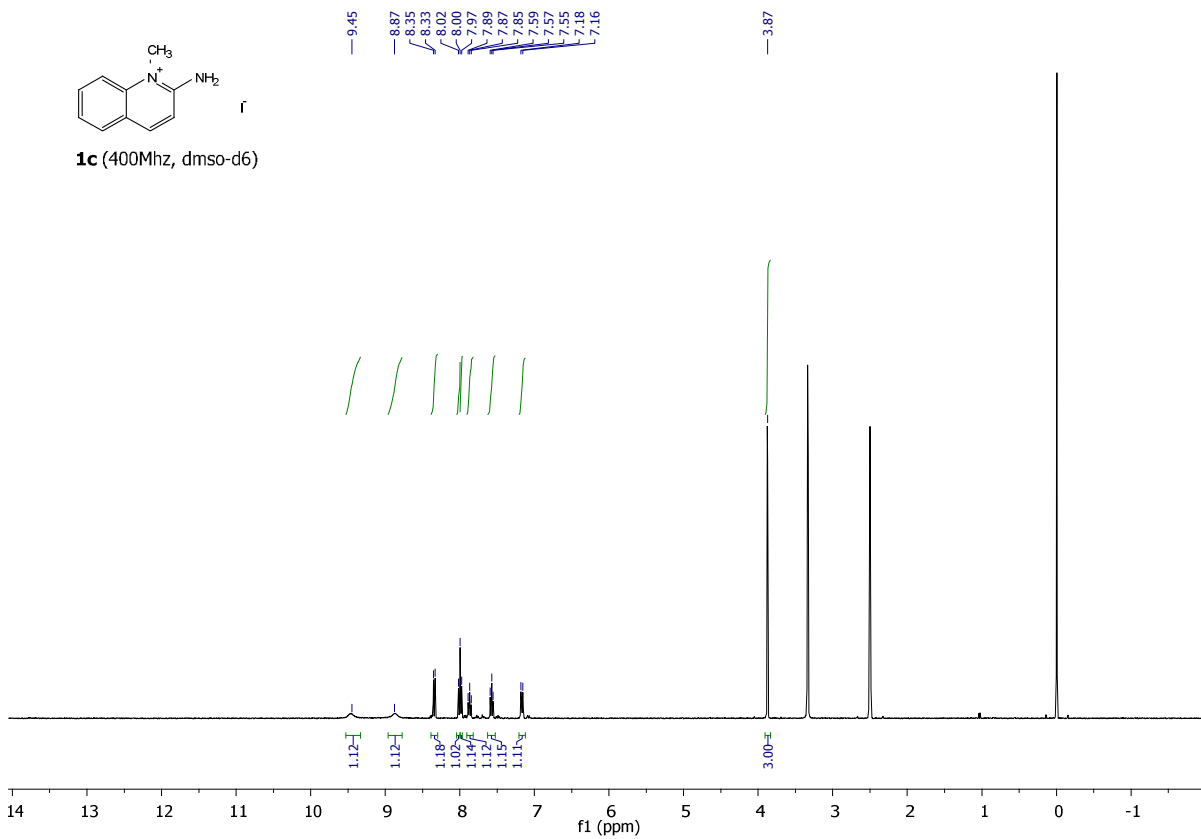
was purified by Biotage flash chromatography (gradient elution, 0-12% EtOAc in hexanes) to obtain the title compound as yellow solid (5.2 g, 27.5 mmol, 79% yield). ¹H NMR (400 MHz, DMSO-d₆) δ 7.92 (m, 1H), 7.40 (dd, *J* = 9.6, 6.8 Hz, 1H), 7.24 (s, 1H), 2.61 (s, 6H), 2.57 (s, 3H); HPLC-MS (AJS-ES): Rt 3.91 min, m/z 190.1 [M+H].

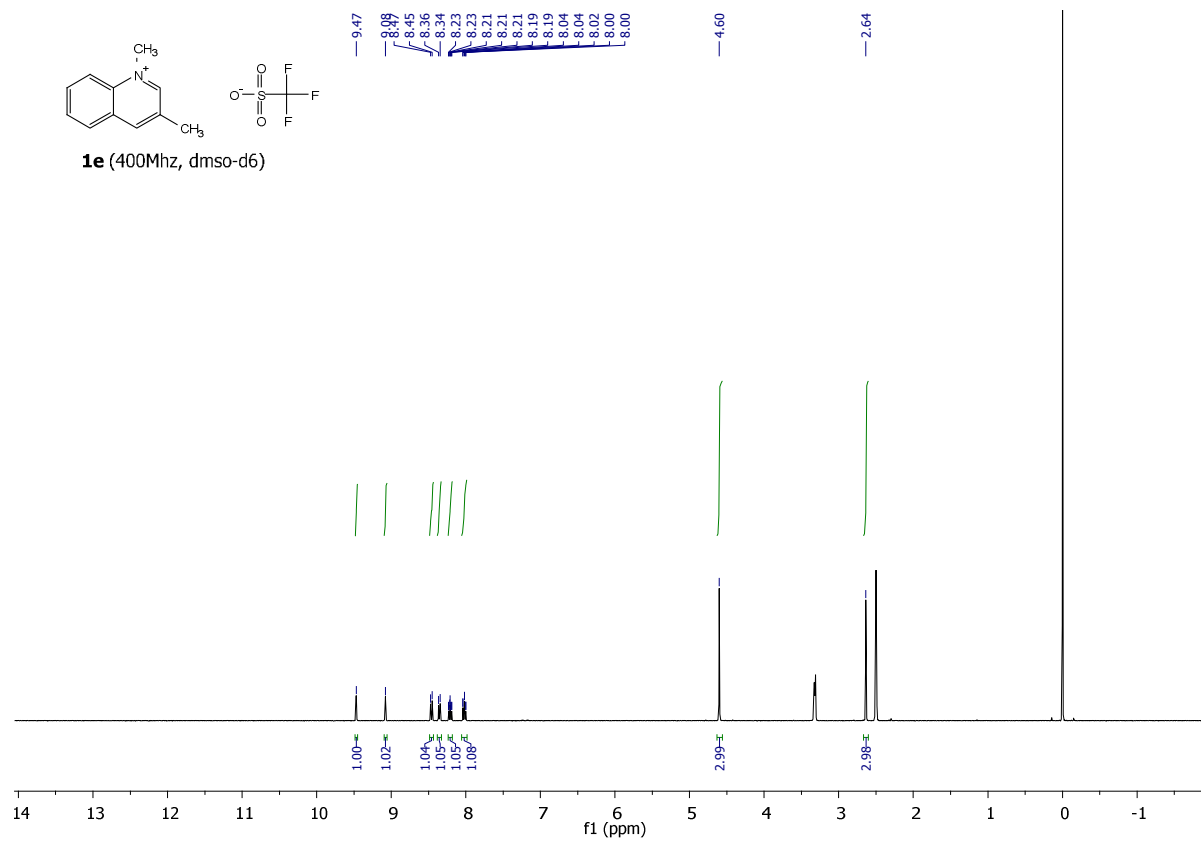
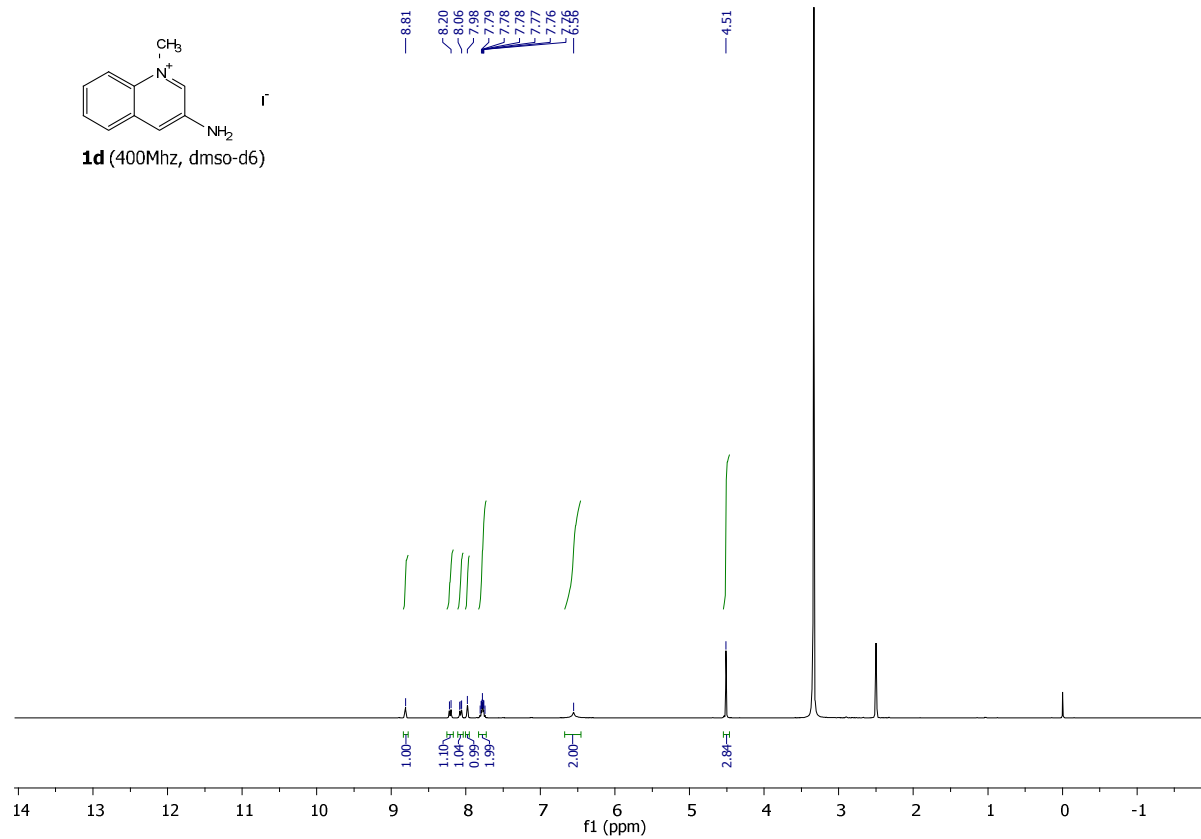


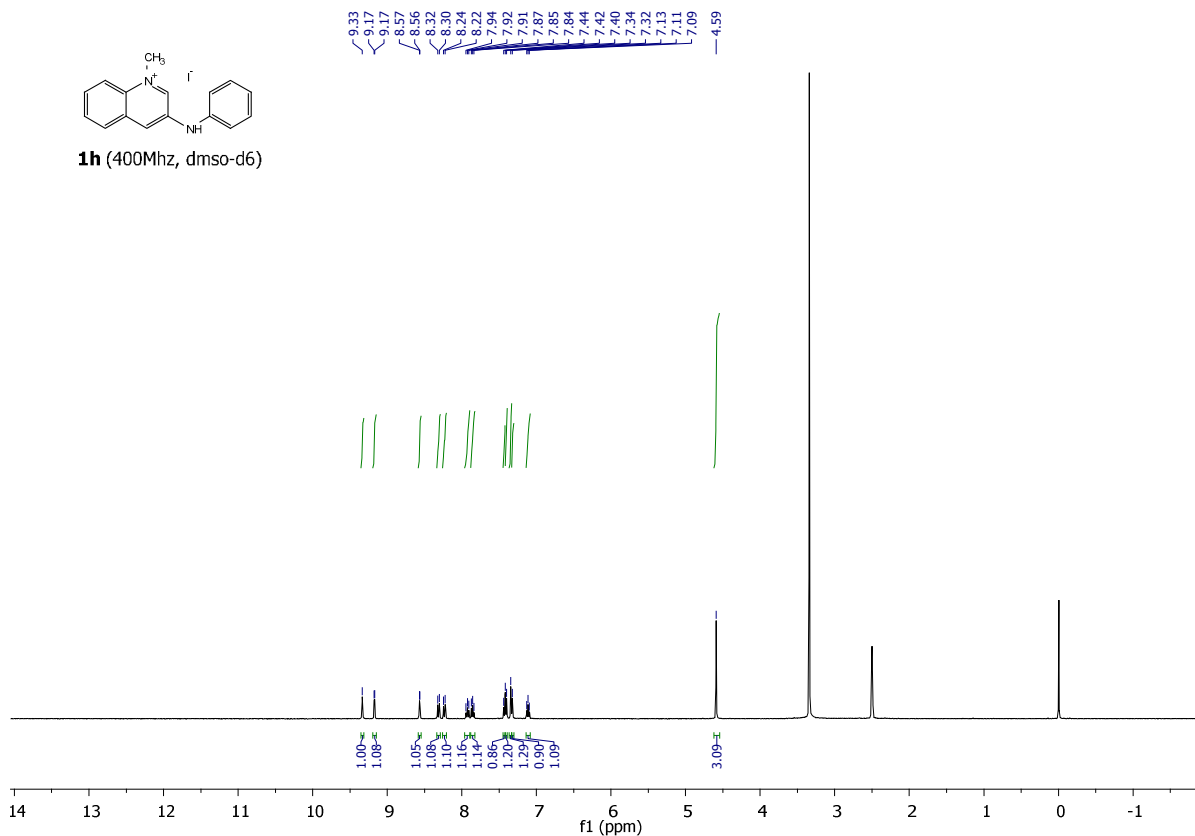
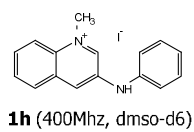
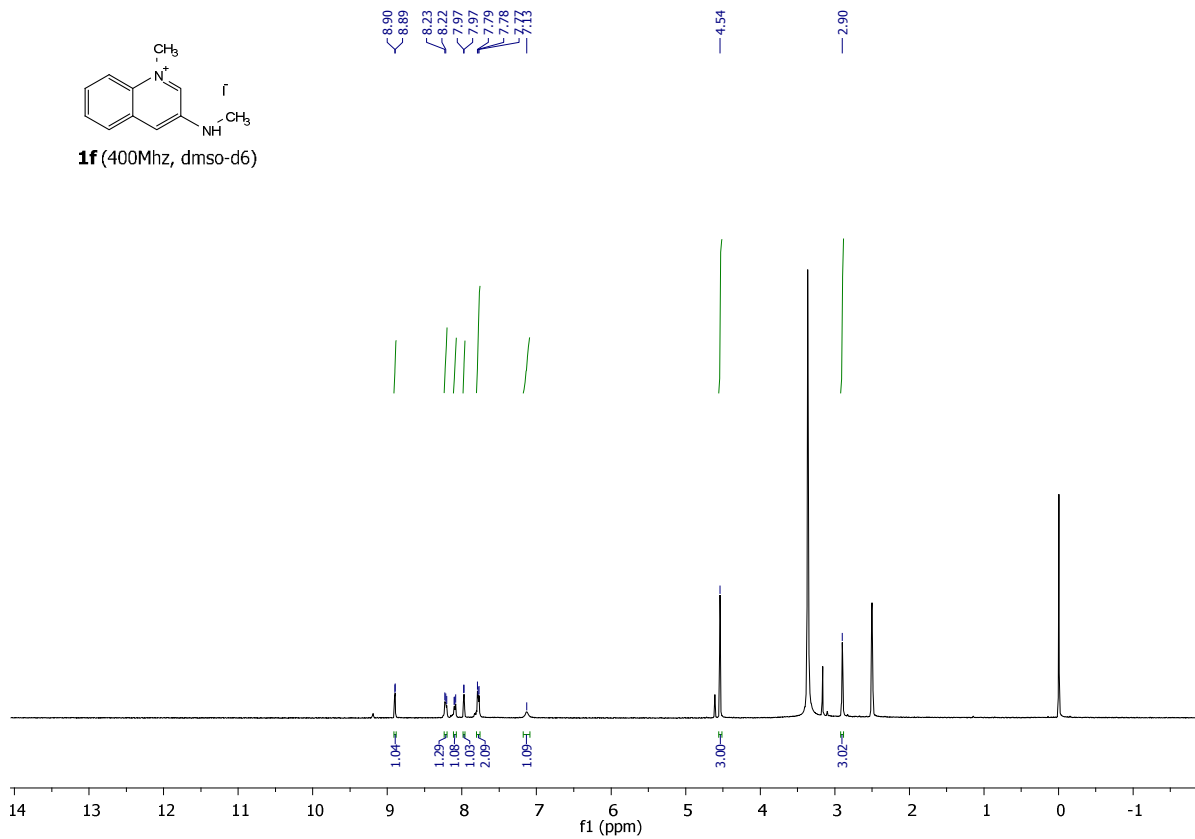
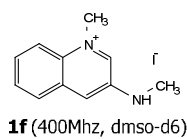
1b (400Mhz, dms0-d6)

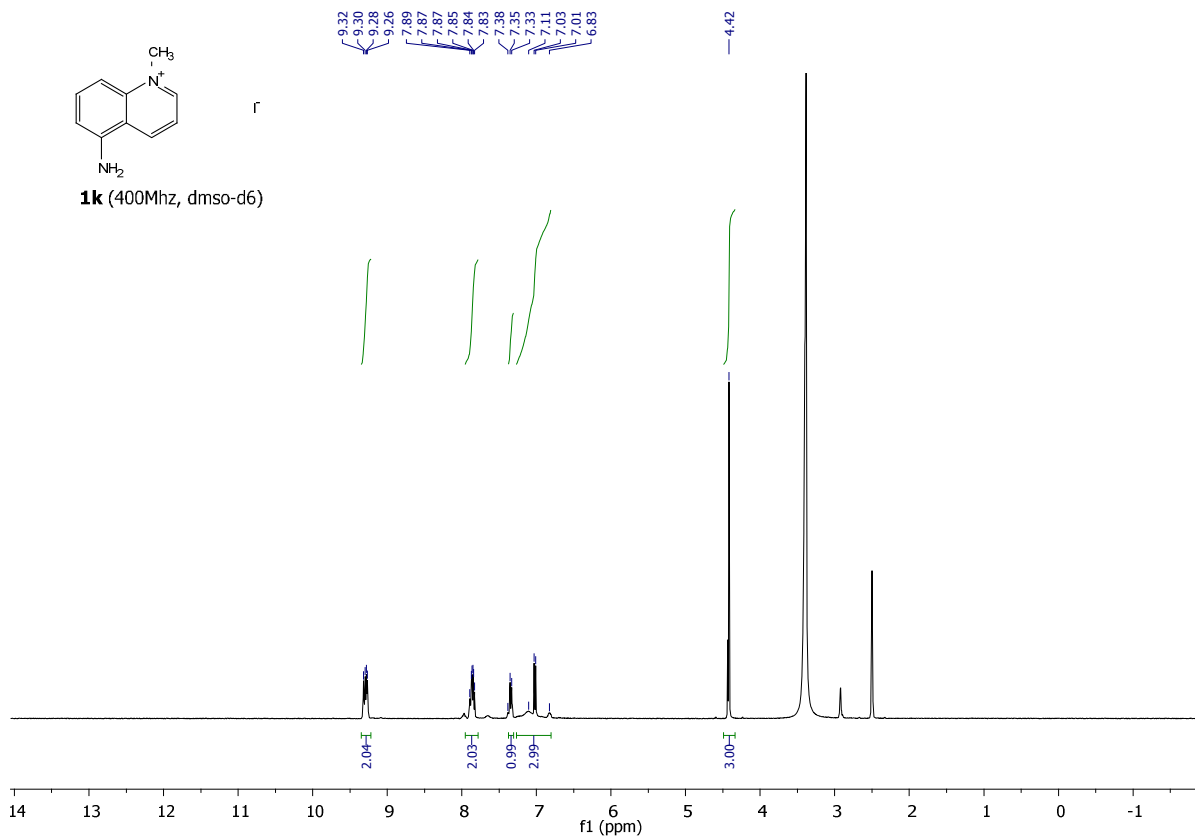
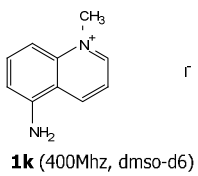
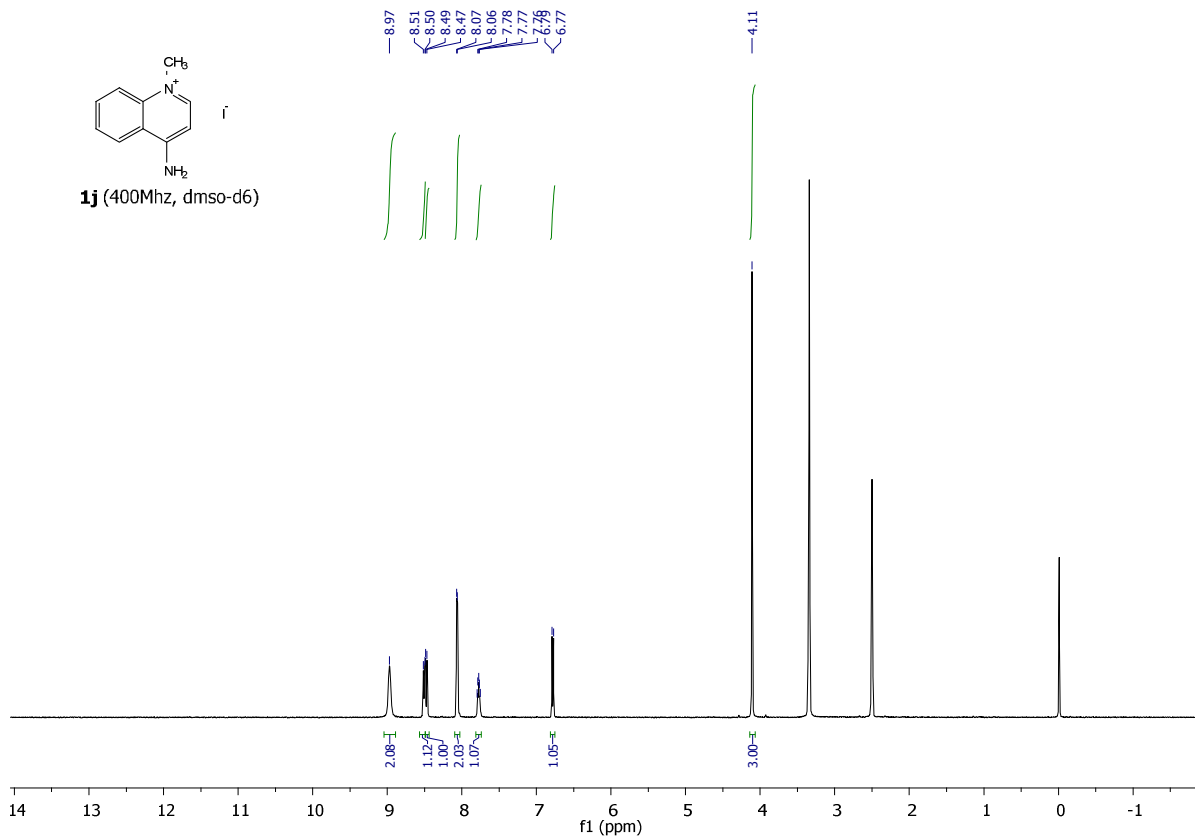
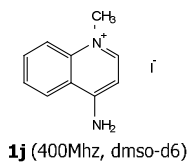


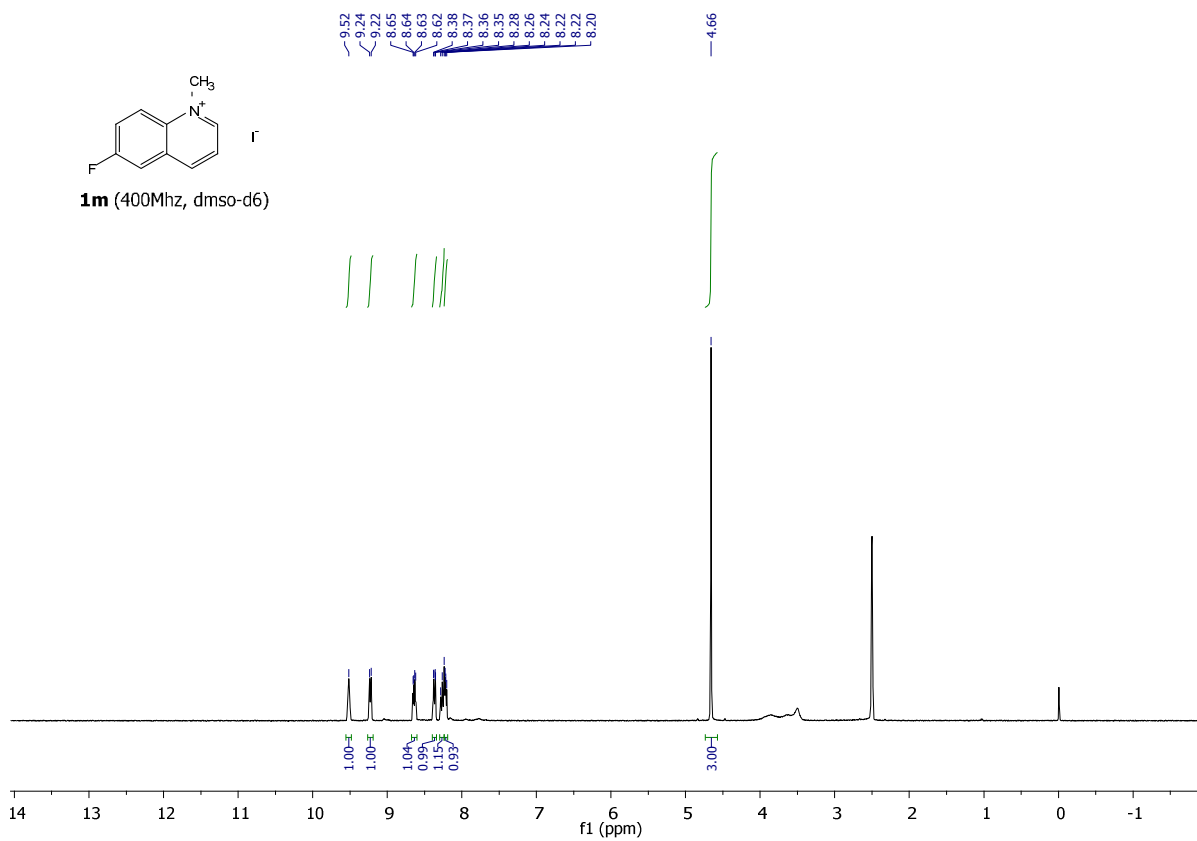
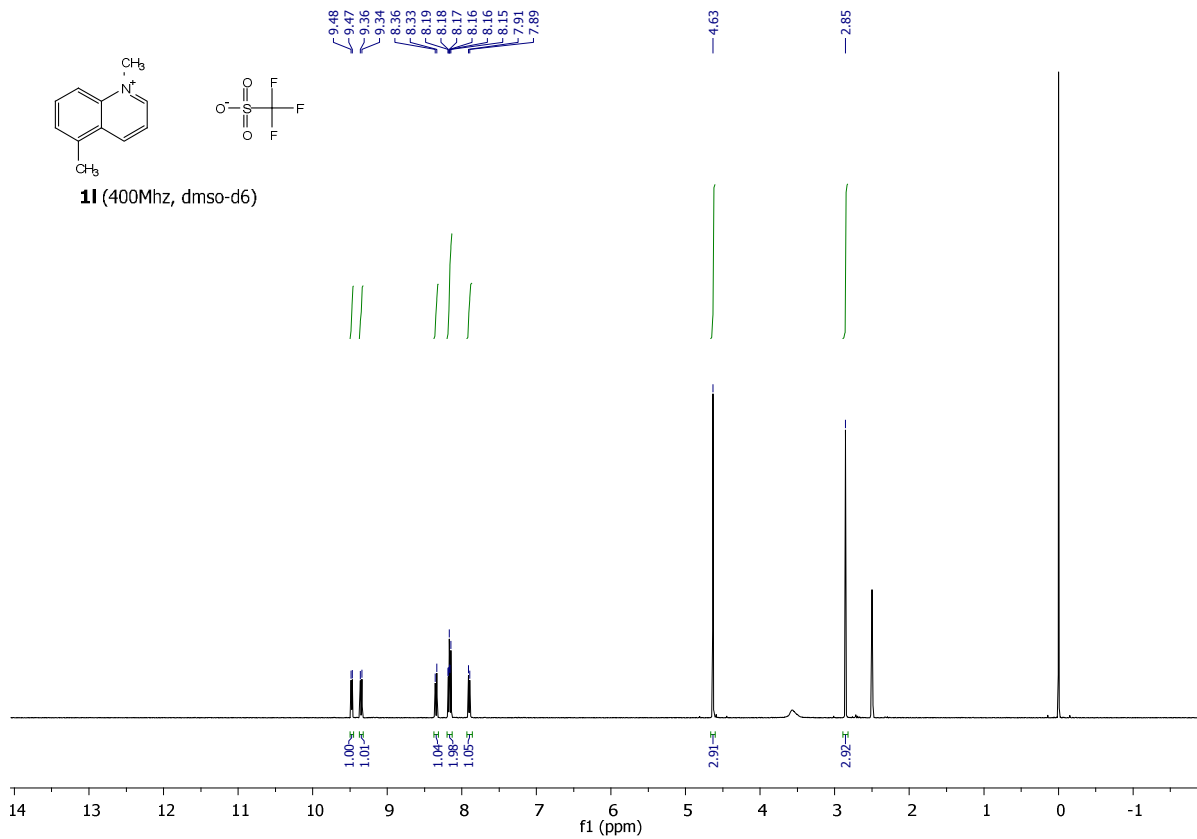
1c (400Mhz, dms0-d6)

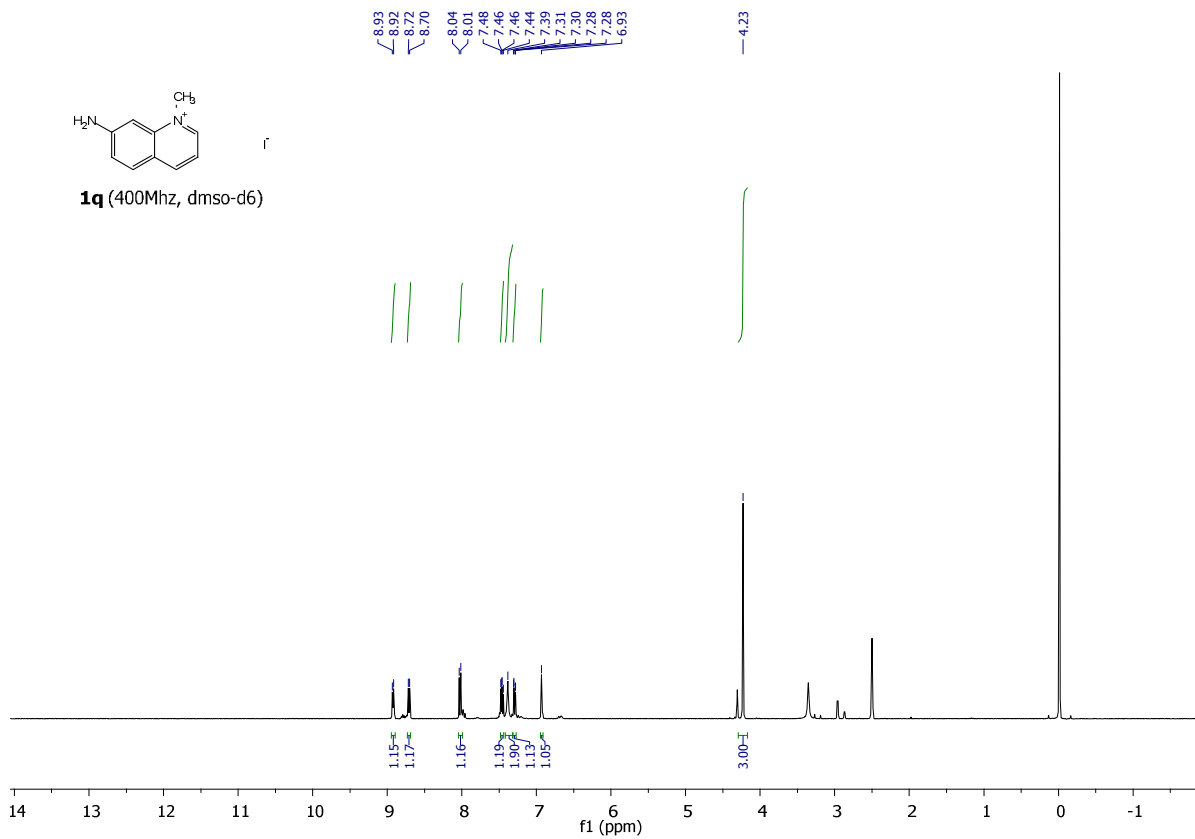
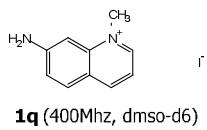
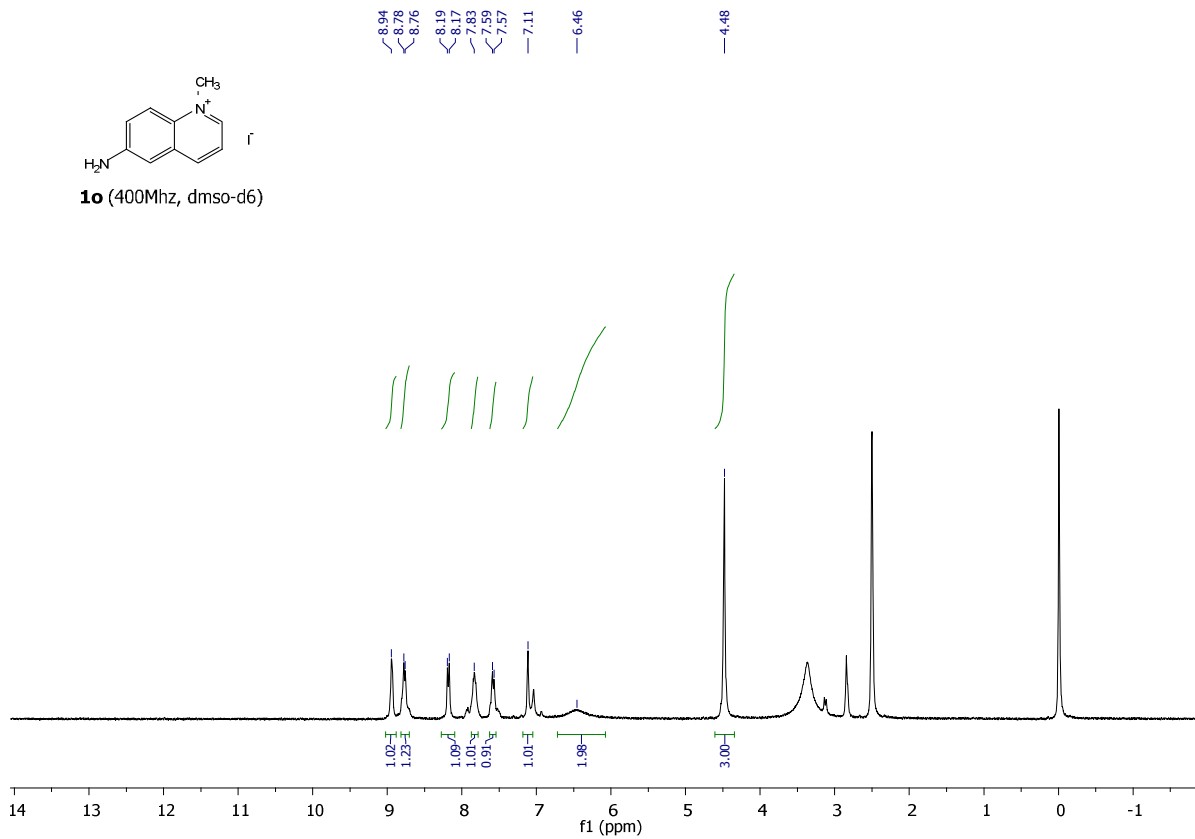
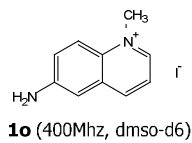


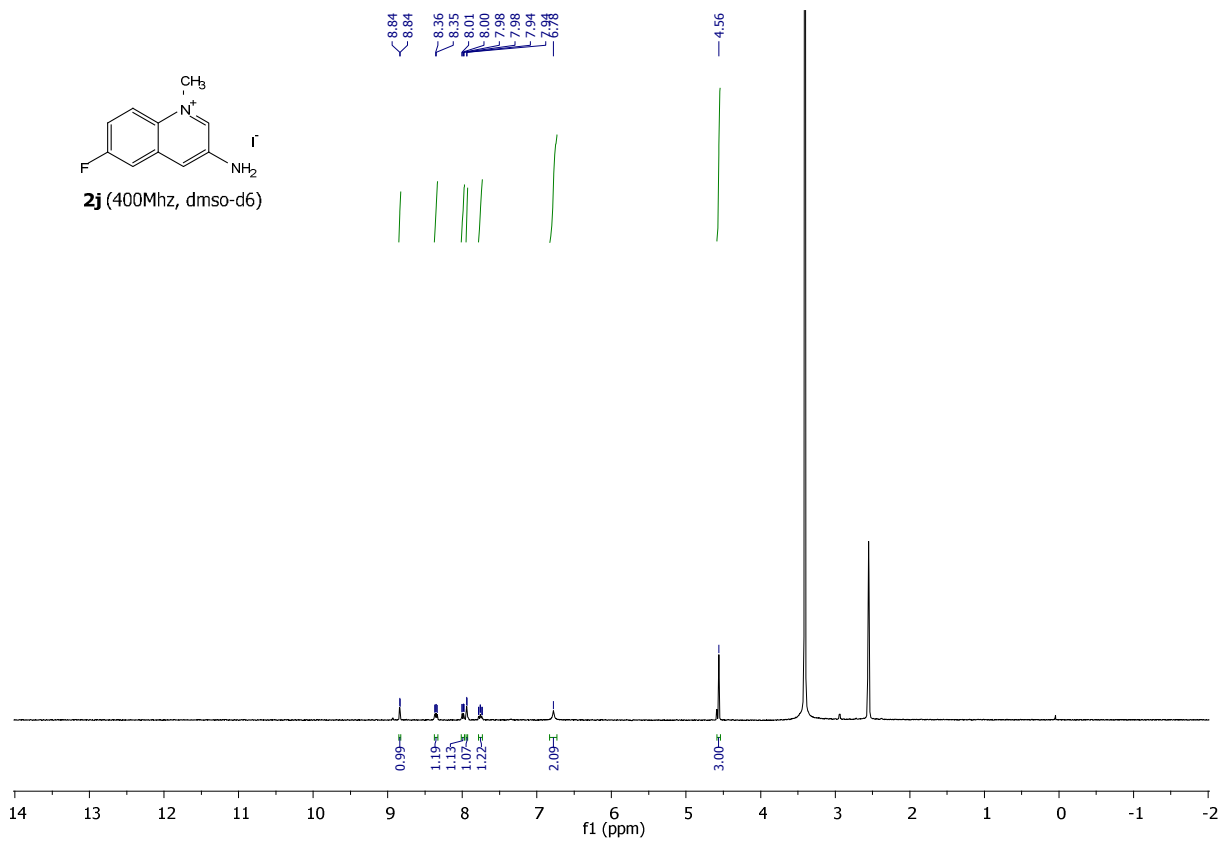
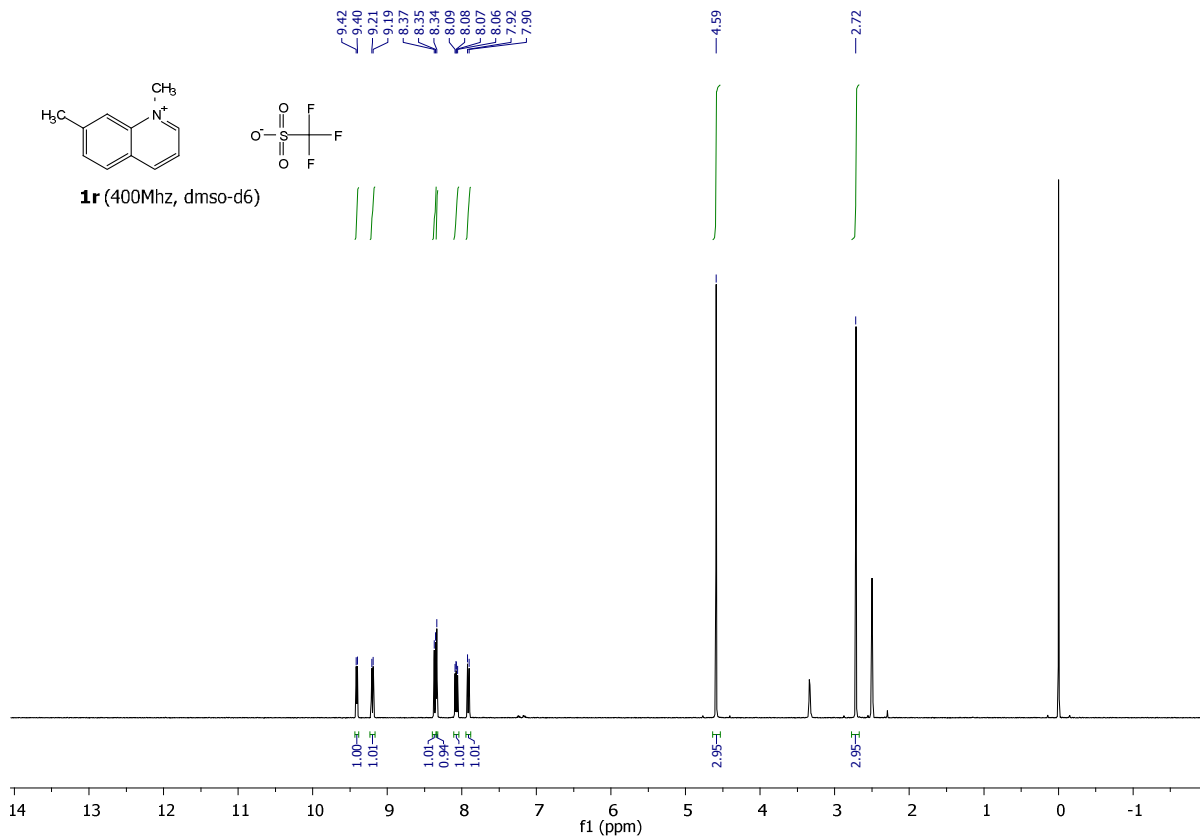


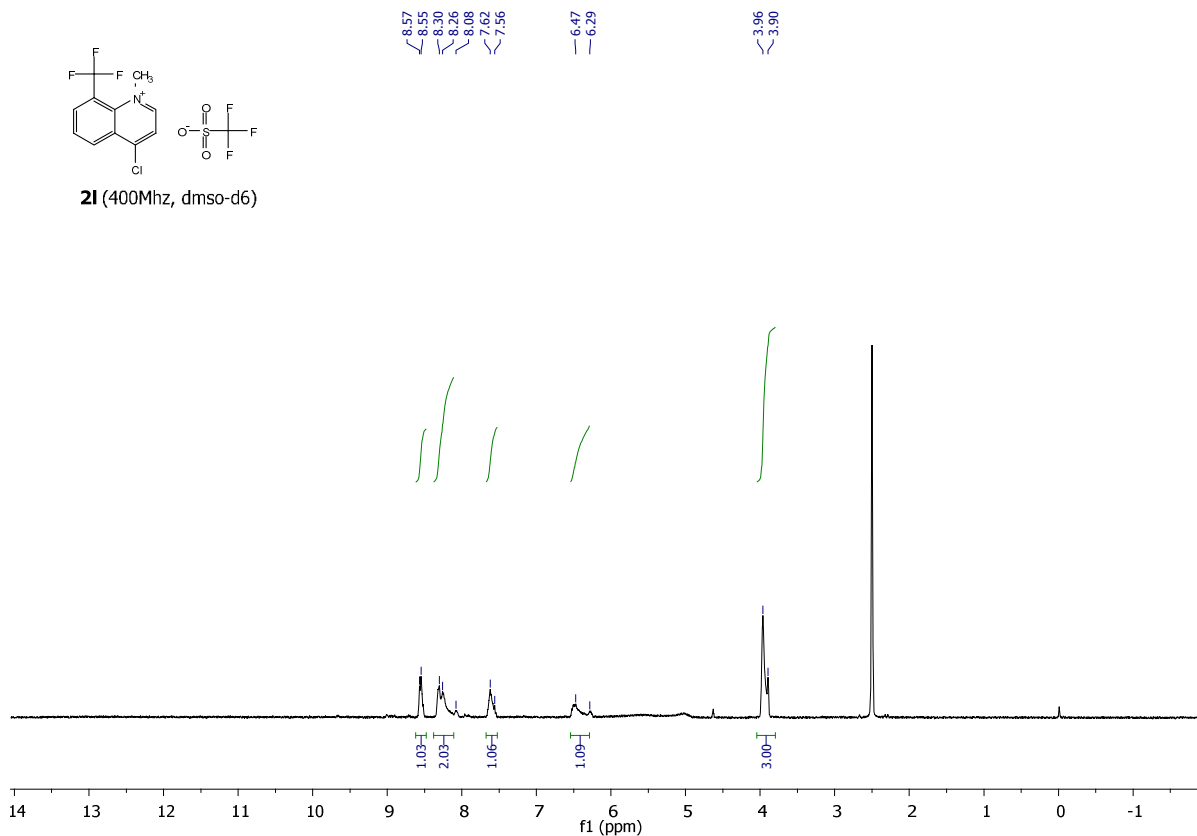
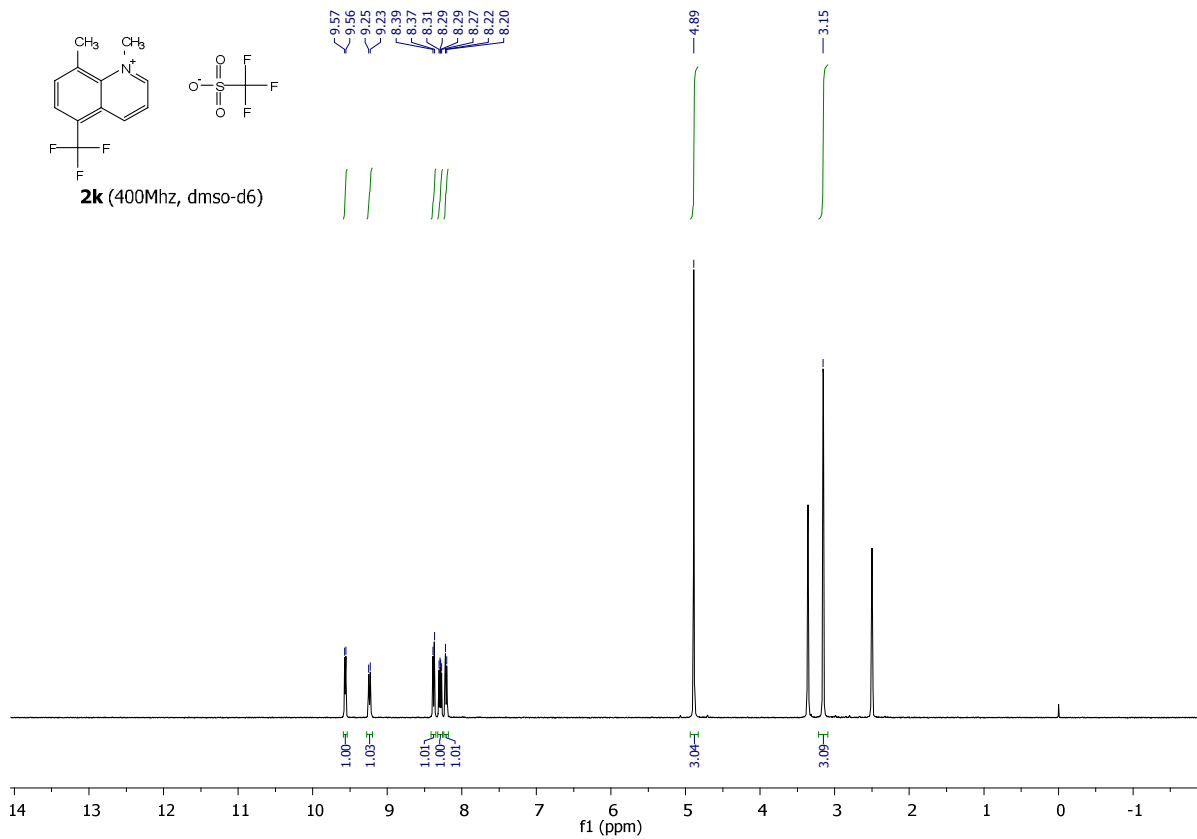


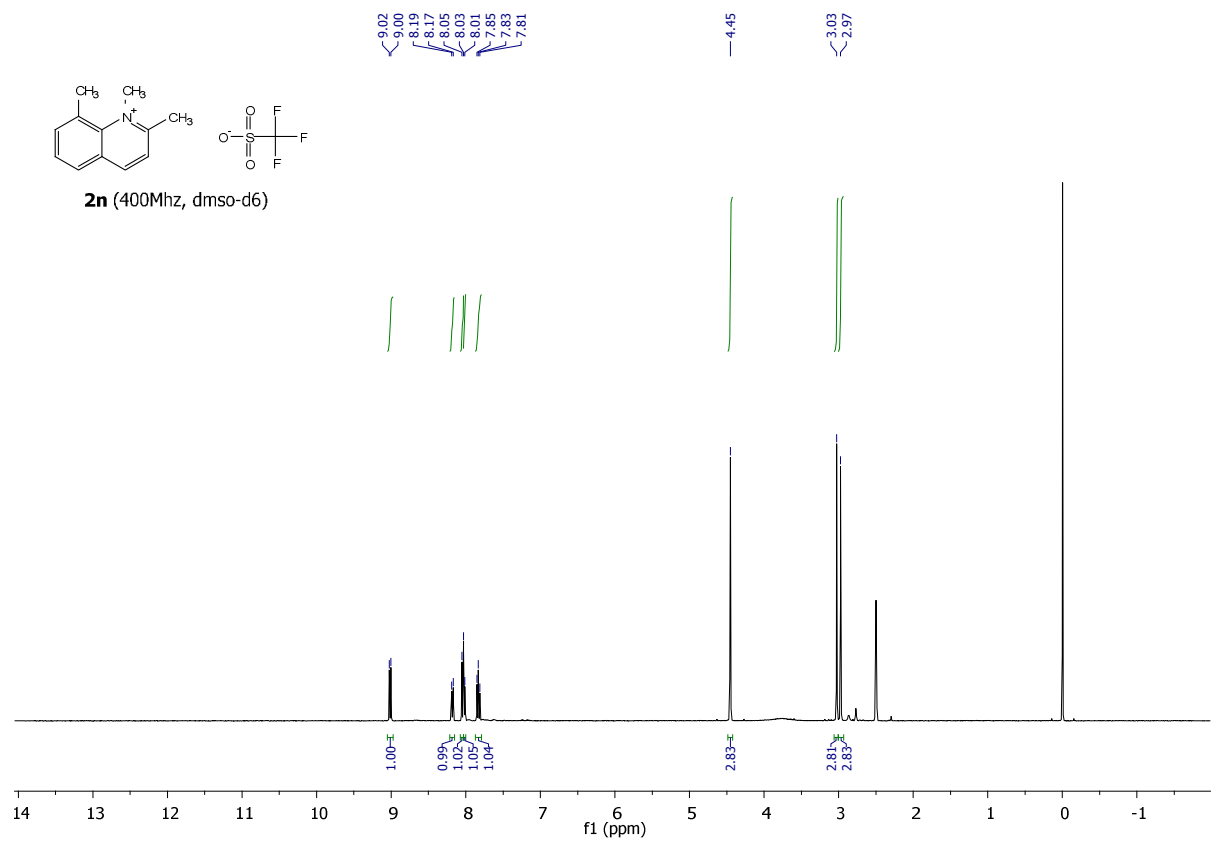
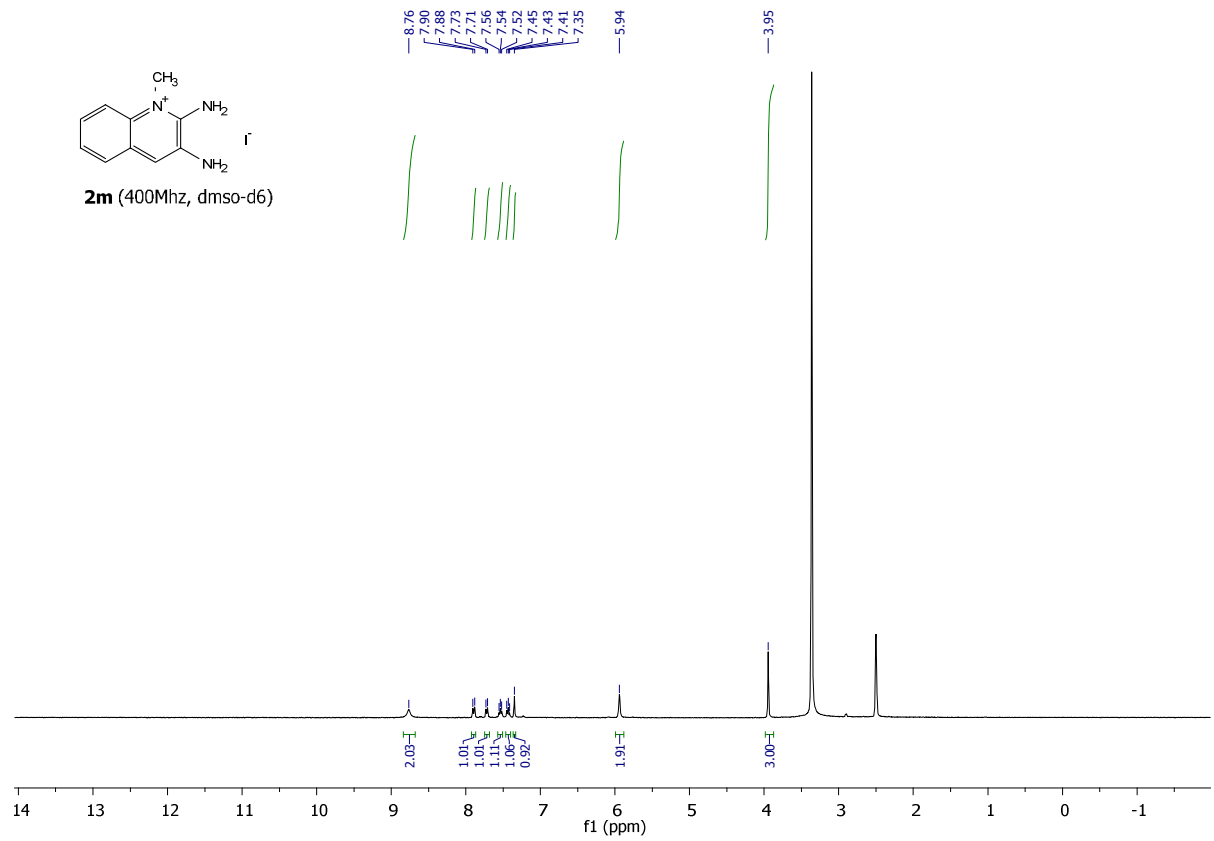


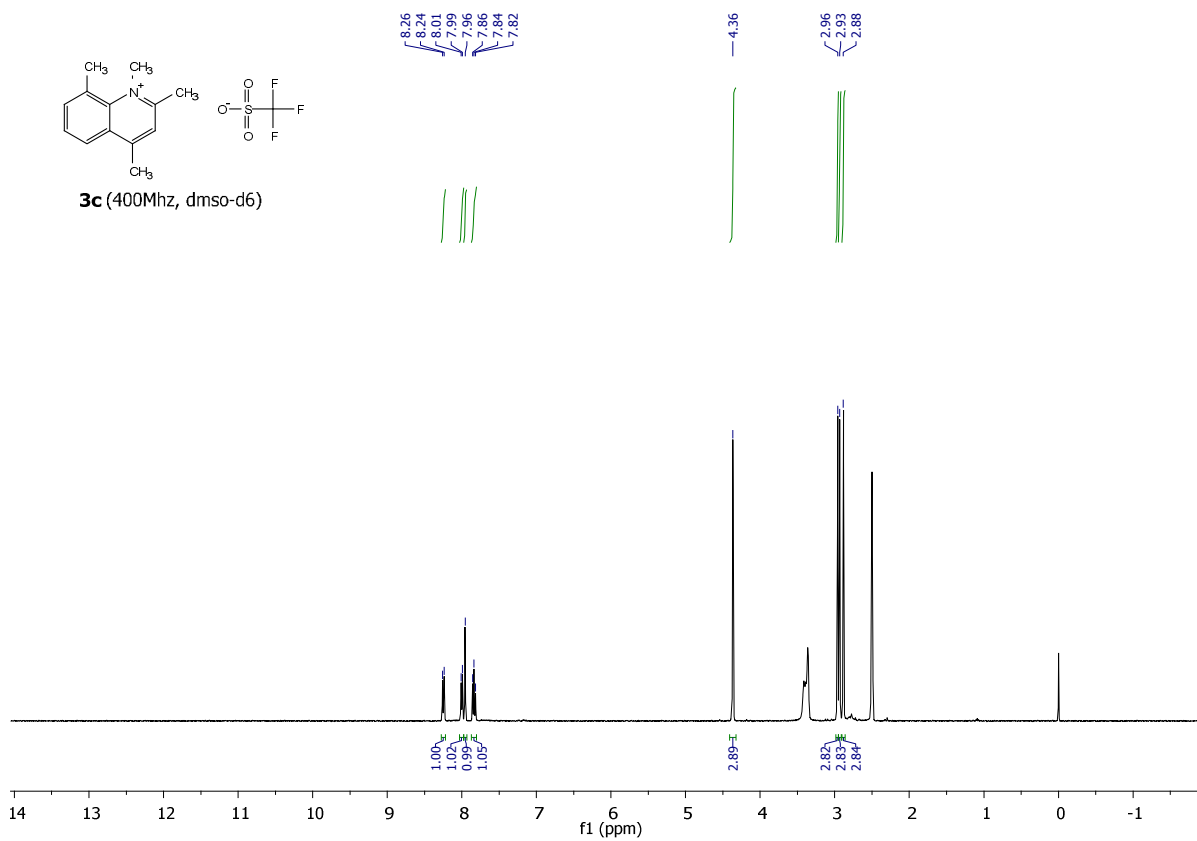
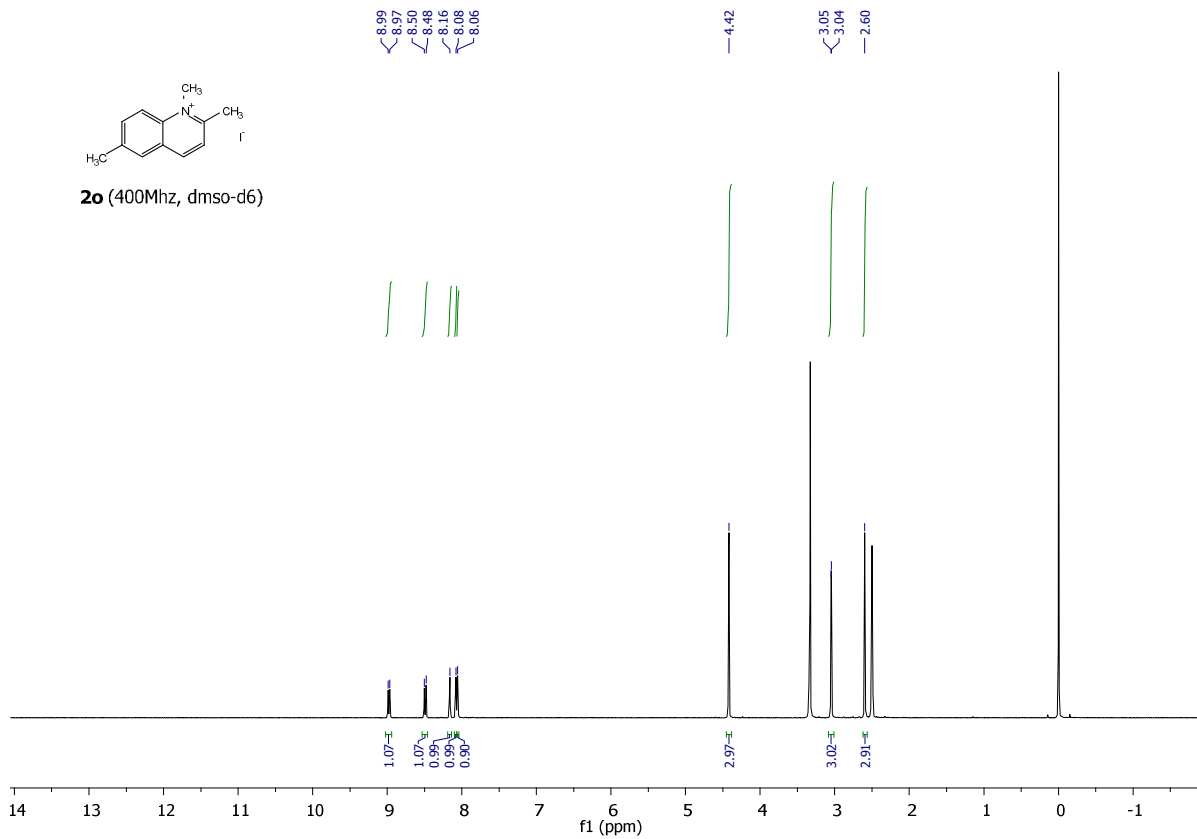


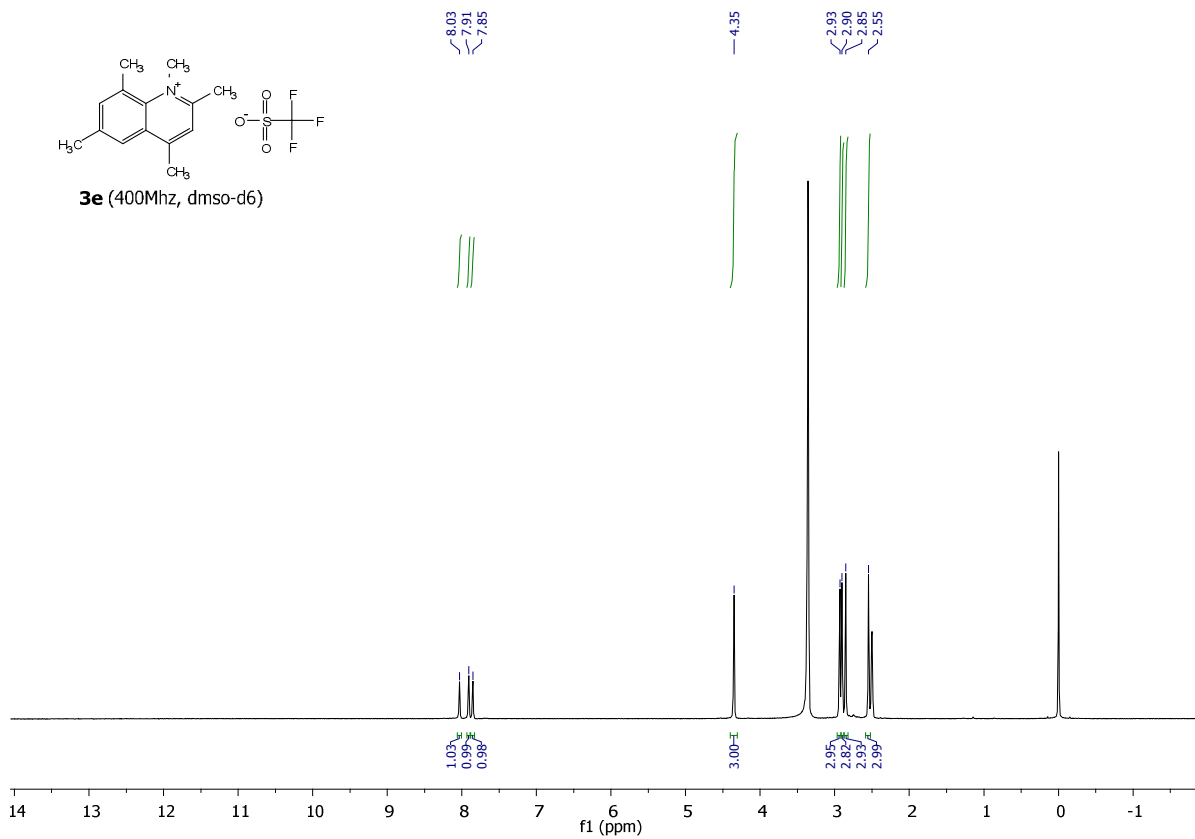
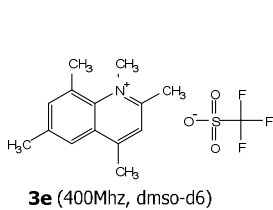
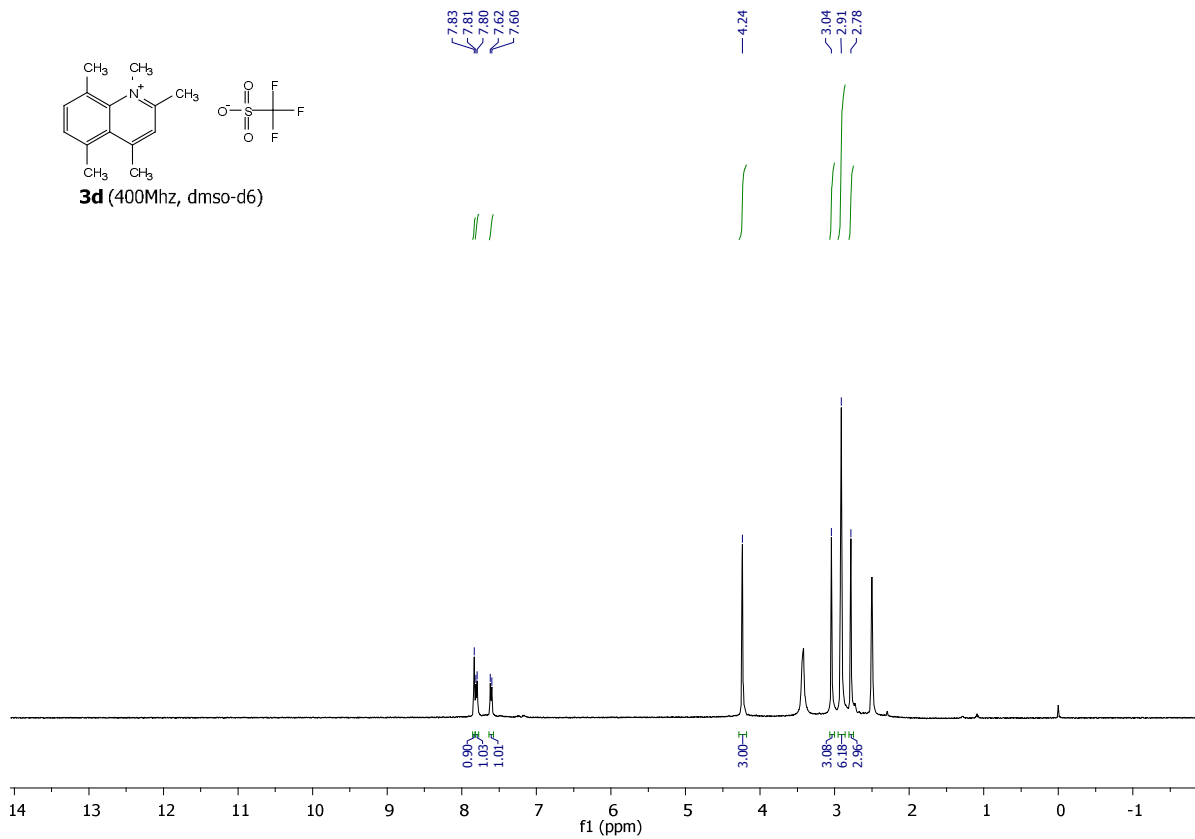
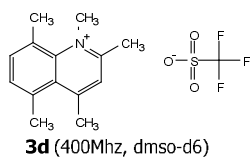


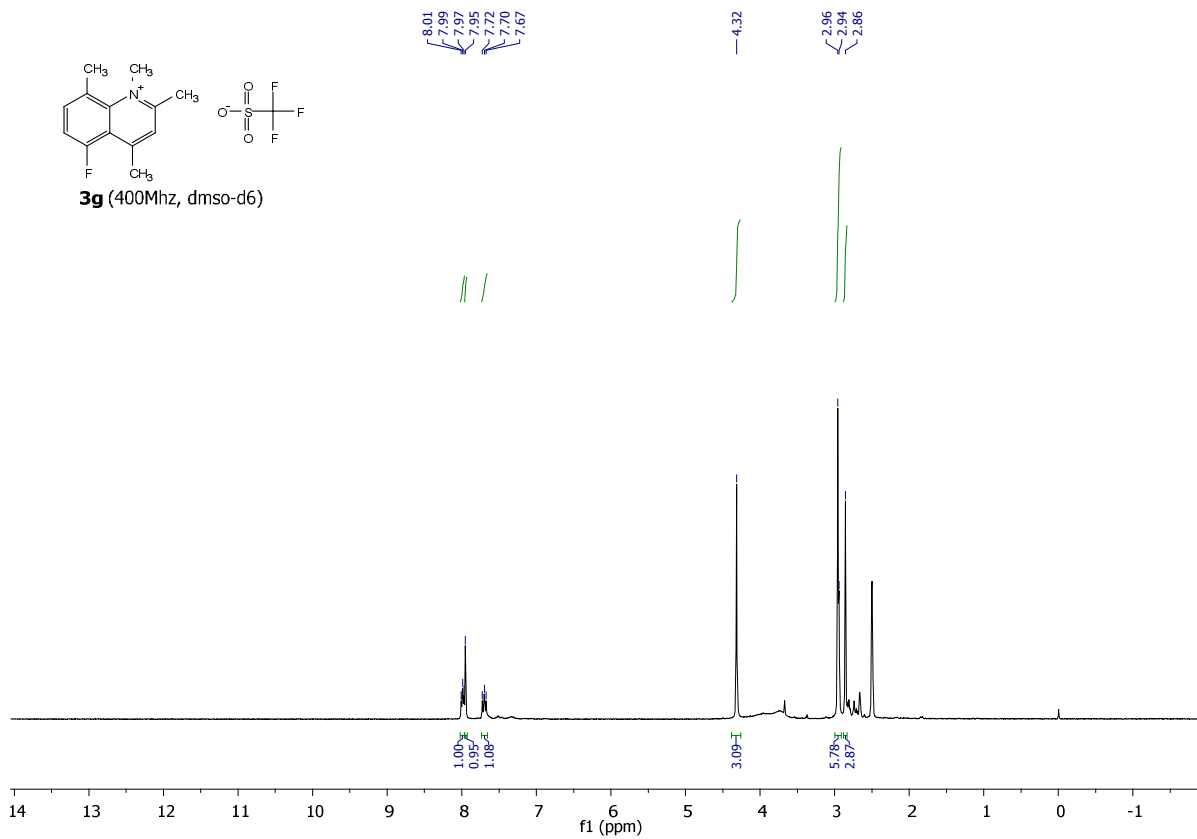
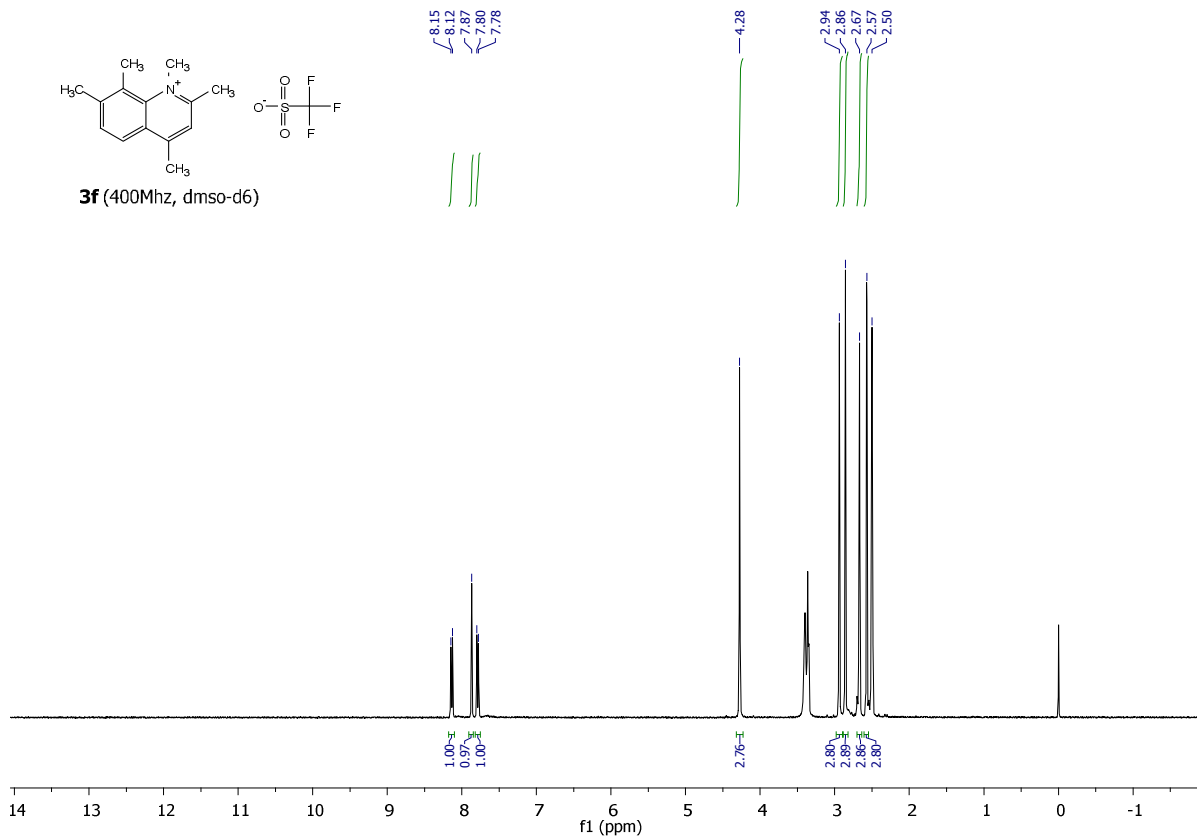


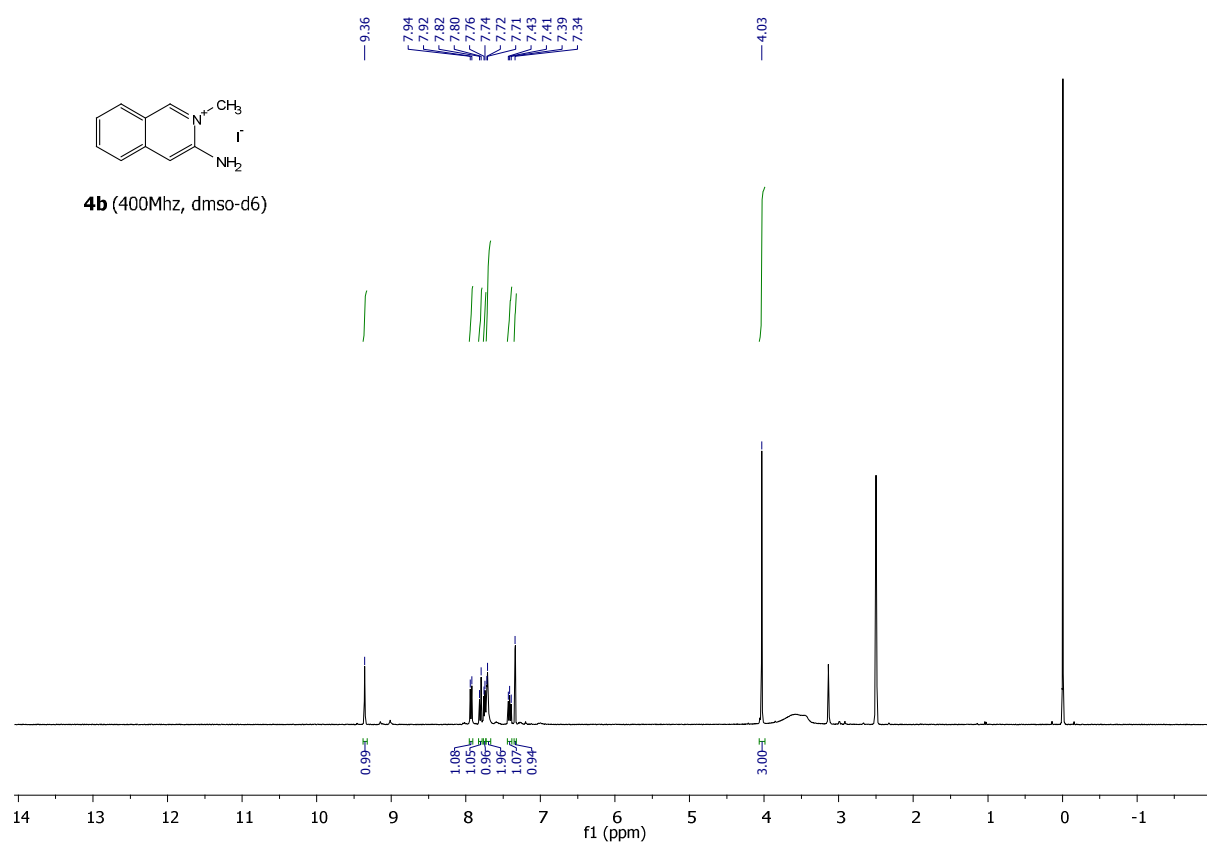
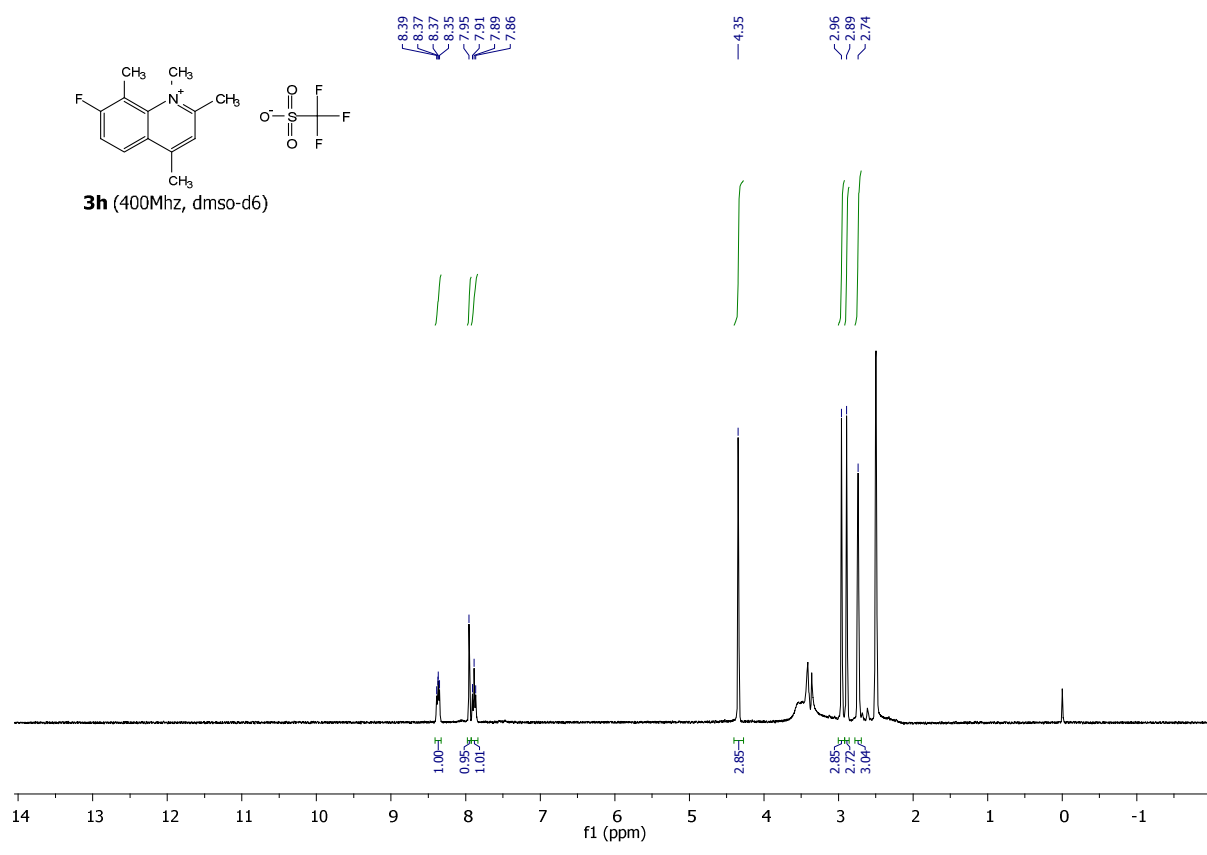


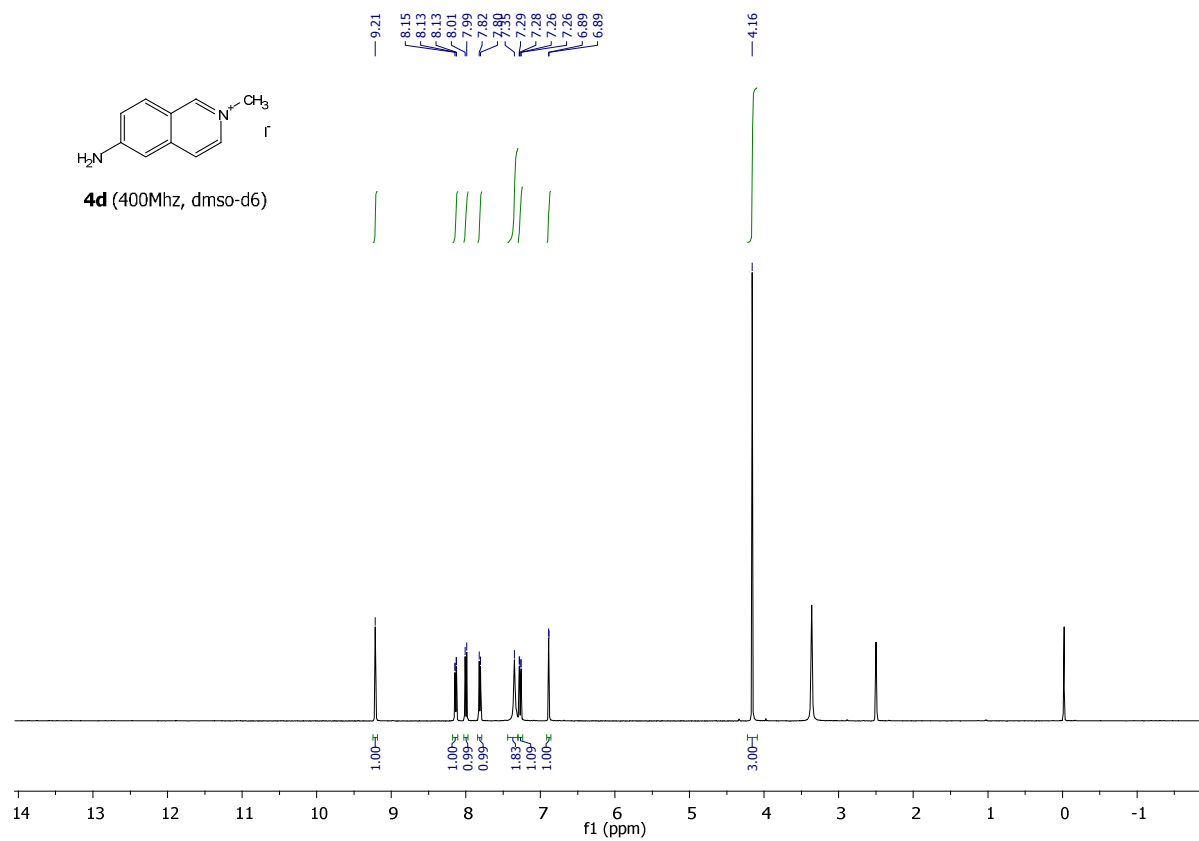
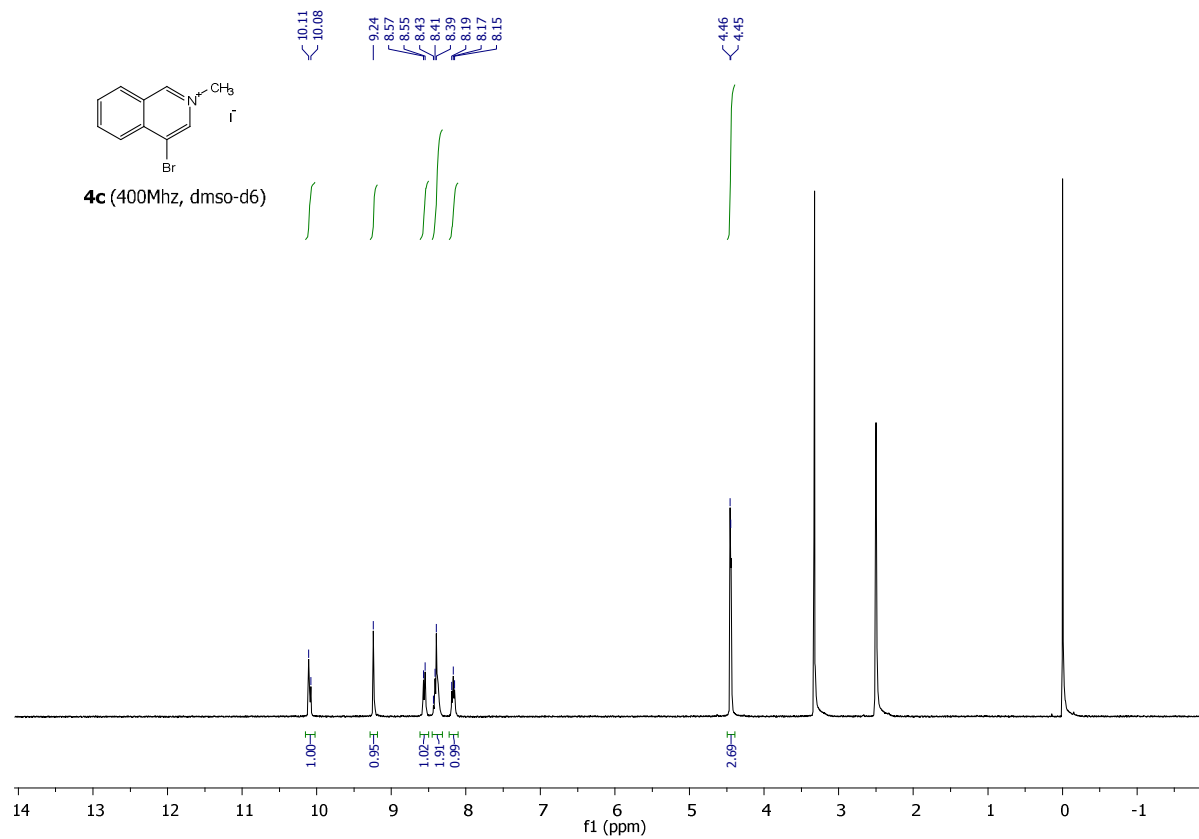


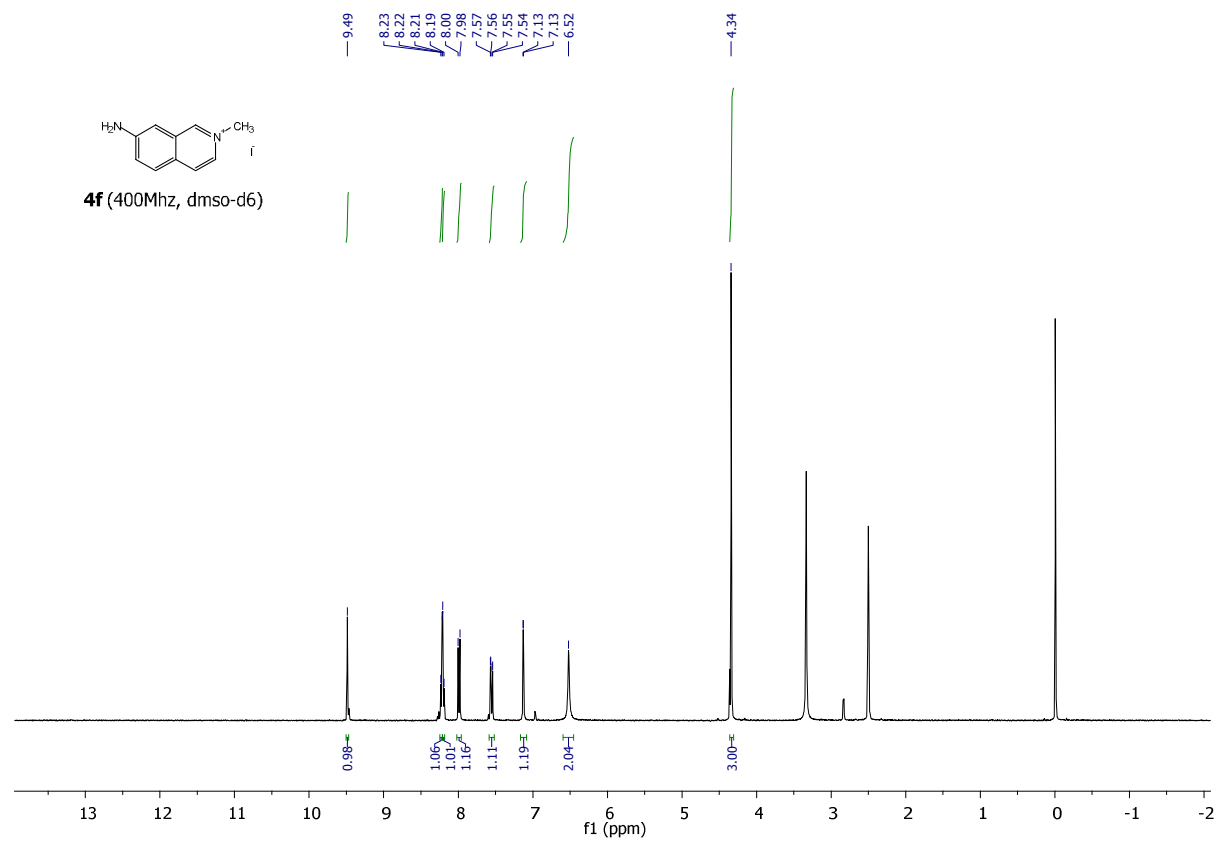
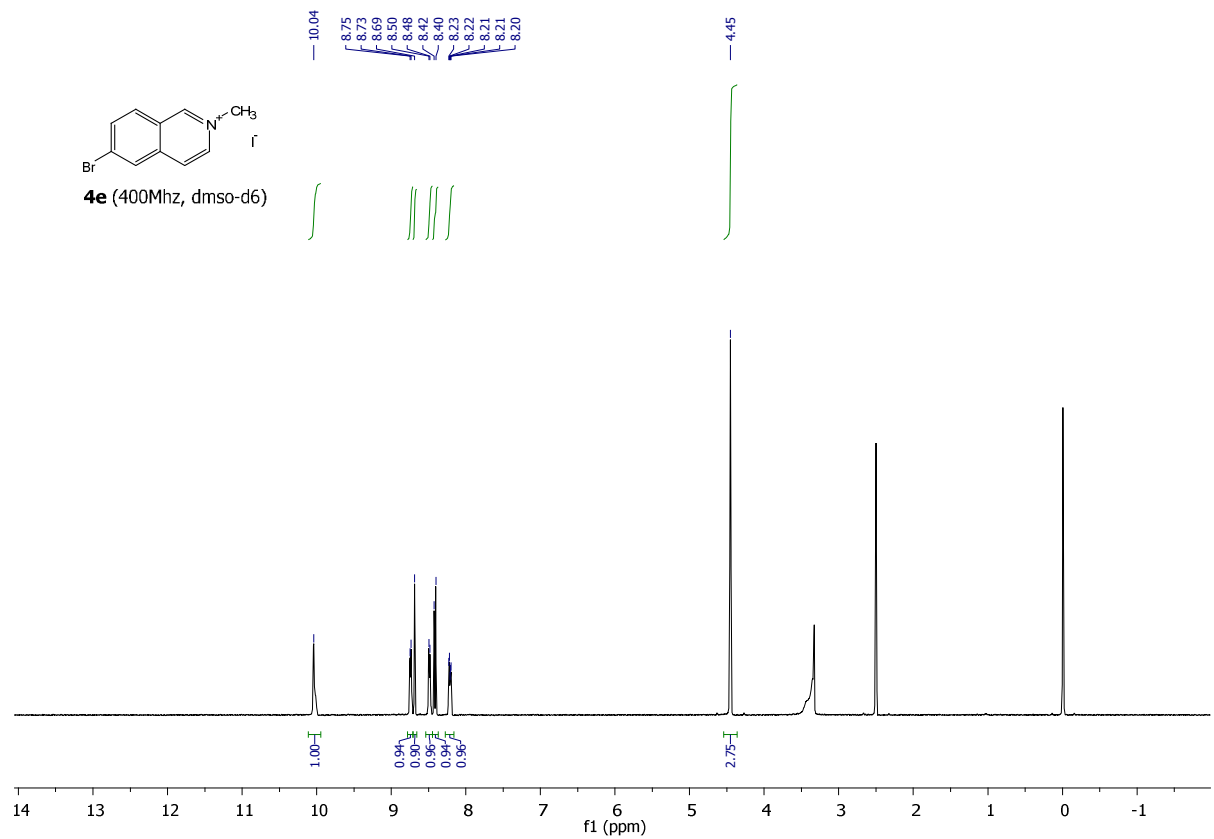


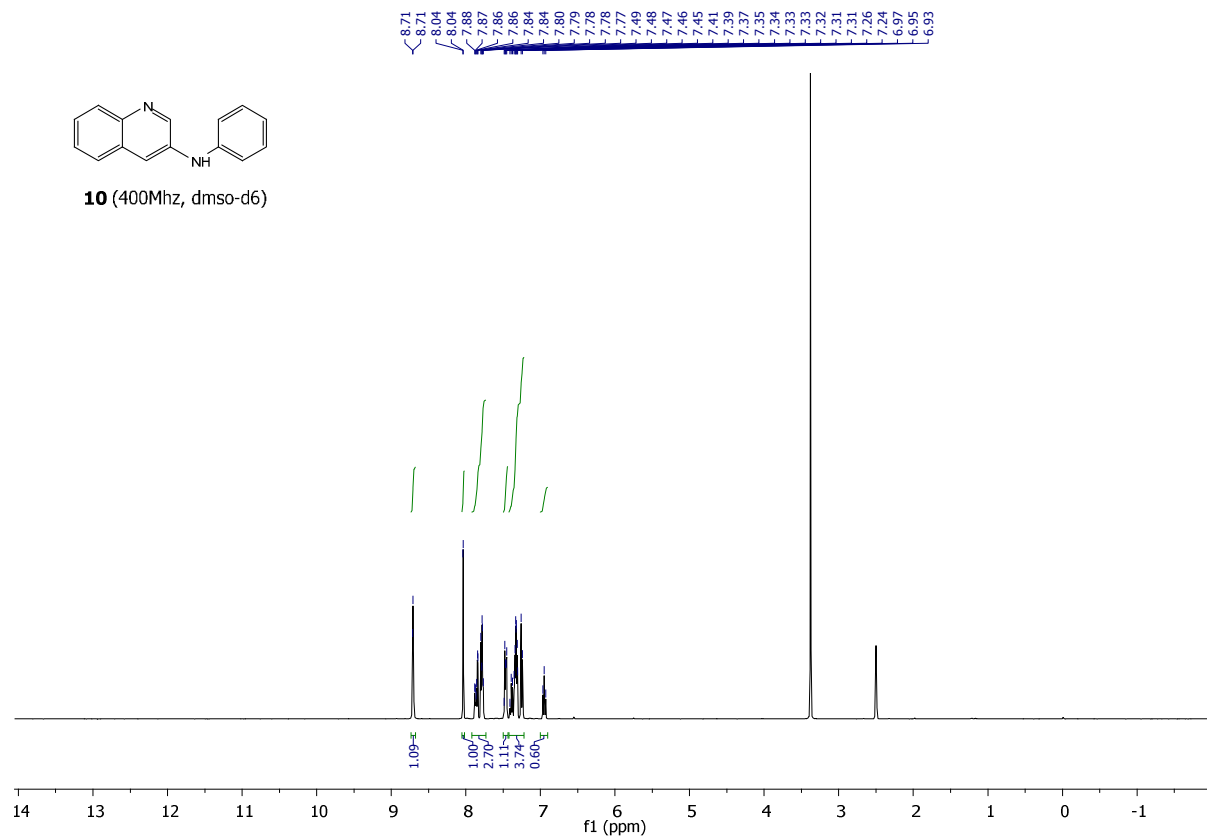
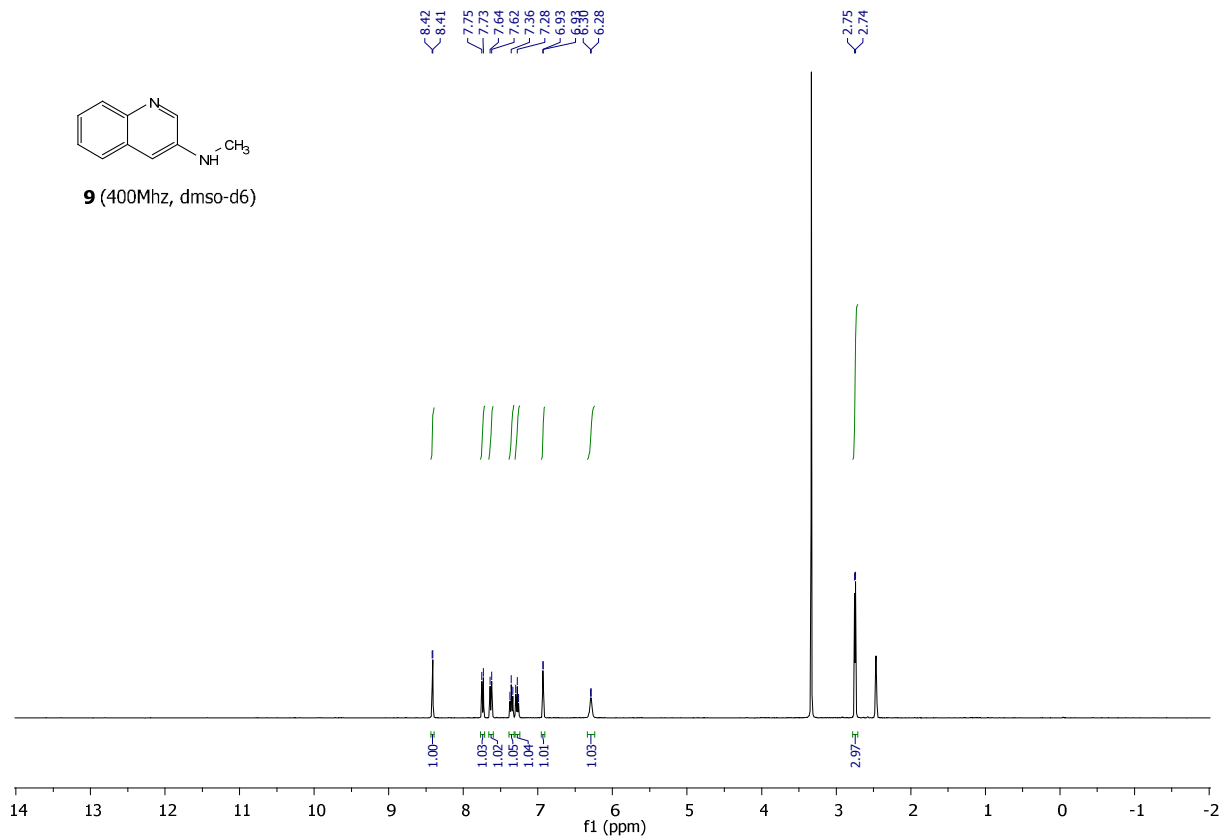


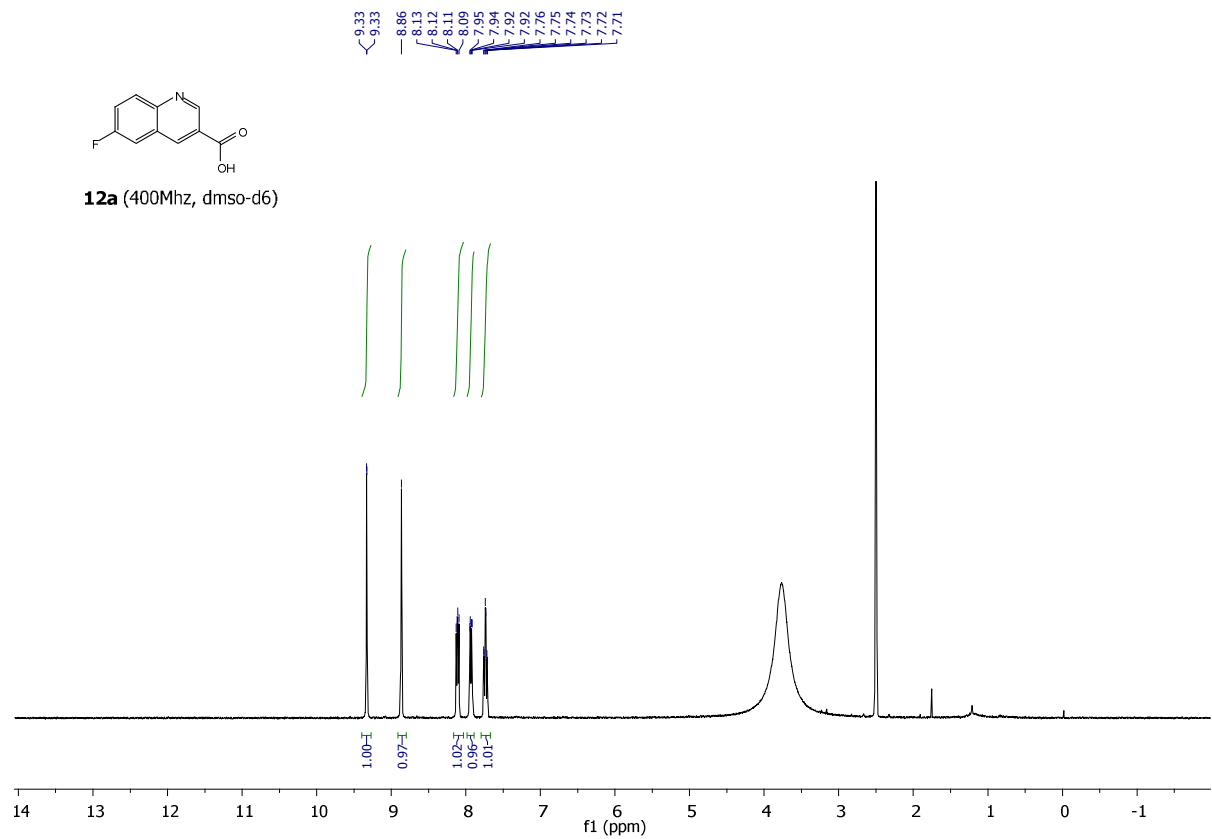
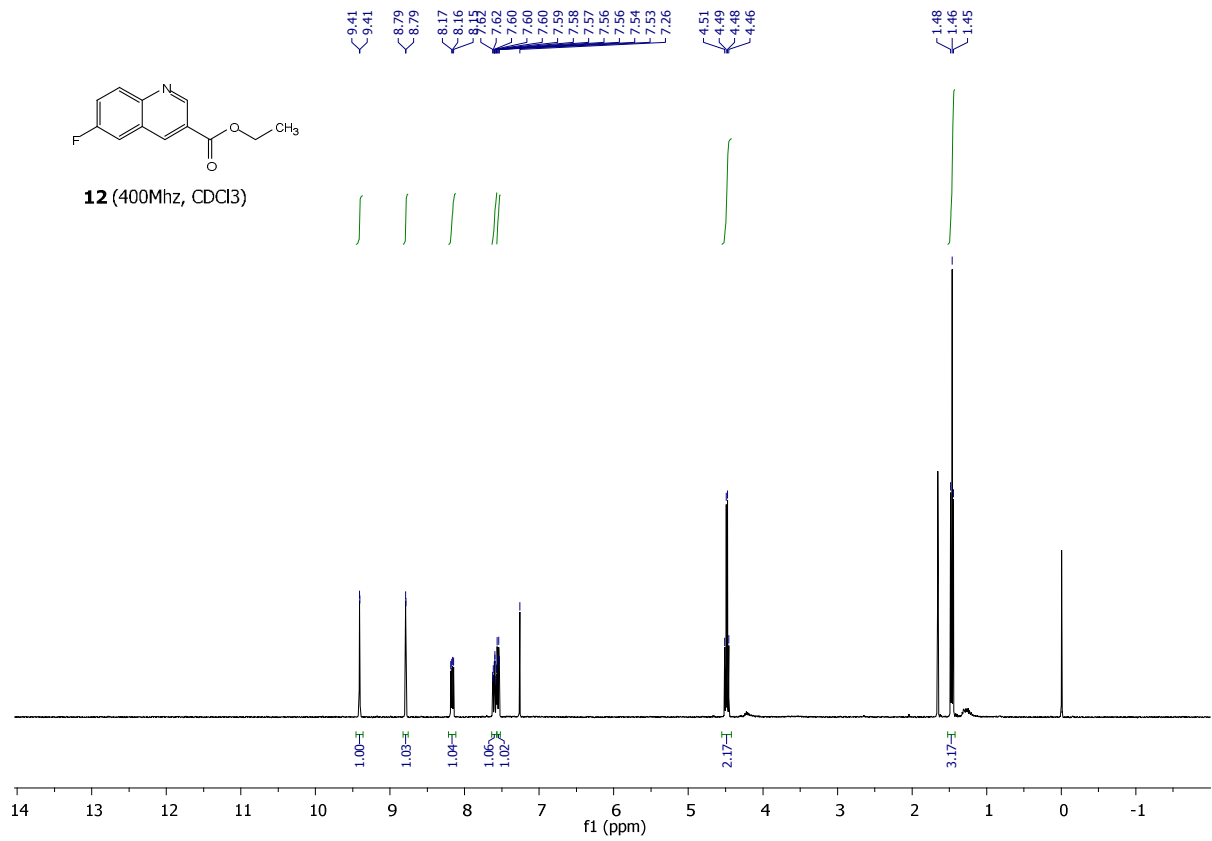


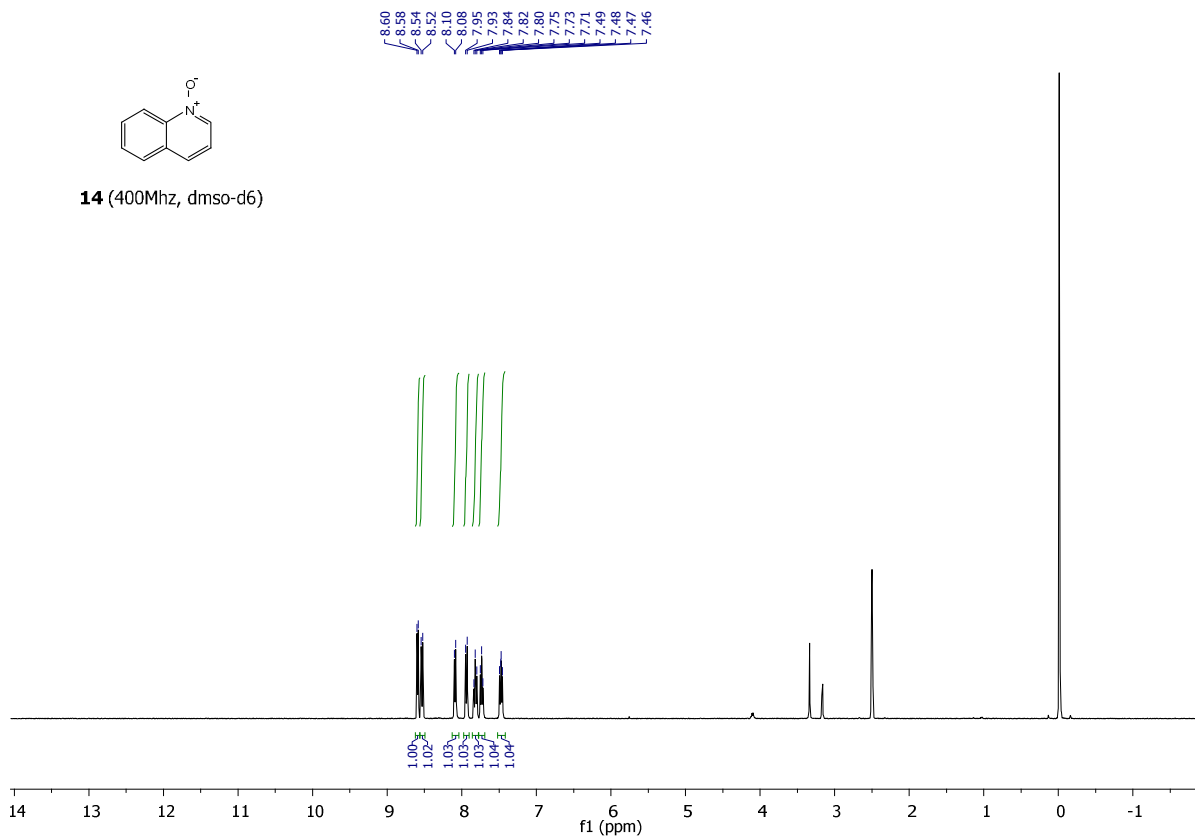
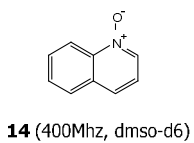
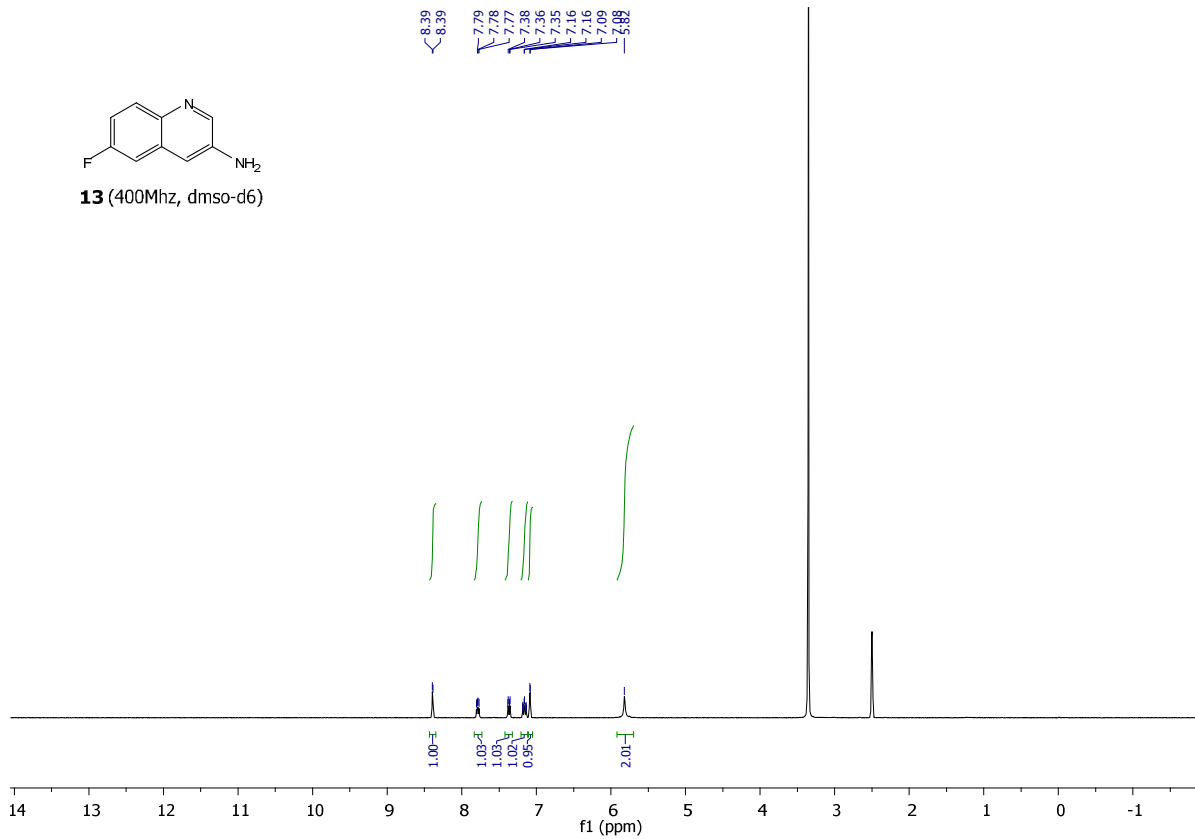
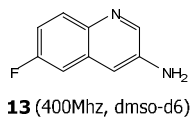


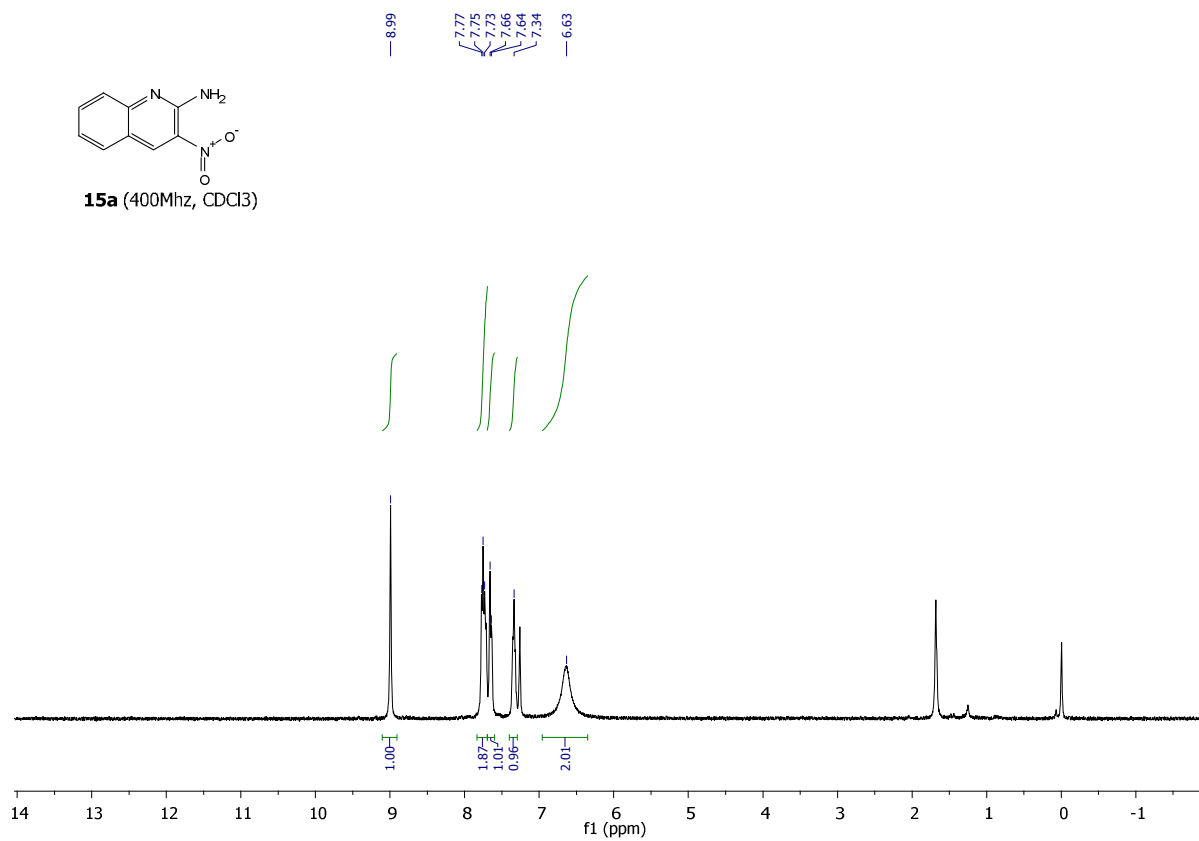
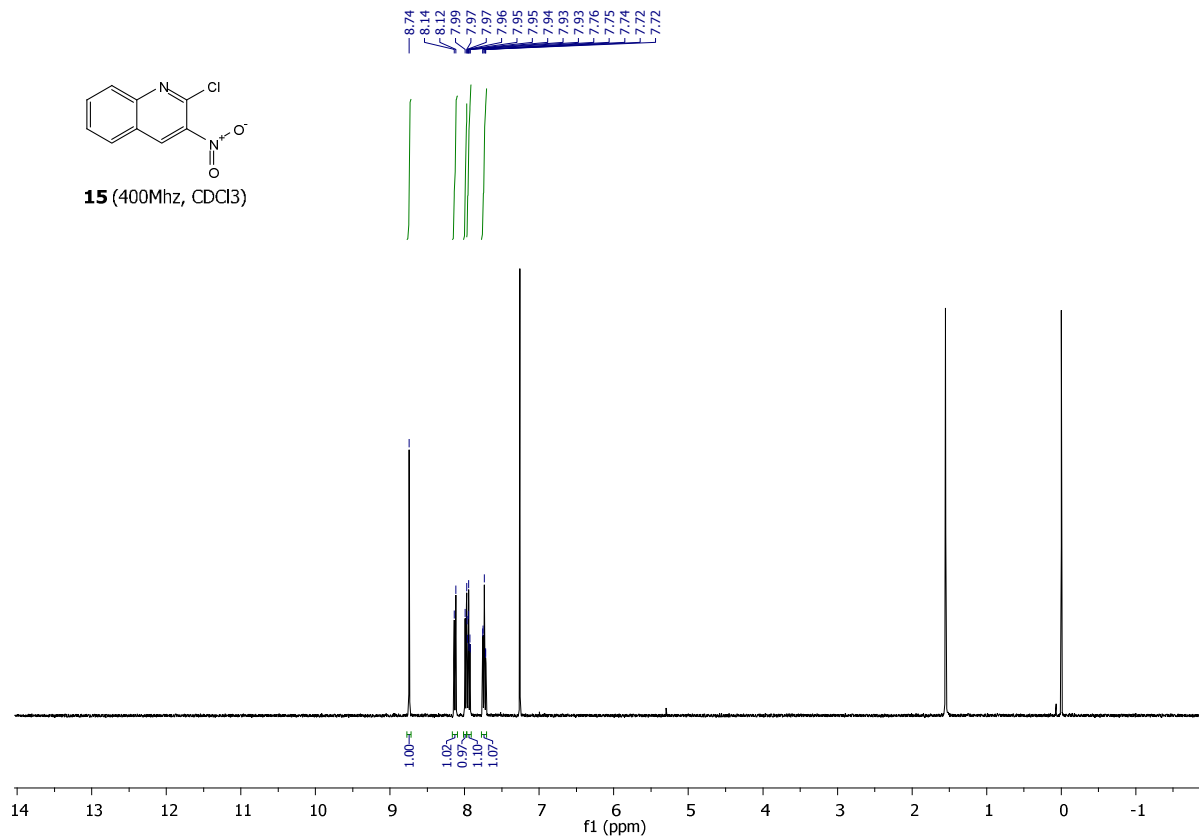


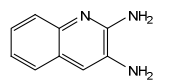




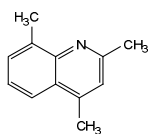
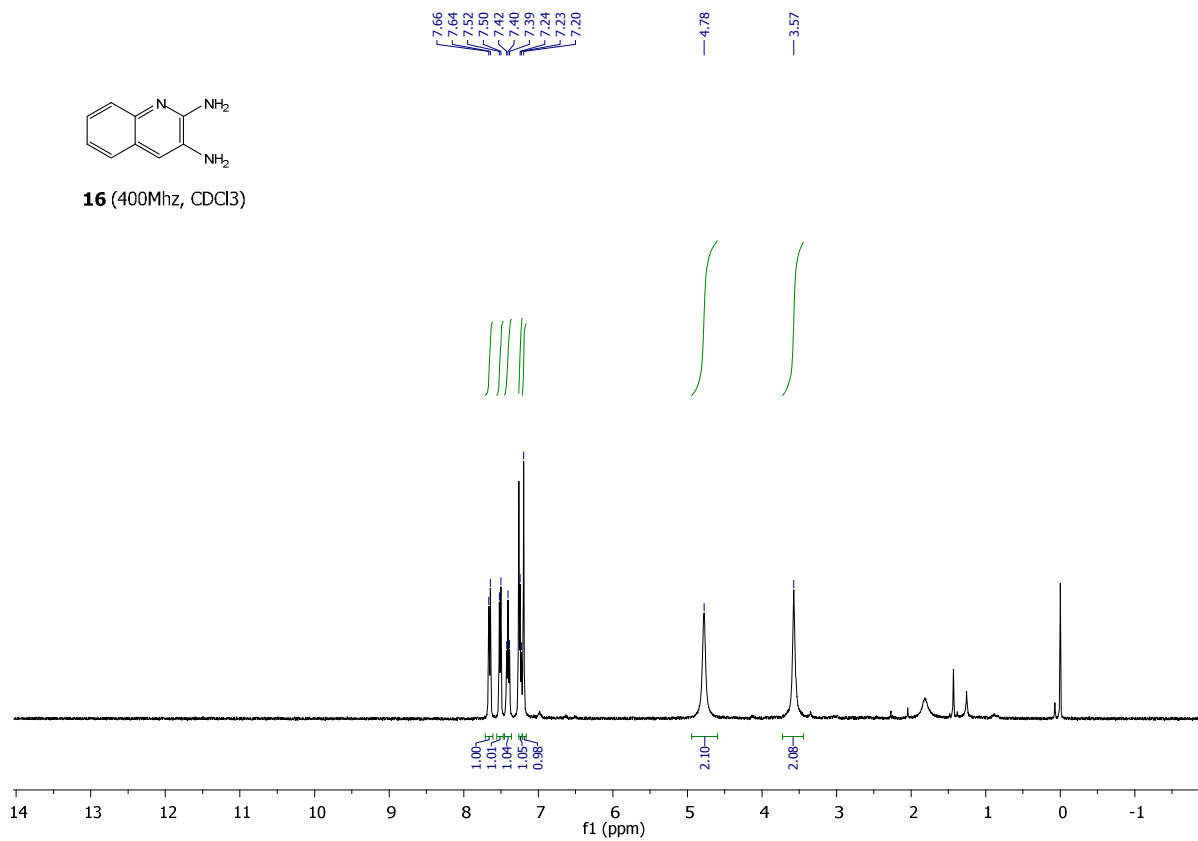




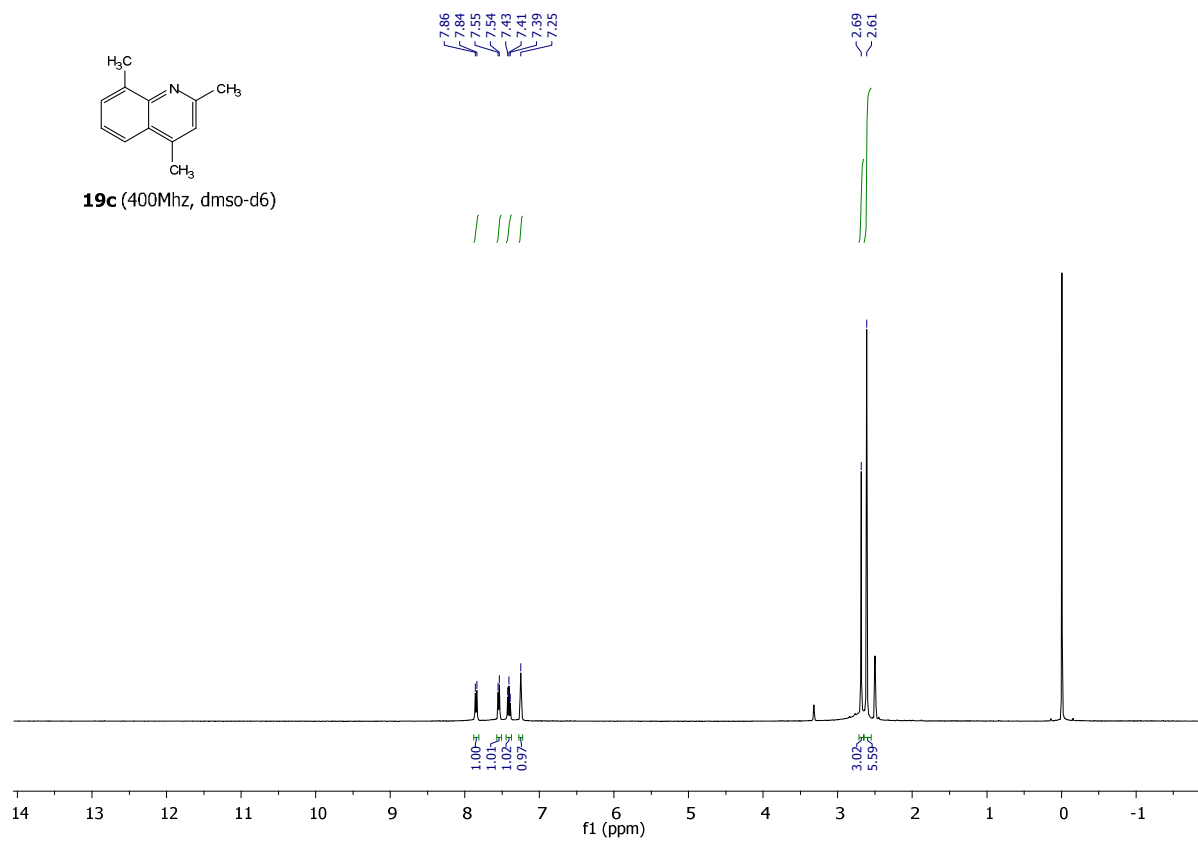


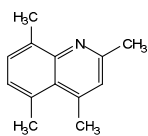


16 (400Mhz, CDCl₃)

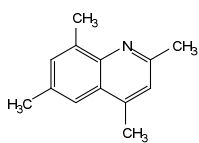
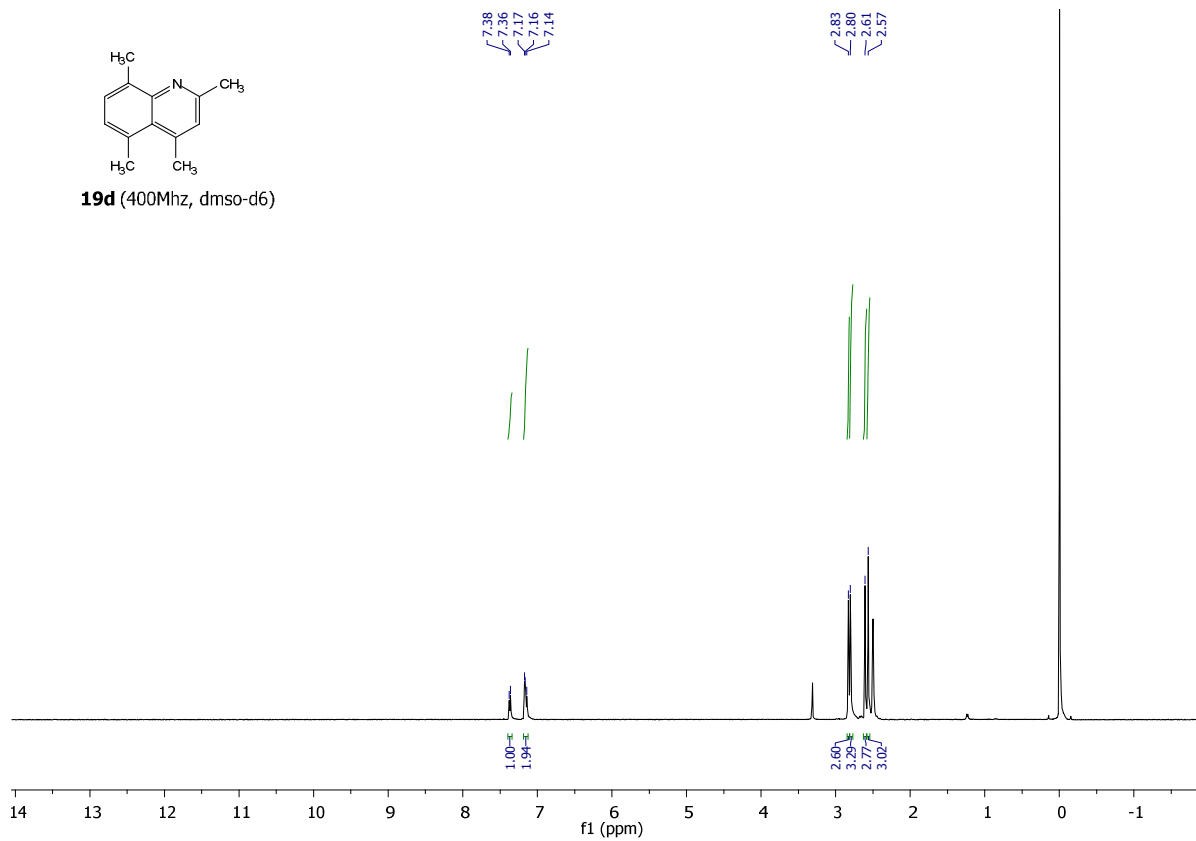


19c (400Mhz, dms_o-d₆)

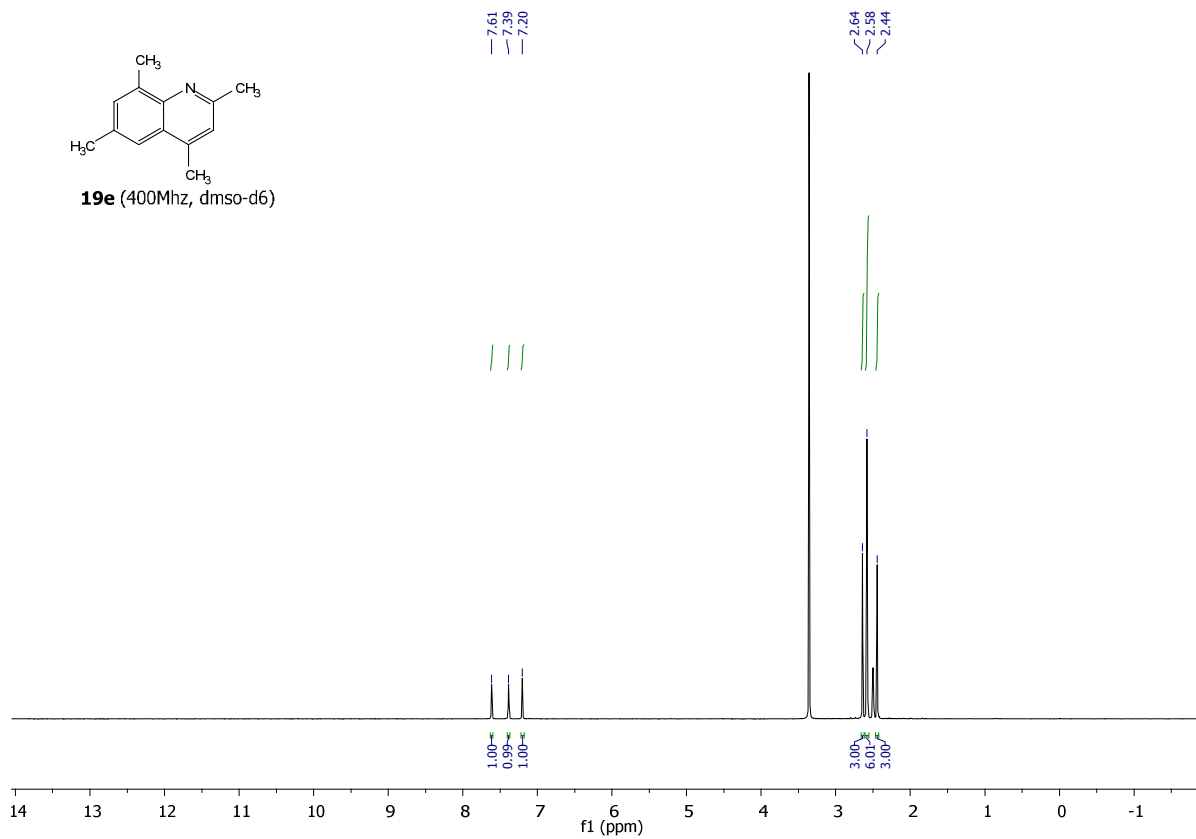


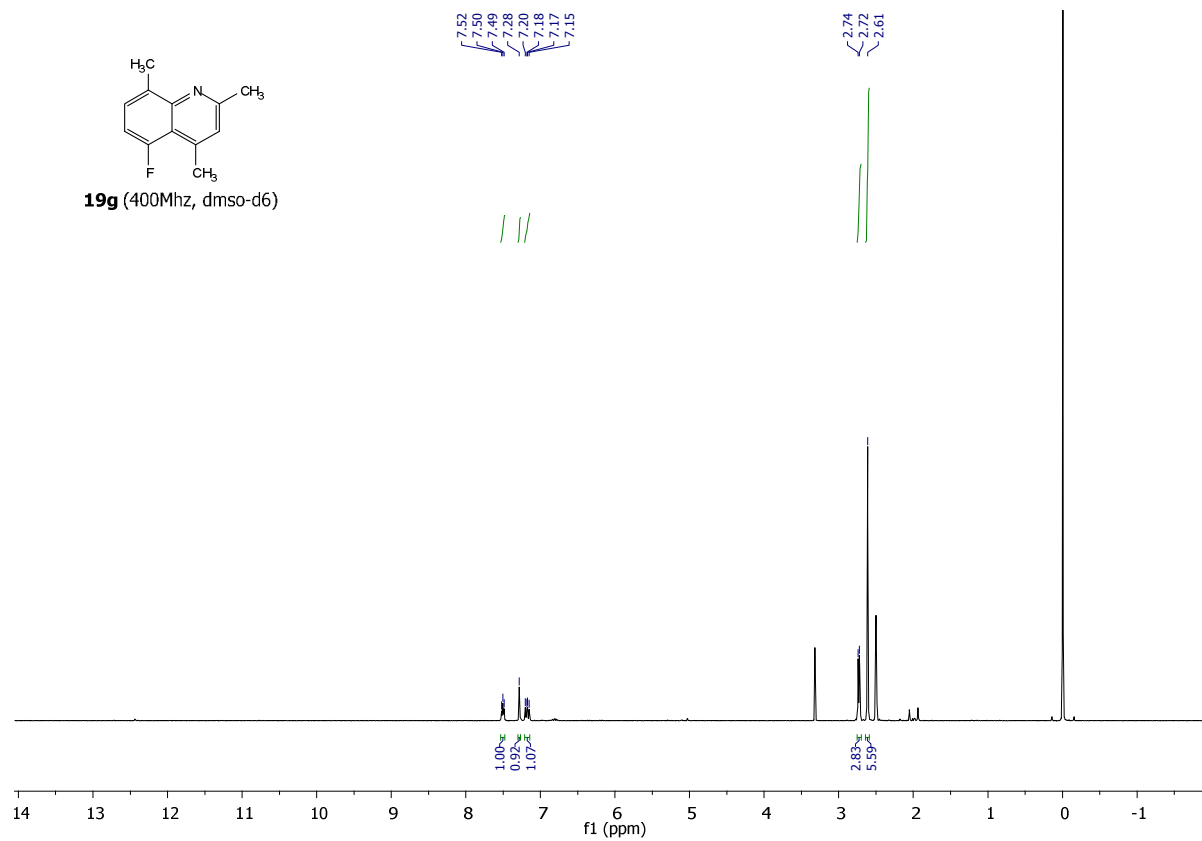
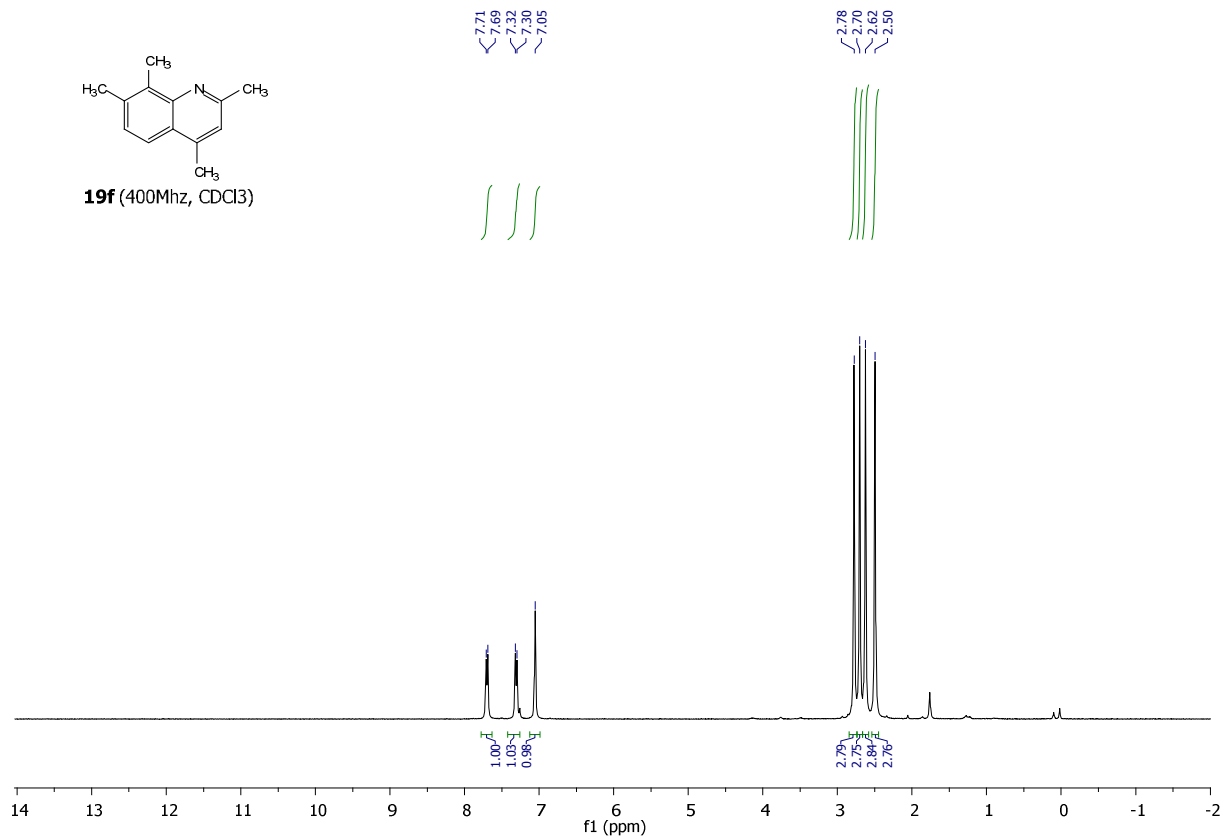


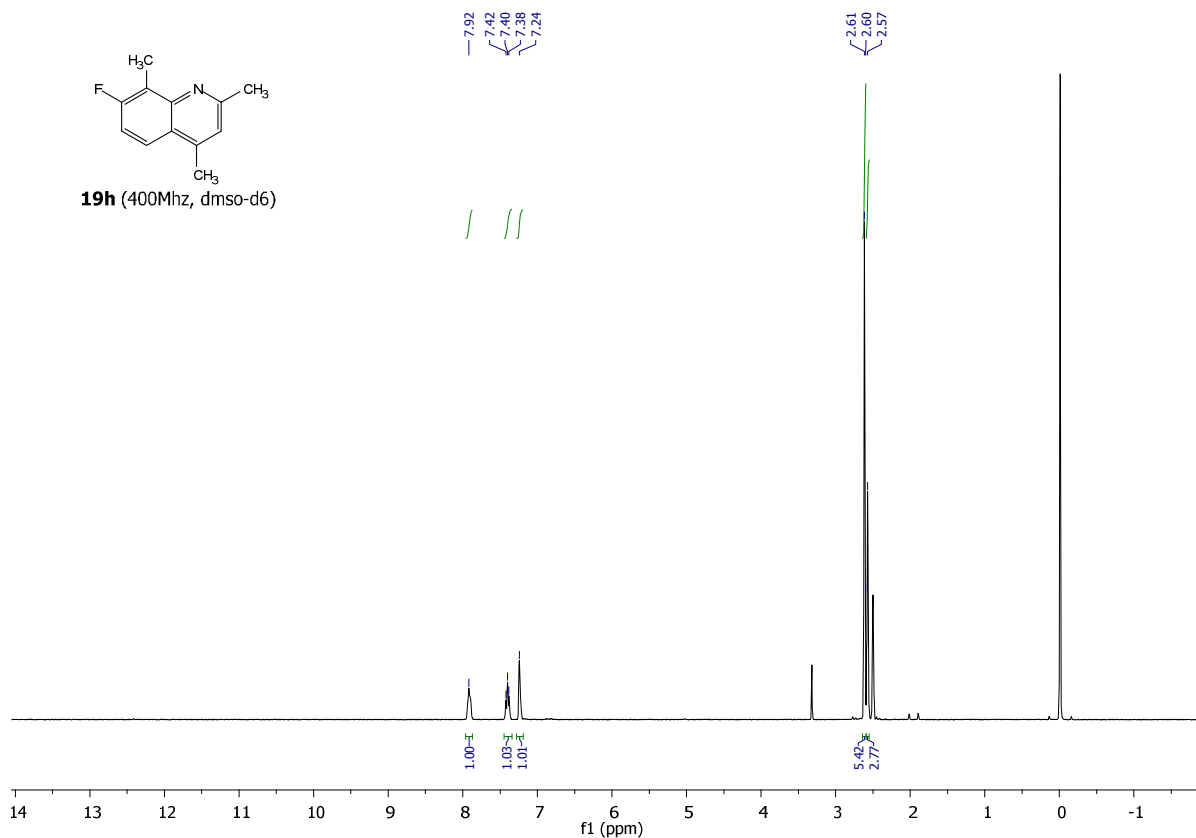
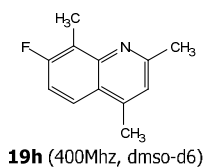
19d (400Mhz, dms0-d6)



19e (400Mhz, dms0-d6)

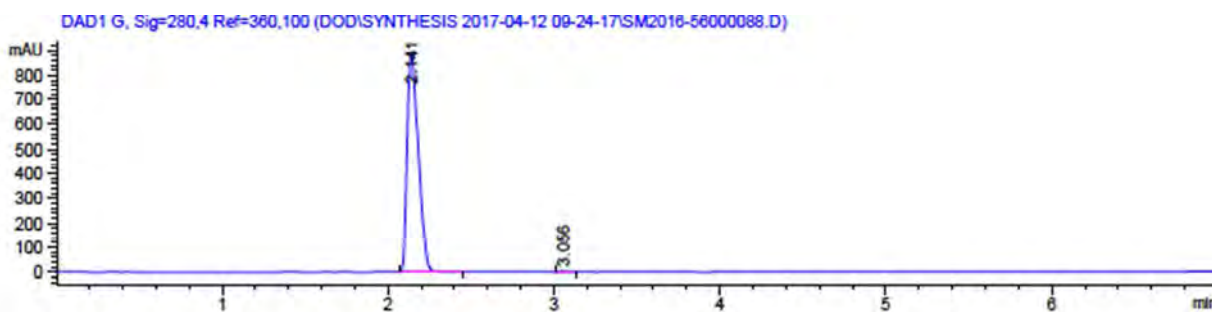






Section 4. Representative examples of HPLC analysis for compound purity

Compound ID: 1h

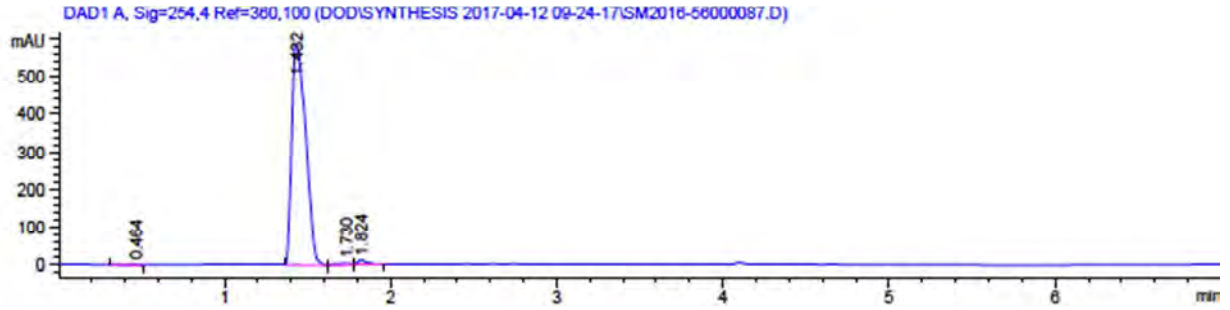


Signal 3: DAD1 G, Sig=280,4 Ref=360,100

Peak #	RetTime [min]	Type	Width [min]	Area [mAU*s]	Height [mAU]	Area %
1	2.141	BB	0.0725	4199.88086	898.40662	99.5756
2	3.056	BB	0.0459	17.89997	6.16931	0.4244

Totals : 4217.78082 904.57593

Compound ID: 3c

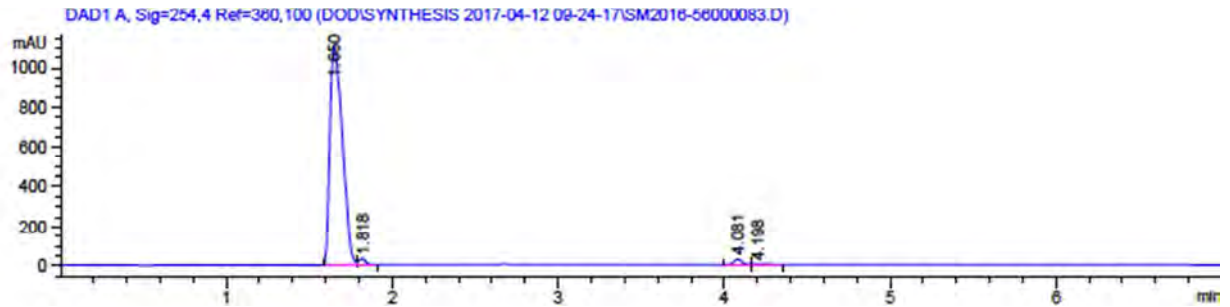


Signal 1: DAD1 A, Sig=254,4 Ref=360,100

Peak #	RetTime [min]	Type	Width [min]	Area [mAU*s]	Height [mAU]	Area %
1	0.464	BV	0.0777	13.45297	2.25304	0.3835
2	1.432	BV	0.0996	3412.29199	588.59271	97.2837
3	1.730	VV	0.0774	28.56310	5.09480	0.8143
4	1.824	VB	0.0625	53.26082	12.29953	1.5185

Totals : 3507.56888 608.24009

Compound ID: 3e

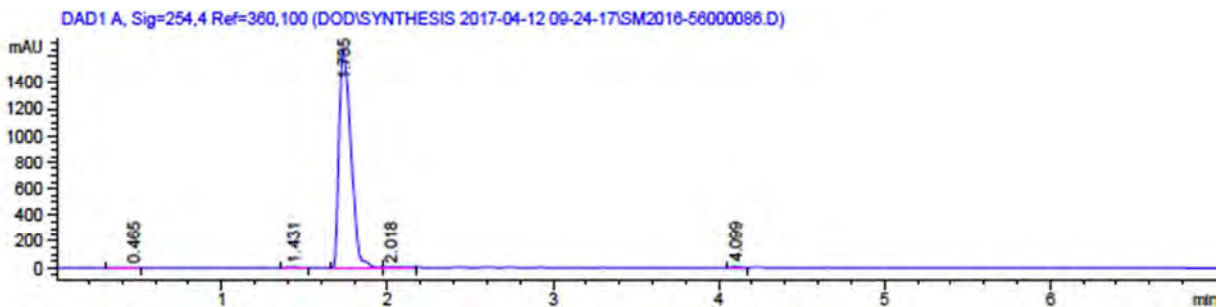


Signal 1: DAD1 A, Sig=254,4 Ref=360,100

Peak #	RetTime [min]	Type	Width [min]	Area [mAU*s]	Height [mAU]	Area %
1	1.650	BV	0.0887	5785.36182	1112.44946	96.5263
2	1.818	VV	0.0482	103.22385	33.25939	1.7222
3	4.081	BV	0.0487	88.92461	28.29437	1.4837
4	4.198	VB	0.0776	16.05269	2.85359	0.2678

Totals : 5993.56297 1176.85681

Compound ID: 3f

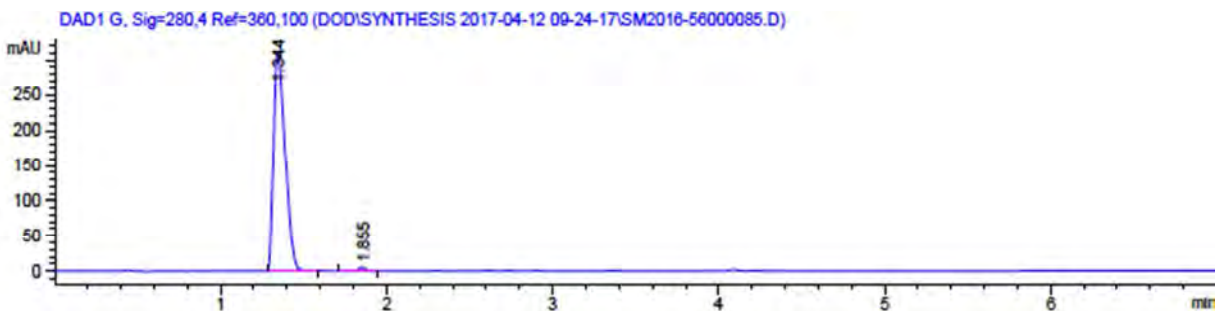


Signal 1: DAD1 A, Sig=254,4 Ref=360,100

Peak #	RetTime [min]	Type	Width [min]	Area [mAU*s]	Height [mAU]	Area %
1	0.465	BV	0.0774	12.31977	2.13157	0.1498
2	1.431	BB	0.0519	13.44873	4.14077	0.1635
3	1.735	BV	0.0791	8160.52441	1666.56018	99.2335
4	2.018	VB	0.0693	15.88238	3.23512	0.1931
5	4.099	BV	0.0492	21.38391	6.70686	0.2600

Totals : 8223.55921 1682.77451

Compound ID: 4e



Signal 3: DAD1 G, Sig=280,4 Ref=360,100

Peak #	RetTime [min]	Type	Width [min]	Area [mAU*s]	Height [mAU]	Area %
1	1.344	BB	0.0738	1503.31348	314.42178	99.0303
2	1.855	BB	0.0476	14.72062	4.82431	0.9697

Totals : 1518.03410 319.24609

Table S1. Analogs purchased from commercial vendors

List of commercial vendors: Sigma-Aldrich (St. Louis, MO); Chembride Corporation (San Diego, CA); ChemDiv (San Diego, CA); Specs (Hopkinton, RI); Cayman Chemical (Ann Arbor, MI); Pfaltz&Bauer (Waterbury, CT)

ID	Vendor	Catalog No.	ID	Vendor	Catalog No.
1a^a	Sigma-Aldrich	S706817	2a	Chemdiv	0099-0209
1g	Sigma-Aldrich	R254789	2b	Specs	AC-907/25005210
1i	Sigma-Aldrich	S395153	2c	Chembridge	CB5107625
1n	Specs	AC-907/25005147	2d	Chembridge	5102042
1p	Chembridge	5102000	2e	Specs	AT-051/43422621
1s	Chemdiv	0599-0777	2f	Chembridge	5102007
1t	Sigma-Aldrich	R461709	2g	Specs	AT-051/43422517
1u	Pfaltz&Bauer	M20475	2h	Chembridge	5102043
1v	Chembridge	5510892	2i	Chembridge	5101989
1w^b	Sigma-Aldrich	S633127	3a	Chemdiv	0691-0006
1x	Chemdiv	0086-0040	3b	Chemdiv	0691-0005
1y	Chemdiv	0986-0271	4a	Sigma-Aldrich	S619213
1z	Chemdiv	4644-0485	5a	Cayman	16604
5b	Specs	AC-907/25004951	5c	Specs	AP-263/40213615
6a	Chembridge	5119869	6b	Chembridge	5657969
6c	Chembridge	5119863	6d	Chembridge	5119941
6e	Chembridge	5107843	6f	Chembridge	5107881
7a	Sigma-Aldrich	R247324	7b	Sigma-Aldrich	S582204
7c	Chembridge	5244600	7d	Chembridge	4003435
7e	Chemdiv	4644-0485	7f	Sigma-Aldrich	S363863
7g	Chembridge	4004623	7h	Chembridge	5663920
7i	Sigma-Aldrich	755508			

^a The counter ion has been corrected from methyl sulfate to iodide.

^b The structure **1w** shown on Sigma-Aldrich website was incorrect and the corrected structure was confirmed with Sigma-Aldrich quality control team. Note: 1 Chembridge and 2 Specs compounds were identified with incorrect structures and not included in the study.

Table S2. N-methyl analogs and associated Vina docking scores

Analog	IC₅₀ (uM)	Vina score	Analog	IC₅₀ (uM)	Vina score
1a	12.1 ± 3.1	-7.1	2l	>1000	-6.0
1b	21.0 ± 2.1	-6.5	2m	2.8 ± 0.5	-6.6
1c	6.3 ± 1.1	-6.8	2n	15.9 ± 7.9	-5.3
1d	2.9 ± 0.7	-7.3	2o	>1000	-6.0 ^a
1e	6.9 ± 3.0	-6.9	3c	115 ± 41	-5.3 ^a
1f	9.9 ± 3.4	-6.2	3d	>1000	-5.0 ^a
1g	23.8 ± 5.6	-6.2	3e	>1000	-4.5 ^a
1h	>1000	-6.6 ^a	3f	>1000	-3.9 ^a
1i	7.5 ± 2.2	-7.4	3g	94.6 ± 76.3	-4.5
1j	11.4 ± 2.1	-7.2	3h	109 ± 59	-4.8
1k	1.2 ± 0.1	-7.4	4a	14.9 ± 6.1	-7.6 ^a
1l	4.6 ± 0.4	-7.8	4b	6.3 ± 2.7	-7.5 ^a
1m	5.7 ± 1.8	-6.6	4c	30.3 ± 7.0	-7.2
1n	13.1 ± 5.1	-6.3 ^a	4d	29.9 ± 9.1	-7.2
1o	34.4 ± 9.6	-7.0	4e	506 ± 199	-7.9 ^a
1p	120 ± 50	-6.2 ^a	4f	39.4 ± 18.0	-7.3 ^a
1q	2.6 ± 0.5	-6.7	5a	9.0 ± 0.6	-6.6
1r	12.0 ± 4.5	-6.4	5b	11.8 ± 3.0	-7.2
1t	1.8 ± 0.5	-7.5	6a	16.7 ± 6.4	-6.1
2j	1.2 ± 0.2	-6.8	6b	82.4 ± 17.4	-6.5
2k	87.0 ± 26.1	-6.8	6d	>1000	-5.0

^a Docked structure was not positioned within nicotinamide binding pocket.

Appendix 3: Neelakantan H, Vance V, Wetzel M, Wang HY, McHardy SF, Finnerty C, Hommel JD, Watowich SJ. Selective and membrane permeable small molecule inhibitor of nicotinamide N-methyltransferase reverses diet-induced obesity in mice. *Biochemical Pharmacology* 147, 141, 2018.



Selective and membrane-permeable small molecule inhibitors of nicotinamide N-methyltransferase reverse high fat diet-induced obesity in mice

Harshini Neelakantan^a, Virginia Vance^a, Michael D. Wetzel^{b,c}, Hua-Yu Leo Wang^d, Stanton F. McHardy^d, Celeste C. Finnerty^{b,c}, Jonathan D. Hommel^e, Stanley J. Watowich^{a,*}

^a Department of Biochemistry and Molecular Biology, University of Texas Medical Branch, Galveston, TX 77550, USA

^b Department of Surgery, University of Texas Medical Branch, Galveston, TX 77550 USA

^c Shriners Hospitals for Children-Galveston, Galveston, TX 77550, USA

^d Department of Chemistry and Center for Innovative Drug Discovery, University of Texas at San Antonio, San Antonio, TX 78249, USA

^e Department of Pharmacology and Toxicology, University of Texas Medical Branch, Galveston, TX 77550, USA

ARTICLE INFO

Article history:

Received 7 September 2017

Accepted 13 November 2017

Available online 15 November 2017

Keywords:

Obesity

Therapeutics

Nicotinamide N-methyltransferase

Inhibitors

Weight loss

ABSTRACT

There is a critical need for new mechanism-of-action drugs that reduce the burden of obesity and associated chronic metabolic comorbidities. A potentially novel target to treat obesity and type 2 diabetes is nicotinamide-N-methyltransferase (NNMT), a cytosolic enzyme with newly identified roles in cellular metabolism and energy homeostasis. To validate NNMT as an anti-obesity drug target, we investigated the permeability, selectivity, mechanistic, and physiological properties of a series of small molecule NNMT inhibitors. Membrane permeability of NNMT inhibitors was characterized using parallel artificial membrane permeability and Caco-2 cell assays. Selectivity was tested against structurally-related methyltransferases and nicotinamide adenine dinucleotide (NAD⁺) salvage pathway enzymes. Effects of NNMT inhibitors on lipogenesis and intracellular levels of metabolites, including NNMT reaction product 1-methylnicotinamide (1-MNA) were evaluated in cultured adipocytes. Effects of a potent NNMT inhibitor on obesity measures and plasma lipid were assessed in diet-induced obese mice fed a high-fat diet. Methylquinolinium scaffolds with primary amine substitutions displayed high permeability from passive and active transport across membranes. Importantly, methylquinolinium analogues displayed high selectivity, not inhibiting related SAM-dependent methyltransferases or enzymes in the NAD⁺ salvage pathway. NNMT inhibitors reduced intracellular 1-MNA, increased intracellular NAD⁺ and S-(5'-adenosyl)-L-methionine (SAM), and suppressed lipogenesis in adipocytes. Treatment of diet-induced obese mice systemically with a potent NNMT inhibitor significantly reduced body weight and white adipose mass, decreased adipocyte size, and lowered plasma total cholesterol levels. Notably, administration of NNMT inhibitors did not impact total food intake nor produce any observable adverse effects. These results support development of small molecule NNMT inhibitors as therapeutics to reverse diet-induced obesity and validate NNMT as a viable target to treat obesity and related metabolic conditions. Increased flux of key cellular energy regulators, including NAD⁺ and SAM, may potentially define the therapeutic mechanism-of-action of NNMT inhibitors.

© 2017 Elsevier Inc. All rights reserved.

1. Introduction

Obesity is a major public health problem around the world that is linked to severe comorbid disease conditions, physical impairment, high mortality rates, and compromised quality of life

[1–4]. Obesity is characterized by the buildup of excessive body fat and extreme dysregulation in whole-body energy expenditure, glucose, hormone, and lipid homeostasis that typically present as adverse metabolic disorders [4,5]. Additionally, the physiological, metabolic, and psychological changes that accompany obesity are major factors in the development of type 2 diabetes (T2D), cardiovascular disease (CVD) (e.g., coronary heart disease, dyslipidemia, hypertension) [6,7], stroke, inflammation, non-alcoholic fatty

* Corresponding author.

E-mail address: watowich@xray.utmb.edu (S.J. Watowich).

liver disease (NAFLD), non-alcoholic steatohepatitis (NASH), osteoarthritis, sleep apnea, and several obesity-linked cancers (e.g., colorectal, breast, kidney, prostate) [6,8]. Lifestyle modifications including diet and exercise may help reverse obesity and improve chronic disease biomarkers (e.g., T2D) [9], but are largely ineffective in achieving sustained weight loss and glycemic control [10]. Pharmacological treatments for obesity exist, but unfortunately most approved anti-obesity drugs have only modest efficacy and/or produce severe adverse effects (e.g., cardiovascular risks, central nervous system effects). Thus, there is a critical need for more effective pharmacological interventions that improve long-term management of obesity and its comorbidities [11].

Recently, nicotinamide-N-methyltransferase (NNMT) has emerged as a novel mechanism-of-action target in the adipose tissue to treat obesity and associated T2D [12–15]. NNMT is a cytosolic enzyme with a newly identified role in modulating cellular energy homeostasis by jointly regulating nicotinamide (NA) and S-(5'-adenosyl)-L-methionine (SAM) flux within the critical intracellular nicotinamide adenine dinucleotide (NAD⁺) salvage pathway and methionine cycle, respectively [15]. NNMT expression is upregulated in the white adipose tissue (WAT) of obese and diabetic mice [12] and has significantly higher activity in the WAT compared to its activity in the brown adipose tissue, liver, and lungs of diet-induced obese mice [16]. Furthermore, plasma levels of the NNMT reaction product 1-methylnicotinamide (1-MNA) correlate with adipose NNMT expression, individuals' body mass index (BMI), and waist circumference, suggesting the target to be clinically relevant [13,14]. Importantly, mice fed a high-fat diet and treated with antisense oligonucleotides (ASOs) that reduced adipose NNMT expression were protected from diet-induced obesity (DIO) and showed reduced adiposity compared to control animals [12].

Using structure-guided design and binding calculations, we recently generated potent small molecule NNMT inhibitors around a methylquinolinium (MQ)-scaffold [17]. In the present study, we extend these findings to show that the small molecule NNMT inhibitors are highly membrane-permeable, selective inhibitors, which reduce intracellular 1-MNA levels and prevent lipogenesis *in vitro*. These amenable properties demonstrated for the small molecules led us to conduct a proof-of-concept *in vivo* study in diet-induced obese mice to test the hypothesis that the most potent inhibitor when administered systemically, would reverse obesity by causing substantial loss of body weight and adiposity without causing any observable adverse effects.

2. Materials and methods

2.1. Chemicals

NNMT inhibitors and standards for LC/MS/MS studies were purchased from established commercial suppliers or synthesized in-house by established synthetic schemes as described previously [17]. SAM, NA, 1-MQ, 1,8-diMQ, NAD⁺, and 6-chloro nicotinamide (6-CN) were obtained from Sigma-Aldrich (St. Louis, MO, USA). 1-MNA and S-(5'-adenosyl)-L-methionine (SAH) were obtained from Cayman Chemical Company (Ann Arbor, MI, USA).

2.2. Parallel artificial membrane permeability assay (PAMPA)

Passive membrane transport properties were measured using a 96-well pre-coated PAMPA plate system with membrane pore size 0.4 μm (Gentest™, Corning; Bedford, MA, USA). Briefly, 1 mM stock solution of each compound was prepared in deionized water, diluted to a final concentration of 400 μM in PBS (Sigma Aldrich; St. Louis, MO), and placed in the plate bottom well (donor well).

After 4 h of incubation at room temperature, the sample concentration in the donor and acceptor wells were measured using a UV-Vis spectrophotometer (Beckman, DU640) set at the wavelength corresponding to the maximum absorption of each compound. Compound concentration in the donor and acceptor wells were calculated from calibration curves spanning 400 to 3.125 μM. Samples were tested in triplicates in three separate experiments.

2.3. Bi-directional permeability assay with Caco-2 cells

Compounds were tested in a Caco-2 cell bi-directional permeability assay using an established contract research organization (Cyprotex; Watertown, MA, USA). Briefly, Caco-2 cells were seeded in 96-well plates and allowed to grow in culture media for three weeks, feeding at 2-day intervals. To ensure a well-defined Caco-2 cell monolayer prior to initiation of experiments, aliquots of the cell buffers were analyzed by fluorescence to determine the transport of the impermeable dye Lucifer yellow. For apical to basolateral (A → B) and basolateral to apical (B → A) permeability, compounds were added at 10 μM concentration to the apical (A) side and basolateral (B) side, respectively, and the corresponding amount of permeation was determined by measuring compound concentration on the B or A side. The A-side buffer contained 100 μM Lucifer yellow dye, in transport buffer (1.98 g/L glucose in 10 mM HEPES, 1x Hank's balanced salt solution, pH 7.4), and the B-side buffer was transport buffer at pH 7.4. Caco-2 cells were incubated with these buffers for 2 h, and the receiver side buffer was removed for analysis by LC/MS/MS (using bucetin as an analytical internal standard). Data were expressed as permeability (P_{app}) calculated using the following formula:

$$P_{app} = \frac{dQ/dt}{c_0A}, \text{ where}$$

dQ/dt, rate of permeation

c_0 , initial concentration of compound
A, area of monolayer (0.11 cm²)

Efflux Ratio (R_e) was calculated using the formula:

$$R_e = \frac{P_{app}(B \rightarrow A)}{P_{app}(A \rightarrow B)}$$

2.4. MTT cell viability assay

3T3-L1 pre-adipocytes cells (catalog CL-173, American Type Culture Collection; Manassas, VA, USA) were seeded at a density of 2×10^3 cells per well in 96-well plates, cultured with standard culture media [DMEM, 4.5 g/L glucose, L-glutamine, sodium pyruvate (Mediatech Inc.; Tewksbury, MA, USA), 10% FBS (Sigma Aldrich; St. Louis, MO, USA), 1% antibiotic-antimycotic solution (Mediatech Inc.; Tewksbury, MA, USA)], and grown for 48 h until >~90% confluent. Cells were treated for 24 h with 0.1–600 μM NNMT inhibitors in cell culture media. A 24 h time point was chosen based on a previous report of using this time period for transfecting or treating 3T3-L1 cells with NNMT anti-sense oligonucleotides or a small molecule NNMT product inhibitor (1-MNA), respectively, for phenotypic measures [12]. MTT (3-(4,5-dimethylthiazol-2-yl)-2,5-diphenyltetrazolium bromide) (ATCC; Manassas, VA, USA) was added to each well and assayed according to the manufacturer's instructions. Absorbance corresponding to the amount of formazan dye produced by treated cells was normalized to that produced by control (untreated) cells to calculate % viable cells in the treated samples.

2.5. Differentiation of 3T3-L1 pre-adipocytes

3T3-L1 pre-adipocytes cells were cultured with standard culture media (DMEM, 4.5 g/L glucose, L-glutamine, sodium pyruvate, 10% FBS, 1% antibiotic-antimycotic solution) and grown for 48 h before initiating differentiation using the manufacturer's suggested protocol and modified from previously published work [18]. Briefly, standard culture medium was supplemented with scheduled addition of adipogenic agents [3-isobutyl-1-methyl xanthine (IBMX), Sigma Aldrich; MO, USA), dexamethasone (Sigma Aldrich; MO, USA), insulin (Gibco Life Technologies Inc.; Grand Island, NY, USA)] over 10 days to promote differentiation of 3T3-L1 fibroblasts into adipocytes; a combination of 1 mM IBMX, 1 μ M dexamethasone, and 10 μ g/ml of insulin in media was added to fully confluent 3T3-L1 fibroblasts for three days (days 0–3) to initiate differentiation. At day 3, the medium was replaced with culture media supplemented with insulin (10 μ g/ml). After day 6, cells were maintained in culture media until described experiments were begun (days 8–10).

2.6. Quantitative measurement of NNMT reaction product 1-MNA in cultured cells

Cellular 1-MNA concentrations were determined using an ultra-sensitive high-resolution AB Sciex 6500 Q-trap mass spectrometer coupled to an Agilent 1260 ultra-high pressure liquid chromatography (LC/MS/MS) system. Using multiple reaction monitoring (MRM) positive ion mode, the 1-MNA NNMT reaction product was quantified from peak area ratios using AB Sciex Analyst and MultiQuant 2.1 software and the parent precursor and Q3 masses set to m/z 137.1 and 94.1, respectively. Fragment ions at m/z of 92.1 and 77.9 were additionally used for the detection and confirmation of 1-MNA, respectively. Processing of undifferentiated 3T3-L1 pre-adipocytes (day 0) and differentiated adipocytes (day 10) were optimized for recovery and reproducibility of 1-MNA levels across cultured batches of 3T3-L1 cells (~passages 7–8) and the 1-MNA levels were compared between the pre-adipocytes and adipocytes. To determine the effect of NNMT inhibitor on NNMT activity in the pre-adipocytes and differentiated adipocytes (8×10^4 cells/well seeded prior to beginning differentiation), cells were treated with 30 μ M inhibitor for 24 h. Similarly, to compare the relative effects of multiple NNMT inhibitors on NNMT activity in cultured adipocytes, differentiated adipocytes in 6-well plates were treated with 10 μ M test compound for 24 h. Following treatment, medium was replaced with 80% (v/v) methanol (cooled to -80°C) containing 500 nmol 6-chloronicotinamide (6-CN) as an internal standard (IS) to extract cellular metabolites. Adherent cells were scrapped, then centrifuged at 4°C and 13,000g for 15 min, and the resulting supernatants processed using established protocols [19]. Intracellular levels of 1-MNA and as well as the IS were determined from LC/MS/MS peak areas. Data were subsequently normalized to the IS peak area and transformed as % control values for cross-sample comparisons. The above procedure was repeated with inhibitor concentrations spanning 0.3–60 μ M for 5-amino-1MQ to determine the effective concentration (EC_{50}) required to inhibit 50% NNMT activity in cultured adipocytes. Choice of inhibitor concentrations and time period was chosen based on the results of the MTT studies.

2.7. Quantitative measurement of selected metabolites in cultured cells

The relative levels of selected metabolites (NA, SAM, SAH, NAD^+) regulated by cellular energy expenditure pathways associated with NNMT were simultaneously detected using LC/MS/MS and MRM ratios. Sample processing was performed as described above. Parent precursor masses of 124.0, 399.3, 385.1, and 665.1

Da and Q3 masses set to m/z 80.0, 250.1, 136.0, and 136.0 were used for the quantitation of NA, SAM, SAH, and NAD^+ , respectively.

2.8. Selectivity of NNMT inhibitors

Test compounds were screened in biochemical assays for activity against three structurally similar methyltransferases, including catechol-O-methyltransferase (COMT), DNA (cytosine-5)-methyltransferase 1 (DNMT1), and protein arginine methyltransferase 3 (PRMT3). Additional biochemical assays were used to test the ability of compounds to inhibit nicotinamide phosphoribosyl transferase (NAMPT) and NAD^+ -dependent protein deacetylase sirtuin 1 (SIRT1), two enzymes in the NAD^+ biosynthesis/salvage pathway. All assays were performed by Reaction Biology Corporation (RBC; Malvern, PA, USA) and complete assay details are noted below. For each test compound, IC_{50} values were calculated from dose-response curves established with 10 concentrations of a half-log dilution series. For each assay, established enzyme specific inhibitors were included as positive controls for enzyme function and assay reproducibility. IC_{50} values were determined by non-linear least-squares fitting of a 4-parameter dose-response curve to collected data points (Graphpad Prism 7.0; La Jolla, CA, USA).

2.8.1. DNMT1 activity assay

A radiometric assay was performed by RBC using 100 μ M–5 nM SAH as an inhibitor positive control. The analogues, 1,8-diMQ and 5-amino-1MQ were tested at concentrations from 200 μ M to 10 nM and 600 μ M to 10 nM, respectively. Reactions were performed with 0.001 mg/ml DNA substrate Poly(dI-dC), 1 μ M radiolabelled S-adenosyl-L-[methyl- ^3H] methionine (SAM) co-substrate, and recombinant human DNMT1 enzyme. Activity was monitored via quantification of radiolabeled reaction product DNA 5-[methyl- ^3H]-cytosine.

2.8.2. PRMT3 activity assay

A radiometric assay was performed by RBC using 100 μ M–5 nM SAH as an inhibitor positive control. The analogues, 1,8-diMQ and 5-amino-1MQ were tested at concentrations from 200 μ M to 10 nM and 600 μ M to 10 nM, respectively. Reactions were performed with 5 μ M histone H3 (histone L-arginine) substrate, 1 μ M radiolabeled S-adenosyl-L-[methyl- ^3H] methionine (SAM) co-substrate, and recombinant human PRMT3 enzyme. Activity was monitored via quantification of radiolabeled reaction product histone [methyl- ^3H]-L-arginine.

2.8.3. 3, COMT activity assay

A radiometric assay was performed by RBC using 1 μ M–50 pM tolcapone as an inhibitor positive control. The analogues, 1,8-diMQ and 5-amino-1MQ were tested at concentrations from 200 μ M to 10 nM and 600 μ M to 10 nM, respectively. Reactions were performed with 0.5 μ M catechol substrate COMT-S01, 1 μ M radiolabelled S-adenosyl-L-[methyl- ^3H] methionine (SAM) co-substrate, and recombinant human COMT enzyme. Activity was monitored via quantification of methylated catechol reaction product (guaiacol [methyl- ^3H]).

2.8.4. NAMPT activity assay

A fluorometric assay was performed by RBC using 1 μ M–50 pM FK866 as an inhibitor positive control. The analogue 5-amino-1MQ was tested at concentrations from 600 μ M to 30 nM. Reactions were performed with 2 μ M nicotinamide and 30 μ M phosphoribosyl pyrophosphate (PRPP) in the presence of 1 mM ATP and recombinant human NAMPT enzyme. Activity was monitored using fluorescence detection and quantification of the nicotinamide mononucleotide (NMN) reaction product.

2.8.5. SIRT-1 activity assay

A fluorometric assay was performed by RBC using 100 μM –5 nM suramin sodium as an inhibitor positive control. The analogue 5-amino-1MQ was tested at concentrations from 600 μM to 30 nM. Reactions were performed with 50 μM RHKKAC, a fluorogenic peptide substrate from p53 residues 379 to 382, 500 μM NAD^+ co-substrate, and recombinant human SIRT-1 (NAD^+ -dependent) enzyme. Activity was monitored by the formation of a fluorescent product (coumarin) generated by a two-step coupled reaction that involved deacetylation of substrate by SIRT-1 followed by secondary release of the fluorophore.

2.9. Efficacy of NNMT inhibitor 5-amino-1MQ in diet-induced obese (DIO) mice

17-Week old, male DIO C57Bl/6 mice that have been fed high-fat diet (HFD) for 11 weeks (starting at week 6) were purchased from Jackson Labs (Jackson Laboratory; Bar Harbour, ME, USA). Mice were initially group housed (three/cage) and allowed to acclimate to the colony environment maintained at a constant temperature (21–23 °C) and humidity (40–50%) on a 12-h light–dark cycle (lights on 0600–1800 h). Upon arrival, mice were continued to be fed HFD (Open Source Diets formula D12451 from Research Diets Inc.; New Brunswick, NJ, USA), containing 45% energy from fat. Water was available *ad libitum*. All experiments were carried out in accordance with the *Guide for the Care and Use of Laboratory Animals* [20] and with approval from the Institutional Animal Care and Use Committee at the University of Texas Medical Branch. Following acclimation for seven days, mice were single-housed and maintained on HFD for 4 additional weeks. Mice were intermittently handled, with body weights and food intake (hopper weights) measured 2–3 times per week. After being fed HFD for a total of 16 weeks (an appropriate rodent model of DIO and comparable to human obesity [21]) and reaching pre-arrival body weights (~ 38 g), mice were randomized into balanced control and treatment cohorts ($n = 9/\text{cohort}$), with similar group average body weight and standard deviation. Mice in the vehicle cohort received three subcutaneous (SC) saline (1 ml/kg) injections/day (~ 0930 , 1330, 1730 h) and mice in the treatment cohort received three SC injections of the NNMT inhibitor 5-amino-1MQ at a dose of 20 mg/kg/injection for a total dose of ~ 34 mg/kg/day of the parent compound (calculated according to free weight) for 11 days. The dose chosen was based on an initial dose escalation study (ranging from 10 mg/kg/day to a total dose of 150 mg/kg/day) in DIO mice ($n = 2$); a total dose of 60 mg/kg/day was well tolerated with no observable adverse effects. Body weight and food intake were measured every other day. On day 12, mice were subjected to a 4 h fast period, then deeply anesthetized using isoflurane and trunk blood was collected by decapitation. Plasma was separated from every sample and the samples were submitted to Texas A&M Veterinary Medical Diagnostic Laboratory (TVMDL; College Station, TX, USA) for plasma lipid-panel measurements (total cholesterol and triglycerides). Triglycerides values were not included for analysis since the measurements were confounded by sample hemolysis that interfered with the triglyceride reagent in the assay. Epididymal fat pads (epididymal white adipose tissue; EWAT) were excised from every mouse, weighed, and fixed in 10% buffered formalin for further processing.

2.10. Histological analysis

Formalin-fixed EWAT samples were paraffin embedded, sectioned (4 μM), and stained with hematoxylin and eosin (H&E). Images were obtained at 20 \times magnification using a light microscope (Leica DM LB) and digitally photographed for automated image analysis. Images were analyzed using the “Adiposoft”

plug-in software in ImageJ (NIH) [22]. Briefly, images were converted to 8-bit images and scaled to 0.366 μm per pixel (corresponding to 20 \times magnification on the Leica microscope). Minimum and maximum diameter parameters were assigned to identify appropriate cells for the automated adipocyte area calculations, and cells along the boundary of the images were excluded from analyses. Three to five images/sample were analyzed, with automated analysis confirmed by visual inspection. Images corresponding to each sample were averaged to obtain the mean adipocyte area (μm^2) per sample and combined to calculate group mean values for control (vehicle-treated EWAT samples) and treatment (NNMT inhibitor-treated EWAT samples) cohorts.

2.11. Effect of NNMT inhibitor on adipocyte differentiation quantitated with oil red O staining

3T3-L1 cells were cultured in 60 mm diameter dishes (8.4×10^4 cells/dish) and treated with NNMT inhibitor dissolved in culture media with/without adipogenic factors (1 mM IBMX, 1 μM dexamethasone, 10 $\mu\text{g}/\text{ml}$ of insulin) during each of the scheduled medium changes during the differentiation process (described above). On day 9 post-differentiation, cells were subjected to quantitative oil red O (Thermo Fisher Scientific; Waltham, MA, USA) staining as adapted and modified from published protocols [12]. Briefly, cells were washed twice with PBS, fixed with 10% formalin for 30 min at room temperature, and stained with oil red O working solution ($\sim 0.2\%$ oil red O in 99% isopropanol) for 30 min. Cells were then washed five times or with sterile water until unincorporated oil red O stain was completely removed. Images of oil red O staining in control and inhibitor-treated cells were digitally photographed using a light microscope (Olympus BX41; Tokyo, Japan). After image capture, 2-propanol (3.5 mL) was added to each dish for 10 min to dissolve the oil red O stain and absorbance was quantified in a plate reader set at 492 nm wavelength. To ensure the absorbance from oil red O staining was within the linear detection range of the plate reader, a calibration curve was established for oil red O staining in adipocytes using a previously described protocol [23].

2.12. Statistical analysis

Statistical analysis for two-group comparisons was conducted using unpaired Student's *t*-test. A one-way analysis of variance (ANOVA) with Dunnett's posthoc test was used to compare multiple groups (different inhibitor treatments or concentration effects in cellular assessments) to controls. Daily NNMT inhibitor effects on body weight measures in DIO mice was analyzed using a repeated measures two-way ANOVA with Sidak's multiple comparison posthoc test. All statistical analyses were performed using Graphpad Prism 7.0 with an experiment-wise error rate of $\alpha = 0.05$.

3. Results

3.1. NNMT inhibitors display high membrane permeability

Compounds spanning ~ 100 -fold IC_{50} values for NNMT inhibition were selected on the basis of positional substitutions around the N-methylated quinolinium scaffold [17] to obtain an estimate of drug-like oral absorption/bioavailability properties and guide the choice of inhibitors for *in vitro* and *in vivo* phenotypic studies. Tables 1 and 2 summarize passive membrane diffusion and active transport membrane permeability, respectively, for select small molecule NNMT inhibitors for which structure activity relationships had been previously developed [17]. 1-MNA, a product inhibitor of NNMT [12,24,25] exhibited no passive permeability

Table 1
NNMT inhibitor permeability from passive transport across membranes as measured using PAMPA.

Name	IC ₅₀ (μM) ^a	Flux (cm/s)	Permeability Classification ^b
Quinoline (highly permeable) ^c	ND	33.9E-06	High permeability
1-Methylnicotinamide (1-MNA)	9.0	0	No permeability
1-Methylquinolinium (1-MQ)	12.1	0	No permeability
1,8-DiMQ	1.8	8.63702E-07	Low permeability
1,2,4,8-TetraMQ	109.2	6.98184E-07	Low permeability
5-Amino-1MQ	1.2	3.01472E-06	High permeability
3-Amino-6-fluoro-1MQ	1.2	1.07832E-06	Moderate permeability
7-Amino-1MQ	2.6	2.05476E-06	High permeability
2,3-Diamine-1MQ	2.8	3.89795E-06	High permeability

ND: Not determined; Quinoline is an NNMT substrate [25].

^a IC₅₀ values from our published SAR study [17].

^b BCS, Biopharmaceutics Classification System.

^c High membrane-permeable comparator compound [51]

Table 2
Active transport across cell membranes and drug efflux ratios for NNMT inhibitors determined using Caco-2 assay.

Name	Mean A → B Papp 10 ⁻⁶ cm/s	Mean B → A Papp 10 ⁻⁶ cm/s	Efflux Ratio (R _e)	Classification
Ranitidine ^a	0.192	1.44	11.9	Low permeability (control)
Talinolol ^a	23.5	15.7	0.673	High permeability (control)
Warfarin ^a	0.0701	5.01	73.2	High efflux (control)
1,8-DiMQ	BLQ	1.78	NC	Low permeability
5-Amino-1MQ	34.2	45.2	1.33	High permeability (no efflux)
7-Amino-1MQ	26.0	39.6	1.52	High permeability (no efflux)
2,3-Diamine-1MQ	5.27	21.2	4.03	Moderate permeability (moderate efflux)

BLQ: No peak detected in receiver side sample for A → B transport.

NC: not calculable.

^a Standard controls used in the assay based on permeability classifications.

(Table 1). Similarly, the quinolinium containing parent analogue 1-MQ also lacked passive diffusion properties (Table 1), suggesting that the lipophilicity and drug-like permeability properties of analogues within the methylquinolinium series had to be improved via chemical modification. To this end, we synthesized a number of per-methylated quinolinium analogues [17] guided by *in silico* calculation of partition coefficient (clogP) [26]. Addition of hydrophobic methyl group substitutions around the quinolinium scaffold (previously shown to negatively impact NNMT inhibitory activity) [17] only slightly improved membrane permeability via passive transport as indicated by the low, but non-zero, permeability values for 1,8-diMQ and 1,2,4,8-tetraMQ (Table 1). In contrast, positional polar amine substitutions around the quinolinium core not only improved NNMT inhibition as noted previously [17], but also enabled favorable passive and active transport across membranes (Tables 1 and 2). Specifically, 5-amino-1MQ and 7-amino-1MQ exhibited high passive and active transport across membrane, with no detectable efflux observed in the Caco-2 cell assay. In contrast, the 2,3-diamino substitution in the 1MQ scaffold (2,3-diamino-1MQ) displayed high passive permeability (Table 1), but moderate bi-directional active transport with moderate efflux ratio (Table 2). Consistent with the PAMPA measurements, the 1,8-diMQ analogue exhibited very low bi-directional transport in the Caco-2 cell assay (Table 2).

3.2. Effects of NNMT inhibitors on 3T3-L1 cell viability

The cytotoxic effects of three membrane-permeable NNMT inhibitors, 5-amino-1MQ, 7-amino-1MQ, and 2,3-diamino-1MQ were evaluated in 3T3-L1 pre-adipocytes. Treatment of cells with 10 μM 5-amino-1MQ or 7-amino-1MQ and 300 μM 2,3-diamino-1MQ for a 24 h period did not impact cell viability (Fig. 1). 5-Amino-1MQ and 7-amino-1MQ produced modest cytotoxicity relative to untreated cells ($P < .01$, treated vs. control untreated cells)

at concentrations ranging from 100 to 300 μM. All three compounds displayed ~40% cytotoxicity at the highest concentration tested ($P < .001$, 600 μM-treated cells vs. control untreated cells).

3.3. Differentiated 3T3-L1 adipocytes provide a relevant cell-based system to validate NNMT inhibitor mechanism-of-action

To determine if differentiated 3T3-L1 adipocytes could be utilized as a cell-based system for mechanism-of-action and phenotypic characterization of NNMT inhibitors, we measured the

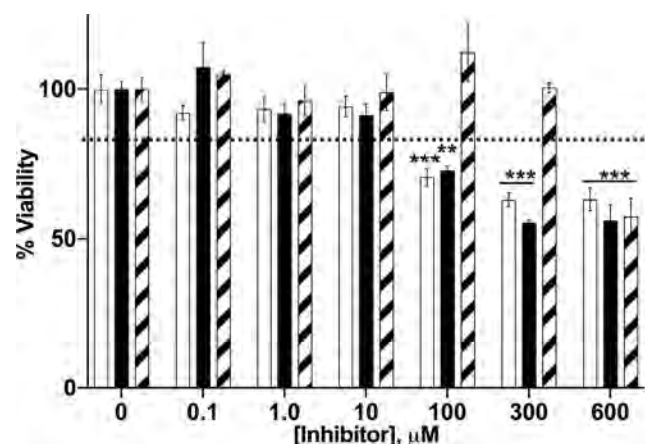


Fig. 1. Effect of NNMT inhibitors on 3T3-L1 cell viability. Data represent average viability of 3T3-L1 cells normalized to untreated (control) cells at different concentrations of 5-amino-1MQ (open bar), 7-amino-1MQ (closed bar), and 2,3-diamino-1MQ (hatched bar) ($n = 3-6$); error bars represent standard error of the mean (SEM). Treatment of 3T3-L1 pre-adipocytes with NNMT inhibitors for 24 h did not impact cell viability up to a concentration of 100 μM. $P > .05$, not significant vs. untreated 3T3-L1 cells (0 μM). $^{**}P < .01$; $^{***}P < .001$ vs. untreated 3T3-L1 cells (0 μM) analyzed by a one-way ANOVA with Dunnett's posthoc.

expression levels of NNMT and used LC/MS/MS to assess the levels of NNMT reaction product 1-MNA in fully differentiated adipocytes (day 9–10 post-differentiation) and undifferentiated pre-adipocytes (day 0). NNMT protein expression was found to be ~37-fold higher in the adipocytes (day 9) vs pre-adipocyte ($P < .0001$, Fig. 2A). Similarly, 1-MNA levels normalized to total cellular protein were ~7.5-fold higher in adipocytes compared to pre-adipocytes ($P < .05$, pre-adipocytes vs. adipocytes, Fig. 2B), suggesting relatively higher activity of the NNMT enzyme in the fully differentiated adipocytes. NNMT inhibition using 5-amino-1MQ (30 μM concentration) in both the pre-adipocytes ($P < .01$, treated pre-adipocytes vs. untreated controls) and the adipocytes ($P < .05$, treated adipocytes vs. untreated controls) resulted in significant reduction in the intracellular levels of 1-MNA (Fig. 2C).

3.4. NNMT inhibitors decrease production of 1-MNA in differentiated adipocytes

The relative effectiveness of NNMT inhibitors to lower 1-MNA levels in the differentiated adipocytes were compared at a single concentration of 10 μM (concentration well below the cytotoxic concentration range for NNMT inhibitors). Treatment of adipocytes with membrane-permeable NNMT inhibitors for 24 h resulted in a significant reduction in cellular 1-MNA levels, relative to the levels

of 1-MNA in untreated control adipocytes ($F_{(5,6)} = 42.64$, $P < .0001$) (Fig. 2D). Dunnett's posthoc tests revealed that all membrane-permeable NNMT inhibitors tested significantly decreased 1-MNA levels in the adipocytes relative to control (5-amino-1MQ, $P < .001$; 3-amino-6-fluoro-1MQ, $P < .01$; and 2,3-diamino-1MQ, $P < .05$ vs. control untreated adipocytes, respectively). In contrast, the poorly membrane-permeable NNMT inhibitor 1,2,4,8-tetraMQ did not significantly decrease intracellular 1-MNA levels compared to untreated controls ($P > .05$, n.s.). 5-amino-1MQ, an analogue from our initial series of NNMT inhibitors with low IC_{50} value ($\text{IC}_{50} \sim 1 \mu\text{M}$ [17]), and high cell membrane permeability (Table 2), produced the greatest reduction of intracellular 1-MNA levels at a concentration of 10 μM among tested inhibitors (Fig. 2D). Based on these results, we monitored changes in intracellular 1-MNA in response to 24 h treatment with varied 5-amino-1MQ concentrations. 5-amino-1MQ showed concentration-dependent inhibition of NNMT in fully differentiated adipocytes that could be fit to a 3-parameter sigmoidal dose-response curve with a calculated $\text{EC}_{50} = 2.3 \pm 1.1 \mu\text{M}$ (Fig. 2E, 2F; goodness-of-fit $R^2 = 0.94$). At inhibitor concentrations ranging from 10 to 60 μM , the relative intracellular 1-MNA levels stabilized at ~40% the level observed for untreated adipocytes; concentrations greater than 60 μM were not tested due to known cytotoxic effects in 3T3-L1 cells (see Fig. 1).

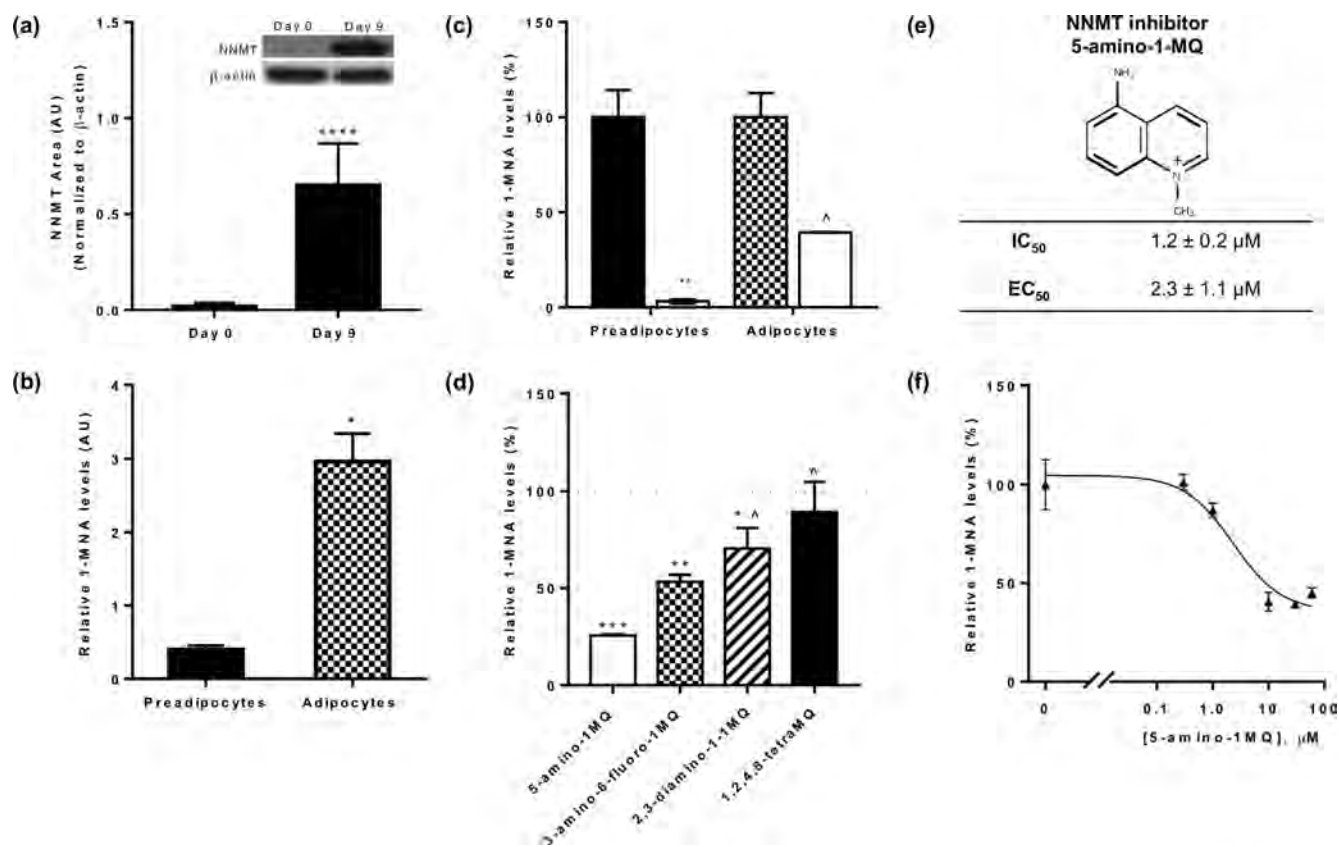


Fig. 2. Relative NNMT protein expression and reaction product 1-MNA levels in the pre-adipocytes vs adipocytes, and the mechanistic validation of NNMT inhibitors in adipocytes. Expression levels of NNMT (normalized to β -actin) in pre-adipocytes (Day 0) and fully differentiated adipocytes (Day 9) (a). Relative levels of 1-MNA in the pre-adipocytes (closed bar) and differentiated adipocytes (checkered bar) per μg of total cellular protein (b). Effects of 5-amino-1MQ (30 μM) (open bar) treatment for 24 h on the intracellular levels of the NNMT reaction product 1-MNA in pre-adipocytes (closed bar) and differentiated adipocytes (checkered bar) (c). Relative effect of NNMT inhibitors on the intracellular levels of 1-MNA in the adipocytes (inhibition of 1-MNA compared at 10 μM concentration of each inhibitor treated for 24 h) (d). Chemical structure and activity of NNMT inhibitor 5-amino-1MQ. IC_{50} for the lead inhibitor 5-amino-1MQ value was determined using a biochemical assay [17] and EC_{50} was determined from data in Fig. 3F (e). Dose-response curve showing intracellular 1-MNA levels in adipocytes following treatment with varied 5-amino-1MQ concentrations (f). Data points represent average 1-MNA levels normalized to an internal standard and transformed to % control values \pm SD ($n = 2$ replicates per data point). The goodness-of-fit R^2 between fitted curves and data was 0.94. * $P < .05$ vs. control pre-adipocytes; ** $P < .05$; *** $P < .01$; **** $P < .001$ vs. control adipocytes; ^ $P < .01$, vs. 5-amino-1MQ (10 μM)-treated adipocytes analyzed by Student's *t*-test or a one-way ANOVA with Dunnett's posthoc where appropriate.

3.5. NNMT inhibition increases intracellular concentrations of NAD⁺ and SAM in differentiated adipocytes

Fig. 3A outlines the major elements of the mammalian NAD⁺ salvage pathway using NA as the starting substrate [27]. Since the NNMT inhibitor 5-amino-1MQ significantly reduced intracellular 1-MNA concentrations (Fig. 2B and C), we hypothesized that NNMT inhibition in adipocytes would increase intracellular concentrations of the co-substrates NA and SAM and shunt more NA into the NAD⁺ salvage cycle. A one-way ANOVA revealed an almost significant main effect of NNMT inhibitor treatment on intracellular NAD⁺ levels ($F_{(5,6)} = 4.131, P = 0.0568$) (Fig. 3B); treatment of the adipocytes with the NNMT inhibitor 5-amino-1MQ resulted in a concentration-dependent increase in the NAD⁺ levels with concentrations in the range of 1–60 μM resulting in ~ 1.2 – 1.6 -fold increase in NAD⁺ levels relative to control adipocytes. Dunnett's posttests revealed a significant increase in NAD⁺ levels at the 10 μM inhibitor concentration ($P < .05$ vs. control; Fig. 3B). Similarly, a one-way ANOVA revealed a significant main effect of NNMT inhibition on intracellular SAM levels ($F_{(5,5)} = 7.35, P = 0.0236$) in the adipocytes (Fig. 3B). Dunnett's posttests revealed a significant increase in the intracellular SAM levels at the higher inhibitor concentration relative to control adipocytes (30 μM , $P < .05$; 60 μM , $P = 0.06$). However, no statistically significant main effect of NNMT inhibitor treatment were observed for the intracellular levels of NA ($F_{(5,6)} = 1.031, P > .05$) and ($F_{(5,6)} = 0.334, P > .05$) SAH (Fig. 3B).

3.6. NNMT inhibitors are selective and do not impact related methyltransferases or enzymes in the NAD⁺ salvage pathway

The selectivity of NNMT inhibitors was confirmed by testing against a panel of structurally similar methyltransferases and two enzymes in the NAD⁺ salvage pathway (NAMPT and SIRT1; Fig. 3). Concentrations of 1,8-diMQ and 5-amino-1MQ ranging from 10 nM to 200 or 600 μM , respectively, did not inhibit DNMT1 or PRMT3 (Fig. 4A and B). Sigmoidal dose-response curves and reliable estimates of IC₅₀ values based on non-linear least-squares fitting to the available data could not be obtained since no significant inhibition of DNMT1 and PRMT3 was observed at the tested NNMT inhibitor concentrations (Table 3). Additionally, 1,8-diMQ and 5-amino-1MQ showed little inhibition of COMT at maximal tested concentrations of 200 μM (20% inhibition) and 600 μM (10% inhibition), respectively, although no clear trend of concentration-dependent inhibition was observed. As was noted for DNMT1 and PRMT3, sigmoidal dose-response curves and reliable estimates of IC₅₀ values could not be obtained since no significant inhibition was observed at the tested NNMT inhibitor concentrations.

5-Amino-1MQ did not inhibit NAMPT up to a tested concentration of 100 μM ; reliable data could not be obtained at 5-amino-1MQ concentrations above 100 μM due to interference with the NAMPT assay readout signal (Fig. 4D, Table 3). However, when the assay was repeated with 5-amino-6-fluoro-1MQ, an analogue of 5-amino-1MQ that did not interfere with the NAMPT assay, no

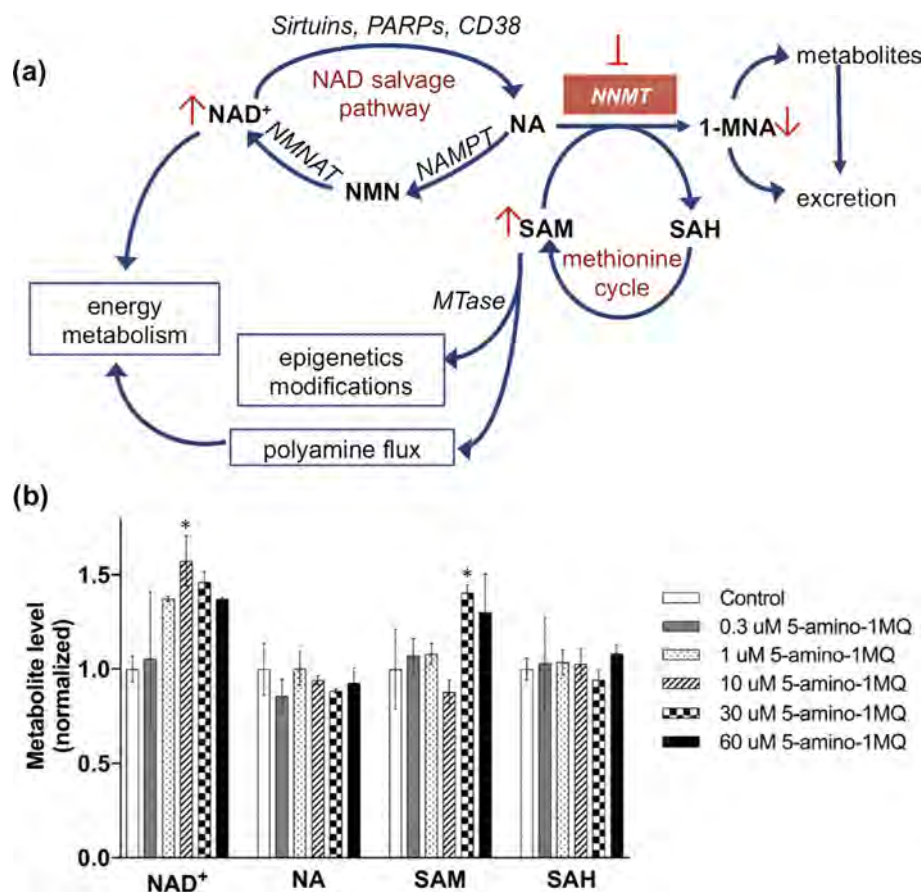


Fig. 3. Effects of NNMT inhibitor on intracellular levels of NAD⁺ salvage pathways and methionine cycle metabolites. Schematic illustration of pathways regulated by NNMT, including the NAD⁺ biosynthesis salvage pathway starting from NA as a precursor that feeds into energy metabolism, methionine cycle that regulates intracellular SAM concentrations and thus cellular epigenetic modifications and polyamine flux, and clearance of NA by conversion to 1-MNA and excretory products. Pathway enzyme abbreviations include NMNAT (nicotinamide mononucleotide adenyltransferase), NAMPT (nicotinamide phosphoribosyltransferase), MTase (SAM-dependent methyltransferases), PARPs (poly-ADP-ribose polymerases), and CD38 (cluster of differentiation 38/cyclic ADP ribose hydrolase) (a). Effects of the NNMT inhibitor 5-amino-1MQ on intracellular levels of NAD⁺, NA, SAM, and SAH metabolites in differentiated adipocytes treated with concentrations 0.3–60 μM for 24 h (b). Data represent mean metabolite levels measured by LC/MS/MS in 5-amino-1MQ-treated adipocytes (open bar) normalized to control untreated adipocyte (closed bar) levels in biological duplicates (\pm SD). * $P < .05$ vs. control untreated adipocytes determined by one-way ANOVAs followed by Dunnett's posttest comparisons.

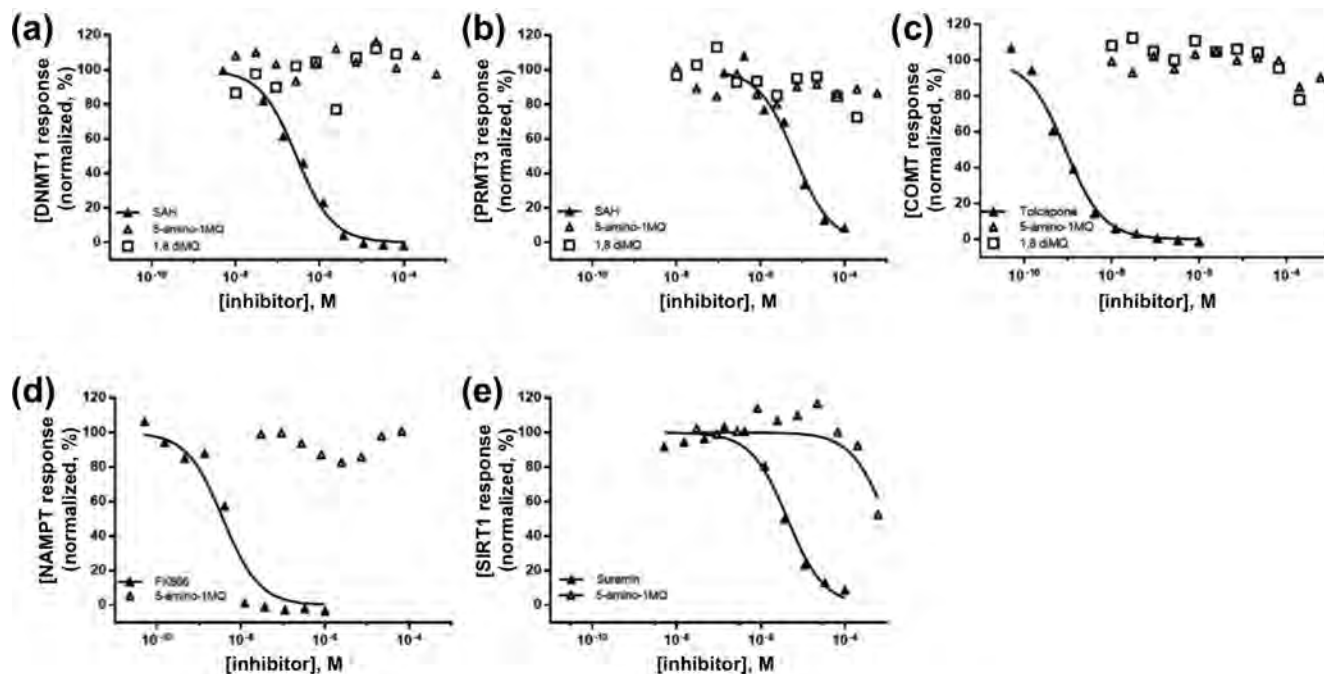


Fig. 4. Normalized response curves for NNMT inhibitors (5-amino-1MQ, open triangle; 1,8-diMQ, open square) against similar methyltransferase enzymes DNMT1 (a), PRMT3 (b), and COMT (c). Normalized response curves for NNMT inhibitor 5-amino-1MQ tested against NAD⁺ salvage pathway enzymes NAMPT (d) and SIRT1 (e). Data points represent normalized enzyme activity in the respective experiments using 10 concentrations of established enzyme-specific (positive control) and NNMT inhibitors in a 3-fold dilution series. The goodness-of-fit for the positive control inhibitors across all experiments and for 5-amino-1MQ against SIRT1 activity was >0.95. All other data points could not be used to generate reliable fitted curves and estimates of IC₅₀ values.

Table 3

Activity for NNMT inhibitors against related methyltransferases and enzymes in the NAD⁺ salvage pathway.

Enzyme	IC ₅₀ (μM)		
	Positive control	1,8-diMQ	5-Amino-1MQ
DNA (cytosine-5)-methyltransferase 1	0.28 ± 0.03 (SAH)	NI	NI
Protein arginine methyltransferase 3	6.6 ± 1.2 (SAH)	NC	NC
Catechol-O-methyltransferase	0.0009 ± 0.0001 (Tolcapone)	NC	NC
Nicotinamide phosphoribosyl transferase	0.0038 ± 0.0001 (FK866)	ND	>100 ^a
NAD ⁺ -dependent protein deacetylase sirtuin 1	4.3 ± 0.6 (Suramin)	ND	NC

NI: no inhibition.

NC: not calculable.

ND: not determined.

^a Concentrations above 100 μM could not be tested due to inference in the assay readout signal.

inhibition of NAMPT was observed with analogue concentrations between 30 and 600 μM (data not shown).

5-Amino-1MQ did not inhibit SIRT1 concentrations ranging from 10 nM to 300 μM, and minor reduction in SIRT1 activity was observed with 600 μM 5-amino-1MQ (Fig. 4E). However, sigmoidal dose-response curves and reliable estimates (i.e., R² > 0.8) of IC₅₀ values could not be obtained since no significant inhibition was observed with the tested concentrations of 5-amino-1MQ. Taken together, these results suggest high selectivity of the small molecule 5-amino-1MQ analogue at pharmacologically relevant concentrations to NNMT-inhibition.

3.7. NNMT inhibitor caused weight loss and reduced adipose tissue mass in DIO mice

Since *in vitro* studies showed 5-amino-1MQ to have high cell permeability, enzyme selectivity, and cell culture efficacy, a sub-chronic (11-day) proof-of-concept *in vivo* study was conducted to test the effect of NNMT inhibition on obesity in HFD fed mice. Three times daily systemic (SC) treatment of DIO mice with

20 mg/kg of 5-amino-1MQ produced a progressive loss of body weight over the treatment period compared to controls (Fig. 5A). A repeated-measures two-way ANOVA revealed a significant main effect of the factors treatment (F_(1,16) = 12.47, P = 0.0028), time (days) (F_(5,80) = 4.437, P = 0.0012), and a significant treatment x time interaction (F_(5,80) = 10.89, P < .0001). Sidak's multiple comparison posttests revealed significant differences in body weight between control and treated DIO mice on days 6 (P < .01), 9 (P < .0001), and 11 (P < .0001) (Fig. 5A). At the end of the 11-day treatment period, control DIO mice showed a cumulative weight gain of 0.6 ± 0.4 g (~1.4% weight gain from baseline measures), while DIO mice treated with the NNMT inhibitor showed a weight loss of 2.0 ± 0.6 g (~5.1% weight loss from baseline measures) (Fig. 5A). Food intake remained the same between the groups suggesting the weight loss effect is primarily related to altered metabolism (i.e., increased energy expenditure) (F_(1,16) = 1.101, P > .05; Fig. 5B); total cumulative food intake in control and treated DIO mice was 28.1 ± 1.2 g and 26.2 ± 1.4 g, respectively (Fig. 5B, inset). Additionally, treatment of DIO mice with the NNMT inhibitor resulted in a substantial ~35% decrease (P < .001) in the mass (Fig. 5C) and size

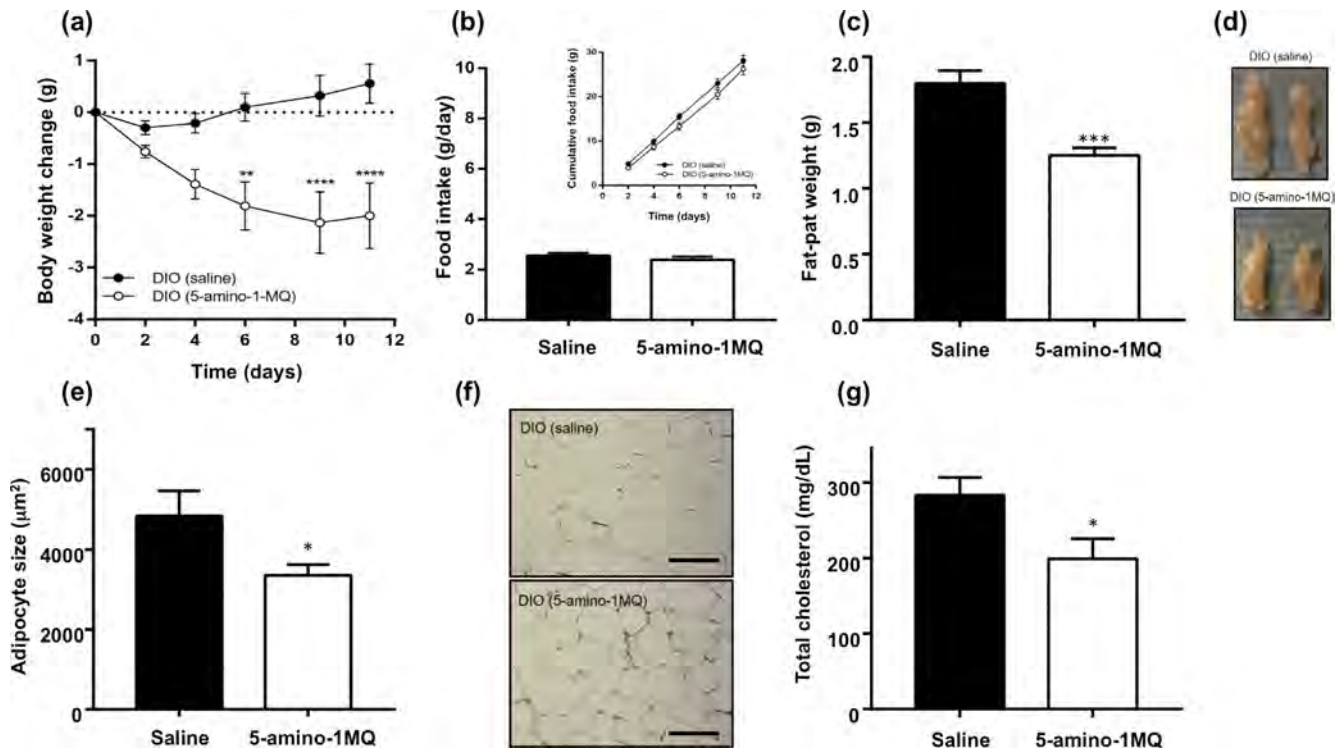


Fig. 5. Effects of saline or NNMT inhibitor (5-amino-1MQ, 20 mg/kg, t.i.d.) administered SC over a 11-day period in DIO mice on body weight changes from baseline (a), average food intake (g/day) and cumulative food intake across 11-days [inset] (b), epididymal fat-pad weight (c), size of the EWAT (representative images) (d), adipocyte size (μm^2) determined in mean number of 20.7 ± 1.8 (DIO, saline) and 28.6 ± 2.3 adipocytes (DIO, 5-amino-1MQ) (e), representative H&E stained images of saline- and 5-amino-1MQ-treated DIO EWAT tissue (scale bar = 200 μm) (f), and total plasma cholesterol levels following a 4-h fasting period (mg/dL) (g). All data points represent the mean values in $n = 9$ mice/group \pm SEM. * $P < .05$; ** $P < .01$, *** $P < .0001$ vs. saline-treated DIO analyzed by unpaired Student's *t*-test or a repeated measures two-way ANOVA with multiple comparisons posthoc tests where applicable.

(Fig. 5D) of the EWAT compared with the control DIO mice. Consistent with these results, histological analysis of the EWAT from treated DIO mice had >30% decrease in adipocyte size ($P < .05$; Fig. 5E and 5F) and >40% decrease in adipocyte volume (data not shown) compared to control DIO mice. Plasma lipid-profile measurements showed that the total cholesterol levels were ~30% lower in treated DIO mice relative to control DIO mice ($P < .05$; Fig. 5G). Total cholesterol levels at the end of our study in the control DIO mice were comparable to cholesterol levels reported by the vendor for age-matched DIO mice. In contrast, cholesterol levels in the NNMT inhibitor-treated DIO mice were similar to

cholesterol levels reported by the vendor for age-matched normal chow-fed C57Bl/6 mice (www.jax.org/jax-mice-and-services/find-and-order-jax-mice/most-popular-jax-mice-strains/dio-b6).

3.8. NNMT inhibition suppresses lipogenesis in 3T3-L1 cells

In order to determine the effect of NNMT inhibition on adipocyte differentiation and lipogenesis, lipid accumulation was determined in adipocytes following treatment of 3T3-L1 cells with the NNMT inhibitor in media containing adipogenic factors. Treatment with 5-amino-1MQ produced concentration-dependent inhibition

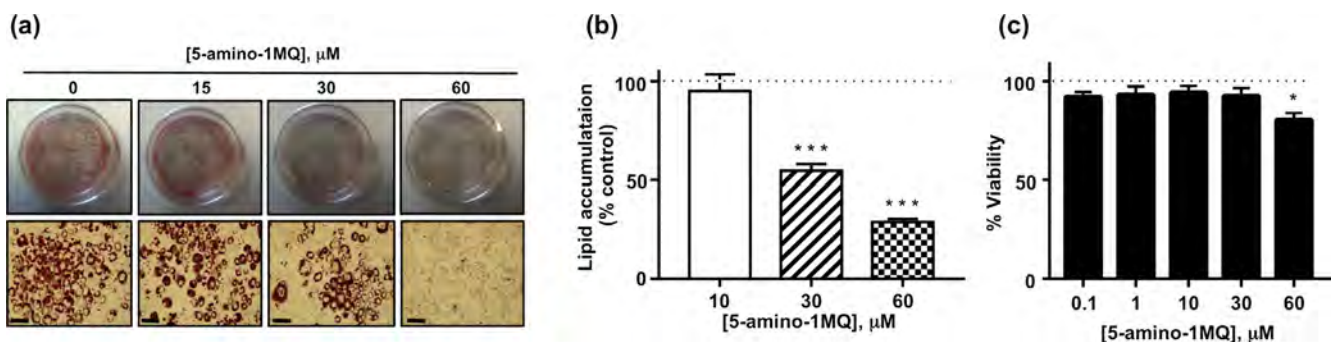


Fig. 6. Effects of 5-amino-1MQ on lipogenesis in differentiating 3T3-L1 cells. Representative images of culture plates (top panels) and microscopic images (20x magnification; scale bar = 50 μm ; bottom panels) following oil red O staining of lipid droplets in the control untreated and 5-amino-1MQ (15, 30, and 60 μM)-treated adipocytes (treatment continued throughout the period of differentiation) (a). Lipid accumulation determined by quantification of oil red O staining in 5-amino-1MQ (15, 30, and 60 μM)-treated adipocytes; data points represent average normalized (% untreated control) values (\pm SEM) in treated adipocyte samples ($n = 2$ replicates per experiment; experiment performed 3 times) (b). Viability of 3T3-L1 cells treated with 5-amino-1MQ (0.1–60 μM); data points represent average normalized (% untreated control) values (\pm SEM) in treated 3T3-L1 samples ($n = 3$ replicates per experiment; experiment performed 3 times). *** $P = 0.0001$ vs. untreated adipocytes (0 μM); * $P < .01$ vs. untreated 3T3-L1 cells analyzed by a one-way ANOVA with Dunnett's posthoc tests (c). (For interpretation of the references to colour in this figure legend, the reader is referred to the web version of this article.)

of lipid accumulation in differentiating pre-adipocytes ($F_{(3,19)} = 39.26$, $P < .0001$; Fig. 6A and B). Concentrations of 30 μM and 60 μM 5-amino-1MQ reduced lipogenesis by 50% and 70%, respectively, compared to control untreated adipocytes ($P = 0.0001$; Fig. 6B). 3T3-L1 cell viability was only slightly reduced at the highest tested concentration of 5-amino-1MQ compared to untreated cell viability ($P < .05$; Fig. 6C).

4. Discussion

Pharmacological treatment of obesity using target-based approaches to either decrease food intake or increase energy expenditure has been a major area of research in recent years [11]. Here, we demonstrated a novel pharmacological approach using small molecule inhibitors of NNMT, a target enzyme with a newly identified role in energy metabolism [15], as a potential intervention to prevent adipogenesis and reverse diet-induced obesity. We rationally developed the first series of highly membrane-permeable and selective small molecule inhibitors of NNMT with pronounced efficacy in reducing the levels of the NNMT reaction product 1-MNA in adipocytes. NNMT structure-activity relationships and physical chemical property-based analysis (e.g., logP) guided the synthesis of these membrane-permeable amino-substituted quinolinium analogues, which were validated with the PAMPA and Caco-2 cell-based empirical results, suggesting high oral absorption and bioavailability for these compounds [28]. Mechanisms of active-transport that mediate the intracellular uptake of these small molecules remain to be studied. However, organic cation transporters (OCTs) [29] may likely play role in the active transport of our charged quinolinium-containing quaternary amine NNMT inhibitors across cell membranes since OCTs have been shown to facilitate cellular uptake of several organic cationic drugs (e.g., metformin) [30,31].

Importantly, quinolinium-based NNMT inhibitors showed exceptional selectivity for NNMT with no apparent activity against either closely-related (i.e., tertiary structure rmsd $< 3 \text{ \AA}$ sequence identity $> 15\%$ relative to NNMT) human methyltransferases (e.g., COMT) or functionally distinct SAM-dependent DNA (e.g., DNMT1) and protein (e.g., PRMT3) methyltransferases with primary and tertiary structures highly similar to NNMT. Additionally, analogues containing the quinolinium scaffold lacked inhibitory activity against enzymes in the NAD^+ salvage pathway that bind nicotinamide-containing substrate, including NAMPT [27,32] and the NAD^+ -dependent SIRT1 enzyme, which deacetylates NAD^+ to produce NA, a product inhibitor of SIRT1 [33]. These results suggest that quinolinium-based NNMT inhibitors achieve selectivity by specifically interacting with the NA-binding pocket of NNMT [17], unlike several known non-selective methyltransferase inhibitors that interact with the SAM-binding pocket, which is highly conserved among SAM-dependent methyltransferases [34,35].

Membrane-permeable NNMT inhibitors reduced intracellular 1-MNA levels in a concentration-dependent manner and at pharmacologically relevant concentrations that did not impact cell viability, suggesting these small molecules interact directly with NNMT in cells. Given that NNMT has been reported to be a primary metabolic enzyme [36] and a major clearance pathway for intracellular NA [15], it is likely that these small molecules are directly and selectively inhibiting the conversion of NA to 1-MNA. We found that intracellular 1-MNA and NNMT protein expression levels were substantially higher in the fully differentiated adipocytes compared to the undifferentiated pre-adipocytes, which is consistent with the differentiation-dependent enhancement in NNMT mRNA levels and enzymatic activity reported previously in the 3T3-L1 cell lines [37]. The higher levels of 1-MNA and NNMT in adipocytes compared to pre-adipocytes may partially account for our observa-

tions that increasing concentrations (10–60 μM) of NNMT inhibitor did not completely eliminate 1-MNA in adipocytes, but did fully suppress 1-MNA accumulation in undifferentiated pre-adipocytes. In addition, the observed differential 1-MNA steady-state levels following NNMT inhibition may reflect differential transcriptional regulation of cellular metabolic pathways across the various stages of 3T3-L1 differentiation [38]; for example, aldehyde oxidase (AOX)-mediated degradation of 1-MNA may be more pronounced in pre-adipocytes compared to adipocytes, thereby synergistically reducing 1-MNA levels to a greater extent in pre-adipocytes compared to adipocytes. Further studies will examine differentiation-specific differences in the metabolic pathways that directly impact the clearance and/or shunting of NA into the NAD^+ salvage pathway.

Our observation that intracellular NA concentrations did not increase following NNMT inhibition extends previous studies that showed NA concentrations were largely unaffected following NNMT knockdown with either adenovirus [39] or anti-sense oligonucleotides (ASOs) [12]. It is possible that significant accumulation of NA in adipocytes (and other tissues) is prevented by rapid conversion of NA to NMN and subsequent NAD^+ synthesis or transport to the extracellular environment [27]. Importantly, NNMT inhibition potentiated the absolute intracellular concentrations of NAD^+ and SAM, without altering the levels of NA and SAH in the adipocytes. These co-factors are critical regulators of cellular energy metabolism, polyamine flux, epigenetic remodeling, and SIRT1 activity in the NAD^+ salvage pathway [12,27,40]. The increased levels of SAM and NAD^+ we observed in cultured adipocytes following NNMT inhibition are consistent with the upregulation of SAM and NAD^+ observed in the WAT of DIO mice treated with NNMT ASO, which correlated with increased cellular energy expenditure, reduced adiposity, and protection against diet-induced obesity [12]. In the present study, systemic treatment of DIO mice with a small molecule NNMT inhibitor caused significant loss of body weight and WAT mass, reduction in adipocyte size, and corresponding improvements in the plasma lipid profile (i.e., decreased circulating cholesterol levels). Notably, NNMT inhibition did not impact food intake in the DIO mice nor produce any overt signs of toxicity or adverse behavioral effects at the pharmacologically effective dose. Together, our observations that a small molecule NNMT inhibitor can increase NAD^+ and SAM concentrations in differentiated adipocytes and reduce adiposity in DIO mice, suggest that treatment with an NNMT inhibitor effectively reverses obesity via modulation of the NAD^+ salvage and SAM-mediated (e.g., polyamine flux) pathways to regulate energy expenditure in the adipose tissue.

A number of studies support NAD^+ regeneration as a therapeutic strategy to benefit patients with obesity [27]. For examples, natural NAD^+ precursor activators such as nicotinamide riboside (NR) administered via dietary supplements to high-fat fed mice protected against diet-induced obesity, increased energy metabolism, and improved insulin sensitivity [41]; some of these effects were shown to be mediated by NAD^+ -dependent SIRT1 activation [42]. Similarly, systemic administration of NMN improved glucose tolerance and diet- and age-related insulin resistant conditions [43,44]. However, dietary supplemental NAD^+ precursors (e.g., NR, NMN) require chronic administration and/or very high pharmacological doses to achieve physiologically beneficial enhancements in the NAD^+ levels, which potentially limit use in humans [27]. It could be predicted that combined administration of sub-maximal doses of dietary supplements and NNMT inhibitors that function as activators of NAD^+ might produce synergistic improvements in diet-induced obesity, and reduce adverse effects associated with chronic high-dose administration of dietary supplemental NAD^+ precursors. Studies testing the efficacy of NNMT inhibition on diet-induced obesity, both alone and combined with dietary agents, are currently in progress.

The present study demonstrated that NNMT inhibitor administered during adipocyte differentiation blocked the accumulation of lipid droplets, suggesting suppressed lipogenesis and programmed development of mature adipocytes from pre-adipocyte 3T3-L1 precursor cells (i.e., “adipogenesis”). Since 24 h of treatment of adipocytes with an NNMT inhibitor increased intracellular levels of SAM and NAD⁺, it is likely that prolonged exposures to NNMT inhibitor during differentiation may have resulted in significantly enhanced intracellular flux of SAM and NAD⁺. Increased absolute concentrations of intracellular NAD⁺ links with activation of NAD⁺-dependent histone deacetylases (e.g., sirtuins) that also mediate epigenetic regulation of gene expression [40] and adipocyte physiology [45]. Similarly, increased intracellular concentrations of SAM, a universal substrate for SAM-dependent histone methyltransferases, could have profound influence on cellular epigenetic modifications, including transcriptional regulation and the expression of genes that regulate adipogenesis and/or thermogenesis promoting browning of adipocytes (e.g., PPAR γ , PRDM16, UCP1, Wnt) [46–48]. NNMT protein expression is relatively lower in the murine brown adipose tissue (BAT) compared to the WAT [37] and *nmmt* (a WAT-selective gene [49,50]) gene expression has been reported to be lower in the BAT of HFD fed mice compared to normal chow-fed mice [49]. Furthermore, NNMT activity is significantly higher in the white fat compared to brown adipose tissue and the other organs (e.g., liver, lungs) in DIO mice [16]. Hence, treatment with an NNMT inhibitor in DIO mice may less likely impact BAT or other tissue NNMT activity, but could be speculated to modulate thermogenic/adipogenic genes in the WAT. Future studies will validate *in vivo* modulation of WAT NAD⁺/SAM and delineate NAD⁺- and SAM-mediated epigenetic mechanisms that may underlie gene regulation in the presence of NNMT inhibitors.

The current study provides conclusive evidence for the use of small molecule, “drug-like” NNMT inhibitors as a viable therapeutic approach to manage diet-induced obesity and related metabolic comorbidities. Our novel NNMT inhibitors display excellent physical chemical properties (e.g., membrane permeability), selectivity, and cellular inhibitory activity against NNMT, concomitantly enhancing the levels of the co-factors SAM and NAD⁺ that independently regulate cellular energy metabolism and epigenetic modifications. Importantly, treatment of DIO mice with our NNMT inhibitors did not impact food intake, but produced marked reductions in body weight, WAT mass, adipocyte size, and cholesterol levels with negligible toxicity or observable adverse effects. Future studies will be focused on optimizing the MQ-scaffold lead series to generate more potent NNMT inhibitors with significantly improved “drug-like” ADME profile. Orally bioavailable lead candidates will be tested in a comprehensive dose-ranging study to confirm efficacy on obesity and co-morbid endpoints.

Acknowledgements

We thank Dr. William Russell (Director, Mass Spectrometry Facility, Department of Biochemistry and Molecular Biology, UTMB) for his assistance in optimizing and running all LC/MS/MS assessments. We thank Dr. Robert Cox and Sam Jacob of the Histopathology Research Laboratory at Shriners Hospital for Children, Galveston for their support in histological processing and light microscopic analysis of the EWAT tissue samples (grant #84060, PI: Dr. Hal Hawkins). We thank Catherine Sampson for her assistance with the mouse blood collection and epididymis fat-pad isolation procedures. This work was supported by the Department of Defense Peer Reviewed Medical Research Program grant PR141776 (S.J.W.), University of Texas Medical Branch Technology Commercialization Award (S.J.W.), and NIH grant R01GM112936 (C.C.F.).

Conflict of interest

The authors declare no conflict of interest.

References

- [1] R.L. Kolotkin, K. Meter, G.R. Williams, Quality of life and obesity, *Obes. Rev.* 2 (4) (2001) 219–229.
- [2] Y.C. Wang, K. McPherson, T. Marsh, S.L. Gortmaker, M. Brown, Health and economic burden of the projected obesity trends in the USA and the UK, *Lancet* 378 (9793) (2011) 815–825.
- [3] K.M. Flegal, B.K. Kit, H. Orpana, B.I. Graubard, Association of all-cause mortality with overweight and obesity using standard body mass index categories: a systematic review and meta-analysis, *JAMA* 309 (1) (2013) 71–82.
- [4] P. Gonzalez-Muniesa, M.A. Martinez-Gonzalez, F.B. Hu, J.P. Despres, Y. Matsuzawa, R.J.F. Loos, L.A. Moreno, G.A. Bray, J.A. Martinez, *Obesity, Nat. Rev. Dis. Primers* 3 (2017) 17034.
- [5] T. Caputo, F. Gilardi, B. Desvergne, From chronic overnutrition to metaflammation and insulin resistance: adipose tissue and liver contributions, *FEBS Lett.* (2017).
- [6] M.D. Jensen, D.H. Ryan, C.M. Apovian, J.D. Ard, A.G. Comuzzie, K.A. Donato, F.B. Hu, V.S. Hubbard, J.M. Jakicic, R.F. Kushner, C.M. Loria, B.E. Millen, C.A. Nonas, F. X. Pi-Sunyer, J. Stevens, V.J. Stevens, T.A. Wadden, B.M. Wolfe, S.Z. Yanovski/American College of Cardiology/American Heart Association Task Force on Practice, S. Obesity, 2013 AHA/ACC/TOS guideline for the management of overweight and obesity in adults: a report of the American College of Cardiology/American Heart Association Task Force on Practice Guidelines and The Obesity Society, *J. Am. Coll. Cardiol.* 63 (25 Pt B) (2014) 2985–3023.
- [7] P. Zimmet, K.G. Alberti, J. Shaw, Global and societal implications of the diabetes epidemic, *Nature* 414 (6865) (2001) 782–787.
- [8] E.E. Calle, C. Rodriguez, K. Walker-Thurmond, M.J. Thun, Overweight, obesity, and mortality from cancer in a prospectively studied cohort of U.S. adults, *N. Engl. J. Med.* 348 (17) (2003) 1625–1638.
- [9] S.R. Colberg, R.J. Sigal, Prescribing exercise for individuals with type 2 diabetes: recommendations and precautions, *Phys. Sportsmed.* 39 (2) (2011) 13–26.
- [10] A. Fildes, J. Charlton, C. Rudisill, P. Littlejohns, A.T. Prevost, M.C. Gulliford, Probability of an obese person attaining normal body weight: cohort study using electronic health records, *Am. J. Public Health* 105 (9) (2015) e54–e59.
- [11] C. Martinussen, K.N. Bojsen-Moller, M.S. Svane, T.F. Dejgaard, S. Madsbad, Emerging drugs for the treatment of obesity, *Expert. Opin. Emerg. Drugs* 22 (1) (2017) 87–99.
- [12] D. Kraus, Q. Yang, D. Kong, A.S. Banks, L. Zhang, J.T. Rodgers, E. Pirinen, T.C. Pulinilkunnil, F. Gong, Y.C. Wang, Y. Cen, A.A. Sauve, J.M. Asara, O.D. Peroni, B.P. Monia, S. Bhanot, L. Alhonen, P. Puigserver, B.B. Kahn, Nicotinamide N-methyltransferase knockdown protects against diet-induced obesity, *Nature* 508 (7495) (2014) 258–262.
- [13] A. Kannt, A. Pfenninger, L. Teichert, A. Tonjes, A. Dietrich, M.R. Schon, N. Kloting, M. Bluher, Association of nicotinamide-N-methyltransferase mRNA expression in human adipose tissue and the plasma concentration of its product, 1-methylnicotinamide, with insulin resistance, *Diabetologia* 58 (4) (2015) 799–808.
- [14] M. Liu, L. Li, J. Chu, B. Zhu, Q. Zhang, X. Yin, W. Jiang, G. Dai, W. Ju, Z. Wang, Q. Yang, Z. Fang, Serum N(1)-methylnicotinamide is associated with obesity and diabetes in Chinese, *J. Clin. Endocrinol. Metab.* 100 (8) (2015) 3112–3117.
- [15] P. Pissios, Nicotinamide N-methyltransferase: more than a vitamin B3 clearance enzyme, *Trends Endocrinol. Metab.* 28 (5) (2017) 340–353.
- [16] B. Rudolphi, B. Zapp, N.A. Kraus, F. Ehebauer, B. Kraus, D. Kraus, Body weight predicts Nicotinamide N-Methyltransferase activity in mouse fat, *Endocr. Res.* (2017) 1–9.
- [17] H. Neelakantan, H.Y. Wang, V. Vance, J.D. Hommel, S.F. McHardy, S.J. Watowich, Structure-activity relationship for small molecule inhibitors of nicotinamide N-methyltransferase, *J. Med. Chem.* 60 (12) (2017) 5015–5028.
- [18] Q.G. Zhou, X. Peng, L.L. Hu, D. Xie, M. Zhou, F.F. Hou, Advanced oxidation protein products inhibit differentiation and activate inflammation in 3T3-L1 preadipocytes, *J. Cell. Physiol.* 225 (1) (2010) 42–51.
- [19] M. Yuan, S.B. Breitkopf, X. Yang, J.M. Asara, A positive/negative ion-switching, targeted mass spectrometry-based metabolomics platform for bodily fluids, cells, and fresh and fixed tissue, *Nat. Protoc.* 7 (5) (2012) 872–881.
- [20] (U.S.) *IoLARGuide for the Care and Use of Laboratory Animals*, 8th ed., National Academies Press, Washington, DC, USA 2011.
- [21] C.Y. Wang, J.K. Liao, A mouse model of diet-induced obesity and insulin resistance, *Methods Mol. Biol.* 821 (2012) 421–433.
- [22] M. Galarraga, J. Campion, A. Munoz-Barrutia, N. Boque, H. Moreno, J.A. Martinez, F. Milagro, C. Ortiz-de-Solorzano, Adiposoft: automated software for the analysis of white adipose tissue cellularity in histological sections, *J. Lipid Res.* 53 (12) (2012) 2791–2796.
- [23] N.A. Kraus, F. Ehebauer, B. Zapp, B. Rudolphi, B.J. Kraus, D. Kraus, Quantitative assessment of adipocyte differentiation in cell culture, *Adipocyte* 5 (4) (2016) 351–358.
- [24] S. Aksoy, C.L. Szumlanski, R.M. Weinshilboum, Human liver nicotinamide N-methyltransferase Cdna Cloning, expression, and biochemical characterization, *J. Biol. Chem.* 269 (20) (1994) 14835–14840.

- [25] H. Neelakantan, V. Vance, H.L. Wang, S.F. McHardy, S.J. Watowich, Noncoupled fluorescent assay for direct real-time monitoring of nicotinamide N-methyltransferase activity, *Biochemistry* 56 (6) (2017) 824–832.
- [26] M.M. Hann, G.M. Keseru, Finding the sweet spot: the role of nature and nurture in medicinal chemistry, *Nat Rev Drug Discov* 11 (5) (2012) 355–365.
- [27] C. Canto, K.J. Menzies, J. Auwerx, NAD(+) metabolism and the control of energy homeostasis: a balancing act between mitochondria and the nucleus, *Cell Metab.* 22 (1) (2015) 31–53.
- [28] J. Ruell, Membrane-based drug assays, *Mod. Drug Disc.* (2003) 28–30.
- [29] T.K. Han, R.S. Everett, W.R. Proctor, C.M. Ng, C.L. Costales, K.L. Brouwer, D.R. Thakker, Organic cation transporter 1 (OCT1/mOct1) is localized in the apical membrane of Caco-2 cell monolayers and enterocytes, *Mol. Pharmacol.* 84 (2) (2013) 182–189.
- [30] J.M. Moreno-Navarrete, F.J. Ortega, J.I. Rodriguez-Hermosa, M. Sabater, G. Pardo, W. Ricart, J.M. Fernandez-Real, OCT1 Expression in adipocytes could contribute to increased metformin action in obese subjects, *Diabetes* 60 (1) (2011) 168–176.
- [31] H. Motohashi, K. Inui, Organic cation transporter OCTs (SLC22) and MATEs (SLC47) in the human kidney, *AAPS J.* 15 (2) (2013) 581–588.
- [32] E.S. Burgos, M.C. Ho, S.C. Almo, V.L. Schramm, A phosphoenzyme mimic, overlapping catalytic sites and reaction coordinate motion for human NAMPT, *Proc. Natl. Acad. Sci. U.S.A.* 106 (33) (2009) 13748–13753.
- [33] S. Imai, The NAD World: a new systemic regulatory network for metabolism and aging—Sirt1, systemic NAD biosynthesis, and their importance, *Cell Biochem. Biophys.* 53 (2) (2009) 65–74.
- [34] R.A. Copeland, M.E. Solomon, V.M. Richon, Protein methyltransferases as a target class for drug discovery, *Nat. Rev. Drug Discov.* 8 (9) (2009) 724–732.
- [35] J.L. Martin, F.M. McMillan, SAM (dependent) I AM: the S-adenosylmethionine-dependent methyltransferase fold, *Curr. Opin. Struct. Biol.* 12 (6) (2002) 783–793.
- [36] T.A. Alston, R.H. Abeles, Substrate specificity of nicotinamide methyltransferase isolated from porcine liver, *Arch. Biochem. Biophys.* 260 (2) (1988) 601–608.
- [37] M. Riederer, W. Erwa, R. Zimmermann, S. Frank, R. Zechner, Adipose tissue as a source of nicotinamide N-methyltransferase and homocysteine, *Atherosclerosis* 204 (2) (2009) 412–417.
- [38] H. Hackl, T.R. Burkard, A. Sturn, R. Rubio, A. Schleiffer, S. Tian, J. Quackenbush, F. Eisenhaber, Z. Trajanoski, Molecular processes during fat cell development revealed by gene expression profiling and functional annotation, *Genome Biol.* 6 (13) (2005) R108.
- [39] S. Hong, J.M. Moreno-Navarrete, X. Wei, Y. Kikukawa, I. Tzameli, D. Prasad, Y. Lee, J.M. Asara, J.M. Fernandez-Real, E. Maratos-Flier, P. Pissios, Nicotinamide N-methyltransferase regulates hepatic nutrient metabolism through Sirt1 protein stabilization, *Nat. Med.* 21 (8) (2015) 887–894.
- [40] R. Janke, A.E. Dodson, J. Rine, Metabolism and epigenetics, *Annu. Rev. Cell Dev. Biol.* 31 (2015) 473–496.
- [41] C. Canto, R.H. Houtkooper, E. Pirinen, D.Y. Youn, M.H. Oosterveer, Y. Cen, P.J. Fernandez-Marcos, H. Yamamoto, P.A. Andreux, P. Cettour-Rose, K. Gademann, C. Rinsch, K. Schoonjans, A.A. Sauve, J. Auwerx, The NAD(+) precursor nicotinamide riboside enhances oxidative metabolism and protects against high-fat diet-induced obesity, *Cell Metab.* 15 (6) (2012) 838–847.
- [42] S. Imai, W. Kiess, Therapeutic potential of SIRT1 and NAMPT-mediated NAD biosynthesis in type 2 diabetes, *Front. Biosci. (Landmark Ed)* 14 (2009) 2983–2995.
- [43] K.M. Ramsey, K.F. Mills, A. Satoh, S. Imai, Age-associated loss of Sirt1-mediated enhancement of glucose-stimulated insulin secretion in beta cell-specific Sirt1-overexpressing (BESTO) mice, *Aging Cell* 7 (1) (2008) 78–88.
- [44] J. Yoshino, K.F. Mills, M.J. Yoon, S. Imai, Nicotinamide mononucleotide, a key NAD(+) intermediate, treats the pathophysiology of diet- and age-induced diabetes in mice, *Cell Metab.* 14 (4) (2011) 528–536.
- [45] K.L. Stromsdorfer, S. Yamaguchi, M.J. Yoon, A.C. Moseley, M.P. Franczyk, S.C. Kelly, N. Qi, S. Imai, J. Yoshino, NAMPT-mediated NAD(+) biosynthesis in adipocytes regulates adipose tissue function and multi-organ insulin sensitivity in mice, *Cell Rep.* 16 (7) (2016) 1851–1860.
- [46] J.E. Lee, K. Ge, Transcriptional and epigenetic regulation of PPARgamma expression during adipogenesis, *Cell. Biosci.* 4 (2014) 29.
- [47] M. Okamura, T. Inagaki, T. Tanaka, J. Sakai, Role of histone methylation and demethylation in adipogenesis and obesity, *Organogenesis* 6 (1) (2010) 24–32.
- [48] K.A. Lo, P.Y. Ng, Z. Kabiri, D. Virshup, L. Sun, Wnt inhibition enhances browning of mouse primary white adipocytes, *Adipocyte* 5 (2) (2016) 224–231.
- [49] C.M. Hung, C.M. Calejman, J. Sanchez-Gurmaches, H. Li, C.B. Clish, S. Hettmer, A.J. Wagers, D.A. Guertin, Rictor/mTORC2 loss in the Myf5 lineage reprograms brown fat metabolism and protects mice against obesity and metabolic disease, *Cell Rep.* 8 (1) (2014) 256–271.
- [50] N.J. Song, S. Choi, P. Rajbhandari, S.H. Chang, S. Kim, L. Vergnes, S.M. Kwon, J.H. Yoon, S. Lee, J.M. Ku, J.S. Lee, K. Reue, S.H. Koo, P. Tontonoz, K.W. Park, Prdm4 induction by the small molecule butein promotes white adipose tissue browning, *Nat. Chem. Biol.* 12 (7) (2016) 479–481.
- [51] V.S. Gopinath, M. Rao, R. Shivahare, P. Vishwakarma, S. Ghose, A. Pradhan, R. Hindupur, K.D. Sarma, S. Gupta, S.K. Puri, D. Launay, D. Martin, Design, synthesis ADME characterization and antileishmanial evaluation of novel substituted quinoline analogs, *Bioorg. Med. Chem. Lett.* 24 (9) (2014) 2046–2052.